Hydrogen production by dry reforming of methane on Ni catalysts based on CeO2, modified CeO2 with Zr or Al, and Mg-Al-O nano-materials

Xiu Liu

CENTRALE LILLE

THÈSE

Présentée en vue d'obtenir
le grade de

DOCTEUR

En
Spécialité : Chimie des matériaux
Par

Xiu LIU

DOCTORAT DELIVRE PAR CENTRALE LILLE

Titre de la thèse :

Production d'hydrogène par reformage à sec de méthane sur catalyseurs au Ni à base de CeO_2, CeO_2 modifiée avec Zr ou Al, et nano-matériaux Mg-Al-O

Hydrogen production by dry reforming of methane on Ni catalysts based on CeO_2, modified CeO_2 with Zr or Al, and Mg-Al-O nano-materials

Soutenue le 8 décembre 2021 devant le jury d'examen :

Président	Arnaud Travert	Professeur	Université de Caen
Rapporteur	Dorothée Laurenti	Directrice de Recherche CNRS	IRCELYON
Rapporteur	Nicolas Bion	Chargé de Recherche CNRS, HDR	IC2MP Poitiers
Examinateur	Marcia Araque Marin	Maître de Conférences	Centrale Lille
Directeur de thèse	Louise Duhamel	Chargée de Recherche CNRS, HDR	Université de Lille
Co-directeur	Sébastien Paul	Professeur	Centrale Lille

Thèse préparée dans le Laboratoire UCCS

École Doctorale SMRE 104

Acknowledgements

First and foremost, I would like to sincerely thank China Scholarship Council for providing me with a scholarship allowing me to perform my PhD studies in France.

I would like to sincerely acknowledge Director of UCCS Franck Dumeignil for welcoming me and allowing me to do this thesis at UCCS. This work is performed in Unité de Catalyse et Chimie du Solide - CNRS UMR8181, and Ecole Centrale de Lille.

I would love to express my sincere and heartfelt gratitude to my supervisor, Dr. Louise Duhamel, who helps me quite a lot in every aspect. I do appreciate her patience, encouragement and professional guidance during my three-year-long PhD studies, leading me to a right way to the independent scientific research. I would like to thank my co-supervisor Pr. Sébastien Paul very much for providing me all the necessary resources for my research.

I would also like to thank Ms. Pardis Simon, Ms. Martine Trentesaux, Mr. Olivier Gardoll who helped me scientifically for the XPS, Raman, TPR and BET analyzes. And I feel grateful to Mr. Stéphane Chambrey, Ms. Mélanie Dubois who helped me during my PhD studies. As well as our friendly colleagues: Dr. Hu Hao, Dr. Bingyu Yang, Dr. Noura Haidar, Dr, Shilipa Sonar, Dr. Belsam Hamieh, Dr. Wafa Ksila, Mr. Mohammad Hellani, Mr. Nicolas Montroussier, Mr. Julien Dupont, Ms. Bertha Farah and Ms. Afef Salhi. The times when we work together leave me very pleasant memories.

I also want to thank my friends in France for having a wonderful time together in these three years. And I also want to thank my boyfriend Wang Zhang, who always be with me, take care of me and encourage me.

I finally would love to express my gratitude to my beloved parents who have always been helping me out of difficulties and supporting me without a word of complaint.

Abstract

The demand for hydrogen, as a chemical product and as energy is increasing, but the main hydrogen production methods are unsustainable and not environmentally friendly. Hydrogen production from renewable resources (such as biogas mainly composed of CH_4 and CO_2) is required. Dry reforming of methane (DRM) is a promising method to produce H_2 and CO from greenhouse gases. It has received a lot of attention due to environmental issues.

In this thesis, Ni-based $CeNi_XO_Y$, $CeZr_{0.5}Ni_XO_Y$, $CeAl_{0.5}Ni_XO_Y$, and $AlMg_2Ni_XO_Y$ catalysts are studied in dry reforming of methane reaction. The effect of reaction temperature, Ni content, in situ H_2 pretreatment, mass of catalyst, calcination, and CO_2/CH_4 ratio are studied. Moreover, long duration stability tests are reported on some chosen samples. The optimized catalytic performance associated with resistance to carbon formation is obtained on partially reduced catalysts.

Various physicochemical characterizations are used to analyze the properties of the catalysts, such as XRD, Raman, XPS, and H_2-TPR. Some chosen catalysts are also characterized after DRM reaction to analyze their evolution.

Finally, an active site involving Ni species in close interactions with other cations is proposed. It is related to a partially reduced catalyst involving anionic vacancies, O^{2-} species, and cations.

Keywords: Dry reforming of methane, Hydrogen production, Ni-based catalysts, Ceria, Zirconium, Aluminum, Mg-Al-O nano-materials.

Table of contents

Chapter 1
Bibliographic studies

Chapter 1 Bibliographic studies

In recent years, the energy crisis, the exhaustion of fossil fuels, and greenhouse gas emissions have attracted the attention of the global community. The energy demands of almost all countries depend on the so-called fossil fuel economy. Most transportation sectors in the world only use petroleum products as fuel. In addition, a large proportion of power plants use fossil fuels such as oil, natural gas, and coal as feedstock. Although fossil fuels play a key role in social development, they have created problems such as air pollution, environmental pollution, global warming, and economic dependence[1].

As of 2017, the World Meteorological Organization (WMO) assessment unveiled the atmospheric content of CO_2 as 405.5 parts / million (ppm), 146% of the pre-industrial era (before 1750). And the atmospheric methane hit a new high of approximately 1859 parts / billion (ppb) in 2017 and now reached 257% of the pre-industrial level. The warning impact of long-lived GHGs on earth rose by 41% since 1990[2].

Global warming is anticipated to be a daunting scientific challenges. Therefore, the development of renewable and clean energy into traditional energy becomes the mainstream development tactic worldwide today. Research on the easy production of clean fuels has become a key research topic[3].

1.1 Hydrogen: energy for future

Hydrogen is one of the most abundant elements on earth, and due to its simplicity, hydrogen is considered an important clean fuel in the future. Hydrogen is an odorless, colorless, highly reactive element, and is the only truly clean chemical fuel. The hydrogen economy is expected to eliminate all the above-mentioned problems related to fossil fuel economy[4]. Hydrogen is a key component of a clean, sustainable energy system or hydrogen economy. A lot of research activities are ongoing, and certain measures are already being taken to prove the potential of the H_2 economy.

The feasibility of the hydrogen economy is based on the research and development results of H_2 production, storage, transportation, and conversion to achieve a sustainable energy economy for various applications in the foreseeable future. Renewable energy sources (such as wind, water, solar and tidal energy) can be used to generate H_2 from water through electrolysis, thereby realizing a sustainable system without any pollution[5]. In the production process of H_2, the electricity cost of the

electrochemical water splitting process is one of the main obstacles to the sustainable energy system and economy.

1.2 Hydrogen utilization and production

1.2.1 Present status of utilization and demand of H_2

Hydrogen is an efficient, clean and expected energy vector, which has a very wide range of applications. It can be used in many systems and technologies, such as refining crude oil, producing ammonia and methanol, surface treatment in metallurgical processes, and other chemical uses[6,7]. Hydrogen holds the key to global energy composition. According to the International Energy Agency report, the global hydrogen production is approximately 73 million tonnes per year in its pure form[8]. Table 1-1 exhibits the current use of H_2 manufacturing worldwide[8]. It is mainly used to produce ammonia and fertilizers, followed by oil refining, then it is used to produce methanol and various applications like transport. It's also employed in thermal processing, metal manufacturing, polysilicon and semiconductor production, metal preparation, chemical tracing, glass production and crystal growth[9,10]. In energy, global total annual hydrogen demand is approximately 330 million tons of oil equivalent (Mtoe), exceeding Germany's primary energy supply[8]. In the past decade, the world's H_2 demand has experienced significant growth. Not only that, hydrogen has long-term application prospects in many fields[11]. It is estimated that by 2050, the power fields, construction and transportation are all promising for applying hydrogen[12].

Table 1-1 World hydrogen consumption by different uses.

Hydrogen uses	Consumption	Percentage
Ammonia production	250	50
Petrochemistry	185	37
Production of other chemical products	65	13

Compared with methane and gasoline, hydrogen has outstanding properties. Down the road, hydrogen may be employed as a fuel in nearly all applications that fossil fuels are applied at present. It is expected that the new growth will mainly come from the low-sulfur fuels refining, oil refining, new energy vehicles and clean energy power generation. For instance, fuel cells are an emerging technique involving turbine use. This is a promising avenue for portable energy equipment, domestic power generation and transportation[13]. The share of hydrogen in the energy market has increased as fuel cell systems are implemented and the need for zero-emission fuels

rises. It's estimated that by 2040, hydrogen used in fuel cell vehicles can replace 18.3 million barrels of oil per day. So far, many studies on the reform procedure of CH_4 have given priority to the production of hydrogen for fuel cells[14].

1.2.2 Global manufacture of H_2 production

The emerging H_2 energy economy and fast-growing demand put forward new requirements for H_2 production capacity. The earliest commercial technology can be traced back to the late 1920s when electrolyzing water to produce pure hydrogen. In the 1960s, the industrial production of hydrogen gradually shifted to fossil-based raw materials, which is the main source of hydrogen production today[15]. At present, the industrial-scale global H_2 production is almost produced by steam reforming hydrocarbon resources, such as steam reforming of natural gas, partial oxidation of methane, auto thermal reforming and hydrocarbon pyrolysis[16,17]. As shown in Figure 1-1, at present, approximately 70 million metric tons of hydrogen are produced globally each year, of which about 98% of the hydrogen is still derived from carbonaceous raw materials, with 76% produced from natural gas via steam reforming of methane, 22% through coal gasification (primarily in China). A small part (2%) comes from using electrolysis[18]. The current H_2 manufacturing route still strongly relies on conventional fossil fuel resources. So far, the development and utilization of fossil fuels has caused a series of social and environmental problems. People have realized the seriousness of the non-renewability of fossil fuels and the damage to the environment, which urgently needs a renewable energy to meet the requirements of the new era.

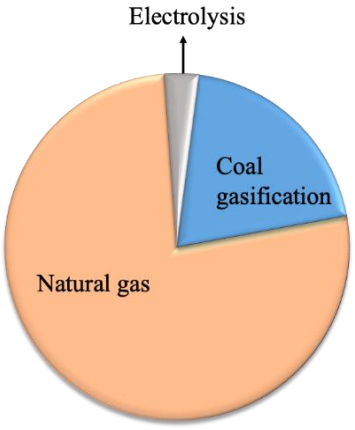

Figure 1-1 Feedstock used in the present global hydrogen production [18].

Water splitting is another approach of producing hydrogen. The electrolysis, thermolysis, and photo-electrolysis techniques is the most promising method[19].

However, the main disadvantage of water electrolysis is that it requires a lot of electricity. Researchers are working to improve efficiency and reduce electricity consumption. From the perspective of environmental benefits, future energy security and sustainable energy development strategies, the conversion of hydrogen from other renewable resources is proposed as another ideal way. For example, it can be used for direct conversion of solar electrolysis photovoltaic power generation, wind energy and biomass production[20]. Among them, the production of H_2 from biomass or biomass-derived materials is of great significance.

1.3 H_2 production from biomass

Biomass is a very important renewable energy source that widely exists in nature, mainly in the form of wood, plants, agriculture crop residues, municipal wastes, etc[21]. Biomass can be largely generated by the photosynthesis reaction in plants, with the advantages of renewability, availability, diversity, and ease of transportation (solid or liquid). It is estimated that the biomass energy stored in plants each year is about 10 times equivalent to the global major fuel consumption, but its utilization as energy remains less than 1% of the total[22].

Biomass is the fourth largest energy source in the world. It accounts for 15% of the world's primary energy consumption[23]. In developing countries such as India, China, and Brazil, it accounts for about 38% of the primary energy consumption. It is estimated that by 2050, the biomass energy production in the United States will reach 5.39 quadrillion British thermal units[24]. Under this circumstance, biomass has great potential to accelerate the realization and use of H_2 as the main fuel in the future. It will also play an important role in meeting global hydrogen demand.

There are two types of biomass feedstocks that can be used to produce hydrogen, one is specific bioenergy crops, and the other is cheaper biomass residues, such as organic waste from conventional agricultural processing. The production of hydrogen from biomass mainly includes thermochemical methods and biological methods. The thermochemical methods are further subdivided into gasification methods, pyrolysis methods, hydrolysis-sugar, and other chemical conversion methods[25],[26,27]. Biological methods can be subdivided into anaerobic digestion, photo fermentation, dark fermentation (sugar conversion), and indirect photolysis, direct photolysis (light conversion)[28,29,30]. In the process of using biomass as a raw material in thermochemical methods, CO_2 is produced as a by-product, but the growing plants can fix it to produce new biomass during photosynthesis. Compared with fossil fuels, the net impact of CO_2

is smaller in thermochemical methods. The gasification method has advantage of simple and obtaining the product directly, but the hydrogen content of lignocellulosic biomass is lower, resulting in a lower H_2 yield in the direct route[31].

Hydrogen production from biomass is an energy-saving, environmentally friendly, and resource-rich process. However, there are still some problems such as high production costs, imperfect supporting facilities, and an incomplete industrial chain. For thermochemical conversion, some technical barriers need to be removed, including the effect of variable feedstock composition on downstream processing, efficient and durable catalysts for gas conditioning, and effective heat integration. Solving these problems requires the joint efforts of all industries[32].

1.4 Biogas production and utilization

Biogas is one of the important renewable biofuel carriers produced by the anaerobic digestion of biomass raw materials. Biogas consists of major CH_4 and CO_2 along with various impurities at very low concentration levels (such as H_2, O_2, N_2, H_2O, H_2S, siloxanes, chlorides, and volatile organic compounds)[33, 34]. Table 1-2 summarizes the chemical composition of biogas, but it may be related to the starting substrate. The biomass used to make biogas comes from different sources such as sewage, sludge, landfill, or industry[35].

Table 1-2 Chemical composition of biogas[36].

Composite	Percentage
CH_4	35-65 (vol%)
CO_2	15-50 (vol%)
H_2S	0-100 (ppm)
NH_3	~5 (ppm)
H_2	0-3 (vol%)
N_2	5-40 (vol%)
O_2	0-5 (vol%)
H_2O	<1 (vol%)

Biogas can be used as energy in two different ways. The first way is to directly heat or use CH_4 in the biogas to generate electricity or use it as an urban gas source for cooking or heating. However, due to the relatively high CO_2 content, the direct use of biogas has two main disadvantages, which not only reduces the calorific value of biogas but also leads to greater carbon dioxide emissions into the atmosphere[37]. The second type of biogas utilization is to convert it to other energy sources, such as syngas or H_2 which is used to synthesize other liquid fuels. Every organic substance can be

degraded to produce biogas, which has clean and renewable reforming properties and can be used in the reforming process[38].

In recent years, the biogas reforming process has increased the utilization of CO_2 and CH_4, reduced the emissions of two greenhouse gases, and converted these greenhouse gases into high-value chemicals, which has attracted more and more attention. In various reforming processes, biogas with appropriate composition can be used as a methane source. Therefore, most of the research on methane reforming can also be applied to biogas reforming[39]. In addition, more and more researches are focusing on the use of different strategies (such as solar energy and plasma) for biogas reforming[40,41]. More and more researchers have also studied the impact of the main impurities (i.e., H_2S) on the biogas reforming process[42].

1.5 H_2 production from catalytic reforming of methane

As mentioned above, the reforming of biogas has the same principle as the reforming of methane, and the reforming of methane has been extensively studied worldwide. There are two strategies for methane conversion, called the indirect method and the direct method. The direct method is to convert methane into methanol, formaldehyde, ethylene, aromatics, or acetic acid[43]. The indirect method is to convert methane to syngas. Among them, the most commonly used method is steam reforming of methane. In the current research, there are three mainstream reactions to convert methane to hydrogen, namely dry reforming of methane (DRM), partial oxidation of methane (POM), and oxidative dry reforming of methane (ODRM). In addition, combining the above two or three reforming processes, many new concepts have been proposed, such as double or triple reforming of methane.

1.5.1 H_2 production from steam reforming of methane

Steam reforming technology is the oldest route to convert methane into hydrogen, it is also the cost-effective method and commonly adopted route for H_2 production. It involves two major reactions:

$$CH_4 + H_2O \rightleftharpoons CO + 3H_2 \quad \Delta H^0_{298K} = 206.2\ \text{kJ/mol} \quad (1\text{-}1)$$

$$CO + H_2O \rightleftharpoons CO_2 + H_2 \quad \Delta H^0_{298K} = -41.2\ \text{kJ/mol} \quad (1\text{-}2)$$

Due to the high endothermic nature of the reaction (Eq. (1-1)), the industrial steam reforming reaction is conducted at high temperatures (800-1100 °C), which is a process of energy consumption[44]. The required heat is usually provided by burning a portion of natural gas. The nickel-based catalysts are widely used due to their low cost

and high conversion efficiency in steam reforming reactions[45]. However, the high operating temperature also caused some other problems, including metal sintering, methane cracking side reaction, coking deposition, which in turn reduced the activity of the catalyst[46]. Usually, excessive steam is added during the reaction to reduce the coke formation. The steam to methane ratio generally used is 2.5-3.0[47]. The high steam to methane ratio promotes the water gas shift (WGS) reaction (Eq. (1-2)) which results in greater hydrogen yield, but also a net CO_2 production. Steam reforming is a mature technology, and continuous improvement of the process has reduced plant costs, including catalysts that resist coke production and avoid sulfur poisoning and developing materials for furnace tubes[48].

In the recent work of Chen et al., CO_2 sorption enhancement was used to optimize the steam methane reforming reaction[49]. The $Ni/Al_2O_3/CaO$ catalysts were prepared by a physical mixing method. The catalytic performance of the SMR reaction was optimized by in situ CO_2 sorption and adjusting the operating conditions, such as the molar ratio of steam to CH_4, space velocity, and temperature. In their study, the sorption-enhanced steam methane reforming reaction produced high-quality H_2 product streams (98.9%) under the conditions of WHSV =2609 $cm^3/g{\cdot}h$, steam to methane ratio = 4, at 550 °C.

The catalytic performance of a highly mesoporous $Ni/MgAl_2O_4$ spinel catalyst was presented in the study of Kim et al[50]. The catalyst showed a CH_4 conversion efficiency of 82.0% at the stream time of 480 min with GHSV of 40 000 mL/g·h at 800 °C. The catalyst showed high CH_4 conversion efficiency, high durability, and excellent resistance to carbon deposition. That was because annealing the catalyst in an N_2 atmosphere increased the specific surface area and mesoporosity, improved the dispersion of nickel nanoparticles in the support, and promoted the interaction between the active phase and the support.

1.5.2 H_2 production from partial oxidation of methane

SRM is an endothermic reaction operated at a temperature above 800 °C, which results in large energy consumption and high cost. Alternatively, partial oxidation of methane (POM) to syngas is a potentially efficient method to reduce energy consumption (Eqs. (1-3) and (1-4)).

$$CH_4 + \frac{1}{2}O_2 \rightleftharpoons CO + 2H_2 \quad \Delta H^0_{298K} = -35.5\ \text{kJ/mol} \quad (1\text{-}3)$$

$$CH_4 + O_2 \rightleftharpoons CO_2 + 2H_2 \quad \Delta H^0_{298K} = -322\ \text{kJ/mol} \quad (1\text{-}4)$$

Partial oxidation of methane operated at low temperatures has the advantages of low energy consumption and high safety. The partial oxidation of methane into synthesis gas is suitable for the production of downstream chemical products, especially methanol and Fischer-Tropsch synthesis products[51,52]. It has a high methane conversion rate, and high selectivity to carbon monoxide.

It is estimated that a total of 6.92 billion cubic meters of coalbed methane has been discovered[53]. It is very exciting to make full use of CH_4 and O_2 in low-concentration coalbed methane to realize the utilization of resources in the coalbed. Catalytic partial oxidation of methane may be an attractive method to convert natural gas into synthesis gas[54].

Generally, noble metals such as Pd[55], Pt[56], Rh[57] and Ru[58] are used as active sites in catalysts for POM reactions and exhibit good catalytic activity. In the past two decades, research on POM has mainly focused on Ni, Co, Pt, and Rh. However, the rapid exothermic reaction sinters the active components, collapses the catalyst structure and deactivates the catalyst. In order to reduce costs, researchers focus on using non-noble metal catalysts, implement different synthesis strategies, develop thermally stable catalysts, and reduce the degree of catalyst sintering[59].

Guo et al. synthesized Pt@ZSM-5 samples with different sodium ion content for the partial oxidation (POM) reaction of methane [53]. The introduction of Na^+ into the zeolite promoted the combination of Pt and hydroxyl groups and produced a large amount of Pt-$O_x(OH)_y$Na active species. The introduced sodium ions also improved the dispersion and stability of Pt atoms and inhibited the catalyst sintering. 1 wt% Na-Pt @ ZSM-5 showed the highest catalytic performance, the conversion rate of methane was 75%, and the ratio of hydrogen to carbon monoxide was 2.3.

Li et al. added Re to the Ru/Al_2O_3 catalyst to prepare a bimetallic catalyst and used it for the POM reaction[60]. Compared with single metal Ru or Re catalysts, this catalyst showed greater activity. Under the reaction conditions of O_2/CH_4 ratio of 0.5, SV = 60000 mL/g·h and 600 °C, the yields of CO and H_2 were increased to 54% and 61%, respectively. They also found that the addition of Re changed the reaction mechanism. It was reported that the main role of Ru was to reduce Re species. The reduced Re species generated formic acid from CH_4 and accelerated the steam reforming reaction. The dual role of Re increased the overall catalytic performance.

1.5.3 H_2 production from dry reforming of methane

Over the past few decades, a large amount of carbon dioxide has been emitted into the atmosphere, causing global warming, melting glaciers, and rising sea levels. Therefore, reducing the amount of carbon dioxide in the atmosphere has caused extensive scientific research on carbon capture, utilization, and storage (CCUS) and its conversion into other valuable chemical resources[61]. Dry reforming of methane not only utilizes CO_2 and CH_4 to reduce greenhouse gas emissions but also produces industrially important syngas, which has received a lot of attention and research. Syngas can be converted into synthetic diesel and gasoline through the Fischer-Tropsch (FT) process[62]. It can also be used for solid oxide fuel cell power generation, methanol production, and dimethyl ether synthesis[63,64,65].

Compared with steam reforming of methane, the dry reforming reaction requires relatively higher thermal energy[66]. It means DRM reaction occurs under high-temperature conditions. However, high temperature promotes two side reactions methane cracking as well as the disproportionation of CO reactions, leading to a coke formation[67]. High temperature also causes the sintering of active components of the catalyst. Although DRM has obvious economic and environmental benefits, it is not regarded as an industrially mature process.

Research on the DRM catalyst must be continued and intensified. Various types of catalysts that have been widely studied for DRM include noble metals, transition metals, supported catalysts, spinels, perovskites, and mesoporous catalysts[68]. In addition, research on the thermodynamics, kinetics, mechanisms, and reactors of DRM has also been reported[69]. The utilization of cheap and stable DRM catalysts with good catalytic performance has been the focal point of research and development in recent times.

DRM conversions of CO_2 and CH_4 to reduce greenhouse gases emissions is of scientific and industrial importance. At the same time, it is expected that the production of chemicals and/or the synthesis of H_2 as a clean fuel or liquid fuels will have a huge demand for syngas in the future. Therefore, it is necessary to develop more efficient and stable catalysts to solve the problems of sintering and carbon deposition, to make the DRM process mature and realize commercialization[70].

1.5.4 H_2 production from oxidative dry reforming of methane

As said before, dry reforming of methane eliminates the emissions of the two greenhouse gases are eliminated by the dry reforming of methane, resulting in the production of syngas. However, the syngas produced by this method has an H_2/CO ratio

of 1, which cannot be directly applied by downstream industries, such as methanol synthesis. Another disadvantage is that it is highly endothermic, and the catalyst is deactivated by carbon deposition. The solution is to add oxygen during the dry reforming of methane process[71,72]. In the 1990s, Ashcroft and Vernon simultaneously demonstrated the feasibility and advantages of dry reforming and partial oxidation of methane to achieve a neutral reaction[73,74]. So far, the concept of adding oxygen to dry reforming has become an attractive research field, and it is often mentioned[75].

Oxidative dry reforming (Eq. 1-5), changing the oxygen concentration, provides the flexibility to adjust the ratio of hydrogen to carbon monoxide (to a certain extent). Compared with the synthetic gas produced by traditional dry reforming, this method is more effective. As a result, downstream industrial applications are more practical[76].

$$3CH_4 + CO_2 + O_2 \rightleftharpoons 4CO + 6H_2 \quad \Delta H^0_{298K} = 58\ \text{kJ/mol} \quad (1\text{-}5)$$

The syngas produced by the combined process with the ratio of hydrogen to carbon monoxide close to 2[77]. Compared with the partial oxidation of methane alone, a small amount of oxygen is added to the feed, and the ratio of oxygen to methane is usually 0.1 -0.5. Thus, large temperature gradients and hot spots in the catalytic bed can be avoided.

The partial oxidation reaction of methane is a mild exothermic process (Eq. (1-3)), which is dangerous because it is self-explanatory in large reactors due to the existence of hot spots and operational difficulties. In recent years, the combination of partial oxidation of methane and carbon dioxide in the alternative circuit for converting natural gas to synthetic gas has attracted the interest of researchers. This process has low energy requirements because of the opposite contribution of the exothermic oxidation of methane and the endothermic reforming of carbon dioxide. The oxygen in the feed has the advantage of preventing the catalyst from losing activity due to carbon. At the same time, the fluidized bed reaction is recommended to efficiently perform the combined response because of its high heat transfer rate and high operational stability. In addition, the pure nickel catalyst prepared by traditional impregnation is rapidly deactivated in the combined oxygen-CO_2 reforming of methane in a fluidized bed reactor[78].

The optimal oxidative dry reforming conditions were proposed to be 550 °C, O_2/CH_4 = 0.47, and CO_2/CH_4 = 0.76, which allowed for an H_2/CO ratio of 1.5 with consumption of both greenhouse gases[79]. At these conditions, the coke-free operation

was achieved with the stable operation for 90 h. STEM analyse suggested negligible coke deposition on a spent 3.4 wt% Ni/$MgAl_2O_4$ catalyst after 90 h on stream.

Wang et al. synthesized Fe-modified Ni-based catalysts by using a microwave-assisted method. A series of xFe-Ni/LDO catalysts were used in DRM and ODRM tests. The results indicated that the addition of oxygen increased CH_4 conversion and decreased coke deposits. Loading a small amount of Fe increased the specific surface area of the catalyst, reduced the Ni particle size, and promoted the formation of Fe-Ni alloys, thereby improving the catalytic activity, stability, and H_2/CO ratio. At 750 °C, $CO_2/CH_4/O_2/N_2$ being 1:1:0.1:1.9, after 80 hours, the methane conversion was of 69%, the carbon dioxide conversion was of 71%, and the ratio of hydrogen to carbon monoxide remained at 0.93[80].

1.5.5 H_2 production from other reforming processes of methane

In addition to the above methods, auto thermal reforming, double reforming, oxidative double reforming, and triple reforming have been also reported in the literature, which can produce H_2 from methane[81]. All processes require the participation of oxidizing agent which oxidizes methane to carbon monoxide. The proportion of hydrogen in the product depends on the oxidant used.

Autothermal reforming is the combination of the reforming and partial oxidation reforming, where steam reforming of hydrocarbons is carried out in the presence of oxygen[82]. By adjusting an appropriate ratio of hydrocarbon: oxygen: steam, the condition of reaction can be selected as exothermic, endothermic, and thermo-neutral conditions[83].

Matus's group prepared a series of 10Ni-M/$Ce_{0.5}Zr_{0.5}O_2/Al_2O_3$ catalysts with a variety of types of metal (Pt, Pd, Re, Mo, Sn) and content. Among them, 10Ni-0.9Re/$Ce_{0.5}Zr_{0.5}O_2/Al_2O_3$ had the best catalytic activity, and the H_2 yield was of 70%, at 850 °C. The designed catalyst had enhanced stability against oxidation and sintering of Ni active component as well as high resistance to coking[84].

The triple reforming of methane combines the SRM, POM, and DRM in a single reactor. Compared to each reaction, triple reforming of methane reduced the amounts of carbon deposits and extended the catalyst stability. In addition, the exothermic reaction of oxygen could improve the energy efficiency of the process. It was also possible by adjusting the triple reforming feed composition to change the H_2/CO ratio to achieve the specifications required for downstream applications[85].

The catalytic performance of a nickel supported on $MgAl_2O_4$ spinel, promoted with $CeZrO_2$ catalysts was presented in the study of Lino et al[86]. An investigation of the effect of O_2/CO_2 ratio and H_2O/CO_2 ratio showed that increasing the supply of oxygen was more effective for reducing coke formation compared to increasing the amount of water. With the O_2/CO_2 ratio equal to 0.17, at 750 °C, the catalyst showed CH_4 and CO_2 conversions of 80% and 60%, respectively, H_2/CO ratio of 1.75, and carbon deposition of 2 mgC/g.

1.6 Dry reforming of methane

Dry reforming of methane uses two greenhouse gases, CO_2 and CH_4, as reactants, reducing greenhouse gas emissions and producing synthesis gas, which can be used in the industrial synthesis. In a typical dry reforming of methane system, the ratio of hydrogen to carbon monoxide in syngas is 1, which is lower than that obtained on steam reforming (H_2/ CO = 3) or partial oxidation (H_2/ CO = 2)[87].

$$CH_4 + CO_2 \rightleftharpoons 2CO + 2H_2 \quad \Delta H^0_{298K} = 260.5\ kJ/mol \quad (1\text{-}6)$$

1.6.1 Thermodynamics of dry reforming of methane

Dry reforming of methane is an endothermic reaction, which operates at a temperature of 650-850°C. The reaction requires high energy consumption and high cost. At the same time, there are some side reactions that occur at high temperatures, which can lead to the formation of carbon deposits, such as methane decomposition (Equation (1-7)), Boudouard reaction (Eq. (1-8)) that can follow not only DRM but also reverse water-gas shift (RWGS) reaction (Eq. (1-9))[88,89], CO and CO_2 hydrogenation reactions (Eqs. (1-10), (1-11)), and/or polymerization reactions after C2 products formation (Eqs. (1-12), (1-13)).

$$CH_4 \rightleftharpoons C + 2H_2 \quad \Delta H^0_{298K} = 75.0\ kJ/mol \quad (1\text{-}7)$$

$$2CO \rightleftharpoons C + CO_2 \quad \Delta H^0_{298K} = -173.0\ kJ/mol \quad (1\text{-}8)$$

$$CO_2 + H_2 \rightleftharpoons CO + H_2O \quad \Delta H^0_{298K} = 41.0\ kJ/mol \quad (1\text{-}9)$$

$$CO_2 + 2H_2 \rightleftharpoons C + 2H_2O \quad \Delta H^0_{298K} = -90\ kJ/mol \quad (1\text{-}10)$$

$$CO + H_2 \rightleftharpoons C + H_2O \quad \Delta H^0_{298K} = -131.3\ kJ/mol \quad (1\text{-}11)$$

$$2CH_4 + CO_2 \rightleftharpoons C_2H_6 + CO + H_2O \quad \Delta H^0_{298K} = 106\ kJ/mol \quad (1\text{-}12)$$

$$2CH_4 + 2CO_2 \rightleftharpoons C_2H_4 + CO + H2O \quad \Delta H^0_{298K} = 294\ kJ/mol \quad (1\text{-}13)$$

Nikoo and Amin[90] identified that methane decomposition (Eq. (1-7)), carbon monoxide disproportionation (i. e. Boudouard reaction) (Eq. (1-8)), hydrogenation of carbon dioxide (Eq. (1-10)), and hydrogenation of carbon monoxide (Eq. (1-11)) are

the four side reactions that cause carbon deposition during DRM. The methane decomposition reaction is promoted at high temperature, while the other three are suppressed at high temperature at 800 K. Moreover, the reverse water-gas shift (RWGS) reaction (Eq. (1-9)) tends to cause the H_2/CO ratio to be less than 1, depending on the equilibrium within a specific temperature range and usually occurs during DRM.

1.6.2 Mechanism of dry reforming of methane

In the literature, two possible mechanisms of dry reforming of methane have been reported, namely monofunctional and bifunctional mechanism. In the monofunctional mechanism, both the activation of carbon dioxide and the dissociation of methane occur on the active sites of nickel. In the bifunctional mechanism, the activation of carbon dioxide occurs on the support, and the dissociation of methane occurs on the active site of nickel[91]. Among them, the bifunctional mechanism is widely accepted[92].

The dissociation of methane on the catalyst is generally considered to be a rate determining step. Each partially dissociated CH_x species adsorbs preferentially on a site which completes its tetravalency, with CH_3 adsorbing on top of metal atoms while CH_2 adsorbs between two metal atoms (bridged adsorption)[66, 93]. The adsorption and dissociation of CO_2 is also affected by surface structure and defects in C-only coordination, C and O coordination or O-only coordination, with both oxygen atoms bonding with the surface metal.

The latter two coordination geometries are more favorable towards dry reforming. This step is generally considered fast. CO_2 tends to adsorb on the metal-support interface[94]. It is known that the water-gas shift reaction is at quasi-equilibrium, meaning that the surface reactions that are related to it are quite fast. Most developed models predict hydrogen migration from the active metal particle to the support where it forms hydroxyl groups at temperatures below 800 °C. Surface oxygen on the metal particle reacts with S-CH_x groups to form S-CH_xO or S-CO. Some authors consider the S-CH_xO groups to be precursors to CO formation while others assert that adsorbed CO_2 forms carbonates that are reduced to CO by carbon on the metal[95]. Other authors claim that S-CO is formed directly without a formate S-CH_xO intermediate[96].

Just as for steam reforming, there is no clear consensus about the details of the reaction mechanism on the surface of the catalyst, and the impact of the catalyst nature and operating conditions is also very important. However, in many cases, the formation and/or decomposition of formates S-CH_xO to CO and hydrogen is considered the rate determining step, especially knowing that the desorption of CO and hydrogen is fast[97].

The monofunctional mechanism is generally considered to occur in the reaction of a catalyst whose support is a relatively inert material like SiO_2[98]. The methane and CO_2 are both activated on metal active site. On an acidic support, CO_2 is activated by formation of formates with the surface hydroxyls. On basic supports, CO_2 is activated by forming oxy-carbonates[99]. However, on an inert support, the catalyst will be deactivated due to the formation of carbon by the dehydrogenation of methane, and the activation of CO_2 and the reaction with carbon are limited[70]. Therefore, catalysts based on inert supports (such as SiO_2) have relatively weaker metal-support interactions and lower stability and activity than weakly acidic (Al_2O_3) or basic (La_2O_3, CeO_2) supports[100,101].

1.6.3 Influence of CO_2 and CH_4 concentrations

Biogas reforming is essentially carbon dioxide reforming of methane or dry reforming of methane. Nevertheless, biogas essentially consists of CH_4 (55-65 vol.%) and CO_2 (30-45 vol.%), and other compounds as reported previously in part 1.3[36,102]. The CO_2 to CH_4 ratio in biogas can vary between 0.45 - 0.8 which is related to the starting substrate[103]. The landfill waste can generate biogas with a CH_4 content of around 40% and CO_2 content of around 40%, agricultural waste can generate biogas containing 70% of CH_4, and 30% of CO_2 [104], the swine farm biogas has 60 % of CH_4 and 40 % CO_2[105]. Therefore, the CO_2 and CH_4 concentrations in the dry reforming reaction should be studied to ensure that the catalyst remains active during the biogas reforming process.

Following the reaction stoichiometry (Eq. (1-6)), the feedstock of CH_4 is equal with CO_2 in DRM reaction. However, in biogas CO_2 concentration is usually lower than CH_4 concentration. Therefore, the CO_2 to CH_4 ratio is an important factor affecting the conversion and the H_2/CO ratio. Many studies on CO_2 and CH_4 concentrations have been reported[103,104].

When the CO_2 concentration was increased, (CO_2/CH_4 ratio higher than unity), led to an increase in methane conversion[106]. However, the CO_2 conversion rate was reduced due to the excess CO_2 in the reaction gas. The CO_2 conversion rate was higher than the equilibrium conversion rate, which could be the result of the participation of RWGS, confirmed by the detection of large amounts of water and CO and the low H_2/CO ratio. The RWGS reaction consumed more H_2, so the selectivity of H_2 was decreased[107]. Moreover, more CO_2 can reduce the deposited carbon through the reverse Boudouard reaction. Excessive H_2O also inhibits carbon deposition by

promoting the gasification of carbon, thereby inhibiting catalyst deactivation. Jin et al. found similar phenomena over Ni/LDO-0.1 catalyst at 700 °C, which indicated that high concentrations of CO_2 could promote the conversion of methane into syngas. When CO_2/CH_4 ratio was 1.4, 93% CH_4 and 75% CO_2 were converted to syngas at the reaction of 28 h[106].

When the concentration of methane was increased in the reactant, the CO_2/CH_4 ratio was lower than 1, the methane conversion decreased, the selectivity of hydrogen was increased, and the H_2/CO ratio was increased[108]. Furthermore, a high concentration of methane promoted methane decomposition, resulting in excessive carbon deposits, reactor blockage in a short time, and reaction unstable. Similar results were reported in the experiment of Yasyerli et al. Catalytic tests were conducted with 1.0Ru@Ni-MCM-41 catalyst using different feed compositions at 600 °C[108]. When the CO_2/CH_4 ratio was less than one, the test stopped at 150 minutes, because of coking and the reaction tube blocked. Lotina et al. studied the effect of the CO_2/CH_4 ratios on the catalytic performance of Ni-based catalyst obtained after calcination of a hydrotalcite-like precursor[109]. CO_2/CH_4 ratios between 0.4 and 1.5 were evaluated. A CO_2/CH_4 ratio between 1 and 0.7 seemed to be the most appropriate to achieve the best CH_4 conversion and H_2 selectivity.

1.7 Catalysts of dry reforming of methane

DRM catalysts have been studied for a long time, Pakhare and Spivey comprehensively reviewed noble metal catalysts, and Seo[110], Li and Gong[111] reviewed strategies to improve the performance and stability of nickel-based catalysts. Other aspects of dry reformation have also been reviewed by Abdulrasheed[112], and Gao et al[113]. Therefore, the latest literature on the synthesis of nickel-based catalysts with parameters related to or similar to this research will be concentrated in this work.

Some catalysts and their DRM performance using CO_2/CH_4 ratio of 1 are summarized in Table 1-3. Dama et al. synthesized $CaZr_{0.8}Ni_{0.2}O_{3-\delta}$ catalysts by conventional citrate gel method for the dry reforming test[114]. The experiments were performed at the temperature of 800 °C with $CH_4/CO_2/N_2$ feed ratios of 1:1:1, 0.6 g catalyst, and space velocity of 28800 h^{-1}. The methane and carbon dioxide conversions remained at 95% and 96%, respectively, after 500 hours.

There are also some researches focusing on low temperature reaction using CO_2/CH_4 ratio of 1, summarized in Table 1-4. As an example, Li et al. used Ni/CeO_2 as catalyst in the dry reforming of methane[115]. The sample was obtained by wetness

impregnation method. The catalytic performance was measured at 500 °C with GHSV = 48000 h^{-1}. The conversions of methane and CO_2 were 30% and 42%, respectively, and elevated reduction temperature promoted migration of ceria from reduced support onto Ni surface, inducing decoration/encapsulation of Ni nanoparticles.

Other studies on various catalysts and their DRM performances using different CO_2/CH_4 ratios, are summarized in Table 1-5. Akbari et al. tested Ni-MgO-Al_2O_3 catalysts for DRM and the effect of feed ratio was examined. The results showed that the increase in CO_2/CH_4 molar ratio from 0.5 to 3.0 increased the methane conversion and decreased the carbon dioxide conversion. With the CO_2/CH_4 ratio of 0.5, the CH_4 and CO_2 conversions were about 58 % and 89 %, respectively, with a H_2/CO ratio of 1.45, on 12.5 wt.% Ni-MgO-Al_2O_3 catalyst at 700 °C and GHSV = 18000 ml/($h \cdot g_{cat}$). With the CO_2/CH_4 ratio of 2, the CH_4 and CO_2 conversions were about 91 % and 63 %, respectively, and H_2/CO ratio of 0.75, in the same conditions[116]. Han et al. intensively studied the CH_4 and CO_2 conversion rates and the syngas yield for different ratios of CO_2/CH_4 (0.5, 1, and 2). The simulation results showed that the optimum CO_2/CH_4 ratio was of 0.5. Under this condition, the CH_4 conversion rate was close to 92 %, and the CO_2 conversion rate was close to 85 %, the H_2/CO ratio of 1.6, at 800 °C on 3wt% Ni/Ce-MgO-ZrO_2/Al_2O_3 catalyst[117].

Table 1-3 Recent catalyst development for DRM at high temperature.

Catalyst	Preparation method	Reaction temperature (°C)	Conv. of CH_4 (%)	Conv. of CO_2 (%)	H_2/CO (molar ratio)	Stability	Operation condition	Ref.
HNiZr3	Coprecipitition	750	86	90	0.88	5h	GHSV=20000 / h 100mL/min $CO_2/CH_4/Ar$=1:1:8	118
$La_2Zr_{2-x}Ni_xO_{7-\delta}$	modified citrate method	700	77	82	0.79	360h	WHSV=30000mL/g*h 100mg $CO_2/CH_4/He$=1:1:3	119
$Fe_{0.012}Ni_{0.058}Mg_{0.93}O$-R	Hydrothermal	760	40	50	0.6	100h	GHSV=86000mL/g*h 50mg 50mL/min CO_2/CH_4=1:1	120
NSZ	Impregnation method	800	90	92	1.0	5h	GHSV=24000mL/g*h 400mg CO_2/CH_4=1:1	121
NiMA-BN-M-R	Impregnation method	750	82	95	1.1	100h	120mg 50mL/min CO_2/CH_4=1:1	122
Ni/d-BN	Impregnation method	750	86	92	1.06	125h	WHSV=25000mL/g*h 120mg 50mL/min CO_2/CH_4=1:1	114
$CaZr_{0.8}Ni_{0.2}O_{3-\delta}$	conventional citrate gel method	800	95	96	1.0	500h	GHSV=28800 /h 600mg 240mL/min $CO_2/CH_4/N_2$=1:1:1	123

Catalyst	Preparation method	Reaction temperature (°C)	Conv. of CH_4 (%)	Conv. of CO_2 (%)	H_2/CO (molar ratio)	Stability	Operation condition	Ref.
5%Ni/SiO_2	Wetness impregnation	700	82	87	/	19h	GHSV=1440 L/g*h 120mL/min $CO_2/CH_4:N_2$=1:1:3	124
10NiOMgO-PACS	Cellulose Paper Assisted SCS (PACS) method	700	78	93	/	25.5h	GHSV=72000 mL/g*h 100mg 120mL/min $CO_2/CH_4:N_2$=1:1:3	125
SiO_2@Ni@ZrO_2	Wetness impregnation	700	56	50	0.69	150h	WHSV=24000 mL/g*h 75mg 30mL/min	126
Fe/Zr@Zr-Ni@Zr	impregnation and nanocoating	750	67	/	/	10h	100mg 200NmL/min CO_2/CH_4/Ar=1:1:0.4	127
$(NiMg)_4Al$		800	80	/	/	40h	WHSV=240 L /h*g 5mg $CO_2/CH_4/N_2$=1:1:8	128
3NZH	Deposition-precipitation method	700	50	57	0.85	5h	GHSV=24000 mL/g*h 400mg CO_2/CH_4 =1:1	129

Catalyst	Preparation method	Reaction temperature (°C)	Conv. of CH_4 (%)	Conv. of CO_2 (%)	H_2/CO (molar ratio)	Stability	Operation condition	Ref.
Ni/ Al-modifiedSBA-15-EG	Impregnate method	700	72	78	0.97	20h	WHSV=18000mL/g*h 100mg 30mL/min CO_2/CH_4 =1:1	130
$La(Co_{0.1}Ni_{0.9})_{0.5}Fe_{0.5}O_3$	solgel self-combustion method	750	70	80	0.88	30h	GHSV=12000 mL/g*h 300mg 60mL/min CO_2/CH_4 =1:1	131
2.5Ni/NS/Zr	Wet Impregnation	800	45	58	0.79	20h	GHSV=240L/g*h 25mg 100mL/min CO_2/CH_4 =1:1	132
Ni@hollow silicate zirconia	hydrothermal posttreatment	800	82	94	0.6	50h	GHSV=54000 mL/g*h $CO_2/CH_4/N_2$=1:1:1	133
Ni-ZrO_2@SiO_2	one-pot method	800	90.5	93.3	1	240 h	50 mg 30mL/min CO_2/CH_4 =1:1	67
Ni-2.5% Ce/W-Zr	Dry impregnation	700	77	83	0.92	100h	GHSV=42 L/g*h 70mL/min $CO_2/CH_4/N_2$=3:3:1	134
Ni/CeO_2-ZrO_2-SiO_2	Incipient wetness impregnation	750	96	97	0.9	20min	500 mg 200mL/min $CO_2/CH_4/N_2$=1:1:38	135

Table 1-4 Recent catalyst development for DRM at low temperature

Catalyst	Preparation method	Reaction temperature (°C)	Conv. of CH_4 (%)	Conv. of CO_2 (%)	H_2/CO (molar ratio)	Stability	Operation condition	Ref.
5%Ni/SiO_2	Wetness impregnation	600	18	35	/	24h	GHSV=1440 L/g·h 120mL/min $CO_2/CH_4/N_2$=1:1:3	124
10NiOMgO-PACS	Cellulose Paper Assisted SCS (PACS) method	600	58	/	0.85	24h	GHSV=72000 mL/g·h 100mg 120mL/min $CO_2/CH_4/N_2$=1:1:3	125
Ni/CeO_2	Wetness impregnation	500	30	42	0.7	10h	GHSV=48000 h^{-1} 30mg CO_2/CH_4=1:1	115
$Ni_{10(TS)}/CaO_{(HT)}$	Hard template (HT) post impregnation	650	55	66	1.05	12h	GHSV=36 L/g·h 100mg $CO_2/CH_4/N_2$=1:1:18	136
Ni-PS@$Ce_{0.95}Zr_{0.05}O_2$	precipitation	600	0.35 mol/ min·g_{Ni}	0.45 mol/ min·g_{Ni}	0.6	20h	WHSV=200 L/g·h CO_2/CH_4=1:1	137
Ni/$MgAl_2O_4$	coprecipitation method	550	31	37	1.0	3h	200 mg 100mL/min $CO_2/CH_4/N_2$=1:1:3	138
0.5Ni/$CeNi_xO_Y$	hydro-hermal treatment	650	57	52	1.06	/	WHSV=72000mL/g·h 50mg 60mL/min $CO_2/CH_4/N_2$=1:1:1	139
HTNi-Zr	Co-precipitation	600	55	55	0.85	/	GHSV=20000 /h 150mg 100 ml/min $CO_2/CH_4/Ar$=1:1:8	140

Table 1-5 Recent catalyst development for DRM using different CO_2/CH_4 ratio

Catalyst	Preparation method	Reaction temperature (°C)	Conv. of CH_4 (%)	Conv. of CO_2 (%)	H_2/CO (molar ratio)	Stability	Operation condition	Ref.
$40LaNi_{0.75}Zr_{0.20}Ce_{0.05}O_3/8MgO\text{-}SiO_2$	Sol-gel method	800	65	92	0.98	6h	100 ml/min 100 mg $CO_2/CH_4/N_2$=2:3:5	103
LNZ10	modified citrate method	700	46	70	/	24h	WHSV=30 L/g·h 100mg CO_2/CH_4=1:1.5	104
Ni-CaO-ZrO_2	Co-precipitation	750	/	/	1.02	50 h	WHSV=48 L/g·h 10mg CO_2/CH_4=0.5:1	107
Ni/LDO-0.1	Treatment with NaOH solution	700	93	75	0.8	28 h	VHSV=48000 mL/g·h 250 mg CO_2/CH_4=1.4:1	106
Ni-based catalyst	Co-precipitation	700	73	92	0.95	2 h	W/F=0.21 g·h/L 250 mg CO_2/CH_4=1.4:1	109
10 wt% Ni/ $Ce_{0.95}Mn_{0.05}O_2$	Co-precipitation	700	34	88	/	2 h	GHSV=12000 mL/h 200mg CO_2/CH_4=0.5:1	141
Ni-MgO-Al_2O_3	Co-precipitation	700	58	89	1.43	/	GHSV=180 L/ g·h 200 mg CO_2/CH_4=0.5:1	116

Catalyst	Preparation method	Reaction temperature (℃)	Conv. of CH_4 (%)	Conv. of CO_2 (%)	H_2/CO (molar ratio)	Stability	Operation condition	Ref.
3wt% Ni/Ce-MgO-ZrO_2/Al_2O_3	impregnation	800	92	85	1.6	/	CO_2/CH_4=0.5:1	117
Ni@S-1	one-pot hydrothermal method	650	25	/	/	100h	WHSV=2×10^4 mL/h·g 50mg CO_2/CH_4:N_2=1:2:1	142
Ni-WC	co-precipitation	800	58	85	0.8	20h	50 mL/min CO_2/CH_4/N_2=32:48:20	143

1.7.1 Active components

Catalysts derived from noble metal precursors such as Ir, Pd, Pt, Rh, and Ru can exhibit higher activity, selectivity, and stability[144]. However, their feasibility in large-scale industrial applications is not economical, mainly due to their high cost and scarcity[112]. Recently, Rh catalyst has attracted significant interest due to its good performance in methane reforming by steam, oxygen, double, and triple reforming methods[145].

$Ru_{0.035}Ni_{0.035}Mg_{0.093}O$-DR catalyst prepared by solvothermal method, presented a CH_4 and CO_2 conversion of 82% and 88 %, and H_2/CO ratio of 0.85, at 760 °C after 100 h[146]. the GHSV was 86000 mL/g*h, 35 mg of catalyst, total flow rate was 50 mL/min, CO_2:CH_4 =1:1.

Yentekakis and co-workers studied Rh catalysts on metal oxide supports for DRM reaction[145]. 50 mg of 1wt%Rh/Al_2O_3 catalyst showed CH_4 conversion of 80%, CO_2 conversion of 90%, and H_2/CO ratio of 0.95, at 750 °C, with CO_2/CH_4 ratio of 1, WGHSV=120000 NmL/g·h, after 12 hours. They also found that the principal active metal site is unambiguously identified as Rh. What's more hydrogen preconditioning is not necessary for the activation of Rh-based DRM catalysts, unlike Ni-based catalysts.

Taking into account economic factors, the focus of research has shifted from precious metals to cheap metals, and it is found that nickel-based catalysts and precious metals have similar effects in terms of catalytic activity, and the price is relatively low[118]. In DRM, cheap metals are currently abundant catalysts that can replace precious metals, because catalyst sintering, coke formation and catalyst surface deposition under reforming conditions will accelerate their loss of activity. This is a very big challenge. Therefore, the trade-off between the cost of the catalyst and its activity, selectivity and stability is the main challenge for dry reforming to produce synthesis gas[112].

Ni catalysts are regarded as the most promising DRM catalysts, as well as catalysts for steam reforming, partial oxidation of methane, and triple reforming due to their comparable activity and stability as precious metal catalysts[147,148,149]. Although a lot of work has been done in the past, they are currently facing the problem: the Ni catalyst used shows rapid deactivation caused by carbon deposition and sintering of Ni particles under severe reaction conditions. Until today, nickel catalysts are still a vacancy in industrial applications[150,151].

Dai and co-workers used an impregnation method, nickel nitrate loaded onto attapulgite (ATP) support [152]. They tested catalyst for DRM at 700 °C with GHSV=18000 h^{-1} (CH_4/ CO_2=1:1). The Ni/ATP catalyst possessed high initial activity; CH_4 conversion was of 51% and CO_2 conversion was of 64%. The conversion decreased quickly with an increase of reaction time, and after 400 min about 13% of conversion was lost. By contrast, adding promoter helped to significantly improve the stability of the catalysts. The CH_4 conversion of Ni-ATP@Ce was 58% and kept stable within 400 mins. The Ce oxide-modified catalyst affected the surface area with strong interaction and catalyst basicity leading to the improvement of catalyst performance.

Lara-Garcia's group investigated dry reforming on $Ni/Ce_{0.95}Nd_{0.05}O_{2-\delta}$ catalyst in the fixed-bed quartz reactor (GHSV=48000 h^{-1}, CO_2/ CH_4/ Ar=1:1:3, T=700 °C)[153]. 58% of CH_4 conversion and 62% of CO_2 conversion are obtained after 24 h of test. In the DRM reaction, the Ni/Nd-Ceria catalyst is more active and stable than the Ni/CeO_2 catalyst, which indicates that the addition of Nd can have a beneficial effect. However, although the number of oxygen vacancies is increasing, the amount of carbon deposited in the used Nd-doped catalyst rises as a function of the dopant concentration. Furthermore, the addition of Nd to cerium oxide results in a change in the acid/basic properties of the carrier, which results in the gasification capacity of carbon residues produced by methane dehydrogenation.

Samrout et al. studied dry reforming over $Ni_{10(TS)}/CaO_{(HT)}$ catalyst at 650 °C, (5% CH_4; CH_4/ CO_2 = 1) with GHSV = 36 $L\cdot g^{-1}\cdot h^{-1}$. After 12 h of test, the CH_4 and CO_2 conversions were at 55 % and 66 %, respectively, and the H_2/CO ratio was equal to 1.05. Moreover, nickel was finely dispersed and stabilized over the support, giving after reduction a stable and selective DRM catalyst. However, the conversion of CH_4 and CO_2 were not enough to meet the needs in the industrial application[154].

Consequently, development of selective and robust DRM catalysts, especially for use at intermediate temperatures, remains a major research challenge in the field of heterogeneous catalysis[155].

1.7.2 Supports

It is known that the support nature significantly impacts the catalytic behavior. Compounds with strong interactions with the support course high resistance to sintering and higher metallic distribution. Manipulating interface structure and interaction between supports and metal is of importance to many catalysts used in heterogeneous catalysis aiming to achieve stable and high activity and selectivity.

Recently, it was exhibited that tuning interface and intensifying interaction between supports and Ni hold the key to synthesizing highly efficient and stable Ni catalysts for DRM[136,156].

A review thus unveiled that the promoter, support structure and shape held the key to producing enhanced surface basic sites, suppressing coke shaping on catalysts. A thorough understanding of the above mentioned important considerations in control of the basic catalyst feature could obviously promote the catalyst designing since it allowed the choice of the right fundamental promoters and supports[157].

Among all kinds of supports, CeO_2 is adopted as a suitable support and promoter for the catalytic reforming reaction, resulting from its one of a kind redox performances (Ce^{4+} to Ce^{3+}) and high content of highly reactive oxygen species, which could constitute local sources or reservoirs for oxygen species, which were involved in reactions occurring on CeO_2 surface[158]. Hence, Ni-CeO_2 interface and interaction were seen crucial for the anti-coke and anti-sintering property on Ni/CeO_2 catalysts[159]. For instance, $CexZr_{1-x}O_{2-\&}$ combined materials, broadly employed in three-way catalytic chemistry resulting from large oxygen storage capacity enhanced the efficiency and long-run stability of Ni catalysts in DRM[160,161].

In literature, CeO_2 was extensively utilized on Ni-based catalysts on account of their high alkaline properties and great capability of oxygen storage/release, as these led to high suppression toward coke deposited. Table 1-6 summarizes the catalysts with CeO_2 for dry reforming of methane. Tu et al. discovered that the employment of flower-like CeO_2 with Ni nanoparticle contents showed an excellent catalytic stability, the degradation of CH_4 conversion of only 3.1% after 50 h of reforming, thanks to the small degree of thermal sintering of the Ni catalyst particles. Moreover, the partial removal of coke amount formed on the catalyst was significant in the presence of the CeO_2 flowers during the reforming process[162]. In another work, Marinho et al. discovered that one step preparation of Ni@CeO_2 and Ni@$CeZrO_2$ catalysts led to Ni nanoparticles embedded in the oxide, which had a positive effect on the stabilization of the Ni particles size during the reduction at high temperature (800 °C). It also generated more oxygen vacancies and increased the interaction with $CeZrO_2$ and CeO_2 in comparison with an impregnated Ni/CeO_2 catalyst [163]. Wang et al. proved that the Ce-incorporated NiAl catalysts demonstrated excellent and stable performance with a slight amount of carbon deposited[164].

Al_2O_3 is another support extensively applied for the Ni active phase caused by large mechanical strength, changeable textural performance and availability. Table 1-7 shows some catalysts involving Al_2O_3 as support. Moreover, in the literature, the integration of Ni, Mg and Al element in catalyst formulation presents interesting outcomes toward the DRM[165]. Wang et al. synthesized Ni/$MgFe_xAl_{2-x}O_4$ catalyst for DRM reaction[166]. The stability and activity of the catalysts featuring a hierarchical support were detected in DRM at 750 °C, 111.3 kPa, and a CH_4/ CO_2 ratio of 1. The Ni/$MgAl_2O_4$ specimen featuring a 0.5 Mg/ Al molar ratio exhibited larger activity than Ni on common $MgAl_2O_4$ resulting from the larger surface area and stronger metal interaction with the hierarchic support. Ni supported on hierarchical Fe-modified $MgAl_2O_4$ proved to have potential and be efficient for methane dry reform.

Moreover, ZrO_2, featuring relatively high thermal stability and surface oxygen mobility, possessing four chemical performances on the surface, acidic and basic performances and oxidizing and reducing performances[167], is also adopted in the DRM as support[168] or promoter[169].

1.7.3 Co-catalysts

Raised Ni distribution is typically acquired through addition of promoter into the system. In general, promoters can be classified into three groups: (I) alkali or alkaline earth metals, (II) rare earth metals and (III) other metals, like Au, Ag, Sn, and Bi. It was also discovered in Gong's investigation that the tiny Au and Pt addition held the key to the catalytic property of bi-/trimetallic catalysts and preventing it from carbon poisoning[170]. The enhancement of stability and catalytic activity acquired for the trimetallic Ni-Au-Pt/Al_2O_3 catalyst resulted from the shaping of highly active Ni-Au-Pt NPs. These interactions have been linked toward anticipating the paths for establishment of DRM reaction kinetics, mechanisms and reactor designing[112].

Table 1-6 Recent advancements in Ce based catalyst development for DRM

Catalyst	Preparation method	Reaction temperature (°C)	Conv. of CH_4 (%)	Conv. of CO_2 (%)	H_2/CO (molar ratio)	Stability	Operation condition	Ref.
CeCo/Mesoporous alumina	Wetness impregnation	750	82.4	88.6	0.95	8h	GHSV=36000 mL/g*h 100mg 60mL/min $CO_2/CH_4/N_2$=1:1:3.1	171
Pt/CeNb/Al2O_3	Wetness impregnation	750	42	55	0.68	24h	100mg 100mL/min CO_2/CH_4=1:1	172
0.8Co-Ni/CeO_2	Incipient wetness co-impregnation	800	77	80	0.9	10h	GHSV=12000 mL/g*h 500mg 100mL/min $CO_2/CH_4/N_2$=3:3:4	173
Paper-structured CeO_2-NiO-5.5	Impregnation method	750	91.9	87	0.9	50h	GHSV=2300 /h 40mL/min CO_2/CH_4=1:1	162
10Ni-5Al-1Ce	/	700	82	91	/	8h	10mg 200mL/min $CO_2/CH_4/N_2$=1:1:18	174
Pt/FeMo/Ni/Al_2O_3-CeO_2	Incipient wetness impregnation	700	81	86	0.91	6h	WHSV=12000mL/g*h 300mg 60mL/min CO_2/CH_4=1:1	175

Catalyst	Preparation method	Reaction temperature (°C)	Conv. of CH_4 (%)	Conv. of CO_2 (%)	H_2/CO (molar ratio)	Stability	Operation condition	Ref.
$1.5CeO_{2-x}$-Nickel silicate nanotubes	Chemical precipitation method	750	82	88	0.9	100h	GHSV=96000 mL/g*h 25mg $CO_2/CH_4:N_2$=1:1:2	176
NiO-CeO_2 solid-solution	sol-gel method exsolution	800	71	80	0.9	90h	GHSV=5000 mL/g*h 150mg CO_2/CH_4=1:1	177
NiCe1C	wetness co-impregnation		56	53	0.95	/	50mL/min CO_2/CH_4=1:1	178
15%Ni/CeO_2-MgO	co-precipitation and impregnation	700	65	72	0.9	5h	GHSV=36000 mL/g*h 100mg 60mL/min $CO_2/CH_4/N_2$=1:1:1	179
Ni/xCeO_2-Al_2O_3	Wetness impregnation	550	57	69	0.63	8h	50mg 100mL/min $CO_2/CH_4/N_2$=1:1:3	180
Ni@$CeZrO_2$	Coprecipetation	800	53	66	0.74	24h	20mg 100mL/min CO_2/CH_4=1:1	163
Ni/nanoceria@boron nitride	wet impregnation	750	69	81	1.0	100h	GHSV = 25 L/g*h 120mg 50mL/min CO_2/CH_4 =1:1	181

Table 1-7 Recent advancements in Al based catalyst development for DRM

Catalyst	Preparation method	Reaction temperature (°C)	Conv. of CH_4 (%)	Conv. of CO_2 (%)	H_2/CO (molar ratio)	Stability	Operation condition	Ref.
Ni/Al_2O_3-F	incipient wetness impregnation	750	80	83	0.88	10h	GHSV=36 L/g*h 200mg CO_2/CH_4 =1:1	182
La.Ni(CA)/$Mg_{1.3}$AlO$_x$.1000	Wet impregn	750	43	89	0.92	100h	GHSV=170L/g*h 50mg CO_2/CH_4 =2:1	183
Ni/30MgAl_S	incipient wetness impregnation	700	35	40	0.8	50h	WHSV=20.3/h 340mg $CO_2/CH_4/N_2$=1:1:3 60 000 Pa	184
0.42CeNi/Al_2O_3HF-ALD	incipient wetness	850	85	/	/	75h	600mg 60mL/min CO_2/CH_4 =1:1	185

1.8 Catalysts deactivation

So far, dry reforming of methane still cannot be industrialized because of the instability and deactivation of the catalyst. Nickel is cheap and abundant in reserves, but Ni-based catalyst is easy to sinter in the dry reforming of methane, and forms carbon and deposits on the surface of the catalyst, which accelerates the deactivation of the catalyst[87].

1.8.1 Carbon formation

In the dry reforming of methane reaction, coke formation on the surface of the catalyst is one of the main reasons for the deactivation of the nickel-based catalyst[186]. According to literature, it is found that increasing the catalyst's ability to adsorb carbon dioxide and activate the carbon dioxide can reduce the formation of carbon deposits. Increasing the adsorbed oxygen species on the catalyst surface can effectively inhibit or remove the deposited carbon[187].

1.8.2 Sintering

Sintering is another major reason for catalyst deactivation. Sintering is caused by the growth of metal particles at high temperatures, and the specific surface area reduced, or the collapse of the pore structure of the supports. Generally, sintering takes place at temperatures above 700 °C and is also promoted by the moisture generated by the RWSG reaction[188]. According to reports, this is the result of the reduction of the surface energy of the kinetic-favorable crystallites and the size-dependent movement of the crystallites on the catalyst support[189].

1.8.3 Methods of anti-deactivation/carbon formation

In order to avoid the sintering of the catalyst and carbon deposition, many studies have been reported to improve the stability of the Ni based catalysts. The properties of nickel active compound, particle size, catalyst preparation methods, the interaction between active site and supports, and the addition of promoters have been studied[190,191]. Research has also combined two or more active metals, adding a variety of promoters to improve catalytic activity and increase stability. The internal interaction of the components in catalyst is also investigated[192].

Several reviews have been reported in catalysts development for DRM reactions on catalysts configuration[193], noble metal catalysts, effect of parameters, coke deposition and management[194], development of oxygen carriers in chemical looping DRM[195], Ni-based catalysts, DRM at low temperature[196] and progress in preparation of

mesoporous SBA-15 supported catalyst[197]. However, it is also essential to study the active sites, oxygen vacancies, basicity, structure, redox property, interactions between active metals and supports of the catalyst[112].

1.9 Objective of the thesis

The demand for hydrogen, as a chemical product and as energy is increasing, but the main hydrogen production methods are unsustainable and not environmentally friendly. Hydrogen production from renewable resources (such as biogas mainly composed of CH_4 and CO_2) is required. Dry reforming of methane (DRM) is a promising method to produce H_2 and CO from greenhouse gases. It has received a lot of attention due to environmental issues.

In this thesis, Ni-based $CeNi_XO_Y$, $CeZr_{0.5}Ni_XO_Y$, $CeAl_{0.5}Ni_XO_Y$, and $AlMg_2Ni_XO_Y$ catalysts are studied in dry reforming of methane reaction. The effect of reaction temperature, Ni content, in situ H_2 pretreatment, mass of catalyst, calcination, and CO_2/CH_4 ratio are studied. Moreover, long duration stability tests are reported on some chosen samples. The optimized catalytic performance associated to resistance to carbon formation are obtained on partially reduced catalysts. Various physicochemical characterizations are used to analyze the properties of the catalysts, such as XRD, Raman, XPS, and H_2-TPR. Some chosen catalysts are also characterized after DRM reaction to analyze their evolution. Finally, an active site involving Ni species in close interactions with other cations is proposed. It is related to a partially reduced catalyst involving anionic vacancies, O^{2-} species, and cations.

Chapter 2
Dry reforming of methane on Ni-based catalysts

Chapter 2 Dry reforming of methane on Ni-based catalysts

The $CeNi_XO_Y$, $CeZr_{0.5}Ni_XO_Y$, $CeAl_{0.5}Ni_XO_Y$, and $AlMg_2Ni_XO_Y$ catalysts are studied on dry reforming of methane reaction (DRM) with different conditions. The experiment process is shown in ***Annex 3***. The influence of time, temperature, pretreatment, mass of catalyst and Ni content are studied, as well as stability in long tests run on some chosen compounds. Meanwhile, different CO_2/CH_4 ratio is conducted on the DRM reaction. The CO_2/CH_4 ratio = 1 ($CH_4/CO_2/N_2$ = 5:5:90%) was tested in part A and CO_2/CH_4 ratio = 0.7 ($CH_4/CO_2/N_2$ = 7:5:88%) presented in part B.

2.A Dry reforming of methane on Ni-based catalysts in CO_2/CH_4 = 1

2.A.1 Catalytic performance at 600 °C on catalysts with H_2 pretreatment

2.A.1.1 On $CeNi_XO_Y$ catalysts

2.A.1.1.a. Influence of time

The results are presented in Fig. 2-1 for $CeNi_{0.2}O_Y$, $CeNi_{0.3}O_Y$, $CeNi_{0.5}O_Y$, catalysts (50 mg) in-situ pretreated in H_2 at 250 °C for 12 h. As illustrated in Fig. 2-1 a, an increase in time leads to a slight decrease in both CH_4 and CO_2 conversions for $CeNi_{0.2}O_Y$ catalyst. The conversions of CH_4 and CO_2 decrease from 52.4 % and 59.5 % to 45.7 % and 48.5 % after 5 hours in feed, respectively. Very close conversions of CO_2 and CH_4 are found in the tested temperatures. The initial CH_4 and CO_2 conversions are of 59.4 % and 63.2 % for $CeNi_{0.3}O_Y$ catalyst. Afterward, the conversions vary slightly during the first hour of reaction. Specifically, the CH_4 conversion increases of 1.7% and CO_2 conversion decreases of 2.1% to the steady-state values after 5 hours. It is a interesting result at the low temperature of 600 °C. In the case of $CeNi_{0.5}O_Y$, the conversion of carbon dioxide decreases from 56.6% to 51.1% after 5 hours, while the CH_4 conversion remains stable at 53.9%. In this study, the H_2/CO ratio is varying between 1.2 and 1.3 for $CeNi_{0.3}O_Y$ catalyst, 1.0-1.15 for $CeNi_{0.5}O_Y$ catalyst, and 0.8-1.1 for $CeNi_{0.2}O_Y$ catalyst. The H_2/CO ratio obtained on $CeNi_{0.3}O_Y$ is higher than the one obtained on $CeNi_{0.2}O_Y$ and $CeNi_{0.5}O_Y$ catalysts. Concretely, the CH_4 conversion on $CeNi_{0.3}O_Y$ is higher compared to the two other catalysts.

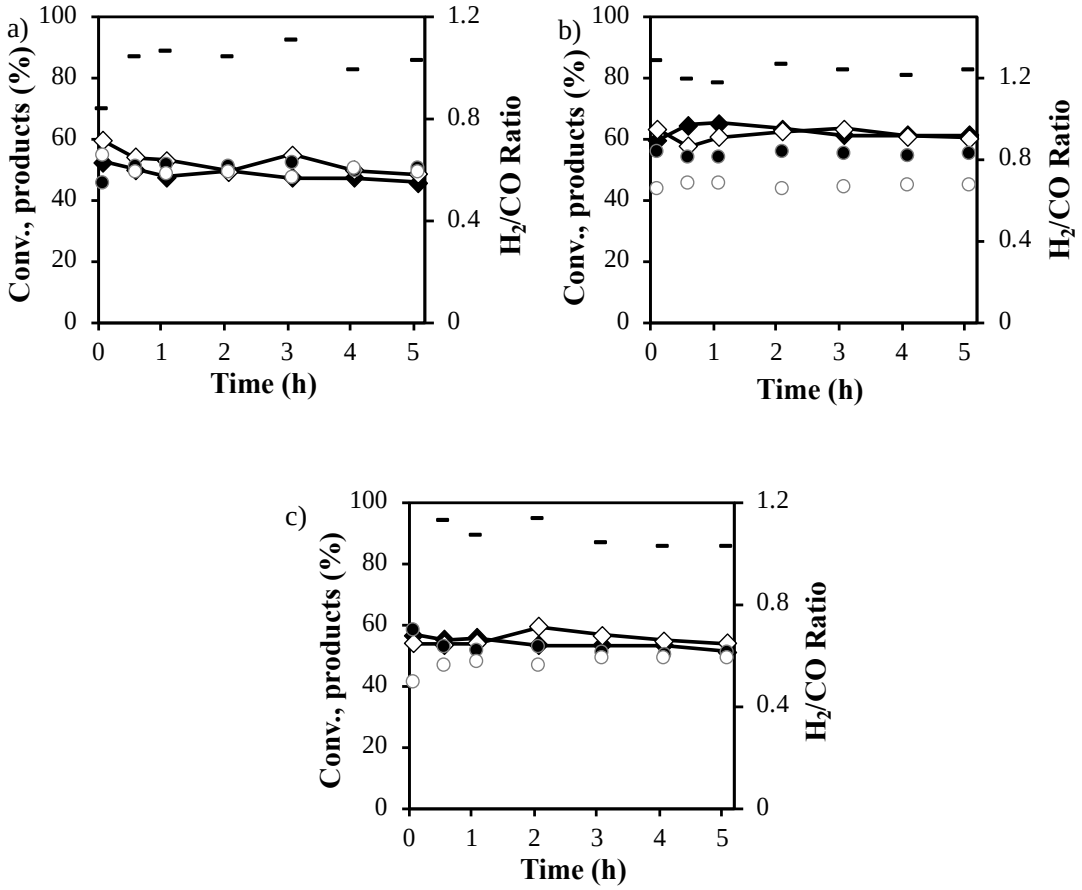

Fig. 2-1 DRM catalytic performance at 600 °C on calcined a) $CeNi_{0.2}O_Y$, b) $CeNi_{0.3}O_Y$, c) $CeNi_{0.5}O_Y$ catalysts (50 mg) with in situ H_2 pretreatment at 250 °C. CH_4 (◆), CO_2 (◇) conversions, H_2 (●), CO (○), in mol % and the H_2/CO ratio (-). $CH_4/CO_2/N_2$ = 5:5:90%.

2.A.1.1.b. Influence of Ni content

Dry reform of methane is investigated in the current work over the $CeNi_XO_Y$ catalysts featuring various Ni concentrations, in a first method with in situ pre-treatment in H_2 at 250 °C. The CH_4 and CO_2 conversions and H_2/CO ratio in the formed products as a function of the Ni concentration (Ni/M_T) are presented in Fig. 2-2 a, and carbon formation rate as a function of the Ni concentration is exhibited in Fig. 2-2 b.

Among the catalysts tested, $CeNi_{0.3}O_Y$ could appear to be the most competitive one as it shows higher conversions, but it exhibits also more carbon deposition. At 600 °C, CH_4 and CO_2 conversions are about 61.1 % and 60.3 % respectively for $CeNi_{0.3}O_Y$ after 5 h of test, with a H_2/CO ratio of around 1.23, and a carbon deposition of 0.22 $g \cdot gcat^{-1} \cdot h^{-1}$ (Fig. 3-1 b). Therefore, the high H_2/CO ratio and CH_4 conversion could be due to the participation of methane decomposition. As the $CeNi_{0.5}O_Y$

compound presents close conversions but much lower carbon formation, it is chosen for long test run.

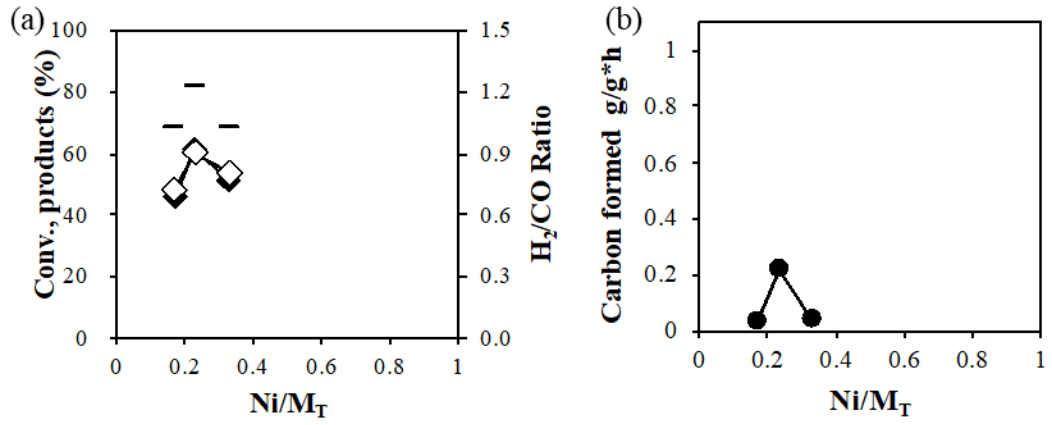

Fig. 2-2 DRM catalytic performance and carbon formation at 600°C on calcined $CeNi_XO_Y$ catalysts (50 mg) with in situ pretreatment in H_2 at 250°C. $CO_2/CH_4/N_2$ = 5:5:90%. CH_4 (◆), CO_2 (◇) and H_2/CO (-) ratio. $Ni/M_T = x/(x+1)$. Time of experiments = 5h.

2.A.1.1.c. Stability test

For clarifying the stability and ultimate deactivation, the catalyst is subjected to long-run detection. The experiment is performed for investigating the $CeNi_{0.5}O_Y$ catalyst property over a 80 h time-on-stream at 600 °C. The acquired conversion values (CH_4 and CO_2) and products ratio (H_2/CO) are plotted as a function of time on stream in Fig. 2-3. A decay in CH_4 and CO_2 conversions are seen during first hours, while after about 20 h they remain relatively stable. The CH_4 conversion drop slightly exceeds the CO_2 conversion drop in the initial stage. After 80 h of reaction at 600 °C, the methane conversion is found at 53.4 % (compared to 75.8 % at the initial state), while CO_2 conversion is of 59.1 % (compared to 72.0 % at the initial state). Furthermore, the initial H_2/CO molar ratio reaches 1.15 and the value decreases after about 20 h and then remains relatively stable and at 0.86 at 80 h. the carbon shaping rate reaches 0.0037 $g \cdot gcat^{-1} \cdot h^{-1}$.

The acquired outcomes are interesting in comparison with literature. Li. et al. Investigated dry reforming over Ni/CeO_2 (5 wt.% Ni) catalyst at 500 °C, (CH_4/CO_2 = 1, with 30 mg of catalyst, GHSV = 48,000 h^{-1}) [115]. The CH_4 and CO_2 conversions reached 30 % and 42 %, separately, and the H_2/CO ratio reached 0.7 after 10 hours on stream. Moreover, carbon in filamentous and graphitic structure was largely formed after test carbon formation rate was 1.6 $mmolcarbon \cdot gcat^{-1} \cdot h^{-1}$. In the current investigation, better outcomes are acquired but at 600 °C.

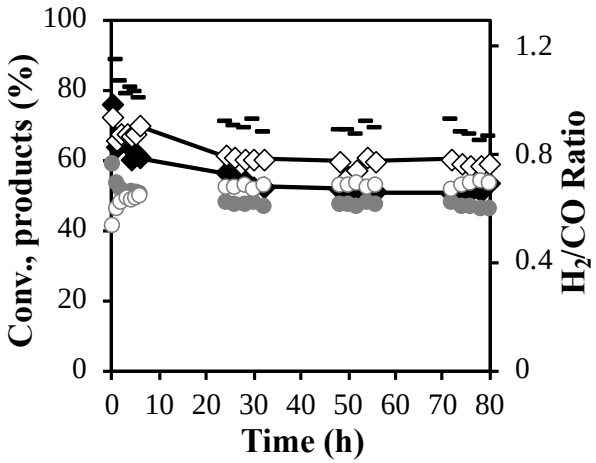

Fig. 2-3 DRM catalytic performance at 600 °C on calcined $CeNi_{0.5}O_Y$ catalyst (50 mg) with in situ H_2 pretreatment at 250 °C. CH_4 (◆), CO_2 (◇), H_2 (●), CO (○), in mol% and H_2/CO (-) ratio. $CO_2/CH_4/N_2$ = 5:5:90%.

2.A.1.2 On $CeZr_{0.5}Ni_XO_Y$ catalysts

2.A.1.2.a Influence of time

The catalytic performance toward DRM is investigated on $CeZr_{0.5}Ni_XO_Y$ catalysts. The CH_4 and CO_2 conversions curves, as well as the values of H_2/CO ratio as a function of time during the methane dry reforming experiments, is shown in Fig. 2-4. For the $CeZr_{0.5}Ni_{0.5}O_Y$, increase of time on stream leads to a slight decrease in conversions, mainly in the first hour, then a relatively good stability is obtained during 5 h. However, for $CeZr_{0.5}Ni_5O_Y$, the growth of time leads to a small increase on both of CH_4 and CO_2 conversions in the test at 600 °C. Minimal amount of carbon seems to be formed in $CeZr_{0.5}Ni_{0.5}O_Y$ case. A mass of carbon formed could be found in the case of $CeZr_{0.5}Ni_1O_Y$ and $CeZr_{0.5}Ni_2O_Y$, (reported later). And the reactor was blocked during the catalytic test for the $CeZr_{0.5}Ni_1O_Y$ and $CeZr_{0.5}Ni_2O_Y$ catalysts.

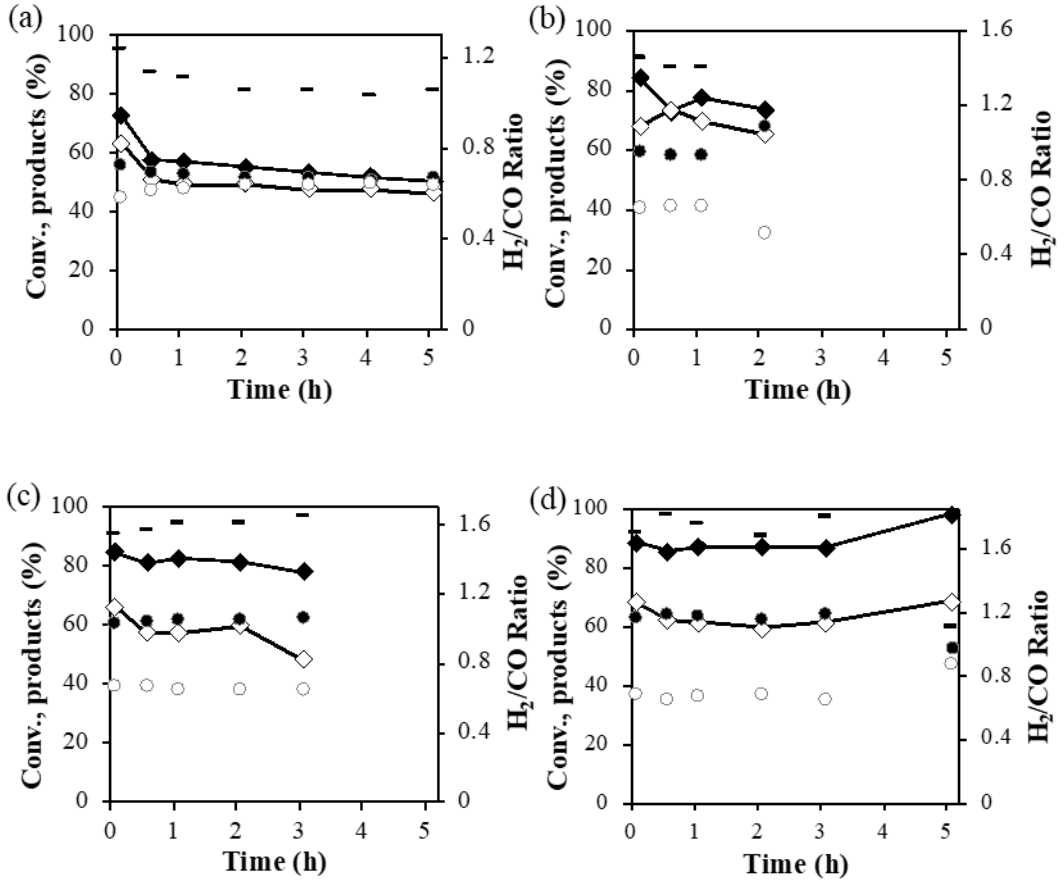

Fig. 2-4 DRM catalytic performance at 600 °C on calcined a) $CeZr_{0.5}Ni_{0.5}O_Y$, b) $CeZr_{0.5}Ni_1O_Y$, c) $CeZr_{0.5}Ni_2O_Y$, d) $CeZr_{0.5}Ni_5O_Y$ catalysts (50 mg) with in situ H_2 pretreatment at 250 °C. CH_4 (◆), CO_2 (◇) conversions, H_2 (●), CO (○), in mol % and the H_2/CO ratio (-). $CH_4/CO_2/N_2$ = 5:5:90%.

2.A.1.2.b Influence of Ni content

The influence of Ni content in DRM at 600 °C is shown in Fig. 2-5. The CH_4 conversion increase with increasing Ni content. The catalyst with lower Ni content results in slightly lower conversion compared to the catalyst with higher Ni content. However, as the Ni content increases, the CO_2 conversion declines. Besides, the reactor was blocked during the catalytic test for the $CeZr_{0.5}Ni_1O_Y$ and $CeZr_{0.5}Ni_2O_Y$ catalysts. As the nickel content increases, the carbon formation rates are 0.047 $g \cdot gcat^{-1} \cdot h^{-1}$, 0.58 $g \cdot gcat^{-1} \cdot h^{-1}$, 0.92 $g \cdot gcat^{-1} \cdot h^{-1}$, and 0.85 $g \cdot gcat^{-1} \cdot h^{-1}$. These observations can be related to the coke formation by methane decomposition and CO disproportionation, leading to producing more CO_2 in the tail gas while more carbon was deposited on catalyst surface. Therefore, the $CeZr_{0.5}Ni_5O_Y$ compound presents the highest performance for CH_4 and CO_2 transformations since 86.9 % and 61.4 % of CH_4 and CO_2 conversions are reached at 600 °C, with a H_2/CO ratio of 0.85.

Compared to literature, Fatesh et al. studied Ni-2.5% Ce/W-Zr catalyst in dry reforming at 700 °C, total flow rate was 70 mL/min, GHSV = 42000 mL/g·h, 0.1 g of catalyst, CH_4 and CO_2 in a ratio of 1:1[134]. The catalyst with large surface area and promoted dispersion showed conversion for CH_4 and CO_2 at 77 % and 83 %, respectively, at 700 °C after 100 h reaction. The H_2/CO ratio was about 0.92 at 700°C. In the present study, similar results are achieved by using harsher conditions (lower temperature at 600 °C and less catalyst 50 mg and higher total flow rate 80 mL/min).

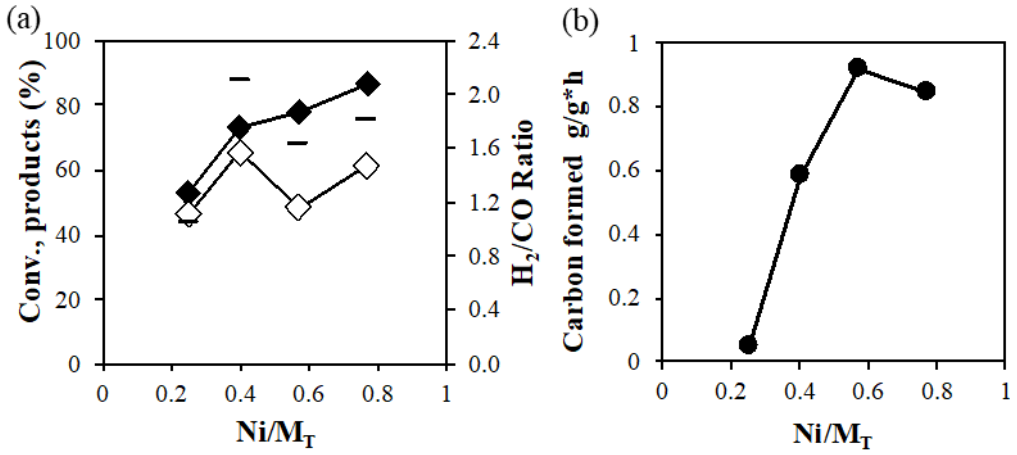

Fig. 2-5 DRM catalytic performance and carbon formation at 600 °C on calcined $CeZr_{0.5}Ni_XO_Y$ catalysts (50 mg) with in situ pretreatment in H_2 at 250°C. $CO_2/CH_4/N_2$ = 5:5:90%. CH_4 (◆), CO_2 (◇) and H_2/CO (-) ratio. Ni/M_T = x/(x+1+0.5). Time of experiments = 5h.

2.A.1.3 On $CeAl_{0.5}Ni_XO_Y$ catalysts

2.A.1.3.a Influence of time

The influence of time of reaction (5 h) is investigated over $CeAl_{0.5}Ni_XO_Y$ catalysts, and the results are shown in Fig. 2-6. The CH_4 and CO_2 conversions are 56 % and 63 % for the $CeAl_{0.5}Ni_{0.5}O_Y$ with in situ pretreatment in H_2 at 250 °C. The $CeAl_{0.5}Ni_1O_Y$ presents a similar result with $CeAl_{0.5}Ni_{0.5}O_Y$, 61.4 % and 63.3 % for CH_4 and CO_2 conversions. For higher Ni content catalysts, $CeAl_{0.5}Ni_2O_Y$ and $CeAl_{0.5}Ni_5O_Y$ show higher and more stable conversions. For $CeAl_{0.5}Ni_2O_Y$, the CH_4 conversion increases of 3 % after 5 hours to 81.5 % and CO_2 conversion stays stable at 74.8 %. A decrease of 1.5 % and 8.5 % for CH_4 and CO_2 conversions during first hour on $CeAl_{0.5}Ni_5O_Y$ catalyst then stays stable. Finally, the steady-state values around 80 % and 69 % for CH_4 and CO_2 conversions are obtained. Therefore, globally after the first hour of reaction, the conversions remain relatively stable on all the studied compounds of this series.

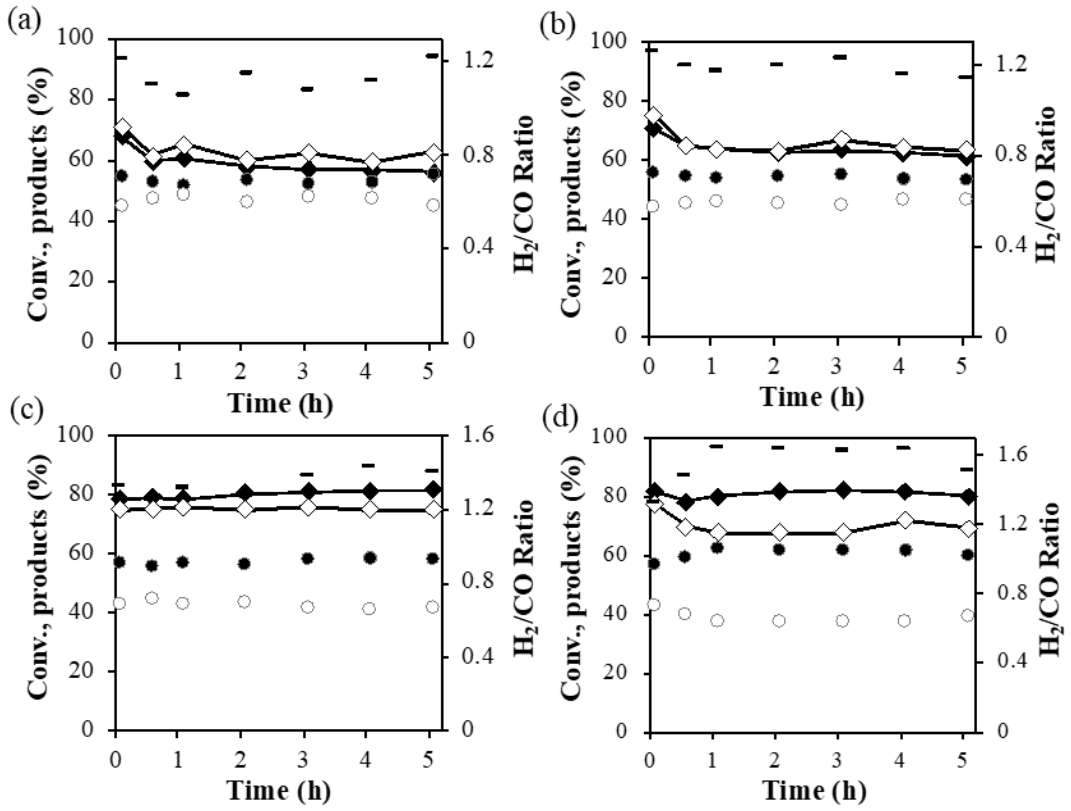

Fig. 2-6 DRM catalytic performance at 600 °C on calcined a) $CeAl_{0.5}Ni_{0.5}O_Y$, b) $CeAl_{0.5}Ni_1O_Y$,c) $CeAl_{0.5}Ni_2O_Y$, d) $CeAl_{0.5}Ni_5O_Y$ catalysts (50 mg) with in situ H_2 pretreatment at 250 °C. CH_4 (◆), CO_2 (◇) conversions, H_2 (●), CO (○), in mol % and the H_2/CO ratio (-). $CH_4/CO_2/N_2$ = 5:5:90%.

2.A.1.3.b Influence of Ni content

The methane and CO_2 conversion outcome determined in the reaction and the H_2/CO ratio vs. Ni content at 600 °C are exhibited in Fig. 2-7. Clearly, the CH_4 and CO_2 conversions globally rise as Ni concentration rises. However, for catalyst $CeAl_{0.5}Ni_5O_Y$, the catalytic performance isn't directly proportional to Ni concentration. Fig. 2-7 b present that among various catalysts detected, the catalyst featuring low Ni concentration exhibits the lowest amount of carbon generated. And the carbon shaping rate rises as the Ni content rises, which are 0.039 $g \cdot gcat^{-1} \cdot h^{-1}$, 0.049 $g \cdot gcat^{-1} \cdot h^{-1}$, 0.27 $g \cdot gcat^{-1} \cdot h^{-1}$, and 0.59 $g \cdot gcat^{-1} \cdot h^{-1}$, respectively. This possibly results from methane decomposition occurring, especially on the catalyst containing a large amount of Ni species. On basis of thermodynamics, carbon-shaping reactions, like direct methane decomposition, $CH_4 = C + 2H_2$, are favored at approximately 600 °C. $CeAl_{0.5}Ni_2O_Y$ appears to be the most competitive since it exhibits similar high conversions and less carbon deposition in comparison with highest Ni concentration catalyst.

Several articles in the current literature report on the performance, stability and selectivity of Ce-Ni-Al based catalysts in DRM. The result can be in comparison with the literature presenting the dry reforming over 10 mg of Ni-Ce-Al catalyst at 700 °C[174]. Approximately 82% of methane and CO_2 conversions were acquired with 10 wt.% of Ni. The reaction conditions used were $CH_4/CO_2/N_2$= 5:5:90 %, and total flow of 200 mL/min. A large amount of fibril-like carbon was found by TEM, but the carbon formation rate was not reported. In the current investigation, similar outcomes are acquired at 600 °C, but with lower total flow, higher mass of catalyst and lower CH_4 %.

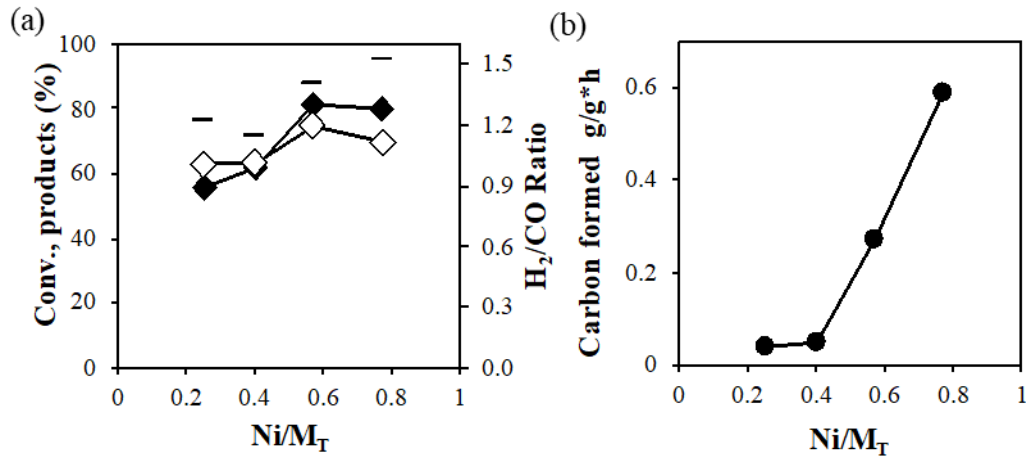

Fig. 2-7 DRM catalytic performance and carbon formation at 600°C on calcined $CeAl_{0.5}Ni_XO_Y$ catalysts (50 mg) with in situ pretreatment in H_2 at 250°C. $CO_2/CH_4/N_2$ = 5:5:90%. CH_4 (◆), CO_2 (◇) and H_2/CO (-) ratio. Ni/M_T = x/(x+1+0.5). Time of experiments = 5h.

2.A.1.4 On $AlMg_2Ni_XO_Y$ catalysts

2.A.1.4.a Influence of time

On the $AlMg_2Ni_XO_Y$ catalysts, as illustrated in Fig. 2-8, CH_4 and CO_2 conversions and products distribution show slight dependence on time with good stability performance with time during 5h. On $AlMg_2Ni_1O_Y$ compound, conversions undergo a slow decrease in first hour from 82.5 % to 78.1 % for CO_2, and 77.6 % to 73.6 % for CH_4. The H_2/CO ratio varies around 1.2. For $AlMg_2Ni_3O_Y$, the CH_4 conversion increases from 82.4 % to 85.0 % but CO_2 conversion decreases from 85.8 % to 79.2 %. And H_2/CO ratio is 1.55. For $AlMg_2Ni_{12}O_Y$, the CH_4 and CO_2 conversions decrease of 3.9 % and 6.1 % after 1 h on reaction, then stay stable at 84.3 % and 73.8 % respectively, the H_2/CO ratio is 1.68.

Fig. 2-8 DRM catalytic performance at 600 °C on calcined a) $AlMg_2Ni_1O_Y$, b) $AlMg_2Ni_3O_Y$, and c) $AlMg_2Ni_{12}O_Y$ catalysts (50 mg) with in situ H_2 pretreatment at 450 °C. CH_4 (◆), CO_2 (◇) conversions, H_2 (●), CO (○), in mol % and the H_2/CO ratio (-). $CH_4/CO_2/N_2$ = 5:5:90%.

2.A.1.4.b Influence of Ni content

Fig. 2-9 demonstrates the influence of Ni content on the catalytic performances of $AlMg_2Ni_XO_Y$ catalysts which are in situ pretreated in H_2 at 450 °C. As the nickel content increases from 21.9 wt.% to 43.7 wt.%, the conversions of methane and carbon dioxide slightly increase. But when the nickel content continues to increase to 61.4%, the conversions of the two reactants decrease. The H_2/CO ratio, as well as carbon formation, is strongly associated with the Ni content. The increase in nickel content greatly increases the H_2/CO ratio and carbon deposition. The carbon formation rates are 0.062 $g \cdot gcat^{-1} \cdot h^{-1}$, 0.41 $g \cdot gcat^{-1} \cdot h^{-1}$, and 0.63 $g \cdot gcat^{-1} \cdot h^{-1}$, respectively. Based on the above results, $AlMg_2Ni_1O_Y$ can be considered to be the best catalyst, however, the conversions being so high, further and deeper analysis could be done using a lower mass of compound.

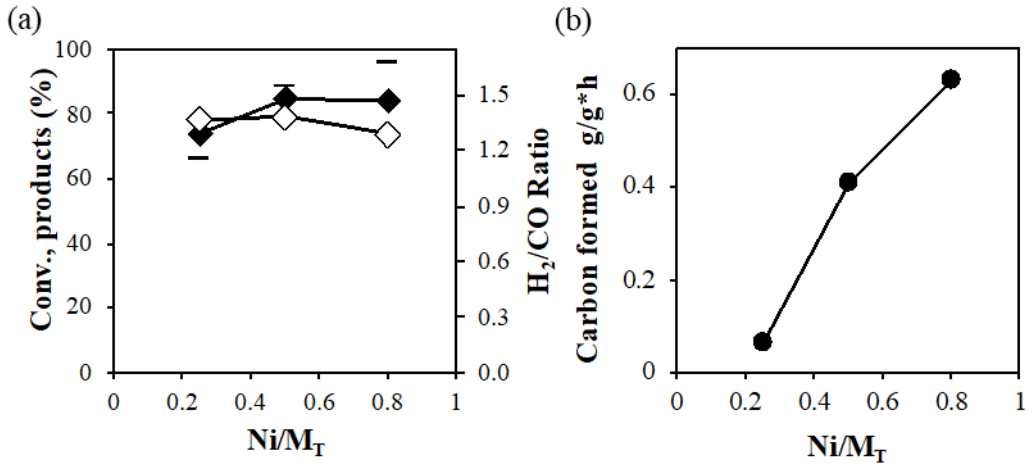

Fig. 2-9 DRM catalytic performance and carbon formation at 600 °C on calcined $AlMg_2Ni_XO_Y$ catalysts (50 mg) with in situ pretreatment in H_2 at 250°C. $CO_2/CH_4/N_2$ = 5:5:90%. CH_4 (◆), CO_2 (◇) and H_2/CO (-) ratio. Ni/M_T = x/(x+1+2). Time of experiments = 5h.

2.A.1.4.c Stability test

For the further study, the stability of calcined $AlMg_2Ni_1O_Y$ catalyst is investigated at 600 °C under same previous conditions (96000 mL/g·h). The stability performances are shown in Figure 2-10. The catalyst exhibits a high and stable catalytic performance for the DRM reaction with initial CH_4 and CO_2 conversions of 83.1 % and 80.1%, respectively. A very good stability is obtained during the 80 hours, after a decline of 8.1 % detected during the first hours for the CH_4 conversion, with a slight variation (ascension) of few % in the CO_2 conversion, in the range of uncertainty. The H_2/CO ratio is 1.2 and carbon formation rate is 0.017 $g \cdot gcat^{-1} \cdot h^{-1}$.

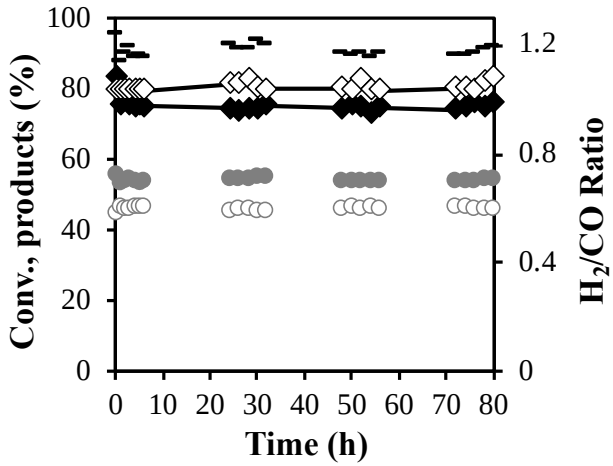

Fig. 2-10 DRM catalytic performance at 600 °C on calcined $AlMg_2Ni_1O_Y$ catalyst (50 mg) with in situ H_2 pretreatment at 450 °C. CH_4 (◆), CO_2 (◇), H_2 (●), CO (○), in mol% and H_2/CO (-) ratio. $CO_2/CH_4/N_2$ = 5:5:90%.

In Azancot's work, similar compound $Ni/MgAl_2O_4$ was prepared by co-precipitation method[138]. It has been found that the catalyst (200 mg) gave 31 % of CH_4 conversion and 37 % of CO_2 conversion in dry reforming at 550 °C with CO_2/ CH_4/ N_2 = 1:1:3, total flow rate = 100 mL/min condition.

2.A.2 Catalytic performance at 600 °C on catalysts without H_2 pretreatment

The following experiments are carried at 600 °C using 50 mg of catalyst without in situ pretreatment in H_2 of the compounds. Concretely, the calcined catalysts are kept in a flow of He during the temperature increase up to 600 °C.

2.A.2.1 On $CeNi_XO_Y$ catalysts

2.A.2.1.a Influence of time

The effect of no pretreatment in H_2 is studied on $CeNi_{0.2}O_Y$, $CeNi_{0.3}O_Y$, $CeNi_{0.5}O_Y$ and $CeNi_2O_Y$. The catalytic performance toward DRM is investigated under stream $CO_2/CH_4/N_2$ = 5:5:90% over 5 h at 600 °C. The CH_4 and CO_2 conversions curves, as well as the values of H_2/CO ratio as a function of time during the methane dry reforming experiments, are shown in Fig. 2-11. For all the compounds, good stability is obtained after 1h or reaction. During the first hour of reaction, the conversions of the reactants decrease on $CeNi_{0.5}O_Y$, while CO_2 conversion decreases on $CeNi_2O_Y$ catalyst. The $CeNi_2O_Y$ catalyst presents the highest methane conversion, with 78.6 % and 58.0 % for CH_4 and CO_2 conversions and H_2/CO ratio of 1.59. Globally, CO_2 conversion is relatively close on all compounds at about 60 %.

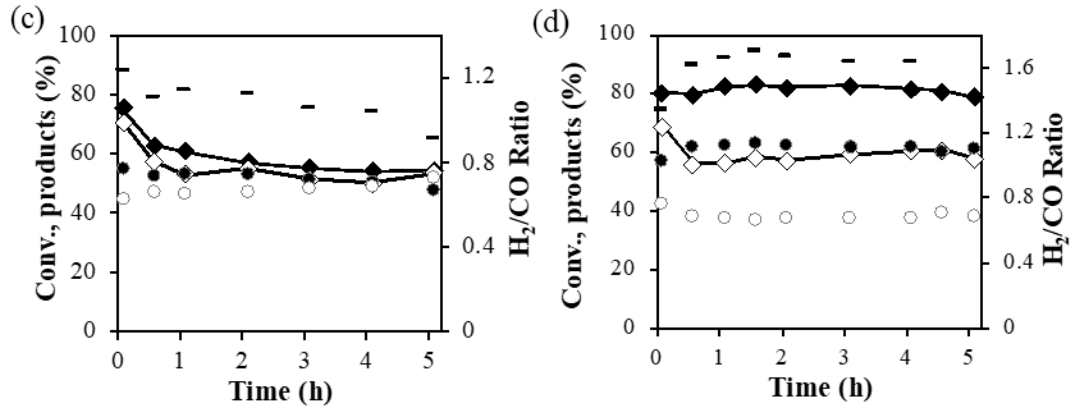

Fig. 2-11 DRM catalytic performance at 600 °C on calcined a) $CeNi_{0.2}O_Y$, b) $CeNi_{0.3}O_Y$, c) $CeNi_{0.5}O_Y$, d) $CeNi_2O_Y$ catalysts (50 mg) without pretreatment. CH_4 (◆), CO_2 (◇) conversions, H_2 (●), CO (○), in mol % and the H_2/CO ratio (-). $CH_4/CO_2/N_2$ = 5:5:90%.

2.A.2.1.b Influence of Ni content

On the $CeNi_XO_Y$ catalysts without pretreatment, the CH_4 and CO_2 conversions and H_2/CO ratio are shown in Fig. 2-12 as a function of the Ni content (Ni/M_T). At the stable state (5h) globally, relatively close conversions are observed at about 60 % up to Ni/M_T = 0.4, while for higher Ni content, CO_2 conversion remains relatively stable but CH_4 conversion increases. H_2/CO ratio is the lowest on the $CeNi_{0.5}O_Y$ catalyst, and the highest on the $CeNi_2O_Y$ catalyst, in relation to the trend of carbon formation (0.71 $g \cdot gcat^{-1} \cdot h^{-1}$), and probably due to methane decomposition. It can be seen that, for $CeNi_2O_Y$ catalyst, higher Ni content leads to a decrease of CO_2 conversion at the beginning of the test, may be due to the high carbon deposit.

Among each catalyst detected, $CeNi_{0.3}O_Y$ (9.5 wt% of Ni) seems to be the most competitive as it presents similar conversions as employing larger concentration of nickel and presents less carbon deposition (0.069 $g \cdot gcat^{-1} \cdot h^{-1)}$. Concretely, at 600 °C, CH_4 and CO_2 conversions are found at approximately 54.5 % and 53.6 % separately, with a H_2/CO ratio of around 0.92.

Regardless of the carbon shaping and catalytic stability, the H_2 generation acquired on the current $CeNi_XO_Y$ catalyst is comparable to the values reported in the recent literature, where the authors reported the dry reforming over 50 mg of $0.5Ni/CeNi_XO_Y$ catalyst at 650 °C, with flow rate of $CO_2/CH_4/N_2$ = 20:20:20 mL/min[139]. Their optimal outcome, 56 % of CH_4 conversion and 52 % of CO_2 conversion were acquired. The H_2/CO ratio reached 1.06. Therefore, $CeNi_XO_Y$ appear as highly efficient, stable catalysts for methane dry reforming regarding the lower

temperature uesd. Moreover, the $CeNi_XO_Y$ will be detected in high temperature resulting from the large potential of performance of this series.

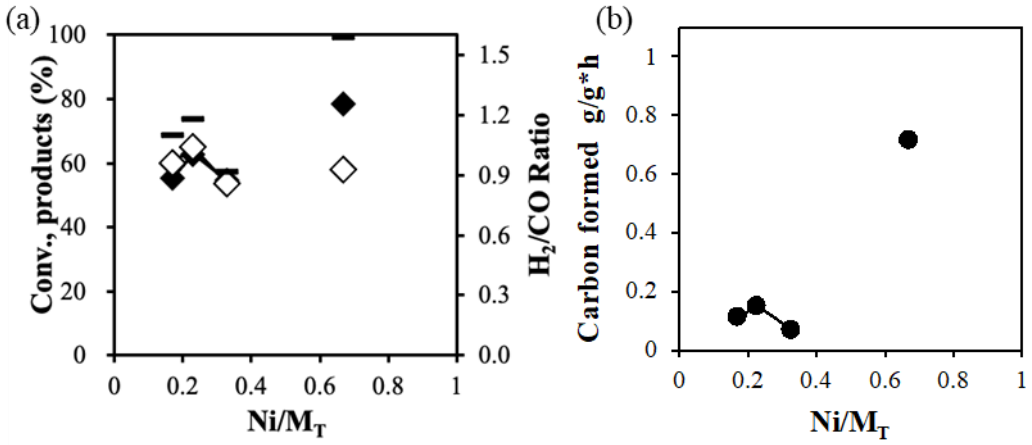

Fig. 2-12 DRM catalytic performance and carbon formation at 600°C on calcined $CeNi_XO_Y$ catalysts (50 mg) without pretreatment. $CO_2/CH_4/N_2$ = 5:5:90%. CH_4 (◆), CO_2 (◇) and H_2/CO (-) ratio. $Ni/M_T = x/(x+1)$. Time of experiments = 5h.

2.A.2.1.c Influence of pretreatment

The effect of H_2 pretreatment on the catalytic performance of the calcined $CeNi_XO_Y$ catalysts at 600 °C is investigated by comparing the results obtained with (Fig.2-2) and without pretreatment (Fig. 2-12). As previously reported (Fig. 2-2, which is shown again here for easy comparison), without pretreatment in H_2 at 250 °C, the CH_4 conversion increases on $CeNi_{0.2}O_Y$, $CeNi_{0.3}O_Y$ and $CeNi_{0.5}O_Y$ catalysts, the CO_2 conversion increased for $CeNi_{0.2}O_Y$ catalyst, stayed the same for $CeNi_{0.3}O_Y$ and $CeNi_{0.5}O_Y$ catalysts. Meanwhile, the H_2/CO ratio did not show any obvious change and remained stable and slightly greater than one. However, after 12 hours of hydrogen pretreatment at 250 °C, the carbon formation is reduced in DRM reaction for $CeNi_{0.2}O_Y$ and $CeNi_{0.5}O_Y$ catalysts. $CeNi_{0.3}O_Y$ catalyst shows the best catalytic performance with and without H_2 pretreatment in this series.

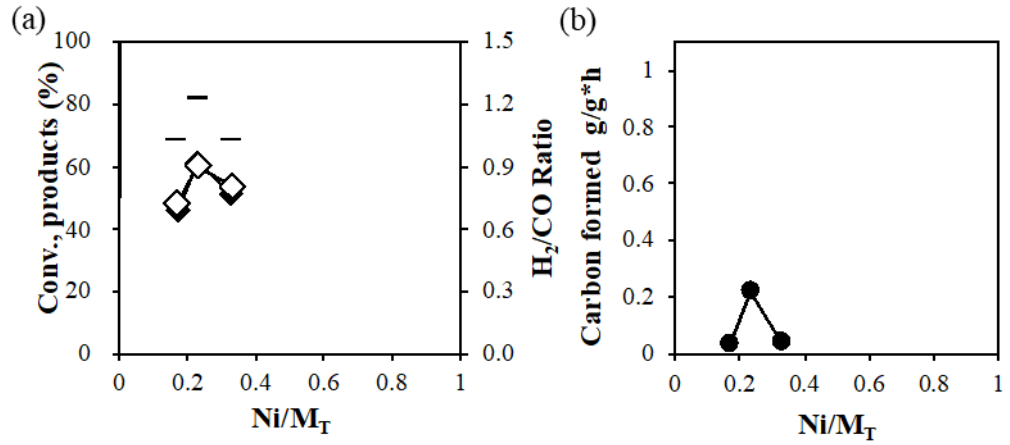

Fig. 2-2 DRM catalytic performance and carbon formation at 600°C on calcined $CeNi_XO_Y$ catalysts (50 mg) with pretreatment in H_2 at 250 °C. $CO_2/CH_4/N_2$ = 5:5:90%. CH_4 (◆), CO_2 (◇) and H_2/CO (-) ratio. Ni/M_T = x/(x+1). Time of experiments = 5h.

2.A.2.2 On $CeZr_{0.5}Ni_XO_Y$ catalysts

2.A.2.2.a Influence of time

The catalytic performance of Zr based compounds without pretreatment are shown in Fig. 2-13. The conversions (after 5 hours), H_2/CO ratio and carbon formation rate versus Ni content are analyzed in Fig. 2-14. $CeZr_{0.5}Ni_{0.5}O_Y$ exhibits the best stability in DRM after 1 hour. The conversions are quite stable after 1h and after the 5 h test, conversions of CH_4 and CO_2 are of 54.6 % and 58.7 %, respectively at 600 °C. The H_2/CO ratio is of 1.01 and the carbon formation rate is only of 0.017 $g \cdot gcat^{-1} \cdot h^{-1}$. While the $CeZr_{0.5}Ni_5O_Y$ shows the highest conversions, with CH_4 and CO_2 conversions of 68.7 % and 66.1 % respectively. It leads to a high H_2/CO ratio of 2.26 in agreement with the high formation of carbon of 1.23 $g \cdot gcat^{-1} \cdot h^{-1}$.

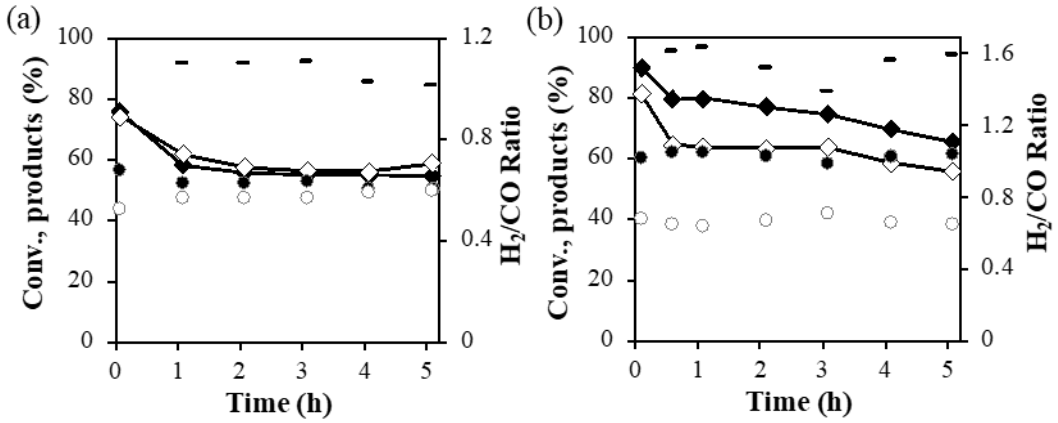

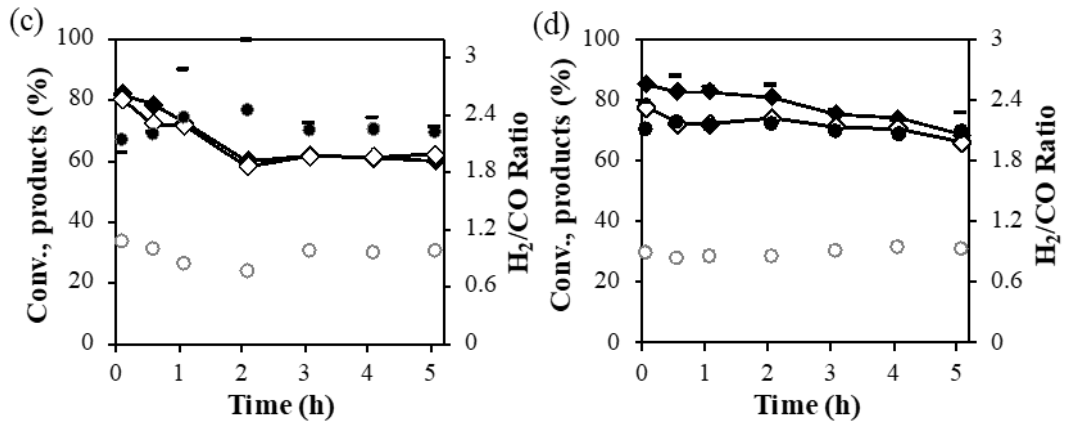

Fig. 2-13 DRM catalytic performance at 600 °C on calcined a) $CeZr_{0.5}Ni_{0.5}O_Y$, b) $CeZr_{0.5}Ni_1O_Y$, c) $CeZr_{0.5}Ni_2O_Y$, and d) $CeZr_{0.5}Ni_5O_Y$ catalysts (50 mg) without pretreatment. CH_4 (◆), CO_2 (◇) conversions, H_2 (●), CO (○), in mol % and the H_2/CO ratio (-). $CH_4/CO_2/N_2$ = 5:5:90%.

2.A.2.2.b Influence of Ni content

On this ternary Zr based compounds, the conversions of reactants increase slightly with the Ni content, while the H_2/CO ratio and carbon formation increase largely. Therefore, the $CeZr_{0.5}Ni_{0.5}O_Y$ catalyst with low Ni content is very performant and leads to the expected H_2/CO ratio of 1 in DRM, with few carbon formations.

Swirk et al. investigated dry reforming on HTNi-Zr catalyst in the continuous fixed-bed flow reactor (GHSV = 20000 h^{-1}, mass of catalyst = 150 mg, total flow rate = 100 ml/min, $CO_2/CH_4/Ar$=1:1:8, T = 600 °C)[140]. 55 % of CH_4 conversion and 55 % of CO_2 conversion were obtained. And the H_2/CO ratio was of 0.85. We get higher conversions values in this study but with less catalyst and with no carbon deposition.

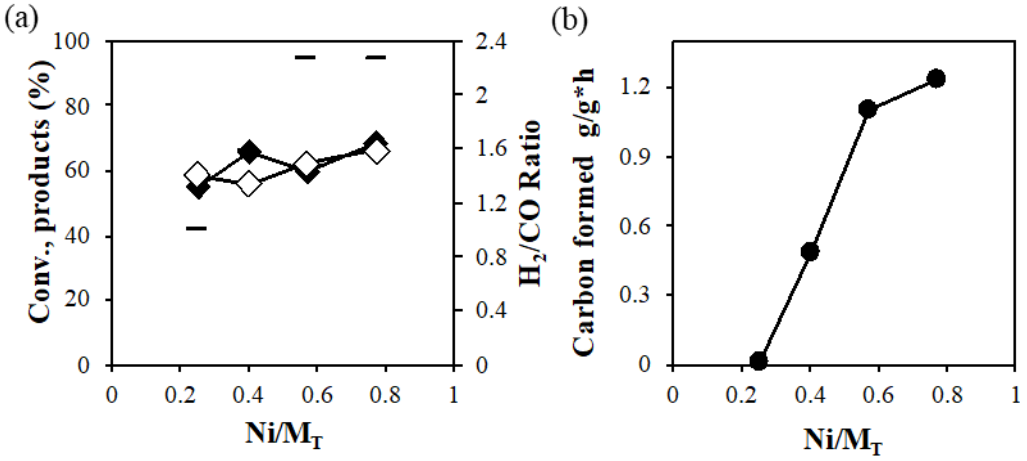

Fig. 2-14 DRM catalytic performance and carbon formation at 600°C on calcined $CeZr_{0.5}Ni_XO_Y$ catalysts (50 mg) without pretreatment. $CO_2/CH_4/N_2$ = 5:5:90%. CH_4 (◆), CO_2 (◇)

and H_2/CO (-) ratio. $Ni/M_T = x/(x+1+0.5)$. Time of experiments = 5h.

2.A.2.2.c Stability test

The catalytic stability test at 600°C on calcined $CeZr_{0.5}Ni_{0.5}O_Y$ catalyst without pretreatment is depicted in Fig. 2-15. A mild decay in CH_4 and CO_2 conversions is seen up to about 30 h of test followed by a relatively good stability up to 80 h under feed. The CO_2 conversion drop mildly exceeds the CH_4 conversion drop in the initial stage. After 80 h of reaction at 600 °C, the methane conversion drops down to 66.2 % (from 72.8 %), while CO_2 conversion drops from 87.7 % to 72.7 %. Furthermore, the initial H_2/CO molar ratio of 1.15 decreases to 1.0, as already observed after 5 h of test.

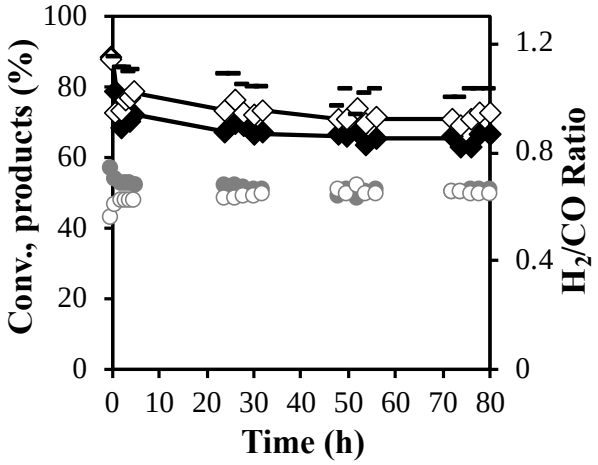

Fig. 2-15 DRM catalytic performance at 600 °C on calcined $CeZr_{0.5}Ni_{0.5}O_Y$ catalyst (50 mg) without pretreatment. CH_4 (◆), CO_2 (◇), H_2 (●), CO (○), in mol% and H_2/CO (-) ratio. $CO_2/CH_4/N_2$ = 5:5:90%.

The acquired outcomes are interesting in comparison with literature. Marinho et al. investigated dry reforming over $Ni@CeZrO_2$ catalyst at 800 °C, (adopting CH_4/CO_2 = 1 and a total flow of 100 mL/min applying 20 mg of catalysts)[163]. The CH_4 and CO_2 conversions reached 53 % and 66 %, separately, and the H_2/CO ratio reached 0.74. Furthermore, carbon in filamentous and graphitic structure largely shaped after detection. In the current investigation, very higher conversions are acquired at much lower temperature but using higher mass of compound.

2.A.2.3 On $CeAl_{0.5}Ni_XO_Y$ catalysts

2.A.2.3.a Influence of time

On calcined $CeAl_{0.5}Ni_XO_Y$ catalysts without pretreatment, the results are reported in Fig. 2-16. Globally, on all the compounds, after the first hour of test relatively good stabilities are observed during 5 h of test. For $CeAl_{0.5}Ni_5O_Y$ catalyst, the comparative

high CH_4 conversion of 82.2 % but lower CO_2 conversion of 75.6 % within the 5 hours on DRM reaction compared with other catalysts indicates the more predominant CH_4 decomposition side reaction of the former, confirmed by the higher H_2/CO ratio of 1.6 and carbon formstion rate of 0.68 $g \cdot gcat^{-1} \cdot h^{-1}$ on this catalyst.

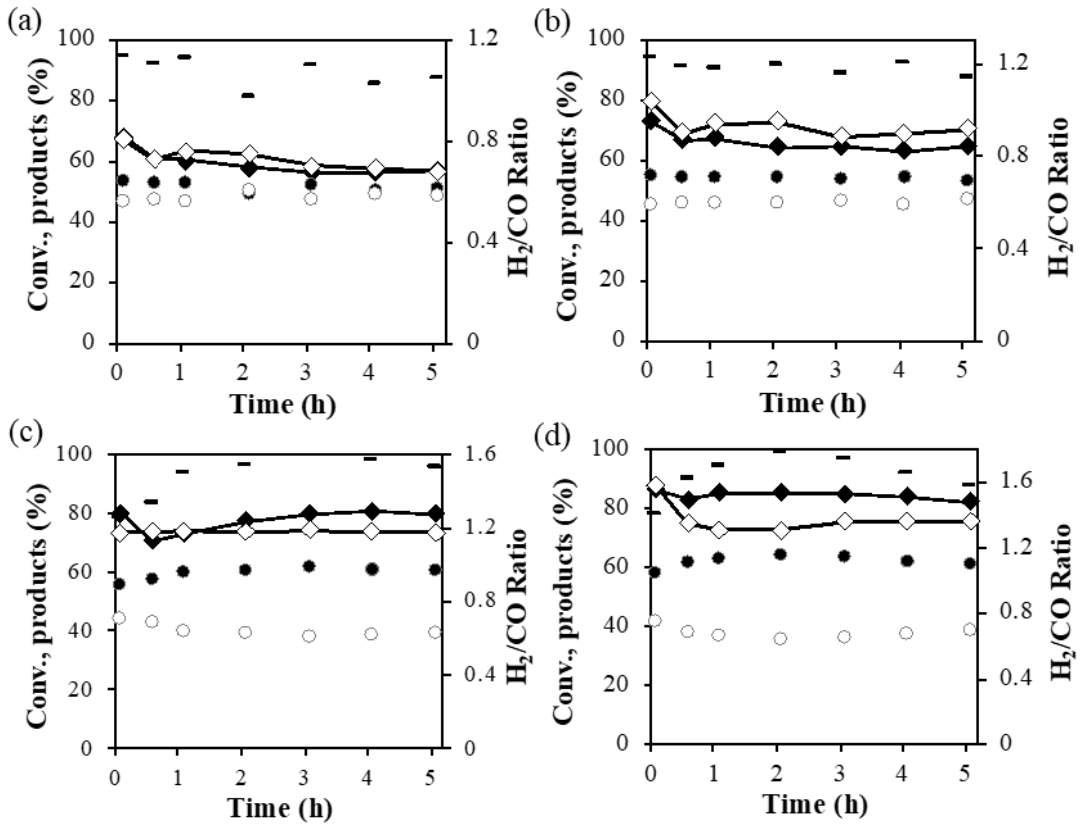

Fig. 2-16 DRM catalytic performance at 600 °C on calcined a) $CeAl_{0.5}Ni_{0.5}O_Y$, b) $CeAl_{0.5}Ni_1O_Y$, c) $CeAl_{0.5}Ni_2O_Y$, d) $CeAl_{0.5}Ni_5O_Y$ catalysts (50 mg) without pretreatment. CH_4 (◆), CO_2 (◇) conversions, H_2 (●), CO (○), in mol % and the H_2/CO ratio (-). $CH_4/CO_2/N_2$ = 5:5:90%.

2.A.2.3.b Influence of Ni content

The methane and carbon dioxide conversions and the H_2/CO ratio as a function of Ni content are reported in Fig. 2-17. The conversions increase with the increasing of Ni content in the studied range. The CO_2 conversion is close to methane conversion for low Ni content catalyst, while CH_4 conversion is higher to CO_2 conversion on the high Ni content catalysts. The carbon deposition on $CeAl_{0.5}Ni_5O_Y$ catalyst is of 0.68 $g \cdot gcat^{-1} \cdot h^{-1}$, whereas on $CeAl_{0.5}Ni_{0.5}O_Y$ catalyst the carbon formation is much lower at 0.05 $g \cdot gcat^{-1} \cdot h^{-1}$. The H_2/CO ratio increases with the increase of Ni content, which are 1.0, 1.1, 1.5, and 1.6 respectively, in agreement with the increase of carbon formation. The best catalytic performance at 600 °C without pretreatment on this series of

compounds is obtained on $CeAl_{0.5}Ni_2O_Y$, with CH_4 and CO_2 conversions of 79.7 % and 73.4 %, respectively, and a H_2/CO ratio of 1.5.

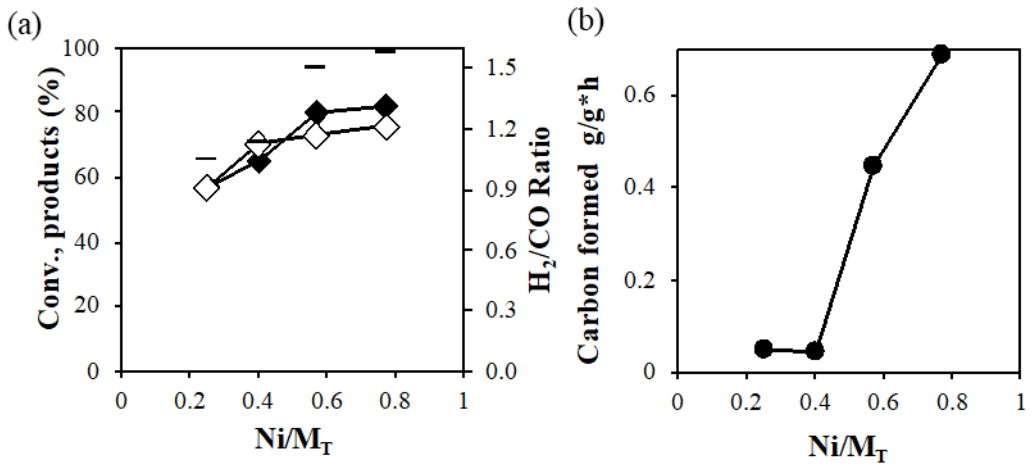

Fig. 2-17 DRM catalytic performance and carbon formation at 600°C on calcined $CeAl_{0.5}Ni_XO_Y$ catalysts (50 mg) without pretreatment. $CO_2/CH_4/N_2$ = 5:5:90%. CH_4 (◆), CO_2 (◇) and H_2/CO (-) ratio. Ni/M_T = x/(x+1+0.5). Time of experiments = 5h.

2.A.2.3.c Stability test

For examining the catalyst stability in the DRM reaction, stability detection of 80 h of time on stream are performed over $CeAl_{0.5}Ni_1O_Y$ featuring low Ni concentration. Fig. 2-18 exhibits the methane and CO_2 conversion and H_2/CO ratio as a function of time during the long-run detection at 600 °C. The catalytic conversion of CH_4 and CO_2 reaches 66.5 % and 72.6 %, separately. The H_2/CO molar ratio acquired reaches 1.07, so a ratio of 1, as expected in DRM. The carbon formation rate is of 0.009 $g \cdot gcat^{-1} \cdot h^{-1}$. Furthermore, the catalyst keeps stable activity without deactivation during 80 h on stream.

In general, the Ni-based catalysts could be less active in longer reaction time or lower reaction temperatures. Despite this, all the outcomes present that $CeAl_{0.5}Ni_1O_Y$ is highly active for DRM reaction and doesn't have activity loss after 80 h of reaction under serious conditions.

Jawad et al. reported that in the test condition of $CO_2/ CH_4/ N_2$ = 1:1:18, total flow of 200 mL/min, with 10 mg of Pt/FeMo/Ni/Al_2O_3-CeO_2 catalyst, at 700 °C, 81 % and 86 % conversions of CH_4 and CO_2, respectively[175]. And the H_2/CO ratio was of 0.91. In the present study, similar conversions are obtained on $CeAl_{0.5}Ni_1O_Y$ without adding noble metal and at lower temperature and lower total flow but using higher mass of catalyst.

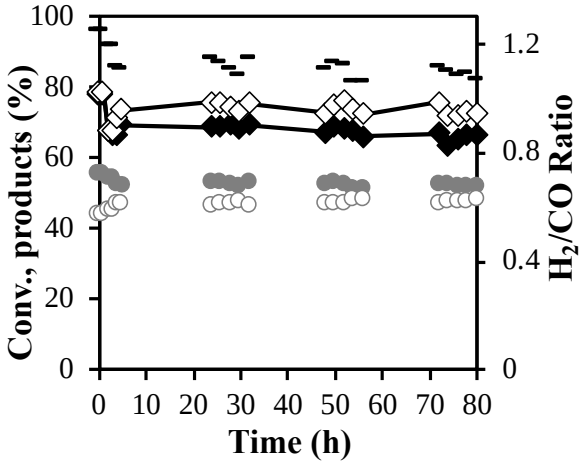

Fig. 2-18 DRM catalytic performance at 600°C on calcined $CeAl_{0.5}Ni_1O_Y$ catalyst (50 mg) without pretreatment. CH_4 (◆), CO_2 (◇), H_2 (●), CO (○), in mol% and H_2/CO (-) ratio. $CO_2/CH_4/N_2$ = 5:5:90%.

2.A.2.4 On $AlMg_2Ni_XO_Y$ catalysts

2.A.2.4.a Influence of time

On $AlMg_2Ni_XO_Y$ catalysts at 600 °C without pretreatment, (96000 mL/g·h) the results are shown in Fig. 2-19. For all the compounds, relatively good stability is observed after 1 h of test and during 5 h. It can be observed that both CH_4 and CO_2 conversions decrease in first one hour for $AlMg_2Ni_1O_Y$ and $AlMg_2Ni_3O_Y$ catalysts. $AlMg_2Ni_{12}O_Y$ exhibits both the highest and the most stable CH_4 and CO_2 conversions. There is a 4 % and 1 % decrease for CH_4 and CO_2 conversions and then stability at 83.6 % and 80.0 % of CH_4 and CO_2 conversions, respectively, after 5 hours on stream is observed.

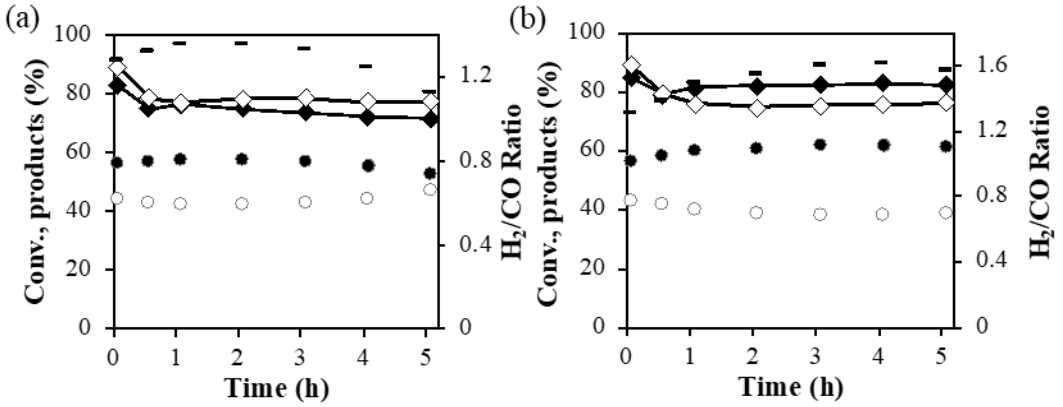

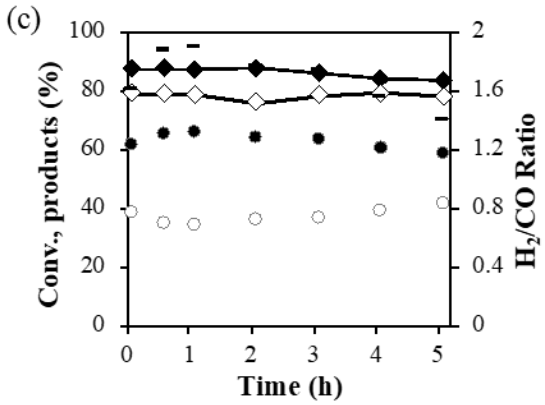

Fig. 2-19 DRM catalytic performance at 600 °C on calcined a) $AlMg_2Ni_1O_Y$, b) $AlMg_2Ni_3O_Y$, and c) $AlMg_2Ni_{12}O_Y$ catalysts (50 mg) without pretreatment in H_2. CH_4 (◆), CO_2 (◇) conversions, H_2 (●), CO (○), in mol % and the H_2/CO ratio (-). $CH_4/CO_2/N_2$ = 5:5:90%.

2.A.2.4.b Influence of Ni content

The effect of nickel content on on this series of samples is shown in Fig. 2-20. Globally the same conversion of CO_2 is obtained on all compounds (close to 80 % and close to CH_4 conversion), while CH_4 conversion increases with Ni content, so CH_4 conversion becomes slightly higher that CO_2 conversion on high Ni content compounds. The H_2/CO ratios are higher than 1 and the lowest value is obtained on low Ni content compound, while carbon formation increases largely with Ni content (from about 0.08 $g \cdot gcat^{-1} \cdot h^{-1}$ up to about 0.61 $g \cdot gcat^{-1} \cdot h^{-1}$).

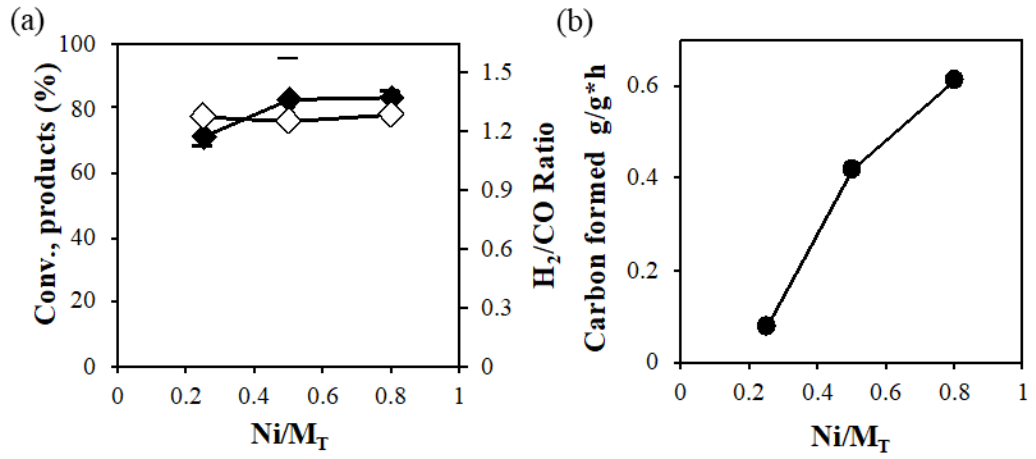

Fig. 2-20 DRM catalytic performance and carbon formation at 600°C on calcined $AlMg_2Ni_XO_Y$ catalysts (50 mg) without H_2 pretreatment. $CO_2/CH_4/N_2$ = 5:5:90%. CH_4 (◆), CO_2 (◇) and H_2/CO (-) ratio. Ni/M_T = x/(x+1+2). Time of experiments = 5h.

2.A.2.4.c Influence of pretreatment

The effect of pretreatment is studied on $AlMg_2Ni_XO_Y$ catalysts when comparing Fig. 2-9 (which is shown again here for easy comparison) and 2-20, both CH_4 and CO_2

conversions are quite same under the conditions without catalyst pretreatment and with in-situ pretreatment in H_2 at 450 °C. Moreover, the H_2/CO ratio and carbon formation rate are similar with or without H_2 pretreatment. For example, $AlMg_2Ni_3O_Y$ catalyst presents 82.4 % and 76.2 % of CH_4 and CO_2 conversions without in situ H_2 pretreatment and 85.0 % and 79.2 % with 12 h in situ H_2 pretreatment. The H_2/CO ratio are 1.57 and 1.55 without and with 12 h in situ H_2 pretreatment respectively. The carbon formation rates are 0.42 and 0.41 $g \cdot gcat^{-1} \cdot h^{-1}$ without and with H_2 pretreatment. Therefore, very interesting results are obtained, as avoiding the pretreatment allows saving energy.

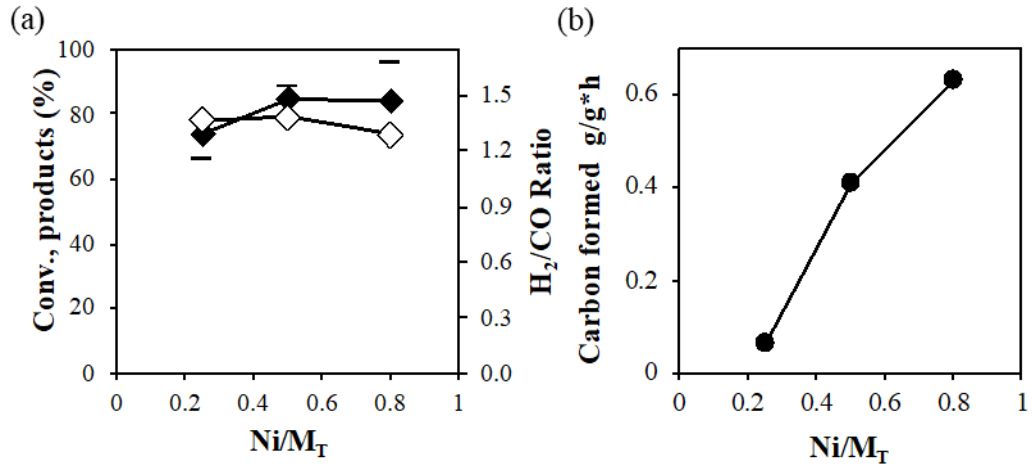

Fig. 2-9 DRM catalytic performance and carbon formation at 600 °C on calcined $AlMg_2Ni_XO_Y$ catalysts (50 mg) with pretreatment in H_2 at 450°C. $CO_2/CH_4/N_2$ = 5:5:90%. CH_4 (◆), CO_2 (◇) and H_2/CO (-) ratio. Ni/M_T = x/(x+1+2). Time of experiments = 5h.

2.A.3 Catalytic performance at 800 °C on catalysts with H_2 pretreatment

Dry reforming of methane experiments are carried out under atmospheric pressure at 800 °C with 10 mg of catalyst in the fixed-bed reactor with CH_4/ CO_2 ratio of 1:1 for 5 hours of time on stream.

2.A.3.1 On $CeNi_XO_Y$ catalysts

2.A.3.1.a Influence of time

DRM catalytic performance at 800 °C with H_2 pretreatment is studied on $CeNi_{0.3}O_Y$ and $CeNi_{0.5}O_Y$ catalysts. The evolutions of methane and carbon dioxide conversion and H_2, CO formation and H_2/CO ratio are analyzed and shown in Fig. 2-21. For the low Ni content $CeNi_{0.3}O_Y$ compound, methane and carbon dioxide conversions are of 22.2 % and 22.5 %, respectively, and H_2/CO ratio is of 0.67 after 5 hours. On $CeNi_{0.5}O_Y$ catalyst, methane and CO_2 conversions of 96.3 and 91.9 % are obtained at first, then decrease within the first three hours and finally stabilize at 26.7 % and 29.3 %.

The H_2/CO ratio obtained on $CeNi_{0.5}O_Y$ after 5 hours is of 0.75. Therefore, good stable state is obtained on these compounds at 5 h of test.

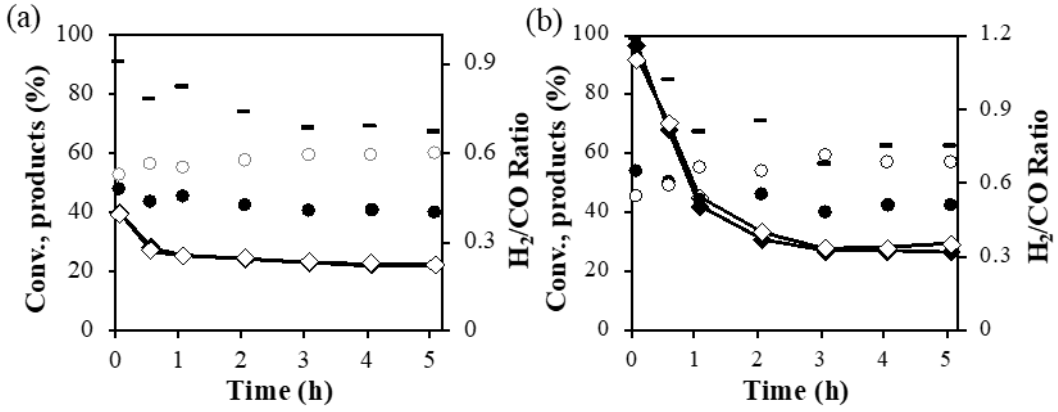

Fig. 2-21 DRM catalytic performance at 800 °C on calcined a) $CeNi_{0.3}O_Y$, and b) $CeNi_{0.5}O_Y$ catalysts (10 mg) with in situ H_2 pretreatment at 250 °C. CH_4 (◆), CO_2 (◇) conversions, H_2 (●), CO (○), in mol % and H_2/CO ratio (-). $CH_4/CO_2/N_2$ = 5:5:90%.

2.A.3.1.b Influence of Ni content

The catalytic results obtained depend on Ni content of $CeNi_XO_Y$ catalysts, as presented in Fig. 2-22. At 800 °C with H_2 pretreatment, as the nickel content increases from 9.5 wt. % to 14 wt.%, the conversions of methane and carbon dioxide slightly increase. On $CeNi_{0.3}O_Y$, 0.15 g/g·h carbon deposition is obtained, while it is of 0.04 g/g·h on $CeNi_{0.5}O_Y$.

Regardless of the carbon shaping and catalytic stability, the H_2 generation acquired on the current $CeNi_XO_Y$ catalyst is comparable to the values reported in the recent literature[173], where authors reported the dry reforming over 500 mg of 0.8Co-Ni/CeO_2 catalyst at 800 °C, adopting total flowing rate of 100 mL/min, and CO_2/ CH_4/ N_2 = 3:3:4. Their optimal outcome, 77 % of CH_4 conversion and 80 % of CO_2 conversion were acquired after 10 h of detection. The H_2/CO ratio reached 0.9. Hence, $CeNi_XO_Y$ appear as highly efficient, stable catalysts for methane dry reforming regarding the low mass of catalyst involved.

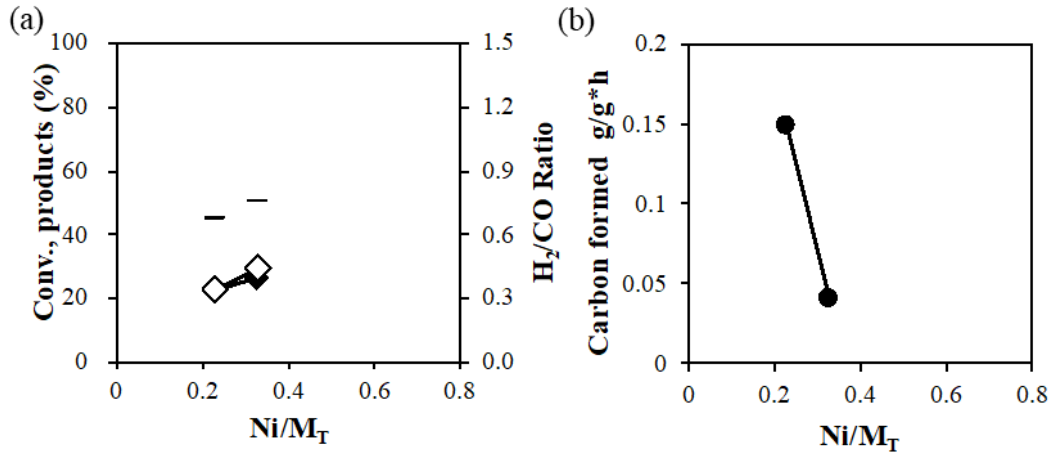

Fig. 2-22 DRM catalytic performance and carbon formation at 800 °C on calcined $CeNi_XO_Y$ catalysts (10 mg) with in situ pretreatment in H_2 at 250°C. $CO_2/CH_4/N_2$ = 5:5:90%. CH_4 (◆), CO_2 (◇) and H_2/CO (-) ratio. $Ni/M_T = x/(x+1)$. Time of experiments = 5h.

2.A.3.2 On dried $CeZr_{0.5}Ni_XO_Y$ catalysts

2.A.3.2.a Influence of time

Fig. 2-23 shows the CH_4 and CO_2 conversions and H_2, CO mol % and H_2/CO ratio with the reaction time on DRM for all the dried Zr compounds catalysts samples. The CH_4 and CO_2 conversions on $CeZr_{0.5}Ni_{0.5}O_Y$ decrease in first 2 hours and stay stable at 16.1 % and 15.1 % till 5 hours. The H_2/CO ratio also decreases with time and stay at 0.53. Similarly, $CeZr_{0.5}Ni_1O_Y$ presents a decay on reactants conversion in first 2 h and stays stable at 62.9 % and 63 % for CH_4 and CO_2 conversions. The H_2/CO ratio is 1.0 after 5 h on reaction. However, $CeZr_{0.5}Ni_2O_Y$ and $CeZr_{0.5}Ni_5O_Y$ show a stable CH_4 and CO_2 conversions around 95 % and 90 %. The H_2/CO ratio also remains stable around 1.15 during the reaction.

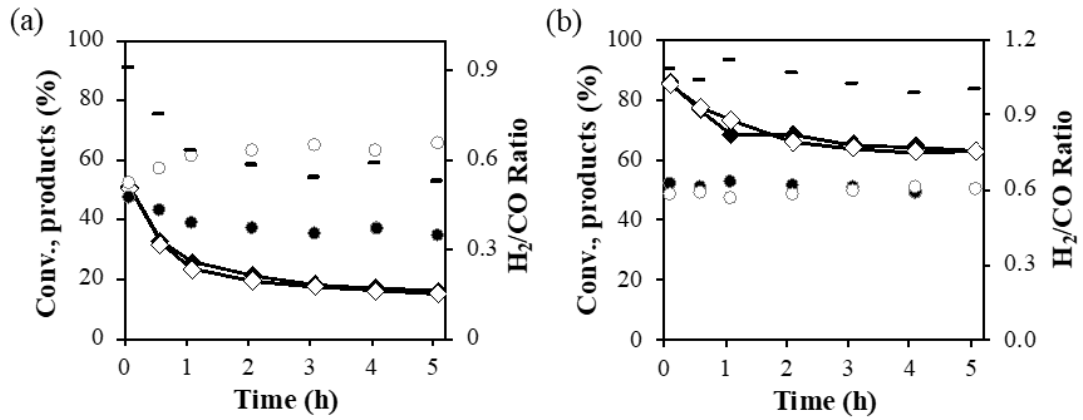

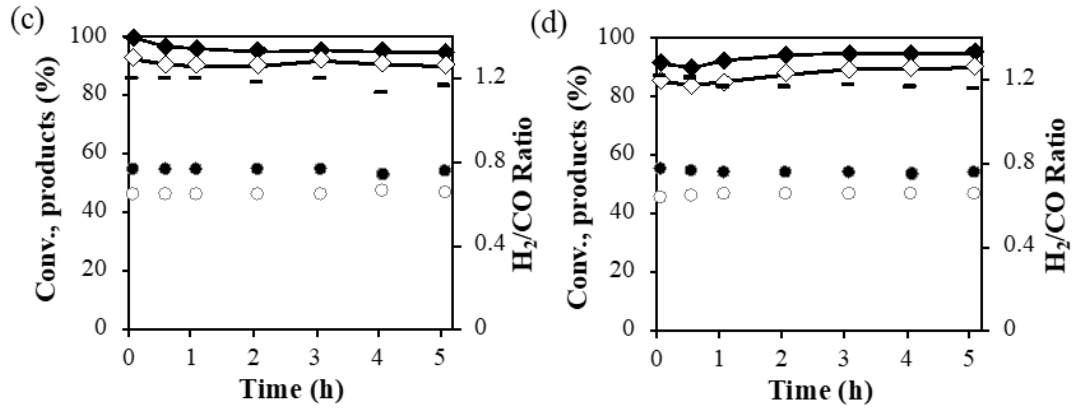

Fig. 2-23 DRM catalytic performance at 800 °C on dried a) $CeZr_{0.5}Ni_{0.5}O_Y$, b) $CeZr_{0.5}Ni_1O_Y$, c) $CeZr_{0.5}Ni_2O_Y$, and d) $CeZr_{0.5}Ni_5O_Y$ catalysts (10 mg) with in situ H_2 pretreatment at 250 °C. CH_4 (◆), CO_2 (◇) conversions, H_2 (●), CO (○), in mol % and H_2/CO ratio (-). $CH_4/CO_2/N_2$ = 5:5:90%.

2.A.3.2.b Influence of Ni content

How Ni concentration affects the catalytic performance of the dried Zr based compounds are exhibited in Fig. 2-24. Generally, CH_4 and CO_2 conversions increase as Ni content rises. As the Ni concentration is raised from 10.8 wt.% to 30.6 wt.%, the CH_4 and CO_2 conversions and the H_2/CO ratio ascend noticeably. The $CeZr_{0.5}Ni_2O_Y$ and $CeZr_{0.5}Ni_5O_Y$ catalysts show the highest CH_4 and CO_2 conversions featuring the highest H_2/CO ratios during the 5 h. The H_2/CO ratio rises as Ni loading rises, rather near 1.2 for the reaction at 800 °C. Side reactions occurrence is possibly acquired, majorly RWGS reaction and CH_4 decomposition. The latter is favored at high temperatures, which could cause enriching H_2 in the blend. At high temperature, the DRM is more popular, and the CH_4 and CO_2 reactants are efficiently transformed. Hence, the lower amount of CO_2 available for the RWGS offers H_2/CO ratio nearer solidarity as anticipated if only the DRM reaction exists. Furthermore, it's known that high temperature also helps steam reforming of methane (SRM), which could be another probable cause of the raised H_2/CO ratio at a high temperature. Globally, the same evolution of the catalytic behavior is acquired on other catalysts featuring various Ni concentrations. In Debek's work, methane conversion approached 86 % and CO_2 conversion got 90 % on HNiZr3 catalyst with the condition of GHSV=20000 / h, total flow = 100 mL/min, CO_2/ CH_4/ Ar = 1:1:8 at 750 °C[118].

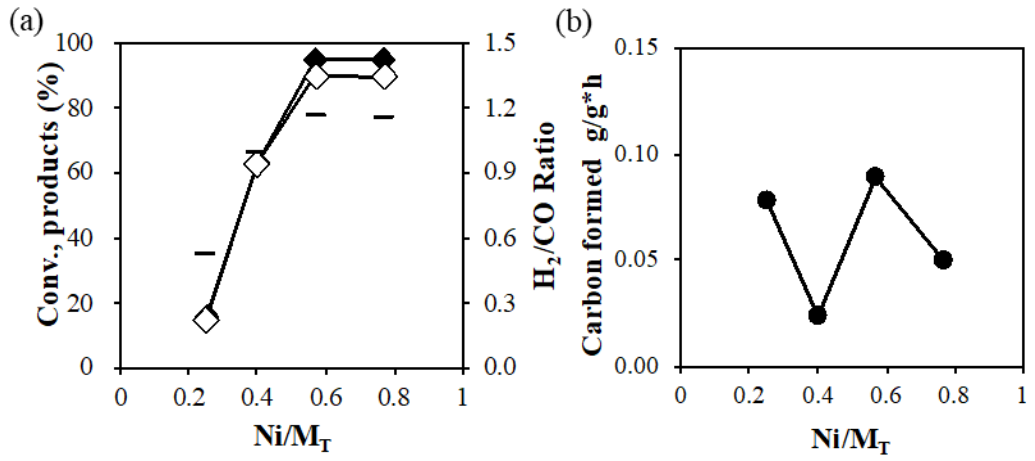

Fig. 2-24 DRM catalytic performance and carbon formation at 800°C on dried $CeZr_{0.5}Ni_XO_Y$ catalysts (10 mg) with in situ pretreatment in H_2 at 250°C. $CO_2/CH_4/N_2$ = 5:5:90%. CH_4 (◆), CO_2 (◇) and H_2/CO (-) ratio. Ni/M_T = x/(x+1+0.5). Time of experiments =5h.

2.A.3.2.c Stability test

The stability test is carried out to investigate the performance of the calcined $CeZr_{0.5}Ni_2O_Y$ catalyst over a long time of 80 h time-on-stream at 800 °C. The obtained conversion values (CH_4 and CO_2) and products ratio (H_2/CO) are plotted as a function of time on stream in Fig. 2-25. At the beginning, CH_4 and CO_2 conversions increase with time in first 10 h. And there is no decay in CH_4 and CO_2 conversions observed after 10 h. After 80 h of reaction at 800 °C, the methane conversion is of 98.8%, while CO_2 conversion is of 93.5%. Moreover, the initial H_2/CO molar ratio is at 1.1 and the value increases to 1.2 in 80 h of time on stream.

In Pavlova et al. work, Ni-$Ce_{0.5}Zr_{0.5}$ catalyst prepared by impregnation method was applied to methane dry reforming reaction. The CH_4 conversion was of 88% and the H_2/CO ratio was at 0.85 after 3 hours in the condition of CH_4/ CO_2/ He = 5%:5%:90%, at 700°C[198].

In the present study, higher conversions and lower carbon formation rate are obtained on $CeNi_{0.5}Zr_2O_Y$. The CH_4 and CO_2 conversions are 98.8% and 93.5%, respectively, and the H_2/CO ratio is 1.2 at 800 °C after 80 hours (with 5 % CH_4; CH_4/CO_2 = 1, total flow of 80 mL/min, 10 mg of catalyst, 480000 $mL \cdot gcat^{-1} \cdot h^{-1}$). Moreover, carbon is formed with a rate of 0.004 $g \cdot g_{cat}^{-1} \cdot h^{-1}$.

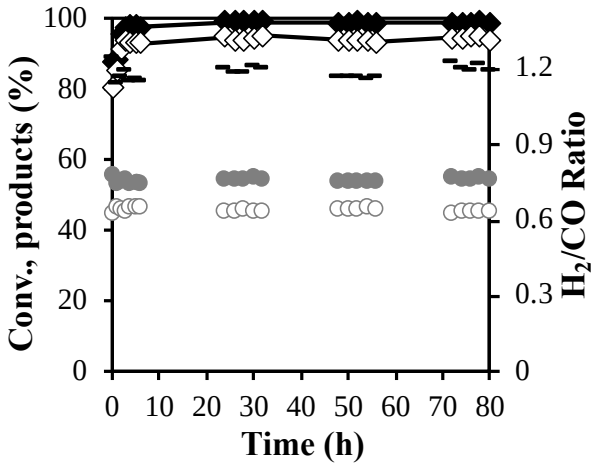

Fig.2-25 DRM catalytic performance at 800 °C on calcined $CeZr_{0.5}Ni_2O_Y$ catalyst (10 mg) with in situ H_2 pretreatment at 250 °C. CH_4 (◆), CO_2 (◇), H_2 (●), CO (○), in mol% and H_2/CO (-) ratio. $CO_2/CH_4/N_2$ = 5:5:90%.

2.A.3.3 Stability of $CeAl_{0.5}Ni_2O_Y$ catalysts

In order to investigate the catalytic performance of the $CeAl_{0.5}Ni_2O_Y$ catalyst a constant temperature test is accomplished at 800 °C for 80 h. As shown in Fig. 2-26, the ternary catalyst exhibits high conversions even using very low mass of 10 mg of catalyst. The CH_4 and CO_2 conversions are 80% and 92%, respectively, and the H_2/CO ratio is quite high at 1.3 at 800°C after 5 hours (10 mg of catalyst, CH_4/CO_2 = 1, 480000 $mL \cdot gcat^{-1} \cdot h^{-1}$), in diluted conditions (5% CH_4). Interestingly, conversions increase with time with a stabilization after about 50 h.

Compared to literature, Damyanova et al. studied $Ni/xCeO_2$-Al_2O_3 catalyst in dry reforming at 550 °C, 50 mg of catalyst were used in the test and the total flow was 100 mL/min, CH_4/ CO_2/ N_2 in a ratio of 1:1:3[180]. The catalyst with large surface area and promoted dispersion showed conversions for CH_4 and CO_2 at 57 % and 69 %, respectively, after 8 h of reaction. The H_2/CO ratio was reported at 0.63.

Similar study was reported by Zhan et al., they performed DRM at 700 °C on a series of Ni-Ce-Al composite oxides with Ce replaced by K, Mg, Y, prepared by self-assembly (EISA) strategy. 100 mg of catalyst was tested in CH_4/ CO_2 =1:1 condition, with a GHSV= 48 L/g·h. The best catalyst with Ce was giving 67 % and 73 % of conversions for CH_4 and CO_2 respectively. The H_2/CO ratio obtained in their study was of 0.83[199].

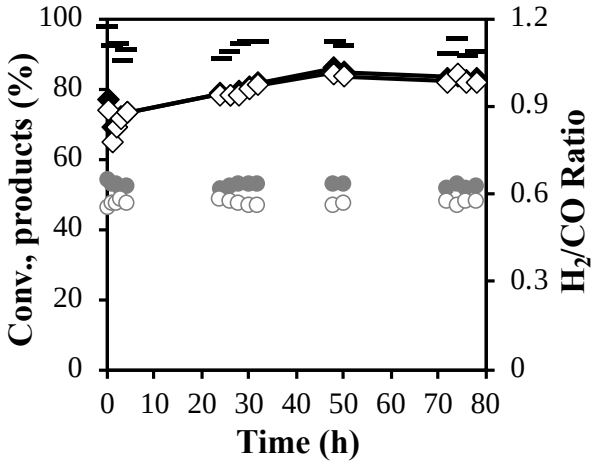

Fig. 2-26 DRM catalytic performance at 800 °C on calcined $CeAl_{0.5}Ni_2O_Y$ catalyst (10 mg) with in situ H_2 pretreatment at 250 °C. CH_4 (◆), CO_2 (◇), H_2 (●), CO (○), in mol% and H_2/CO (-) ratio. $CO_2/CH_4/N_2$ = 5:5:90%.

2.A.3.4 Stability of $AlMg_2Ni_{12}O_Y$ catalysts

The catalytic performance of the $AlMg_2Ni_{12}O_Y$ catalyst is shown in Fig. 2-27. The $AlMg_2Ni_{12}O_Y$ exhibits high CH_4 and CO_2 conversions (99.7 % and 93.8 %, respectively) and long-term stability (80 hours). The CH_4 conversion is higher than CO_2 conversion, and the H_2/CO ratio is 1.2 higher than unit. The carbon formation rate in this case is of 0.006 $g \cdot gcat^{-1} \cdot h^{-1}$. The $AlMg_2Ni_{12}O_Y$ catalyst exhibits a good carbon resistant performance.

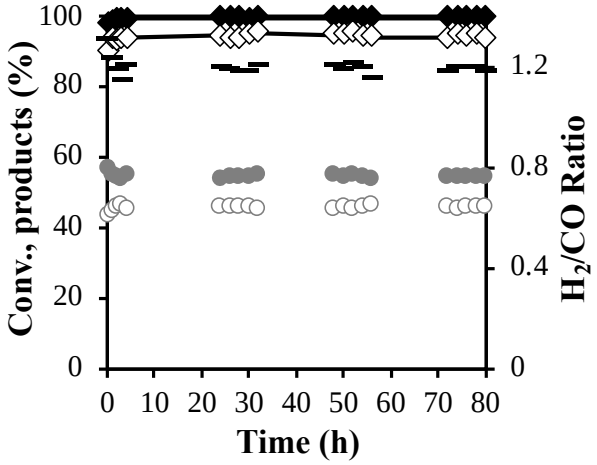

Fig. 2-27 DRM catalytic performance at 800 °C on calcined $AlMg_2Ni_{12}O_Y$ catalyst (10 mg) with in situ H_2 pretreatment at 450 °C. CH_4 (◆), CO_2 (◇), H_2 (●), CO (○), in mol% and H_2/CO (-) ratio. $CO_2/CH_4/N_2$ = 5:5:90%.

2.A.4 Catalytic performance at 800 °C on catalysts without H_2 pretreatment

2.A.4.1 Stability of $CeNi_1O_Y$ catalysts

The performance of the $CeNi_1O_Y$ catalyst without H_2 pretreatment is investigated over a long time of 80 h time-on-stream at 800°C t in reactants mixture of CH_4/ CO_2/ N_2 = 5 %:5 %:90 %.

As is shown in Figure 2-28, for the non-pretreated catalyst, a rapid decline of conversions (that are close to 90-100 % for first hours) and H_2/CO ratio are observed within the 50 hours of time on stream. Then 50.7 % conversion of CH_4 and 55.8 % conversion of CO_2 are obtained after 80 hours. Moreover, the initial H_2/CO molar ratio of 1.19 decreases to 0.90 in 80 h of time on stream.

The obtained results are interesting when compared to literature. Tu et al. studied dry reforming over paper-structured CeO_2-NiO-5.5 catalyst at a temperature of 750 °C, (GHSV = 2300 /h, 40 mL/min CO_2/ CH_4 =1:1)[162]. The CH_4 and CO_2 conversions were of 91.9 % and 87 %, respectively, and the H_2/CO ratio was 0.9 after 50 hours. Besides, carbon in filamentous and graphitic structure was largely formed after test.

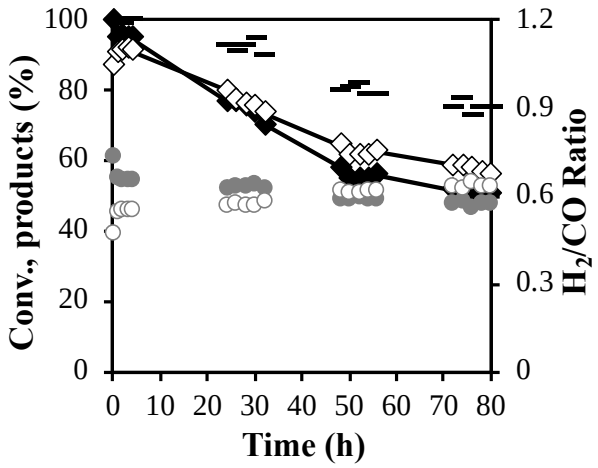

Fig. 2-28 DRM catalytic performance at 800 °C on calcined $CeNi_1O_Y$ catalyst (10 mg) without H_2 pretreatment. CH_4 (◆), CO_2 (◇), H_2 (●), CO (○), in mol% and H_2/CO (-) ratio. $CO_2/CH_4/N_2$ = 5:5:90%.

2.A.4.2 On dried $CeZr_{0.5}Ni_XO_Y$ catalysts

Another objective is to explore the dried Zr based catalysts in the DRM reaction at 800 °C and stability. On this purpose, dried $CeZr_{0.5}Ni_XO_Y$ **(**10 mg) is carried in the reactor without any pretreatment in H_2. As before, the reaction conditions used are CH_4/ CO_2/ N_2 = 5:5:90%.

2.A.4.2.a Influence of time

The results obtained on dried $CeZr_{0.5}Ni_XO_Y$ are shown in Fig. 2-29. The result for $CeZr_{0.5}Ni_5O_Y$ is impressive due to very high conversions of CH_4 and CO_2 in all the period of time (CH_4 and CO_2 conversions at 98.7 % and 93.9 %, respectively). A H_2/CO ratio of 1.19 is obtained on $CeZr_{0.5}Ni_5O_Y$ catalyst in such conditions. $CeZr_{0.5}Ni_2O_Y$ catalyst presents a similar result to $CeZr_{0.5}Ni_5O_Y$, with CH_4 and CO_2 conversions at 96.0 % and 90.6 %, respectively. But the carbon deposition rate on $CeZr_{0.5}Ni_2O_Y$ (0.23 $g \cdot gcat^{-1} \cdot h^{-1}$) is much higher than on $CeZr_{0.5}Ni_5O_Y$ (0.02 $g \cdot gcat^{-1} \cdot h^{-1}$). For low Ni content catalysts, $CeZr_{0.5}Ni_{0.5}O_Y$ provides 20.8 % and 18.9 % of CH_4 and CO_2 conversions, respectively. However, the H_2/CO ratio is of 0.59. For $CeZr_{0.5}Ni_1O_Y$, methane and carbon dioxide conversions are maintained at 69.1 % and 69.3 % respectively, and the H_2/CO ratio is equal to unity after 5 hours of reaction.

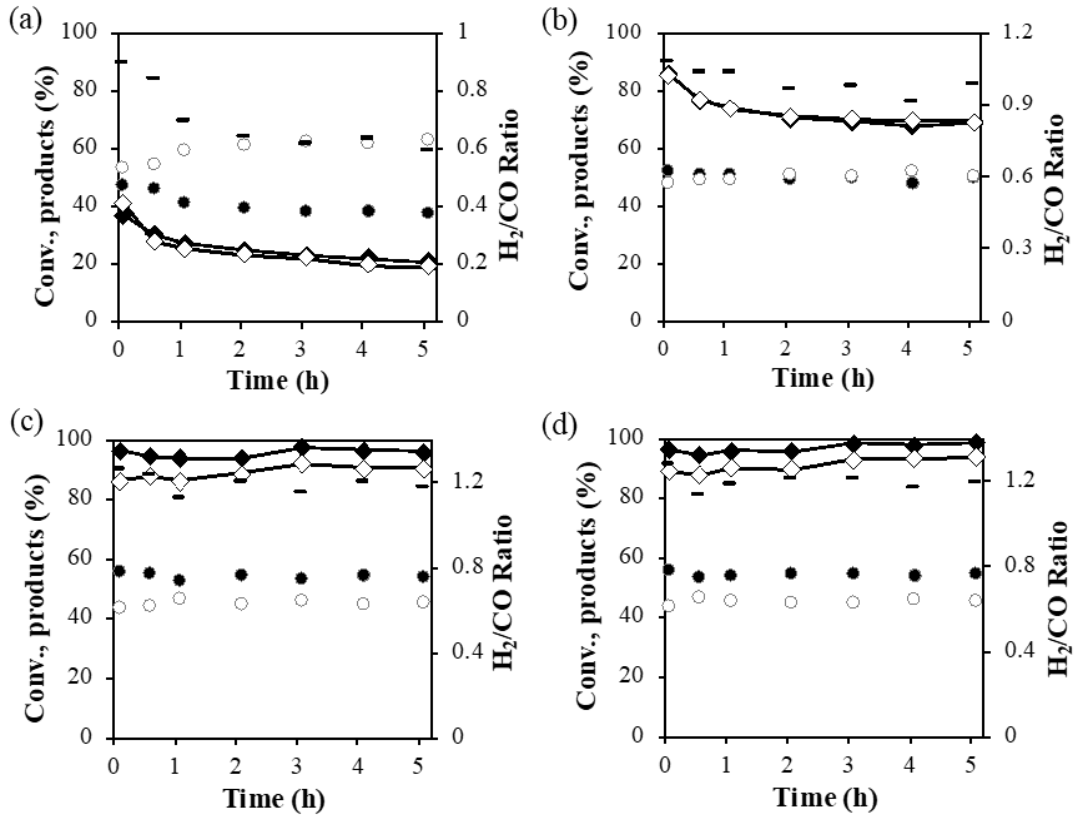

Fig. 2-29 DRM catalytic performance at 800 °C on dried a) $CeZr_{0.5}Ni_{0.5}O_Y$, b) $CeZr_{0.5}Ni_1O_Y$, c) $CeZr_{0.5}Ni_2O_Y$, and d) $CeZr_{0.5}Ni_5O_Y$ catalysts (10 mg) without H_2 pretreatment. CH_4 (◆), CO_2 (◇) conversions, H_2 (●), CO (○), in mol % and the H_2/CO ratio (-). $CH_4/CO_2/N_2$ = 5:5:90%.

2.A.4.2.b Influence of Ni content

For easy analysis of the effect of Ni content, the results of CH_4 and CO_2 conversions and H_2/CO ratio at 800 °C are shown in Fig. 2-30 versus Ni content (Ni/M_T

ratio). It is clear that the CH_4 and CO_2 conversions globally increase with increasing Ni content.

At 800 °C, on the catalysts containing a large amount of Ni ($CeZr_{0.5}Ni_2O_Y$ and $CeZr_{0.5}Ni_5O_Y$), the initial CH_4 and CO_2 conversions are rather high. Moreover, the carbon formation rate on $CeZr_{0.5}Ni_5O_Y$ reaches 0.024 $g \cdot gcat^{-1} \cdot h^{-1}$, lower compared to some lower Ni content catalysts. The link between carbon shaping and Ni concentration isn't linear since the amount of carbon deposited on catalyst $CeZr_{0.5}Ni_1O_Y$ is rather large, indicating that possibly the Ni concentration determines the carbon deposit, and other considerations also, as particle morphology or structure might impact carbon deposition. Furthermore, the conversions are improved in comparison to values reported on the binary Ni-Ce based catalyst. This will be profoundly discussed later on in comparison part.

Deng et al. investigated dry reforming on Ni/CeO_2-ZrO_2-SiO_2 catalyst in the continuous fixed-bed flow reactor (mass of catalyst = 500 mg, $CO_2/CH_4/N_2$=1:1:38, T = 750 °C)[135]. 96 % of CH_4 conversion and 97 % of CO_2 conversion were obtained after 20 mins of test. And the H_2/CO ratio was of 0.9. We get same conversions values in this study but with less catalyst and (in harsher conditions) and with a simple preparation method. Moreover, the catalyst is more stable than the one reported in literature.

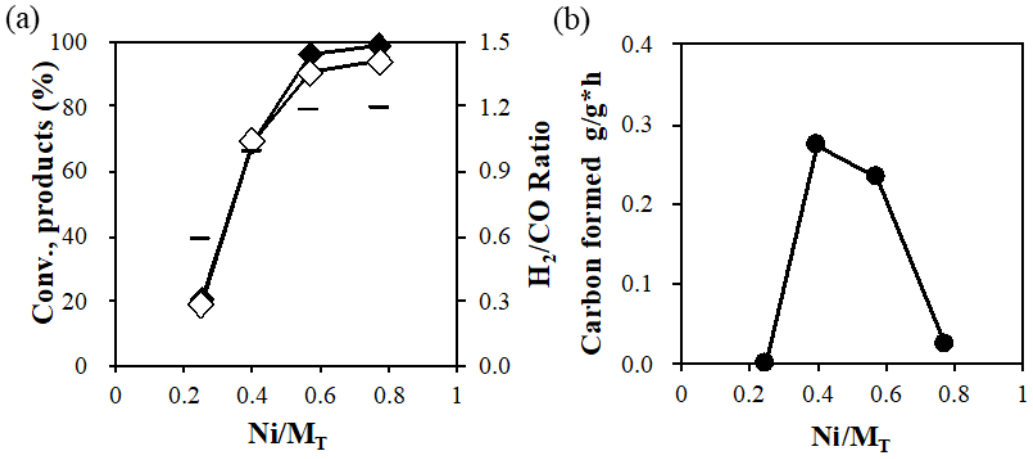

Fig. 2-30 DRM catalytic performance and carbon formation at 800 °C on dried $CeZr_{0.5}Ni_XO_Y$ catalysts (10 mg) without H_2 pretreatment. $CO_2/CH_4/N_2$ = 5:5:90%. CH_4 (◆), CO_2 (◇) and H_2/CO (-) ratio. Ni/M_T = x/(x+1+0.5). Time of experiments = 5h.

2.A.4.2.c Stability test

The study is further carried out with dried $CeZr_{0.5}Ni_2O_Y$ catalyst during 80 hours of reaction. As shown in Fig. 2-31, the catalyst exhibits stable performances all the time on stream. The catalyst exhibits a very high stability without any decline in CH_4 and

CO_2 conversions with time on stream. The loss in CH_4 conversion for $CeZr_{0.5}Ni_2O_Y$ catalyst is about 1.1 % after 80 hours, staying at 95.8 %. The CO_2 conversion is of 86.6 % at beginning and increases to 91.7 % after 80 h. The H_2/CO molar ratio is about 1.2 during the reaction. Moreover, the carbon deposition of 0.0151 $g \cdot gcat^{-1} \cdot h^{-1}$ is much lower than 0.23 $g \cdot gcat^{-1} \cdot h^{-1}$ after 5 h (Fig. 2-30) meaning that carbon formation is not linear with time, and C is probably mainly formed at the beginning of the test.

The result is competitive compared to the literature which presented the dry reforming over $CaZr_{0.8}Ni_{0.2}O_{3-\delta}$ catalyst at 800 °C, approximately 95 % of methane and CO_2 conversions were obtained with GHSV=28800 /h, 600 mg catalyst, CO_2/ CH_4/ N_2 = 1:1:1[123]. In this study, 95 % of methane conversion obtained only with 10 mg $CeZr_{0.5}Ni_2O_Y$ catalyst.

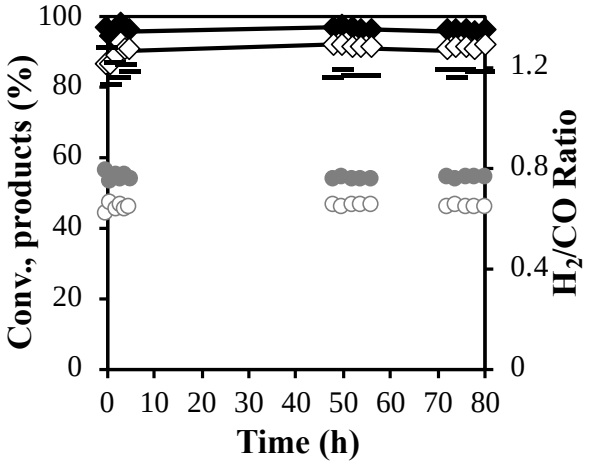

Fig. 2-31 DRM catalytic performance at 800 °C on dried $CeZr_{0.5}Ni_2O_Y$ catalyst (10 mg) without H_2 pretreatment. CH_4 (◆), CO_2 (◇), H_2 (●), CO (○), in mol% and H_2/CO (-) ratio. $CO_2/CH_4/N_2$ = 5:5:90%.

Conclusion of part A

In this part, $CeNi_XO_Y$, $CeZr_{0.5}Ni_XO_Y$, $CeAl_{0.5}Ni_XO_Y$, and $AlMg_2Ni_XO_Y$ catalysts are studied in DRM reaction with CO_2/CH_4 ratio = 1. First 50 mg of catalysts are in situ pretreated in H_2 overnight, tested on stream at 600 °C for 5 h. Among the binary catalysts tested, $CeNi_{0.3}O_Y$ has the best performance in terms of conversions (CH_4 and CO_2 conversions of 61.1 % and 60.3 %) but highest carbon deposition rate of 0.22 $g \cdot gcat^{-1} \cdot h^{-1}$. $CeNi_{0.5}O_Y$ catalyst presents CH_4 and CO_2 conversions of 53.4% and 59.1% after stability test of 80 h. For ternary catalysts, $CeZr_{0.5}Ni_5O_Y$ shows CH_4 and CO_2 conversions of 86.9 % and 61.4 %, with a H_2/CO ratio of 1.8, and a carbon deposition rate of 0.85 $g \cdot gcat^{-1} \cdot h^{-1}$. $CeAl_{0.5}Ni_2O_Y$ is the most competitive one in Al doped

compounds with CH_4 and CO_2 conversions of 81.5 % and 74.8 %, a H_2/CO ratio of 1.4 and carbon deposition rate of 0.27 $g \cdot gcat^{-1} \cdot h^{-1}$. For $AlMg_2Ni_XO_Y$ catalysts, $AlMg_2Ni_1O_Y$ is tested on stream for 80 hours, and 75.9 % and 83.2 % of CH_4 and CO_2 conversions are obtained, with a H_2/CO ratio of 1.2, and carbon deposition rate of 0.017 $g \cdot gcat^{-1} \cdot h^{-1}$.

The catalysts are also tested at 600 °C, but without in situ H_2 pretreatment. $CeNi_{0.3}O_Y$ compound shows similar result without pretreatment with a lower carbon deposition rate of 0.14 $g \cdot gcat^{-1} \cdot h^{-1}$. While the $CeZr_{0.5}Ni_5O_Y$ catalyst shows a lower CH_4 conversion of 68.7 % without pretreatment. $CeZr_{0.5}Ni_{0.5}O_Y$ shows CH_4 and CO_2 conversions of 66.2 % and 72.7 % and carbon formation rate of 0.004 $g \cdot gcat^{-1} \cdot h^{-1}$ after 80 h of stability test. $CeAl_{0.5}Ni_2O_Y$ shows no different CH_4 and CO_2 conversions but higher carbon formation rate without pretreatment. The stability test is conducted over $CeAl_{0.5}Ni_1O_Y$, and conversions of CH_4 and CO_2 reach 66.5 % and 72.6 %, respectively. The H_2/CO molar ratio obtained is about 1.07. The carbon formation rate is of 0.009 $g \cdot gcat^{-1} \cdot h^{-1}$. For $AlMg_2Ni_XO_Y$ catalysts, the CH_4 and CO_2 conversions are around 80 % and there is no effect of H_2 pretreatment.

At 600 °C, H_2 pretreatment decreases the reactants conversions of $CeNi_{0.2}O_Y$ also decreases the carbon formation rate of $CeNi_{0.2}O_Y$ and $CeNi_{0.5}O_Y$. In situ H_2 pretreatment has influence on ternary compounds. For $CeZr_{0.5}Ni_XO_Y$ catalysts, H_2 pretreatment increases the CH_4 conversions and decreases the carbon formation rate. For $CeAl_{0.5}Ni_XO_Y$ catalysts, H_2 pretreatment decreases the carbon formation. For $AlMg_2Ni_XO_Y$ catalysts, there is no effect of H_2 pretreatment.

The catalysts are examined in DRM reaction at 800 °C, with 10 mg catalyst pretreated, and under CH_4/ CO_2 ratio = 1. For binary catalysts, $CeNi_{0.5}O_Y$ shows CH_4 and CO_2 conversions of 26.7 % and 29.3 %, the H_2/CO ratio of 0.75, while carbon formation rate is of 0.04 $g \cdot gcat^{-1} \cdot h^{-1}$ after 5 h. For ternary compounds, best result is obtained on $CeNi_{0.5}Zr_2O_Y$, with CH_4 and CO_2 conversions of 98.8% and 93.5%, a H_2/CO ratio of 1.2, and carbon formation rate of 0.004 $g \cdot gcat^{-1} \cdot h^{-1}$ after 80 hours. The $CeAl_{0.5}Ni_2O_Y$ compound also presents a good result, with CH_4 and CO_2 conversions around 82%, a H_2/CO ratio is 1.1, and carbon formation rate of 0.008 $g \cdot gcat^{-1} \cdot h^{-1}$ after 80 hours. For $AlMg_2Ni_{12}O_Y$, the conversions of methane and CO_2 are of 99.7 % and 93.8 % after 80 hours, H_2/CO ratio is of 1.2, and carbon formation rate is of 0.006 $g \cdot gcat^{-1} \cdot h^{-1}$.

The catalysts are also studied in DRM at 800 °C, on 10 mg of catalyst, but without pretreatment. Calcined $CeNi_1O_Y$ catalyst shows conversions of CH_4 and CO_2 of 50.7 % and 55.8 %, H_2/CO ratio of 0.9, and carbon formation rate of 0.018 $g \cdot gcat^{-1} \cdot h^{-1}$ after 80 hours. Dried $CeZr_{0.5}Ni_2O_Y$ presents methane and CO_2 conversions of 95.8 % and 91.7 % after 80 h. The H_2/CO molar ratio is about 1.2 during the reaction. Moreover, the carbon deposition is of 0.0151 $g \cdot gcat^{-1} \cdot h^{-1}$.

2.B Dry reforming of methane on Ni-based catalysts in CO_2/CH_4 = 0.7

Dry reforming of methane with CO_2/CH_4 = 0.7 is studied in the present part over the catalysts with different formulations, and Ni contents, in approach with or without H_2 pretreatment, at 600 °C and 800 °C. The catalytic performance toward DRM is investigated under $CO_2/CH_4/N_2$ = 5:7:88% stream.

2.B.1 Catalytic performance at 600 °C on catalysts with H_2 pretreatment

2.B.1.1 On $CeNi_XO_Y$ catalysts

2.B.1.1.a Influence of time

The CH_4 and CO_2 conversions and H_2/CO ratio in the products as a function of the time are shown in Fig. 2-32. The 5 hours of catalytic test indicates that the conversion of CH_4 and CO_2 keep constant over $CeNi_{0.3}O_Y$, $CeNi_{0.5}O_Y$ and $CeNi_1O_Y$ catalysts, while a decline is noticeable in the $CeNi_{0.1}O_Y$ and $CeNi_{0.2}O_Y$ catalysts, for first hour. Some differences are also observed in H_2/CO ratio. CH_4 conversions are lower compared to CO_2 conversions, unless for $CeNi_2O_Y$. At 600 °C, CH_4 and CO_2 conversions are about 52.9% and 67.1% respectively for $CeNi_{0.5}O_Y$ after 5 h of test, with a H_2/CO ratio of around 1.28. It can be seen that, for $CeNi_2O_Y$ catalyst the reaction was stopped at about 2 h. Higher Ni content leads to blockage of the reactor probably due to the high carbon deposit of 1.1 $g \cdot gcat^{-1} \cdot h^{-1}$ on $CeNi_2O_Y$, in agreement with the high H_2/CO ratio obtained close to 2.4.

Compared to the results obtained on the same catalysts with CO_2/CH_4 = 1, the CO_2 conversions of $CeNi_{0.2}O_Y$ and $CeNi_{0.3}O_Y$ with CO_2/CH_4 = 0.7 are about the same, but CH_4 conversions with CO_2/CH_4 = 0.7 are lower than the results with CO_2/CH_4 = 1. Moreover, the H_2/CO ratio and carbon formation rate of $CeNi_{0.3}O_Y$ and $CeNi_{0.5}O_Y$ with CO_2/CH_4 = 0.7 are higher than that obtained with CO_2/CH_4 = 1. For example, on $CeNi_{0.3}O_Y$ catalyst, with CO_2/CH_4 = 1, 61 % and 60 % of CH_4 and CO_2 conversions are achieved, with H_2/CO ratio of 1.23 and carbon formation rate of 0.22 $g \cdot gcat^{-1} \cdot h^{-1}$. With CO_2/CH_4 = 0.7, 47 % and 59 % of CH_4 and CO_2 conversions are obtained, with H_2/CO ratio of 1.29 and carbon formation rate 0.36 $g \cdot gcat^{-1} \cdot h^{-1}$.

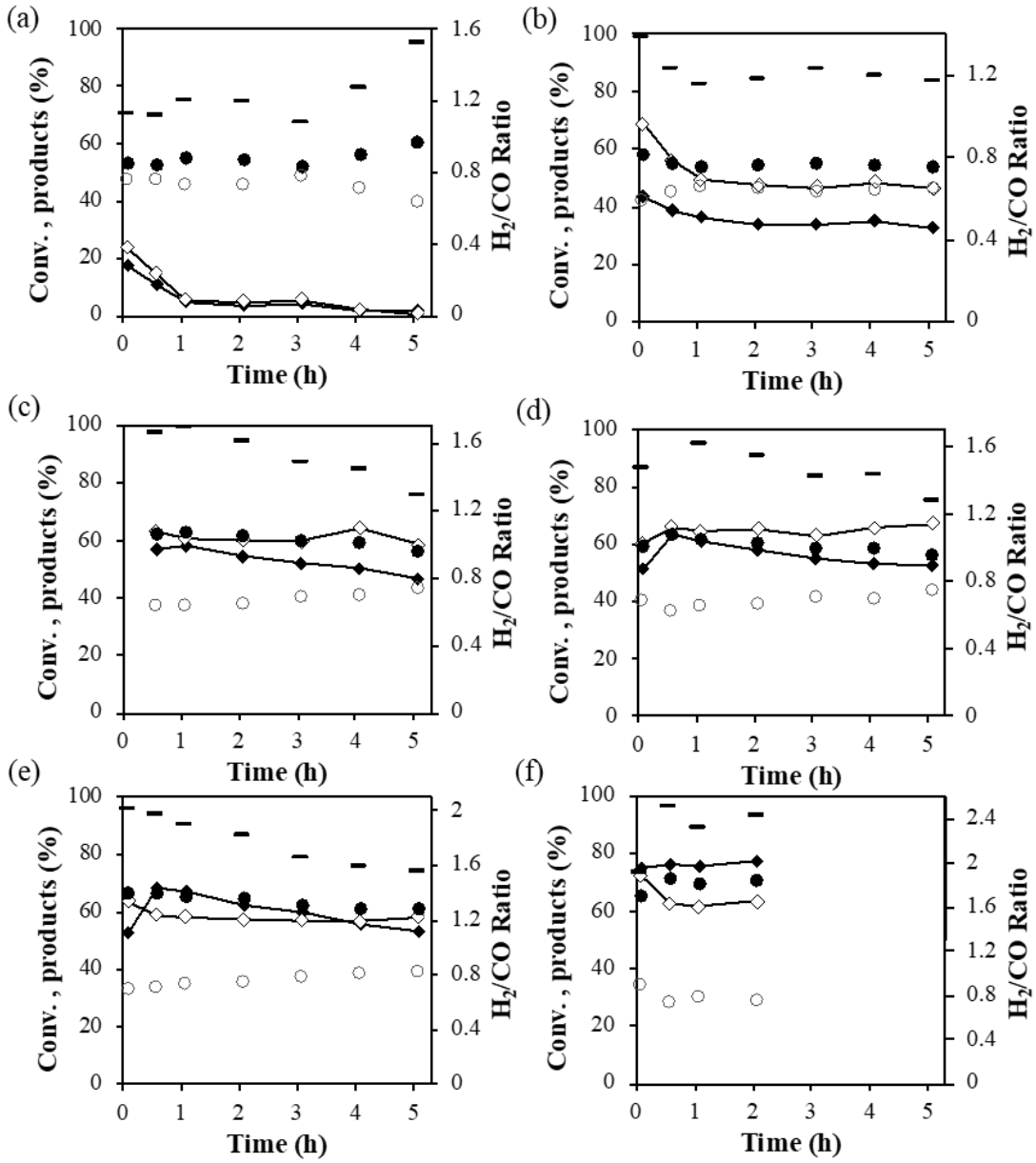

Fig. 2-32 DRM catalytic performance at 600 °C on calcined a) $CeNi_{0.1}O_Y$, b) $CeNi_{0.2}O_Y$, c) $CeNi_{0.3}O_Y$, d) $CeNi_{0.5}O_Y$, e) $CeNi_1O_Y$, and f) $CeNi_2O_Y$, catalysts (50 mg) with in situ H_2 pretreatment at 250 °C. CH_4 (◆), CO_2 (◇) conversions, H_2 (●), CO (○), in mol % and H_2/CO ratio (-). $CH_4/CO_2/N_2$ = 7:5:88%.

2.B.1.1.b Influence of Ni content

The CH_4 and CO_2 conversions, H_2/CO ratio and carbon formation as a function of the Ni content (Ni/M_T) are shown in Fig. 2-33. The catalytic performance strongly depends on the Ni content. In particular, at 600 °C the highest methane conversion is obtained on $CeNi_2O_Y$ catalyst with a value of 77.4 %. The CO_2 conversions are higher than methane conversions on most of catalysts, and the H_2/CO ratio is higher than unity

on all catalysts. Moreover, the carbon formation rate increases with the increasing of Ni content.

Kong et.al studied the Ni@S-1 catalyst on DRM reaction with CO_2/CH_4 ratio = 0.5[142]. The catalyst was prepared by one-pot hydrothermal method and shown CH_4 conversion of 25 % at 650 °C. The condition used was WHSV = $2*10^4$ mL/h·g, 50 mg catalyst, CO_2/ CH_4/ N_2 = 1:2:1.

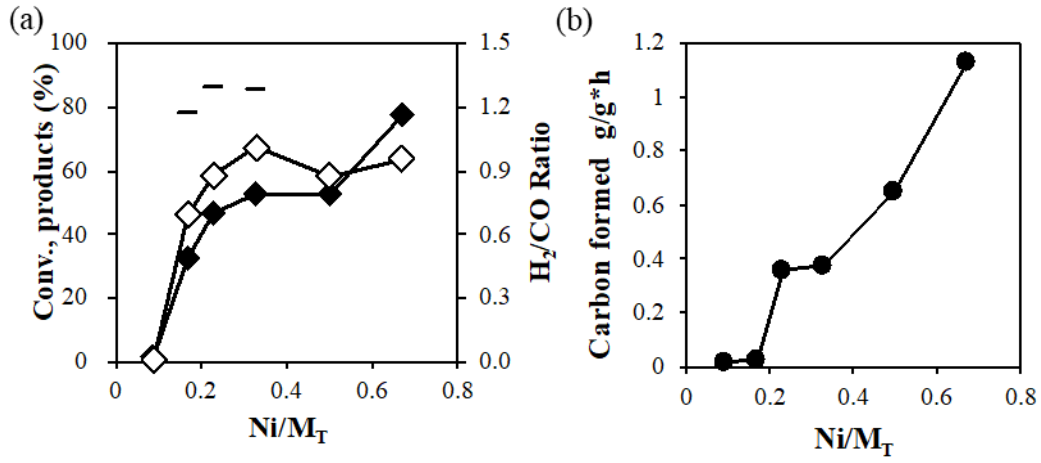

Fig. 2-33 DRM catalytic performance and carbon formation at 600 °C on calcined $CeNi_XO_Y$ catalysts (50 mg) with in situ pretreatment in H_2 at 250°C. $CO_2/CH_4/N_2$ = 5:7:88%. CH_4 (◆), CO_2 (◇) and H_2/CO (-) ratio. Ni/M_T = x/(x+1). Time of experiments = 5h.

2.B.1.1.c On dried $CeNi_XO_Y$ catalysts

The CH_4 and CO_2 conversions at 600 °C on dried $CeNi_XO_Y$ catalysts are shown in Fig. 2-34. The CH_4 and CO_2 conversions of dried $CeNi_{0.3}O_Y$ catalyst decrease with time on stream, stay 18.2 % and 29.9 % after 5 hours of reaction. The dried $CeNi_{0.5}O_Y$ catalyst presents a CH_4 and CO_2 conversions increase with time at 50.1 % and 64.0 % after 5 h. The dried $CeNi_2O_Y$ catalyst shows CH_4 and CO_2 conversions 77.7 % and 60.2 % in first 1 h then the reactor is blocked due to the carbon deposition. The H_2/CO ratio and carbon formation rate increase with Ni content. The H_2/CO ratio for $CeNi_{0.3}O_Y$, $CeNi_{0.5}O_Y$, and $CeNi_2O_Y$ catalyst are 1.1, 1.3 and 2.3 respectively. The carbon formation rate are 0.16 $g \cdot gcat^{-1} \cdot h^{-1}$, 0.15 $g \cdot gcat^{-1} \cdot h^{-1}$, 1.06 $g \cdot gcat^{-1} \cdot h^{-1}$.

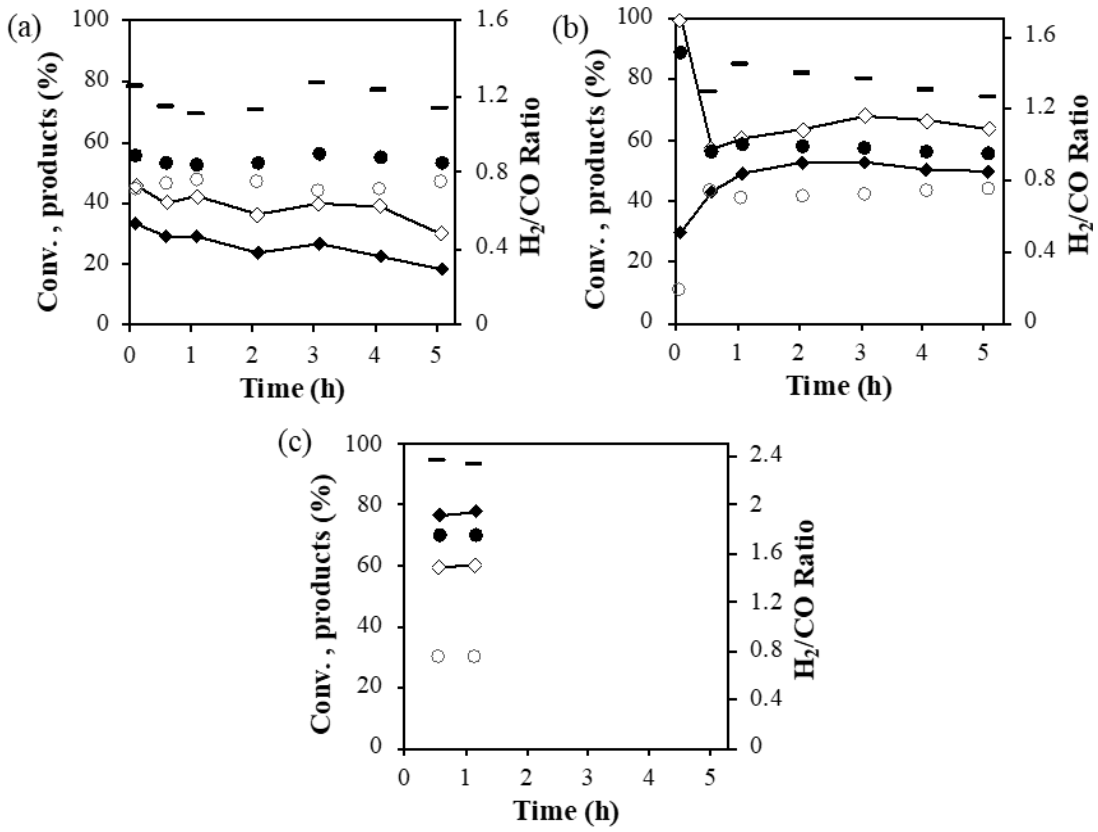

Fig. 2-34 DRM catalytic performance at 600 °C on dried a) $CeNi_{0.3}O_Y$, b) $CeNi_{0.5}O_Y$, and c) $CeNi_2O_Y$ catalysts (50 mg) with in situ H_2 pretreatment at 250 °C. CH_4 (◆), CO_2 (◇) conversions, H_2 (●), CO (○), in mol % and the H_2/CO ratio (-). $CH_4/CO_2/N_2$ = 7:5:88%.

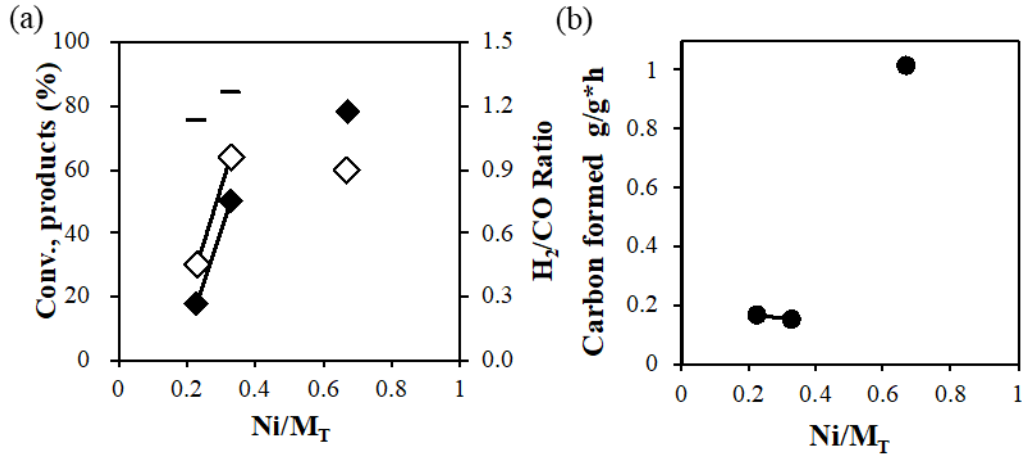

Fig. 2-35 DRM catalytic performance and carbon formation at 600 °C on dried $CeNi_XO_Y$ catalysts (50 mg) with in situ pretreatment in H_2 at 250°C. $CO_2/CH_4/N_2$ = 5:7:88%. CH_4 (◆), CO_2 (◇) and H_2/CO (-) ratio. Ni/M_T = x/(x+1). Time of experiments = 5h.

Comparing the results obtained on calcined and dried $CeNi_XO_Y$ catalysts (Fig 2-32 and 2-34), calcination increased the CO_4 and CO_2 conversions when the Ni content is low, as a matter of fact, for the $CeNi_{0.3}O_Y$, calcination leads to an increase in catalytic performance. However, for higher Ni contents there is almost no difference for the

conversions and H_2/CO ratio between the dried and calcined compounds, which is interesting as a step of pretreatment of the catalyst can be avoided, saving energy. For $CeNi_2O_Y$, the calcination leads to a slight increase on CO_2 conversion in the test at 600 °C.

2.B.1.2 On $CeAl_{0.5}Ni_XO_Y$ catalysts

2.B.1.2.a Influence of time

For the $CeAl_{0.5}Ni_xO_Y$ compounds, the results reported in Fig. 2-36 show relatively good stabilization after 1 hour under feed. The catalytic performance of the $CeAl_{0.5}Ni_{0.5}O_Y$ and the $CeAl_{0.5}Ni_1O_Y$ catalysts decrease slightly with time and the CO_2 conversion after 5 h is of 66.2 % (degraded by 12.3 %) for the $CeAl_{0.5}Ni_{0.5}O_Y$ and of 64.5 % (degraded by 13.3 %) for the $CeAl_{0.5}Ni_{0.5}O_Y$ compound. For the $CeAl_{0.5}Ni_2O_Y$ catalyst with the amount of Ni up to 57 wt%, the percentage of CO_2 conversion is of 65.9 %.

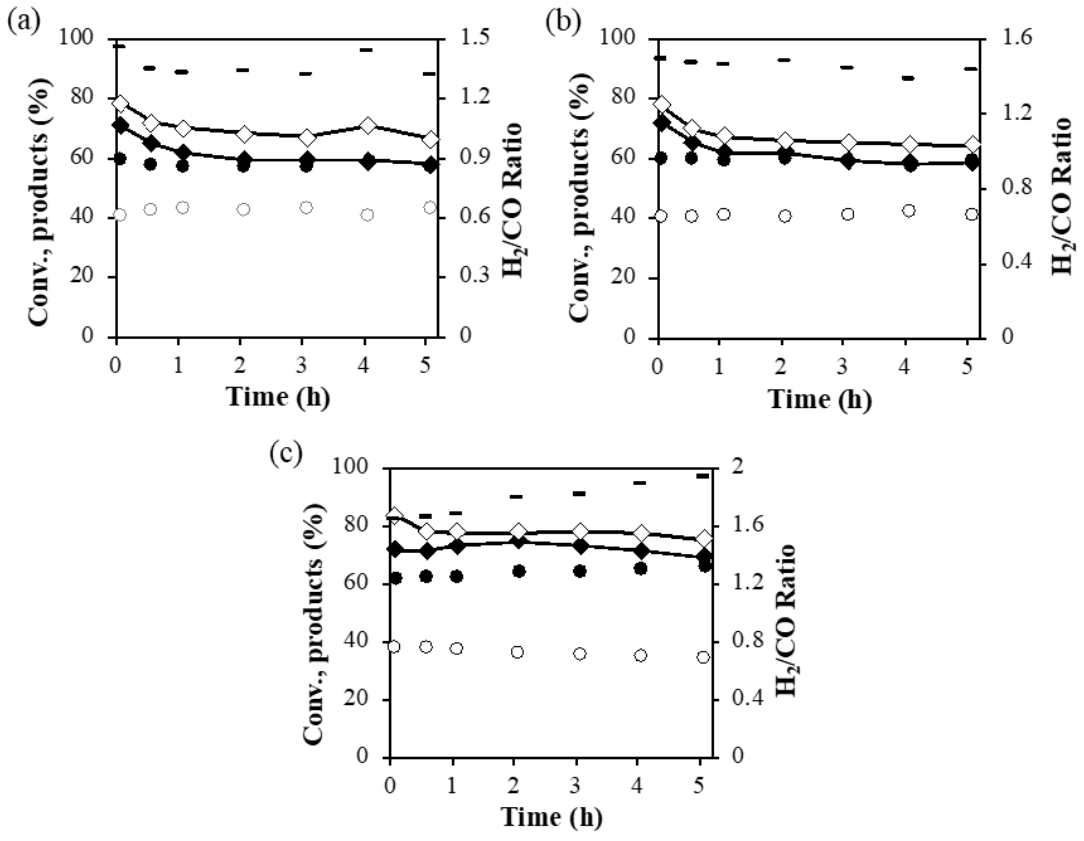

Fig. 2-36 DRM catalytic performance at 600 °C on calcined a) $CeAl_{0.5}Ni_{0.5}O_Y$, b) $CeAl_{0.5}Ni_1O_Y$, c) and $CeAl_{0.5}Ni_2O_Y$ catalysts (50 mg) with in situ H_2 pretreatment at 250 °C. CH_4 (◆), CO_2 (◇) conversions, H_2 (●), CO (○), in mol % and the H_2/CO ratio (-). $CH_4/CO_2/N_2$ = 7:5:88%.

2.B.1.2.b Influence of Ni content

Fig. 2-37 shows the CH_4 and CO_2 conversions and H_2/CO ratio in the products as a function of the Ni content (Ni/M_T). It shows that CH_4 conversion and H_2/CO ratio increase when Ni content increases. The CO_2 conversion is not significantly affected by Ni content. The carbon formation rate also increases with the upgrade of Ni content. The analysis of the reaction products reveals that the increase of the Ni content produces a slight increase of the H_2/CO ratio. This result is probably a consequence of the two effects: the more Ni active sites for methane decomposition and the decrease of coke elimination.

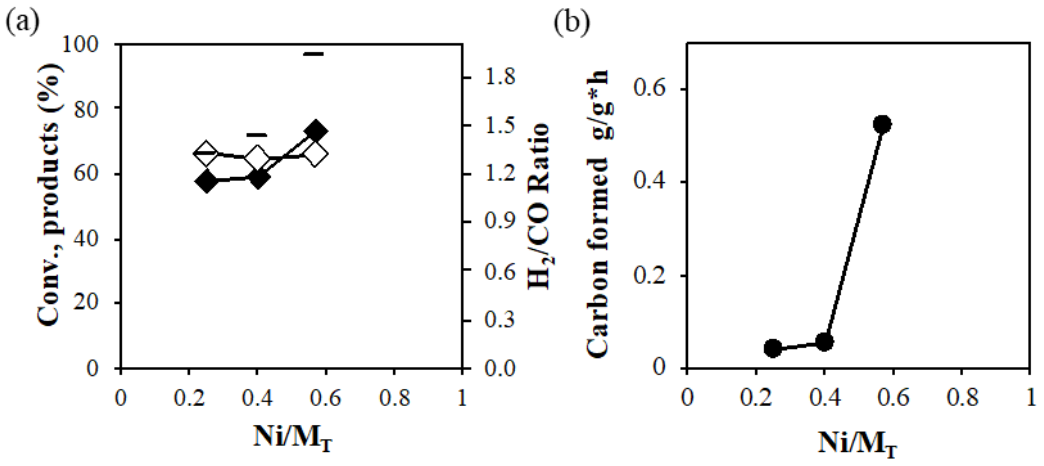

Fig. 2-37 DRM catalytic performance and carbon formation at 600 °C on calcined $CeAl_{0.5}Ni_XO_Y$ catalysts (50 mg) with in situ pretreatment in H_2 at 250°C. $CO_2/CH_4/N_2$ = 5:7:88%. CH_4 (◆), CO_2 (◇) and H_2/CO (-) ratio. Ni/M_T = x/(x+1+0.5). Time of experiments = 5h.

2.B.2 Catalytic performance at 600 °C on catalysts without H_2 pretreatment

2.B.2.1 On $CeNi_XO_Y$ catalysts

2.B.2.1.a Influence of time and Ni content

Fig. 2-38 describes the CH_4, CO_2 conversions and H_2/CO ratio determined in the DRM experiments conducted at 600 °C on $CeNi_XO_Y$ catalyst without H_2 pretreatment, and the outcomes are reported after 5 h (at the steady stage) versus Ni concentration in Fig. 2-39. Clearly, the CH_4 and CO_2 conversions rise as Ni concentration rises. To our surprise, the $CeNi_{0.5}O_Y$ specimen, featuring 12 wt.% of nickel, presents comparable property to catalyst featuring much higher Ni content $CeNi_1O_Y$. $CeNi_1O_Y$ catalyst presents the highest property at 600 °C concerning CH_4 and CO_2 conversions. Nevertheless, on this compound, the evolution of the conversions with time, present after 1 h of test, a minimum for CO_2 conversion and a maximum for CH_4 conversion. Globally, when comparing to initial state, CH_4 and CO_2 conversions over $CeNi_1O_Y$ drop mildly from 63.1 % to 59.8 % and from 80.0 % to 76.6 % in 5 h, respectively.

The H_2/CO ratio is always above 1 and affected by the nickel content, mainly for the lowest Ni content compound (2.1 on $CeNi_{0.1}O_Y$). However, for the lowest Ni content compound, the conversions being very low, the uncertainty is high. Globally, H_2/CO is at about 1.2 at the steady state for the studied compounds (Fig. 2-39). The H_2/CO ratio decrease from 2.1 on $CeNi_{0.1}O_Y$ to around 1.3 on $CeNi_1O_Y$ at 600 °C. the carbon formation increases from 0.013 $g \cdot gcat^{-1} \cdot h^{-1}$ on $CeNi_1O_Y$ to 0.75 $g \cdot gcat^{-1} \cdot h^{-1}$ on $CeNi_1O_Y$.

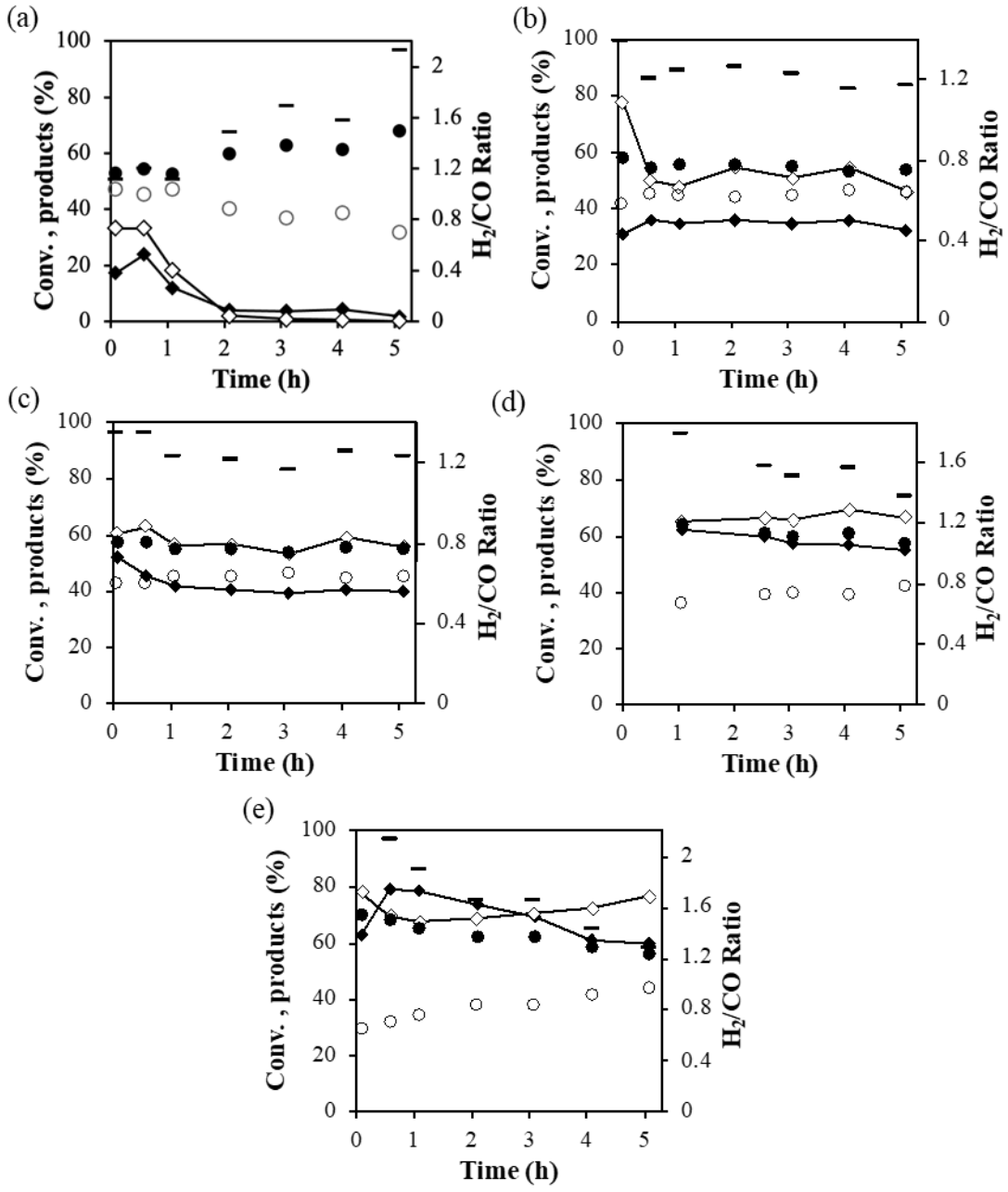

Fig. 2-38 DRM catalytic performance at 600 °C on calcined a) $CeNi_{0.1}O_Y$, b) $CeNi_{0.2}O_Y$, c) $CeNi_{0.3}O_Y$, d) $CeNi_{0.5}O_Y$, and e) $CeNi_1O_Y$ catalysts (50 mg) without H_2 pretreatment. CH_4 (◆), CO_2 (◇) conversions, H_2 (●), CO (○), in mol % and the H_2/CO ratio (-). $CH_4/CO_2/N_2$ = 7:5:88%.

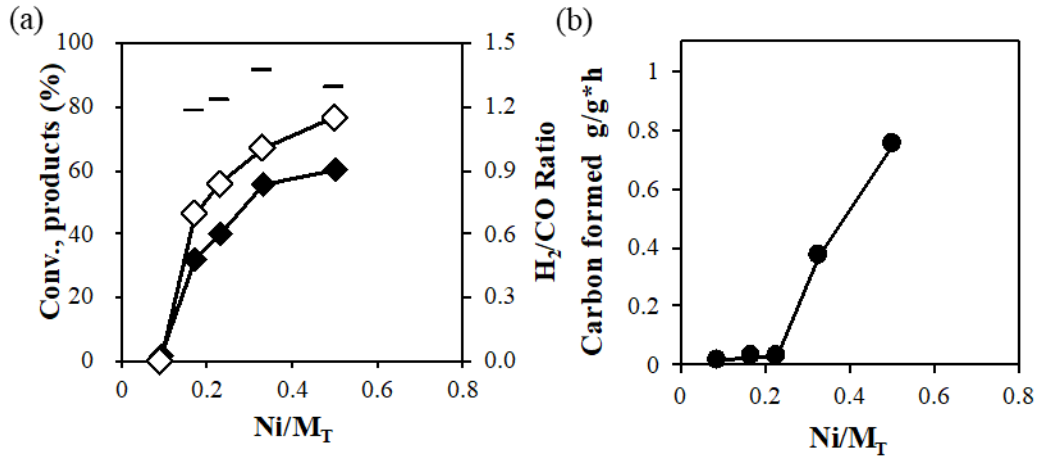

Fig. 2-39 DRM catalytic performance and carbon formation at 600 °C on calcined $CeNi_XO_Y$ catalysts (50 mg) without H_2 pretreatment. $CO_2/CH_4/N_2$ = 5:7:88%. CH_4 (◆), CO_2 (◇) and H_2/CO (-) ratio. $Ni/M_T = x/(x+1)$. Time of experiments =5 h.

2.B.2.1.b Influence of calcination

Fig. 2-40 shows DRM reaction results at 600 °C on dried $CeNi_{0.3}O_Y$ and $CeNi_{0.5}O_Y$ catalysts without pretreatment in H_2. By comparing the results reported in Fig. 2-39 and 2-41 it can be seen that calcination has no big influence on the reactants conversion, the H_2/CO ratio and carbon formation rate. On $CeNi_{0.3}O_Y$, after calcination the CH_4 and CO_2 conversions changes from 40.5 % and 58.3 % to 40.1 % and 55.8 %, H_2/CO ratio stays at 1.2 and carbon formation rate decreases from 0.049 $g \cdot gcat^{-1} \cdot h^{-1}$ to 0.029 $g \cdot gcat^{-1} \cdot h^{-1}$. It indicates calcination is not necessary in this case and it allows saving energy.

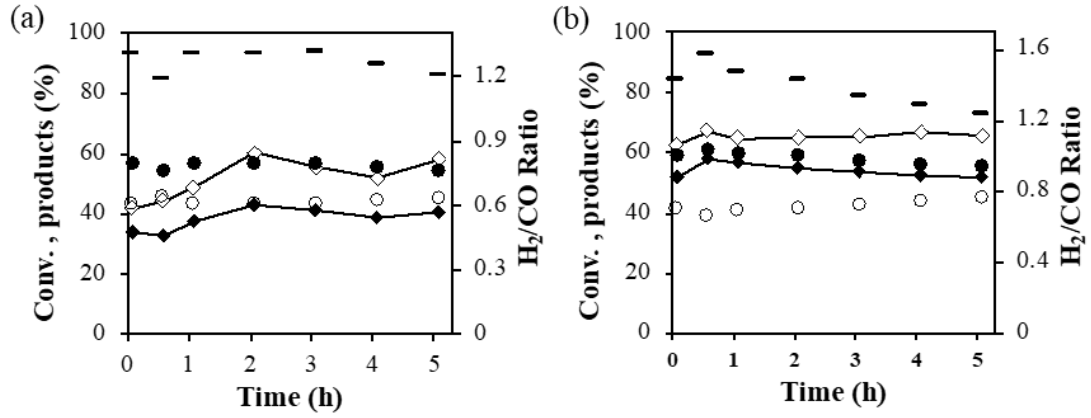

Fig. 2-40 DRM catalytic performance at 600 °C on dried a) $CeNi_{0.3}O_Y$, and b) $CeNi_{0.5}O_Y$ catalysts (50 mg) without H_2 pretreatment. CH_4 (◆), CO_2 (◇) conversions, H_2 (●), CO (○), in mol % and the H_2/CO ratio (-). $CH_4/CO_2/N_2$ = 7:5:88%.

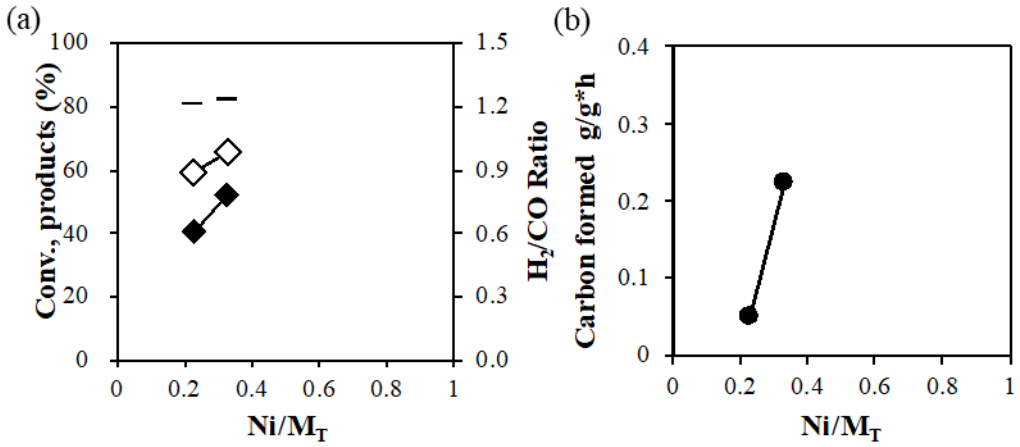

Fig. 2-41 DRM catalytic performance and carbon formation at 600 °C on dried $CeNi_XO_Y$ catalysts (50 mg) without H_2 pretreatment. $CO_2/CH_4/N_2$ = 5:7:88%. CH_4 (◆), CO_2 (◇) and H_2/CO (-) ratio. Ni/M_T = x/(x+1). Time of experiments = 5h.

2.B.2.1.c Influence of pretreatment

The effect of pretreatment in H_2 at 250°C can be compared to without pretreatment in H_2 on $CeNi_XO_Y$ catalysts in Fig. 2-32 and 2-38. Both CH_4 and CO_2 conversions (32% for CH_4 and 46% for CO_2) are quite similar under the conditions without catalyst pretreatment and with in-situ pretreatment in H_2 at 250 °C of the catalyst. Nevertheless, the pretreatment in H_2 leads to more stable conversions for both CH_4 and CO_2.

For easy comparison, Fig. 2-42 shows the conversions after 5h of test on the $CeNi_XO_Y$ catalysts pretreated in H_2 at 250 °C and catalysts without H_2 pretreatment. It is visible that the pretreatment has no great influence. For $CeNi_{0.3}O_Y$ catalyst, after pretreatment, CH_4 conversion and CO_2 conversion increase by 6.5% and 2.8% respectively. However, CH_4 conversion decreases from 59.8% to 53% and CO_2 conversion decreases from 76.6% to 58.1% for the $CeNi_1O_Y$ catalyst.

Catalytic results in combination with carbon deposition data (Table 2-1) indicate that catalysts with $Ni/M_T \leq 0.33$ in-situ pretreated in H_2 at 250°C and without pretreatment show similar carbon generation in the products. However, on $CeNi_1O_Y$ catalyst a pretreatment in H_2 at 250 °C leads to a carbon formation of 0.72 $g \cdot gcat^{-1} \cdot h^{-1}$ which is lower compared to the carbon formation of 0.82 $g \cdot gcat^{-1} \cdot h^{-1}$ obtained on the catalyst without pretreatment.

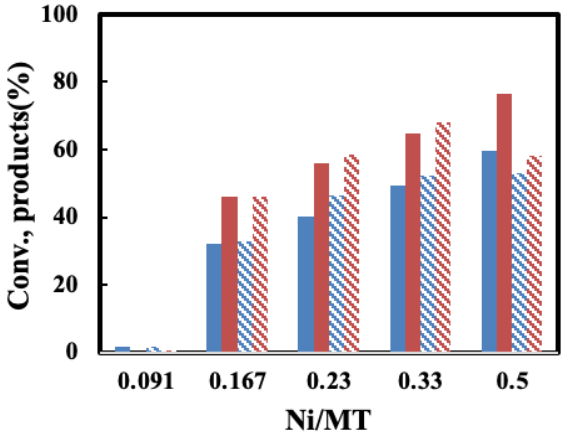

Fig. 2-42 CH_4 conversion (blue), CO_2 conversion (red) obtained at 600 ºC on $CeNi_XO_Y$ catalyst (50 mg) without H_2 pretreatment (filled by full color) and with in situ H_2 pretreatment at 250 °C. (filled by shadow). $CO_2/CH_4/N_2$ = 5:7:88%. Ni/M_T molar ratio = x/(x+1). Time of experiments = 5h.

Table 2-1 Carbon formation rate ($g \cdot gcat^{-1} \cdot h^{-1}$) on $CeNi_XO_Y$ catalysts with with in situ H_2 pretreatment and without. Results are reported after 5h of test.

Ni/M_T molar ratio	0.091	0.167	0.23	0.33	0.5
With pretreatment	0.00078	0.0014	0.019	0.012	0.72
Without pretreatment	0.00076	0.0013	0.019	0.011	0.82

Therefore, a notable feature is that the catalyst has been activated even without the pre-treatment under H_2. Plenty energy can be saved through avoidance of treatment process. The catalyst can be active toward DRM beginning directly at the oxide stage. Thus, the pretreatment stage test is an amazing attempt in technology and economy. Apparently, the 600 °C reaction temperature at the experiment beginning makes the activation under 5 % concentration of the reactants, on this type of catalysts.

2.B.2.2 On $CeZr_{0.5}Ni_XO_Y$ catalysts

2.B.2.2.a Influence of time

The $CeZr_{0.5}Ni_XO_Y$ catalysts have been previously shown highly efficient for H_2 production from DRM at 600 °C without pretreatment under CH_4/ CO_2/ N_2 = 5:5:90 % feed. In such a context, calcined $CeZr_{0.5}Ni_XO_Y$ compounds with different Ni contents are investigated for H_2 production from DRM with CO_2/CH_4 = 0.7 and the results are displayed in Fig. 2-43.

It is obvious to disclose that with the CO_2/CH_4 ratio of 0.7 $CeZr_{0.5}Ni_XO_Y$ compounds present a higher CO_2 conversion than CH_4 conversion. For $CeZr_{0.5}Ni_{0.5}O_Y$ catalyst, CO_2 conversion is of 95.0 % at beginning, then drops to 65.9 % after 0.5 h, and

stays at 56.8 % after 5 hours on stream. CH_4 conversion drops slightly from 52.9 % to 40.5 %. The H_2/CO ratio is around 1.2 during the reaction. For $CeZr_{0.5}Ni_1O_Y$ catalyst, the CH_4 and CO_2 conversions are quite same around 80 % at the beginning with a H_2/CO ratio around 1.8. After 4 h on stream, the CH_4 and CO_2 conversions are of 55.4 % and 68.5 %, respectively. The H_2/CO ratio is of 1.37. The carbon formation rate is high (around 0.75 $g \cdot gcat^{-1} \cdot h^{-1}$) and the test has to be stopped after 4.5 hour on stream due to blockage of the reactor by carbon deposition.

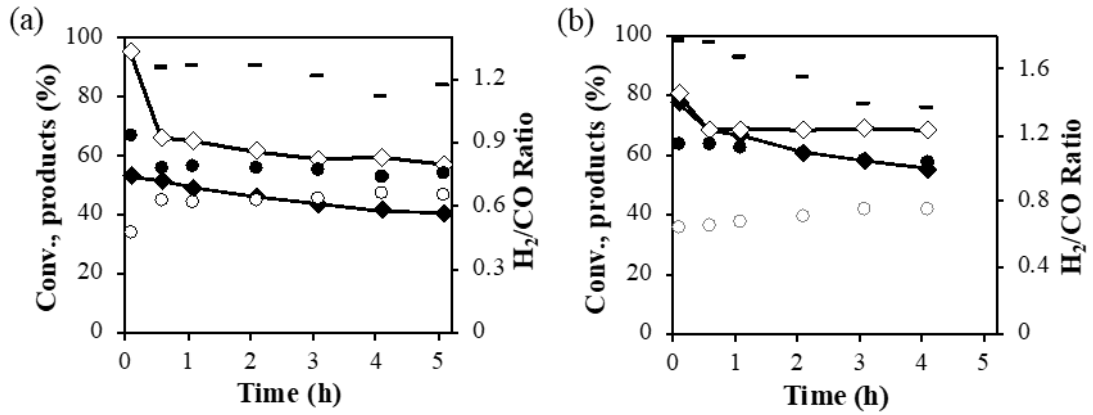

Fig. 2-43 DRM catalytic performance at 600 °C on calcined a) $CeZr_{0.5}Ni_{0.5}O_Y$, and b) $CeZr_{0.5}Ni_1O_Y$ catalysts (50 mg) without H_2 pretreatment. CH_4 (◆), CO_2 (◇) conversions, H_2 (●), CO (○), in mol % and H_2/CO ratio (-). $CH_4/CO_2/N_2$ = 7:5:88%.

2.B.2.2.b Influence of Ni content

Among the compounds studied (x from 0.5 to 1), the CH_4 and CO_2 conversions increase with the Ni content. Moreover, the H_2/CO ratio and carbon formation rate also increase with Ni content probably due to the methane decomposition reaction.

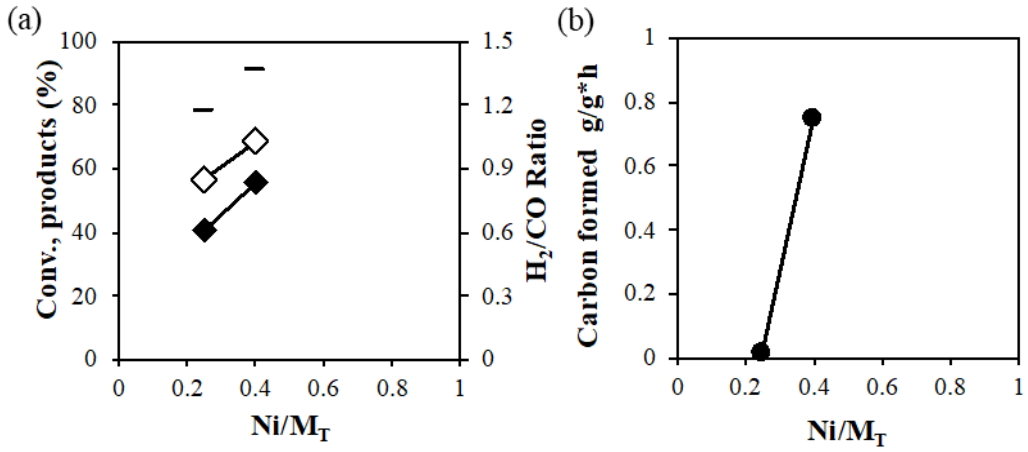

Fig. 2-44 DRM catalytic performance and carbon formation at 600 °C on calcined $CeZr_{0.5}Ni_XO_Y$ catalysts (50 mg) without H_2 pretreatment. $CO_2/CH_4/N_2$ = 5:7:88%. CH_4 (◆), CO_2 (◇) and H_2/CO (-) ratio. Ni/M_T = x/(x+1+0.5). Time of experiments = 5h.

2.B.2.3 On $CeAl_{0.5}Ni_XO_Y$ catalysts

2.B.2.3.a Influence of time

The catalytic performance of the $CeAl_{0.5}Ni_XO_Y$ in terms of CH_4 and CO_2 conversions are studied at 600 °C without pretreatment as shown in Fig. 2-45. Globally very good stability is obtained after 1 h under feed and during 5 h, while during the first hour of reaction small decrease of the conversions is observed. The conversions of CO_2 are higher than those of CH_4. The $CeAl_{0.5}Ni_{0.5}O_Y$ catalyst (12 Ni wt. %) shows conversion of CH_4 and CO_2 at 51.8 % and 68.8 %, respectively. The $CeAl_{0.5}Ni_1O_Y$ catalyst presents conversions of methane and of CO_2 at 64.8 % and 70.5 %, respectively. The $CeAl_{0.5}Ni_2O_Y$ shows the conversion of methane and CO_2 of 79.8 5 and 73.4%. The highest conversions of CH_4 and CO_2 are obtained (82.2 % and 75.6 %, respectively) on $CeAl_{0.5}Ni_5O_Y$ catalyst.

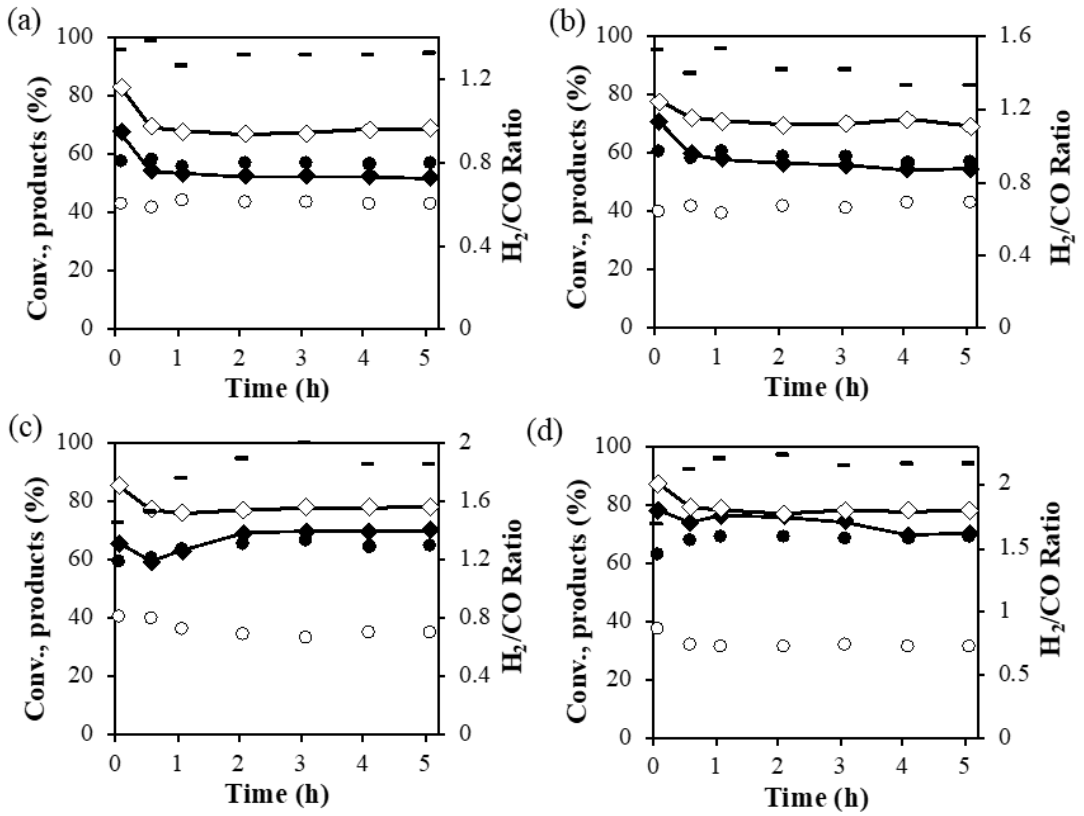

Fig. 2-45 DRM catalytic performance at 600 °C on calcined a) $CeAl_{0.5}Ni_{0.5}O_Y$, b) $CeAl_{0.5}Ni_1O_Y$, c) $CeAl_{0.5}Ni_2O_Y$, and d) $CeAl_{0.5}Ni_5O_Y$ catalysts (50 mg) without H_2 pretreatment. CH_4 (◆), CO_2 (◇) conversions, H_2 (●), CO (○), in mol % and H_2/CO ratio (-). $CH_4/CO_2/N_2$ = 7:5:88%.

2.B.2.3.b Influence of Ni content

Fig. 2-46 shows the CH_4 and CO_2 conversions and H_2/CO ratio in the products as a function of the Ni content (Ni/M_T). It shows that CH_4 conversion and H_2/CO ratio

increase when Ni content increases. The CO_2 conversion is not significantly affected by Ni content. The carbon formation rate is also promoted from 0.05 $g \cdot gcat^{-1} \cdot h^{-1}$ on $CeAl_{0.5}Ni_1O_Y$ to 0.72 $g \cdot gcat^{-1} \cdot h^{-1}$ on $CeAl_{0.5}Ni_2O_Y$ when the Ni content increases from 19.5 wt.% to 30.8 wt.%.

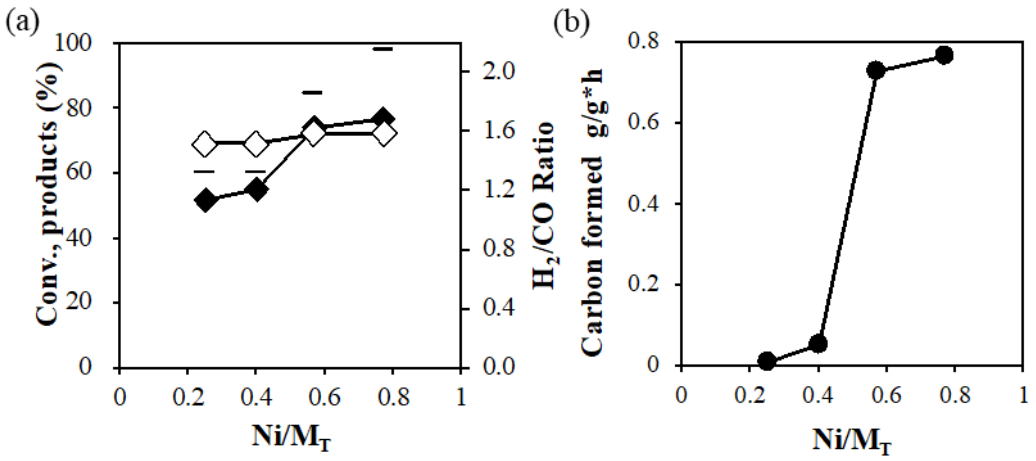

Fig. 2-46 DRM catalytic performance and carbon formation at 600 °C on calcined $CeAl_{0.5}Ni_XO_Y$ catalysts (50 mg) without H_2 pretreatment. $CO_2/CH_4/N_2$ = 5:7:88%. CH_4 (◆), CO_2 (◇) and H_2/CO (-) ratio. Ni/M_T = x/(x+1+0.5). Time of experiments = 5h.

2.B.3 Catalytic performance at 800 °C on catalysts with H_2 pretreatment

2.B.3.1 On $CeNi_XO_Y$ catalysts

2.B.3.1.a Influence of time and Ni content

The DRM catalytic performance of the $CeNi_XO_Y$ at 800 °C with the CO_2/CH_4 ratio = 0.7 is shown in Fig. 2-47. The $CeNi_{0.1}O_Y$ shows very low reactant conversions in first one hour, then there is no reactants conversion observed. For all the compounds, there is a decrease of the conversions in the first hour, then a relatively good stabilization is obtained during 5h. At the steady state, almost all other catalysts show relatively low CH_4 and CO_2 conversions around 20 %, except on $CeNi_{0.2}O_Y$ that shows CH_4 and CO_2 conversions of 31.8 % and 38.2 %, respectively (Fig. 2-48). The H_2/CO ratio of $CeNi_{0.2}O_Y$ catalysts is 1.27 and carbon formation rate is 0 $g \cdot gcat^{-1} \cdot h^{-1}$. The $CeNi_XO_Y$ catalysts show a good stability but low conversions due to the particularly low mass of catalyst used (10 mg).

Compared to the results with CO_2/CH_4 ratio = 1, CH_4 and CO_2 conversions obtained with CO_2/CH_4 ratio = 0.7 are lower, but H_2/CO ratios are higher. For example, on $CeNi_{0.3}O_Y$ catalyst, CH_4 and CO_2 conversions are 22.2 % and 22.5 % with CO_2/CH_4 ratio =1, and 15.8 % and 6 % with CO_2/CH_4 ratio = 0.7. The H_2/CO ratio is 0.7 with CO_2/CH_4 ratio = 1, 1.9 with CO_2/CH_4 ratio = 0.7.

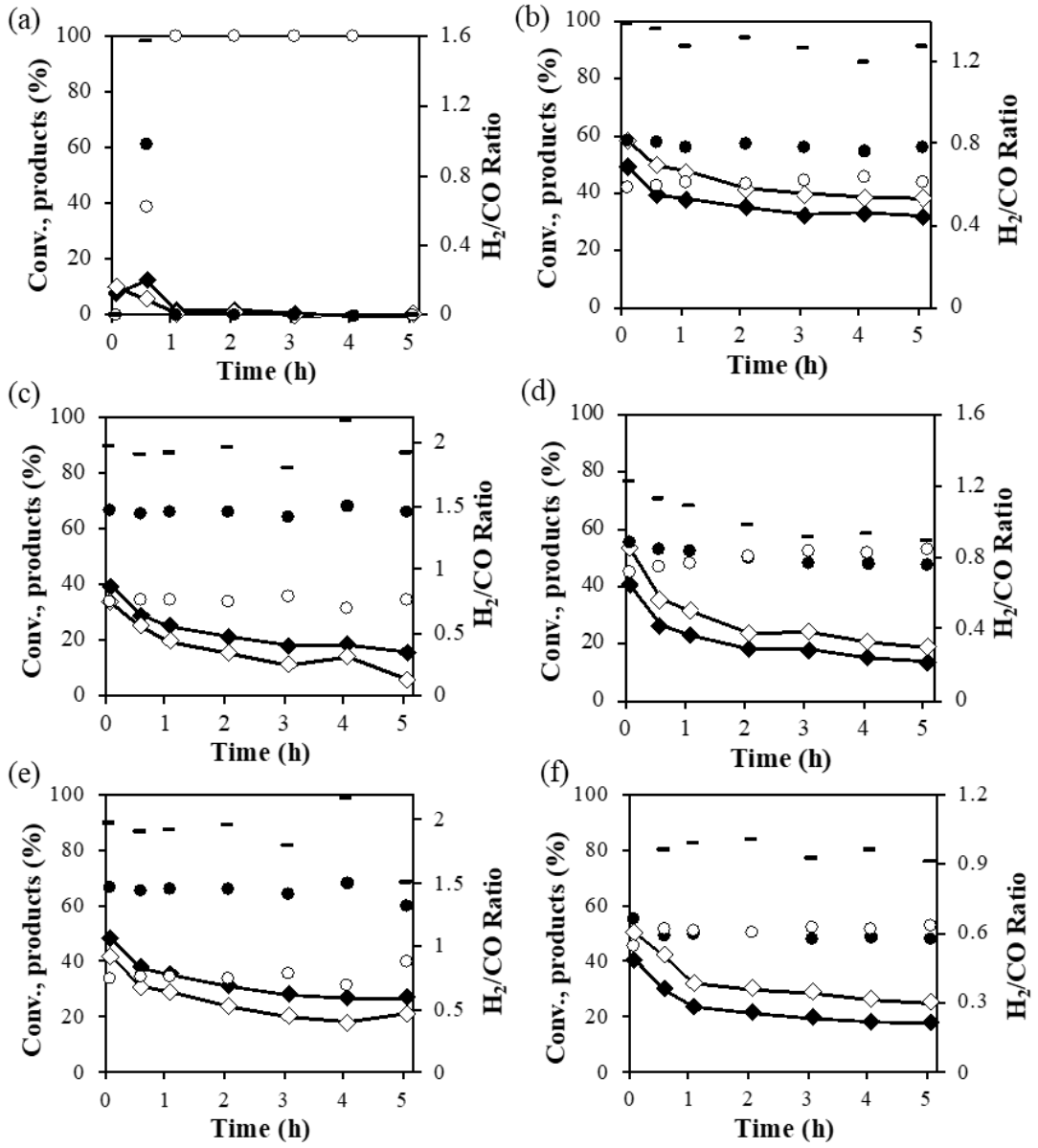

Fig. 2-47 DRM catalytic performance at 800 °C on calcined a) $CeNi_{0.1}O_Y$, b) $CeNi_{0.2}O_Y$, c) $CeNi_{0.3}O_Y$, d) $CeNi_{0.5}O_Y$, e) $CeNi_1O_Y$, and f) $CeNi_2O_Y$ catalysts (10 mg) with in situ H_2 pretreatment at 250 °C. CH_4 (◆), CO_2 (◇) conversions, H_2 (●), CO (○), in mol % and the H_2/CO ratio (-). $CH_4/CO_2/N_2$ = 7:5:88%.

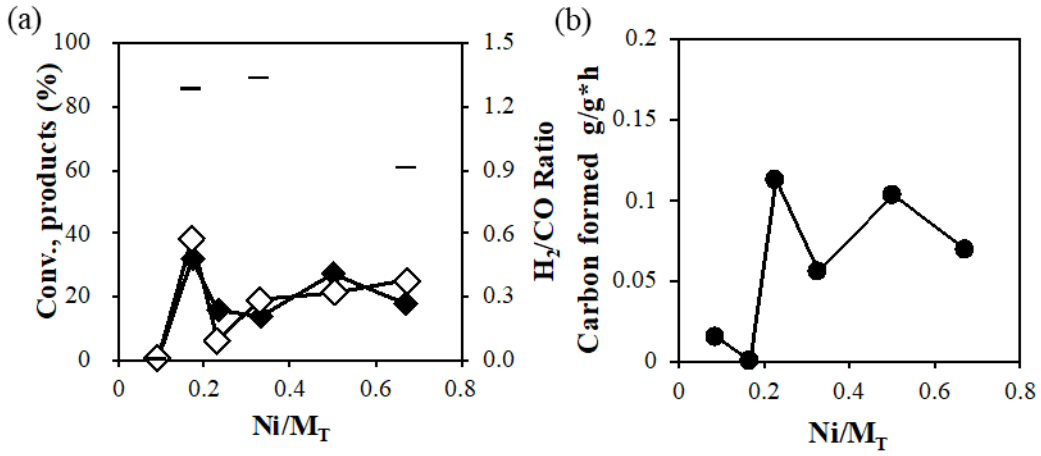

Fig. 2-48 DRM catalytic performance and carbon formation at 800 °C on calcined $CeNi_XO_Y$ catalysts (10 mg) with in situ pretreatment in H_2 at 250°C. $CO_2/CH_4/N_2$ = 5:7:88%. CH_4 (◆), CO_2 (◇) and H_2/CO (-) ratio. Ni/M_T = x/(x+1). Time of experiments = 5h.

In literature, Mousavi et. al reported 10 wt.% $Ni/Ce_{0.95}Mn_{0.05}O_2$ prepared by co-precipitation method used in DRM reaction[141]. At 700 °C, catalyst showed CH_4 and CO_2 conversions of 34 % and 88 % in the condition of GHSV = 12000 mL/h, 200 mg catalyst, CO_2/ CH_4 =0.5:1. Here in this work, the $CeNi_{0.2}O_Y$ shows 31.8 % of methane conversion but with only 50 mg of catalyst.

2.B.3.1.b Influence of mass of catalysts

It appears interesting to analyze the performance with a higher amount of catalyst and tests are carried out in the condition of $CO_2/ CH_4/ N_2$ = 5:7:88 % on $CeNi_XO_Y$ with a mass of 50 mg. As shown in Fig. 2-49, CH_4 and CO_2 conversions become higher as the mass increases. Globally, H_2/CO ratio and carbon formation are relatively lower than the case with 10 mg. In this condition, the carbon formation rates are lower than 0.02 $g \cdot gcat^{-1} \cdot h^{-1}$ Fig. 2-50). The $CeNi_{0.2}O_Y$ catalyst also presents the best catalytic performance with 50 mg catalyst (Fig. 2-50). The conversion of CH_4 and CO_2 are 74.0 % and 93.9 %, respectively. H_2/CO ratio is 1.3 and carbon formation rate is 0.08 $g \cdot gcat^{-1} \cdot h^{-1}$. It is meaning that even with a low Ni content in this series of compounds, high conversions can be reached by increasing the catalyst mass. Most prominently, carbon formation is diminished in this case.

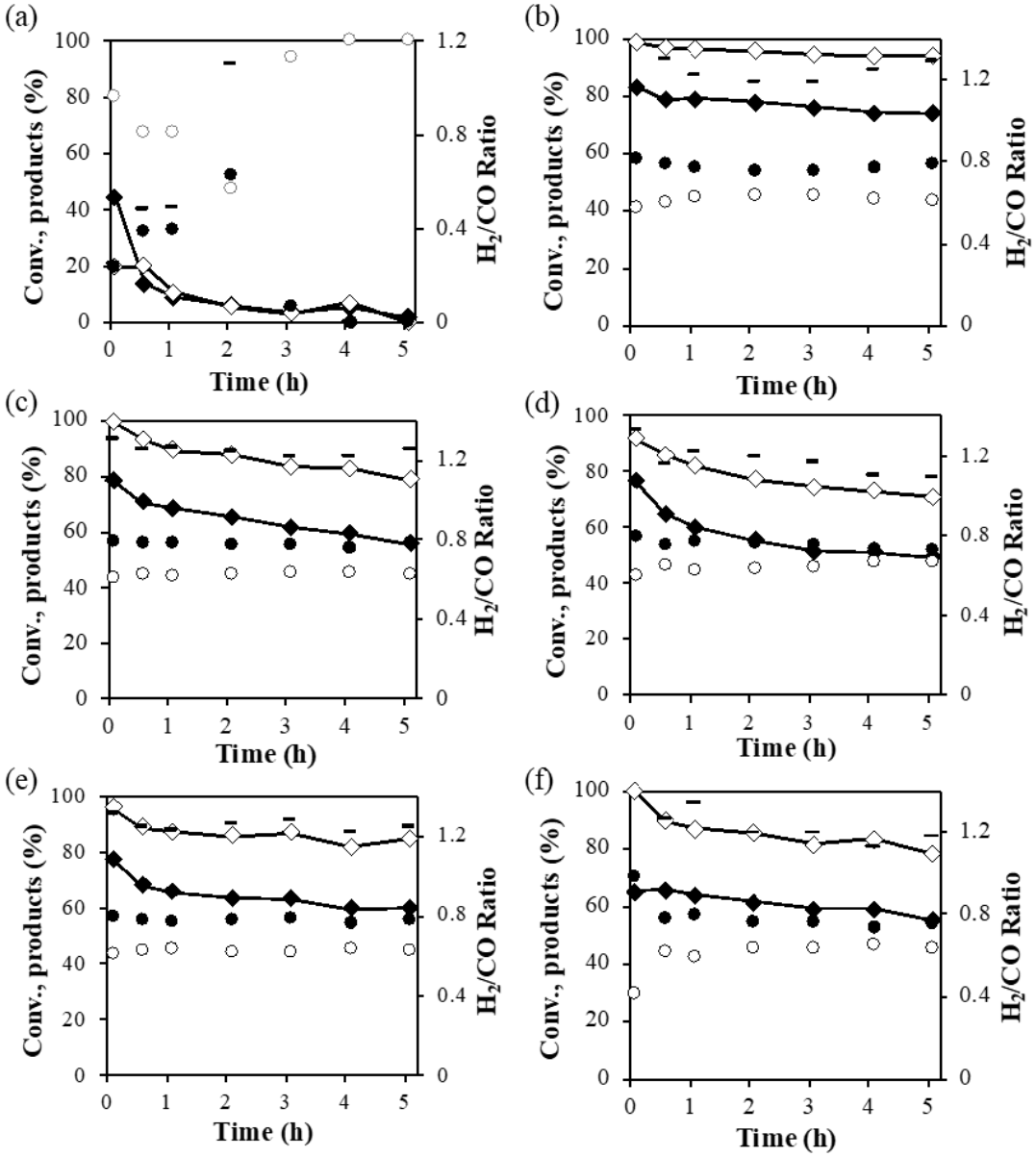

Fig. 2-49 DRM catalytic performance at 800 °C on calcined a) $CeNi_{0.1}O_Y$, b) $CeNi_{0.2}O_Y$, c) $CeNi_{0.3}O_Y$, d) $CeNi_{0.5}O_Y$, e) $CeNi_1O_Y$, and f) $CeNi_2O_Y$ catalysts (50 mg) with in suit H_2 pretreatment at 250 °C. CH_4 (◆), CO_2 (◇) conversions, H_2 (●), CO (○), in mol % and H_2/CO ratio (-). $CH_4/CO_2/N_2$ = 7:5:88%.

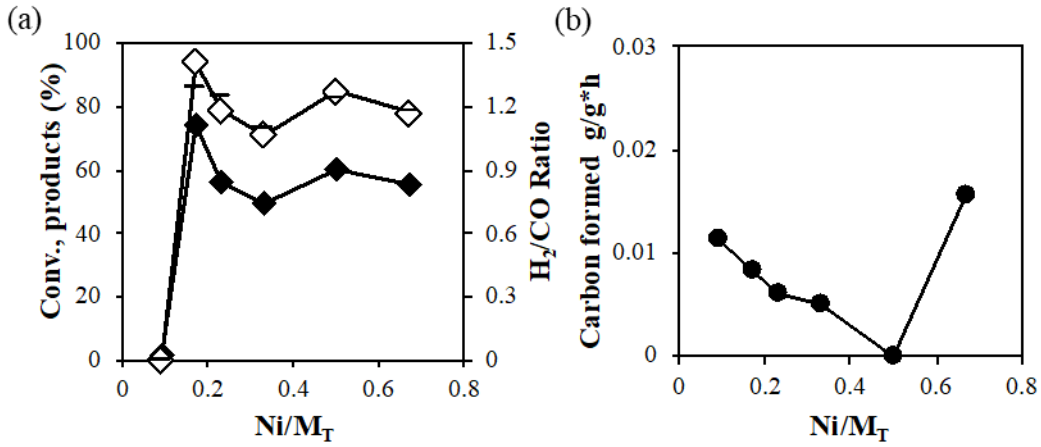

Fig. 2-50 DRM catalytic performance and carbon formation at 800 °C on calcined $CeNi_XO_Y$ catalysts (50 mg) with in suit pretreatment in H_2 at 250 °C. $CO_2/CH_4/N_2$ = 5:7:88%. CH_4 (◆), CO_2 (◇) and H_2/CO (-) ratio. Ni/M_T = x/(x+1). Time of experiments = 5h.

Barbosa et al. reported DRM performance at variated ratio of CH_4/CO_2 on Ni-WC catalyst (55.1 wt.% NiO in precursor) at 800 °C[143]. 58 % and 85 % of CH_4 and CO_2 conversions and H_2/CO ratio of 0.8 were obtained with CH_4/CO_2 ratio = 1.5 and total flow rate of 50 mL/min with 20 % of N_2 as the internal standard. In this study, higher CH_4 and CO_2 conversions achieved on lower Ni content catalyst $CeNi_{0.2}O_Y$ (6.2 wt.% Ni).

2.B.3.1.c Influence of reaction temperature

For easy comparison of the influence of reaction temperature the results previously reported in Fig. 2-33 and 2-50 are shown again together, as for example, on the $CeNi_{0.5}O_Y$ catalyst (50mg) in-situ pretreated at 250 °C in H_2 tested at 600 °C and 800 °C. As illustrated, a rise of temperature causes a rise in CH_4 and CO_2 conversions, resulting from the DRM reaction endothermic nature. CH_4 and CO_2 conversions rise from 51.6% and 60.4% at 600 °C to 68.0% and 80.5% at 800°C, separately. The CO_2 conversion exceeds CH_4 conversion in the detected temperatures.

LNZ10 catalyst was prepared by a modified citrate method in literature[104104]. 100 mg of catalyst were used in dry reforming of methane at 700 °C, WHSV was of 30 L/g·h, and CH_4 and CO_2 in a ratio of 1.5:1. The catalyst showed conversion for CH_4 and CO_2 at 46 % and 70 %, respectively.

In the present study, similar results are achieved by using lower Ni content catalyst (14% wt. Ni). The CH_4 and CO_2 conversions are 87% and 96% at the beginning and the H_2/CO ratio is of 1.2 at 800°C (CO_2/CH_4 = 0.7, 7 % CH_4, total flow of 80 mL/min, 50 mg of catalyst). After 5h of reaction, the deactivation of about 10%

is observed, which could result from the sintering of metallic nickel particles or/and carbon deposition.

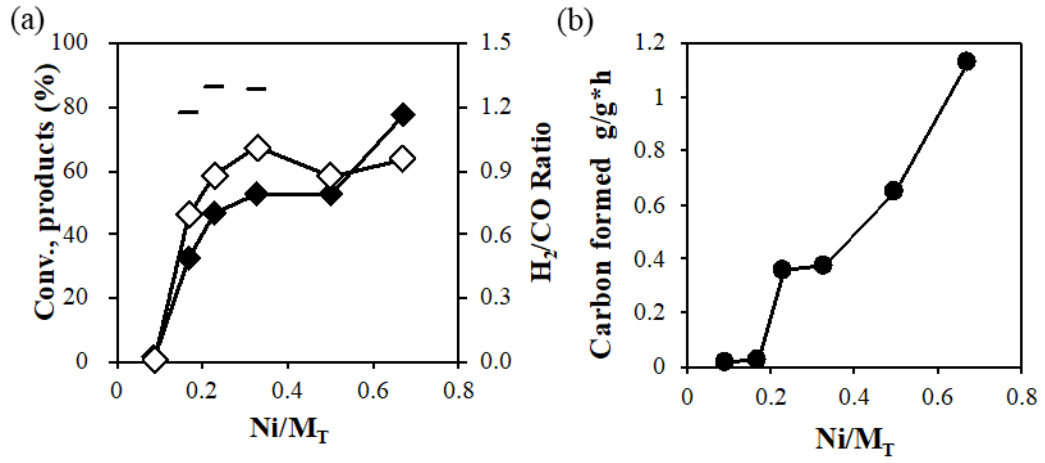

Fig. 2-33 DRM catalytic performance and carbon formation at 600 °C on calcined $CeNi_XO_Y$ catalysts (50 mg) with in situ H_2 pretreatment at 250 °C. $CO_2/CH_4/N_2$ = 5:7:88%. CH_4 (◆), CO_2 (◇) and H_2/CO (-) ratio. $Ni/M_T = x/(x+1)$. Time of experiments = 5h.

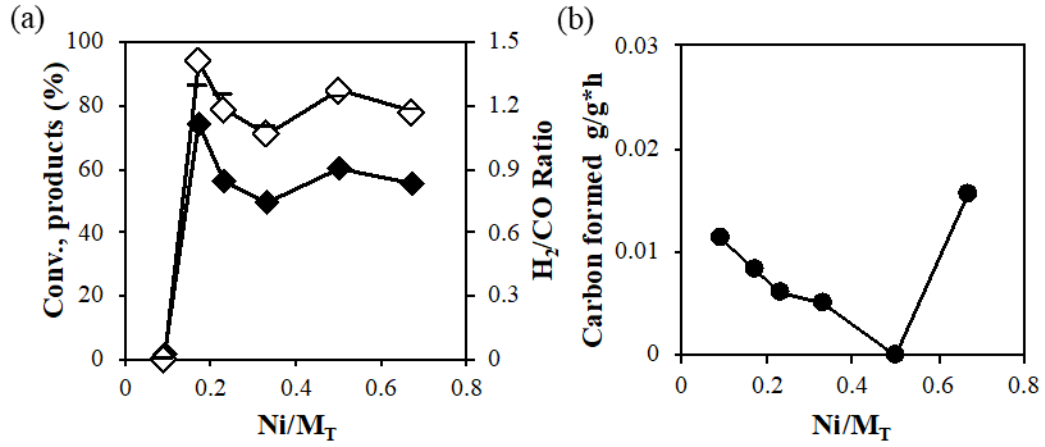

Fig. 2-50 DRM catalytic performance and carbon formation at 800 °C on calcined $CeNi_XO_Y$ catalysts (50 mg) with in situ pretreatment in H_2 at 250°C. $CO_2/CH_4/N_2$ = 5:7:88%. CH_4 (◆), CO_2 (◇) and H_2/CO (-) ratio. $Ni/M_T = x/(x+1)$. Time of experiments = 5h.

2.B.3.1.d Stability test

In order to investigate the catalytic stability of the $CeNi_1O_Y$ catalyst a constant temperature test is accomplished at 800 °C for 80 hours. As shown in Fig. 2-51, the $CeNi_1O_Y$ catalyst exhibits a slight deactivation along with the DRM process. The conversions of methane and CO_2 over $CeNi_1O_Y$ catalyst are of 57.2 % and 55.6 % at the beginning, respectively. The conversions present a decrease. The conversion of methane and CO_2 remain relatively stable after 50 h and are finally of 23.8 % and

21.0 %, respectively. The carbon formation rate is of 0.0012 $g \cdot gcat^{-1} \cdot h^{-1}$. The H_2/CO ratio also decreases from 1.0. to 0.9 after 80 h.

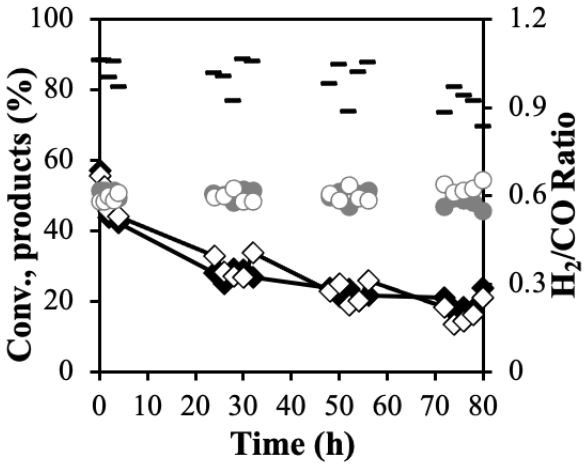

Fig. 2-51 DRM catalytic performance at 800 °C on calcined $CeNi_1O_Y$ catalyst (10 mg) with in situ H_2 pretreatment at 250 °C. CH_4 (◆), CO_2 (◇), H_2 (●), CO (○), in mol% and H_2/CO (-) ratio. $CO_2/CH_4/N_2$ = 5:7:88%.

2.B.3.2 On $CeZr_{0.5}Ni_XO_Y$ catalysts

2.B.3.2.a Influence of time

The $CeZr_{0.5}Ni_XO_Y$ catalysts tested in same conditions are shown in Fig. 2-52. The $CeZr_{0.5}Ni_{0.5}O_Y$ presents conversions decreasing in the first hour. The conversion of methane and CO_2 are of 82.7 % and 93.2 % at the beginning, respectively, and of 57.5 % and 63.7 %, respectively after 5 hours. The carbon formation rate is 0 $g \cdot gcat^{-1} \cdot h^{-1}$ and H_2/CO ratio around 1.3 all the process. For all the other compounds with higher Ni content stable catalytic performance is obtained, there is no decrease in methane and CO_2 conversions during the 5 h DRM reaction at 800 °C.

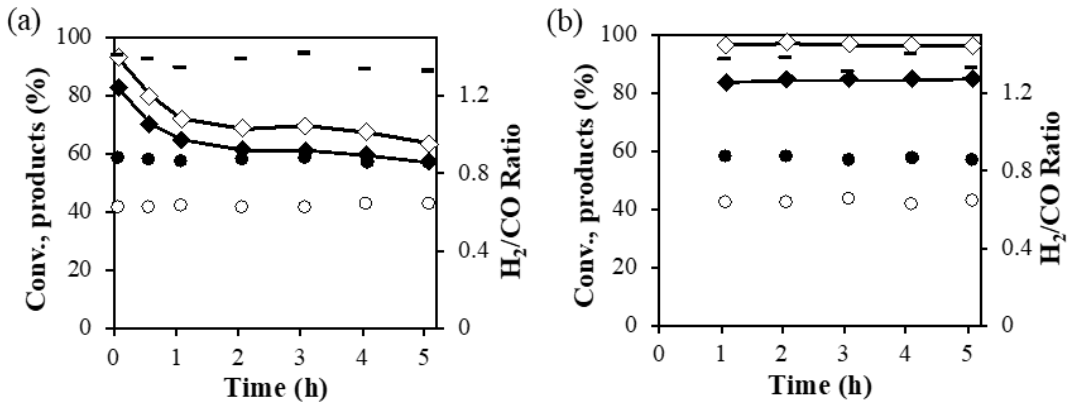

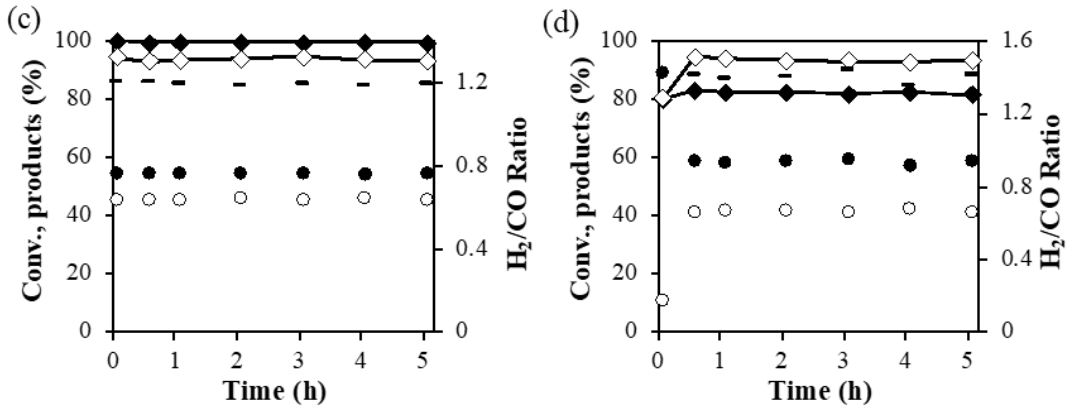

Fig. 2-52 DRM catalytic performance at 800 °C on calcined a) $CeZr_{0.5}Ni_{0.5}O_Y$, b) $CeZr_{0.5}Ni_1O_Y$, c) $CeZr_{0.5}Ni_2O_Y$, and d) $CeZr_{0.5}Ni_5O_Y$ catalysts (10 mg) with in situ H_2 pretreatment at 250 °C. CH_4 (◆), CO_2 (◇) conversions, H_2 (●), CO (○), in mol % and the H_2/CO ratio (-). $CH_4/CO_2/N_2$ = 7:5:88%.

2.B.3.2.b Influence of Ni content

To examine the catalytic performance of the samples with various Ni contents, the CH_4 and CO_2 conversions and H_2/CO ratio in the products as a function of the Ni content (Ni/M_T) are shown in Fig. 2-53. Both CH_4 and CO_2 conversions increase with the increase in Ni amount up to 30.6 wt. % (Ni/M_T close to 0.6), leading to almost total conversions, and the employment of higher Ni content (48.3 wt.%) decreases them in a small extent. In overall, the CO_2 and CH_4 conversions decrease in the order of $CeZr_{0.5}Ni_2O_Y$ > $CeZr_{0.5}Ni_1O_Y$ > $CeZr_{0.5}Ni_5O_Y$ > $CeZr_{0.5}Ni_{0.5}O_Y$. The Ni content has no effect on the H_2/CO ratio, H_2/CO ratio of Zr dropping compounds in this condition around 1.3. Carbon formation rate generally increases with increasing of nickel content, $CeZr_{0.5}Ni_{0.5}O_Y$ has lowest carbon formation rate of 0 $g \cdot gcat^{-1} \cdot h^{-1}$, and $CeZr_{0.5}Ni_{0.5}O_Y$ has higest carbon formation rate of 0.29 $g \cdot gcat^{-1} \cdot h^{-1}$.

Yadav et al. investigated the catalytic performance of $40LaNi_{0.75}Zr_{0.20}Ce_{0.05}O_3/8MgO\text{-}SiO_2$ catalyst[103]. The catalyst synthesized by sol-gel method showed methane conversion of about 65 % and CO_2 conversion of 92 %, stability of 6 h. The test was conducted at 800 °C, with 100 mg catalyst, CO_2/ CH_4/ N_2 = 2:3:5, total flow of 100 mL/min. Although, the catalyst showed excellent catalytic performance, but it is costly and different to synthesis.

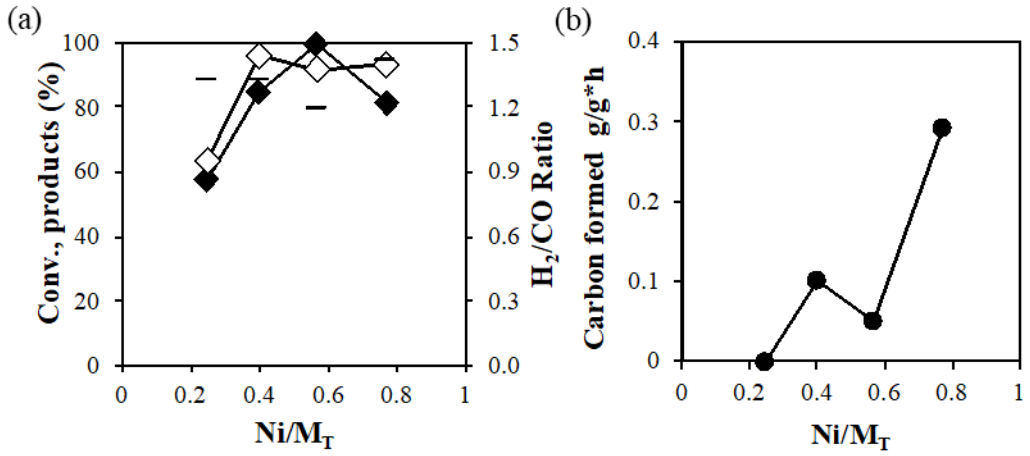

Fig. 2-53 DRM catalytic performance and carbon formation at 800 °C on calcined $CeZr_{0.5}Ni_XO_Y$ catalysts (10 mg) with in situ pretreatment in H_2 at 250°C. $CO_2/CH_4/N_2$ = 5:7:88%. CH_4 (◆), CO_2 (◇) and H_2/CO (-) ratio. Ni/M_T = x/(x+1+0.5). Time of experiments = 5h.

2.B.3.2.c Stability test

In order to investigate the catalytic stability of the $CeZr_{0.5}Ni_2O_Y$ catalyst, a test is conducted at 800 °C for 80 hours. As shown in Fig. 2-54, the $CeZr_{0.5}Ni_2O_Y$ catalyst exhibits a deactivation along with the DRM process. The conversions of methane and CO_2 are of 78.8 % and 95.6 % at the beginning, respectively. Then final conversion of methane and CO_2 are of 59.1 % and 65.1 %, respectively. The carbon formation rate is of 0.045 $g \cdot gcat^{-1} \cdot h^{-1}$.

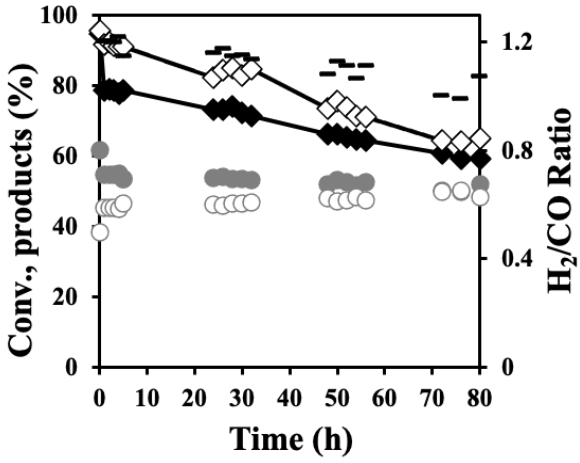

Fig. 2-54 DRM catalytic performance at 800 °C on calcined $CeZr_{0.5}Ni_2O_Y$ catalysts (10 mg) with in situ H_2 pretreatment at 250 °C. CH_4 (◆), CO_2 (◇), H_2 (●), CO (○), in mol% and H_2/CO (-) ratio. $CO_2/CH_4/N_2$ = 5:7:88%.

2.B.3.3 On $CeAl_{0.5}Ni_XO_Y$ catalysts

2.B.3.3.a Influence of time

On the $CeAl_{0.5}Ni_XO_Y$ catalysts the conversions and H_2/CO ratio as a function of time are plotted and shown in Fig. 2-55. Results show that the CO_2 conversion is greater than CH_4 conversion in all the catalysts. For $CeAl_{0.5}Ni_{0.5}O_Y$ catalyst, the CH_4 and CO_2 conversions are of 71.3 % and 80.1 % at first, then drop to 55.3 % and 65.0 % after 5 hours on stream. The H_2/CO ratio is of 1.3 and the carbon formation rate is of 0.058 $g \cdot gcat^{-1} \cdot h^{-1}$. The $CeAl_{0.5}Ni_1O_Y$ shows CH_4 and CO_2 conversions decreasing in first 2 h then increasing to 74.2 % and 89.1% after 5 h. The H_2/CO ratio stays stable around 1.3 and carbon formation rate is of 0.095 $g \cdot gcat^{-1} \cdot h^{-1}$. The $CeAl_{0.5}Ni_2O_Y$ presents an increasing in DRM performance, the CH_4 conversion upgrades from 60.6 % to 80.4 % and CO_2 conversion from 72.0 % to 93.5 %. The H_2/CO ratio decreases from 1.5 to 1.3. The $CeAl_{0.5}Ni_{0.5}O_Y$ catalyst presents a relatively stable performance. The CH_4 and CO_2 conversions are of 80.0 % and 93.6 % and the H_2/CO ratio is of 1.3 after 5 hours.

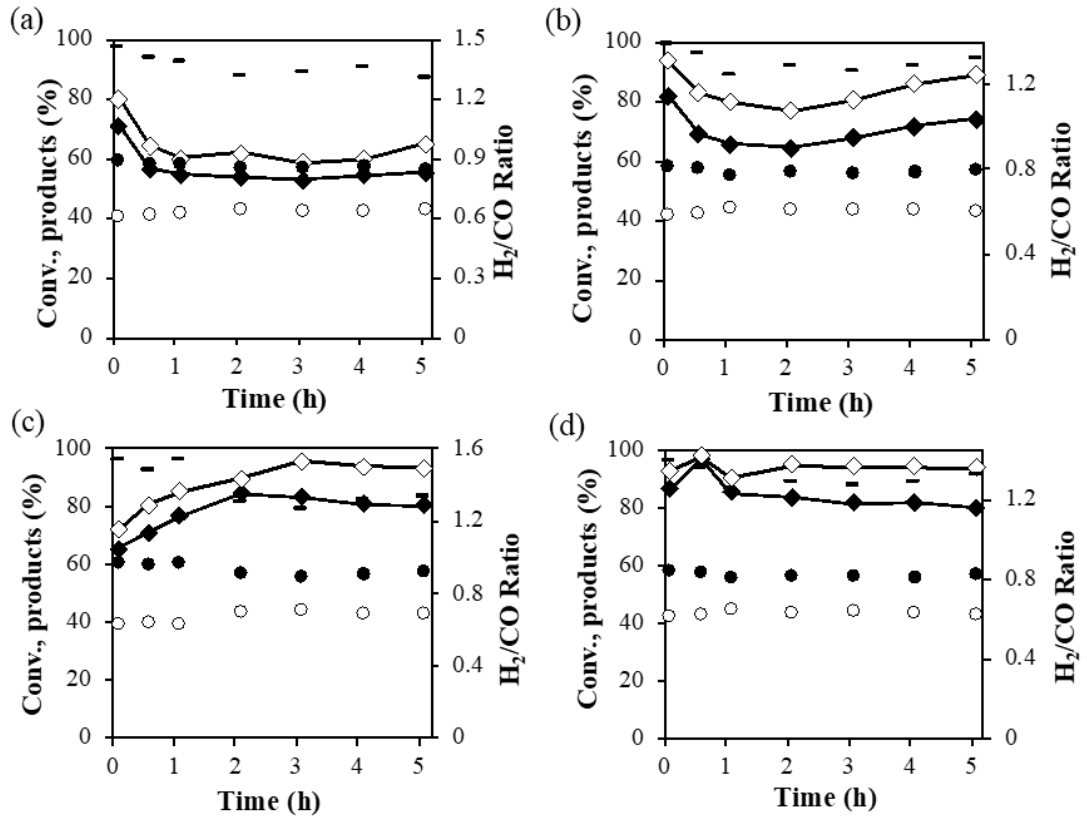

Fig. 2-55 DRM catalytic performance at 800 °C on calcined a) $CeAl_{0.5}Ni_{0.5}O_Y$, b) $CeAl_{0.5}Ni_1O_Y$, c) $CeAl_{0.5}Ni_2O_Y$, and d) $CeAl_{0.5}Ni_5O_Y$ catalysts (50 mg) with in situ H_2 pretreatment at 250 °C.CH_4 (◆), CO_2 (◇) conversions, H_2 (●), CO (○), in mol % and the H_2/CO ratio (-). $CH_4/CO_2/N_2$ = 7:5:88%.

2.B.3.3.b Influence of Ni content

Fig. 2-56 shows that the reactant conversions increase when the Ni content increase up to Ni/M_T ratio of 0.6 (from 12 wt.% to 30.8 wt.% in Ni), where CO_2 conversion is almost total. The conversions stay the same value when Ni content increase up to Ni/M_T ratio of 0.8 (from 30.8 wt.% to 49.2 wt.% Ni). The carbon formation rate increases with increasing the Ni content, while the H_2/CO molar ratio stays stable around 1.3 for all the Al based catalysts.

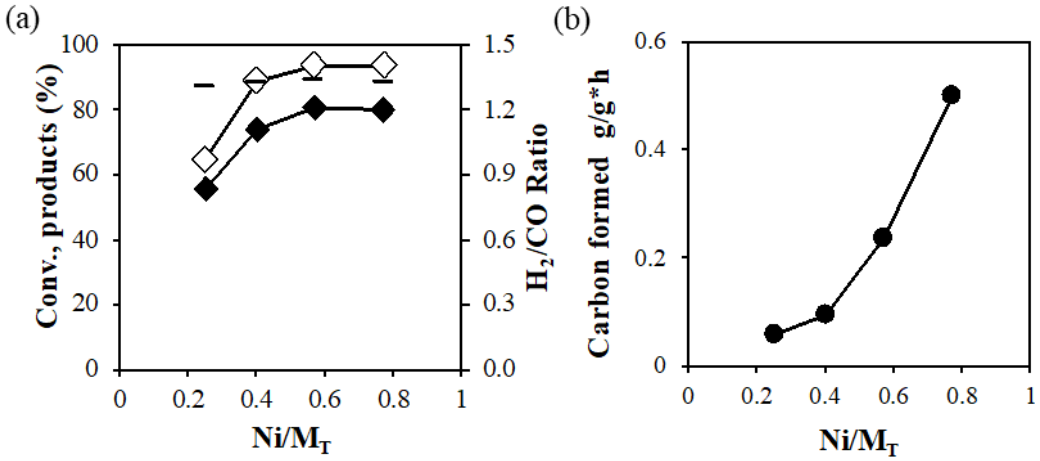

Fig. 2-56 DRM catalytic performance and carbon formation at 800 °C on calcined $CeAl_{0.5}Ni_XO_Y$ catalysts (10 mg) with in situ pretreatment in H_2 at 250°C. $CO_2/CH_4/N_2$ = 5:7:88%. CH_4 (◆), CO_2 (◇) and H_2/CO (-) ratio. $Ni/M_T = x/(x+1+0.5)$. Time of experiments = 5h.

2.B.3.4 On $AlMg_2Ni_XO_Y$ catalysts

2.B.3.4.a Influence of time

The catalytic performance of the $AlMg_2Ni_XO_Y$ catalysts with H_2 pretreatment at 450 °C as a function of time are shown in Fig. 2-57 All the catalysts in this series present an excellent stability during 5 h, with very high conversions (even if a very low mass of catalyst of 10 mg is used). For $AlMg_2Ni_1O_Y$ and $AlMg_2Ni_3O_Y$ catalysts, the CO_2 conversion is higher than CH_4 conversion. The $AlMg_2Ni_{12}O_Y$ catalyst shows almost total conversions of CH_4 and CO_2.

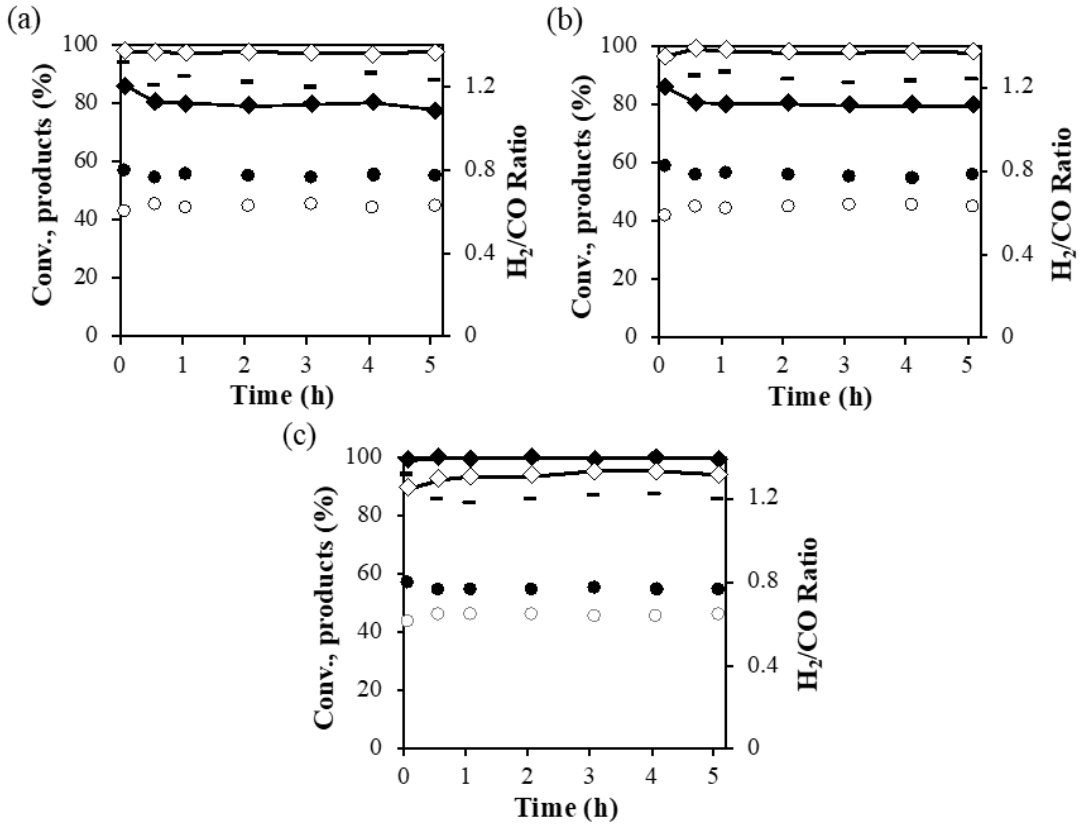

Fig. 2-57 DRM catalytic performance at 800 °C on calcined a) $AlMg_2Ni_1O_Y$, b) $AlMg_2Ni_3O_Y$, and c) $AlMg_2Ni_{12}O_Y$ catalysts (10 mg) with in situ H_2 pretreatment at 450 °C. CH_4 (◆), CO_2 (◇) conversions, H_2 (●), CO (○), in mol % and H_2/CO ratio (-). $CH_4/CO_2/N_2$ = 7:5:88%.

2.B.3.4.b Influence of Ni content

To analyze the influence of Ni content, the reactant conversions and H_2/CO molar ratio are shown in Fig. 2-58 versus Ni content. As shown in Fig. 2-58, the Ni content has little effect on the conversions of reactants (in the range of Ni contents studied). When Ni content increases from 21.9 wt.% to 43.7 wt.%, the conversions stay same. The nickel content has no effect on the H_2/CO ratio (at about 1.2), but for $AlMg_2Ni_3O_Y$ catalyst, the highest carbon formation rate at around 0.08 $g \cdot gcat^{-1} \cdot h^{-1}$ is found. The $AlMg_2Ni_{12}O_Y$ compound presents the best catalytic performance with CH_4 and CO_2 conversions of 99.4 % and 92.1 % respectively, and lowest carbon formation rate of 0.02 $g \cdot gcat^{-1} \cdot h^{-1}$.

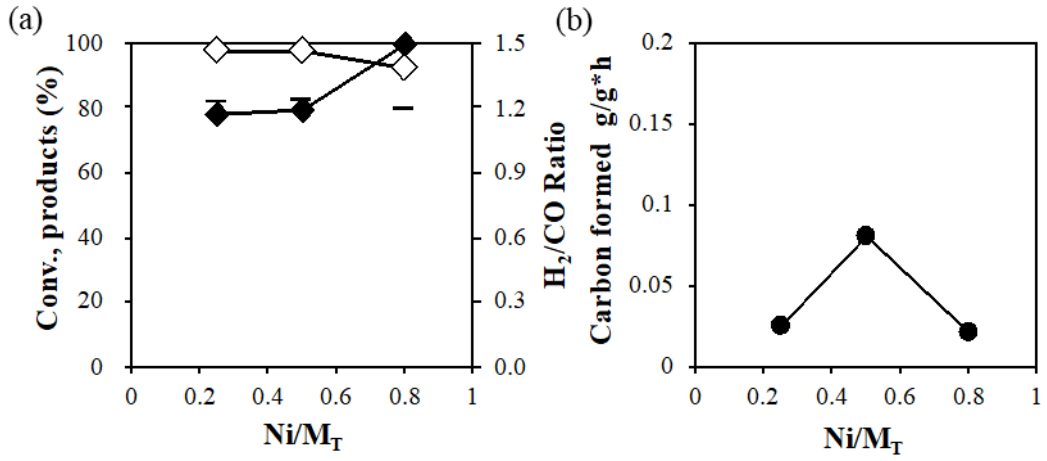

Fig. 2-58 DRM catalytic performance and carbon formation at 800 °C on calcined $AlMg_2Ni_XO_Y$ catalysts (10 mg) with in situ pretreatment in H_2 at 250°C. $CO_2/CH_4/N_2$ = 5:7:88%. CH_4 (◆), CO_2 (◇) and H_2/CO (-) ratio. Ni/M_T = x/(x+1+2). Time of experiments = 5h.

2.B.3.4.c Stability test

The stability of the $AlMg_2Ni_{12}O_Y$ catalyst during 80 h is shown in Fig. 2-59. he CH_4 and CO_2 conversions starting with the value of 90.3 % and 95.2 %, decrease during the first 30 h and then become stable up to 80 h, they are of 76.8 % and 84.1 %, respectively, after 80 h. The H_2/CO ratio of 1.1 suggest the occurrence of side reactions which result in higher H_2 production, such as CH_4 decomposition. The carbon formation rate is of 0.0081 $g \cdot gcat^{-1} \cdot h^{-1}$.

Akbari et al reported the DRM catalytic performance of Ni-MgO-Al_2O_3 catalyst with CO_2/CH_4 = 0.5[116]. The catalyst prepared by co-precipitation method showed CH_4 and CO_2 conversions of 58 % and 89 %, respectively, at 700 °C.

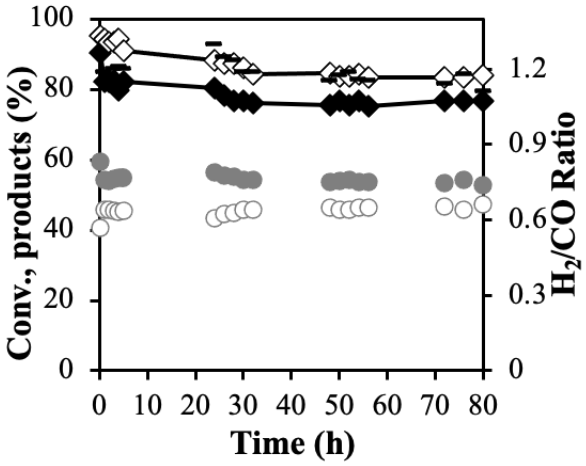

Fig. 2-59 DRM catalytic performance at 800 °C on calcined $AlMg_2Ni_{12}O_Y$ catalyst (10 mg) with in situ H_2 pretreatment at 250 °C. CH_4 (◆), CO_2 (◇), H_2 (●), CO (○), in mol% and H_2/CO (-) ratio. $CO_2/CH_4/N_2$ = 5:7:88%.

2.B.4 Catalytic performance at 800 °C on catalysts without H_2 pretreatment

2.B.4.1 On $CeNi_XO_Y$ catalysts

2.B.4.1.a Influence of time and Ni content

The catalysts without H_2 pretreatment are examined for DRM performance at 800 °C, as shown in Fig. 2-60. Globally, all the catalysts suffer a decline in both reactant conversions during the first hour, and then a stabilization is obtained over the 5 h. The $CeNi_2O_Y$ catalyst leads to CH_4 and CO_2 conversions of 62.7 % and 83.5 %, respectively, with a H_2/CO ratio of 1.27. Generally, the reactants conversion increases with the increase of nickel content, but $CeNi_{0.2}O_Y$ catalyst presents a relatively excellent catalytic performance, 43.2 % and 53.6 % of CH_4 and CO_2 conversions with 6.2 wt.% of Ni. The H_2/CO ratio of $CeNi_{0.2}O_Y$ is 1.23 and carbon formation rate is 0.0067 $g \cdot gcat^{-1} \cdot h^{-1}$.

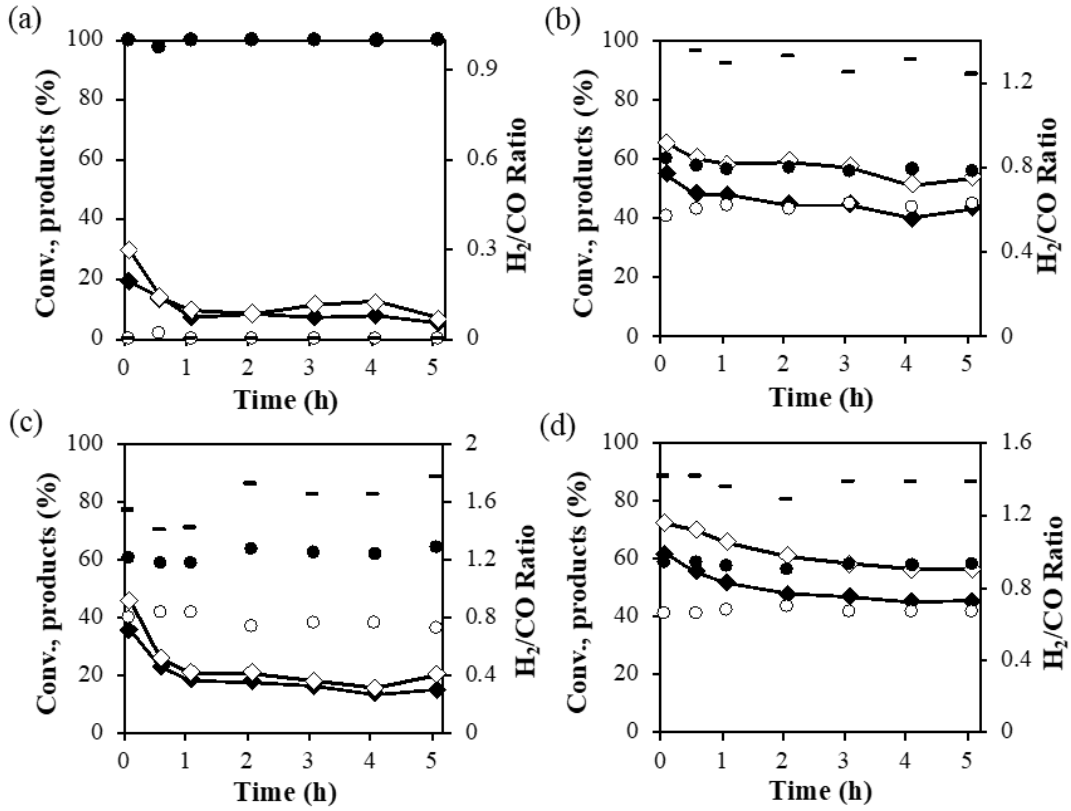

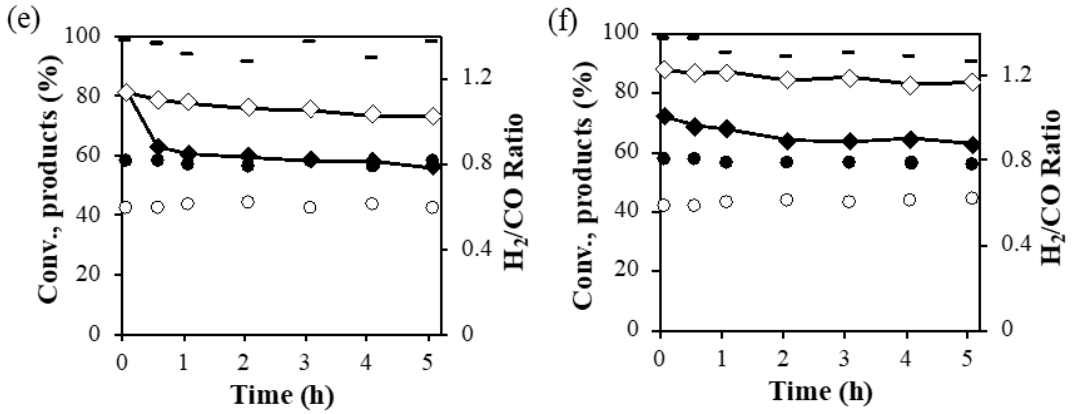

Fig. 2-60 DRM catalytic performance at 800 °C on calcined a) $CeNi_{0.1}O_Y$, b) $CeNi_{0.2}O_Y$, c) $CeNi_{0.3}O_Y$, d) $CeNi_{0.5}O_Y$, e) $CeNi_1O_Y$, and f) $CeNi_2O_Y$ catalysts (10 mg) without H_2 pretreatment. CH_4 (◆), CO_2 (◇) conversions, H_2 (●), CO (○), in mol % and H_2/CO ratio (-). $CH_4/CO_2/N_2$ = 7:5:88%.

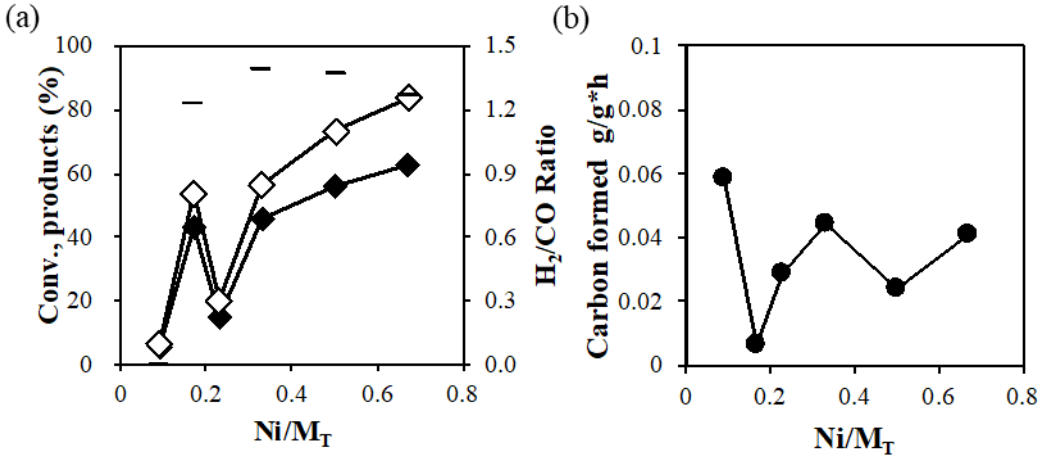

Fig. 2-61 DRM catalytic performance and carbon formation at 800 °C on calcined $CeNi_XO_Y$ catalysts (10 mg) without H_2 pretreatment. $CO_2/CH_4/N_2$ = 5:7:88%. CH_4 (◆), CO_2 (◇) and H_2/CO (-) ratio. $Ni/M_T = x/(x+1)$. Time of experiments = 5h.

2.B.4.1.b Influence of mass of catalysts

The DRM performance with a higher amount of 50 mg catalyst is tested with the condition of $CO_2/CH_4/N_2$ = 5:7:88% and without in situ H_2 pretreatment on $CeNi_XO_Y$. As shown in Fig. 2-62, CH_4 and CO_2 conversions are improved as the mass of catalysts increases for $CeNi_{0.3}O_Y$, $CeNi_{0.5}O_Y$, and $CeNi_1O_Y$ catalysts. Globally, H_2/CO ratio are not affected by add the mass of catalysts. With 50 mg of catalysts, the carbon formation rates are lower than that obtained with 10 mg catalysts. The $CeNi_2O_Y$ catalyst presents the best catalytic performance with 50 mg catalyst (Fig. 2-62). The conversion of CH_4 and CO_2 are 65.6 % and 88.2 %, respectively. H_2/CO ratio is 1.2 and carbon formation rate is 0.013 $g \cdot gcat^{-1} \cdot h^{-1}$.

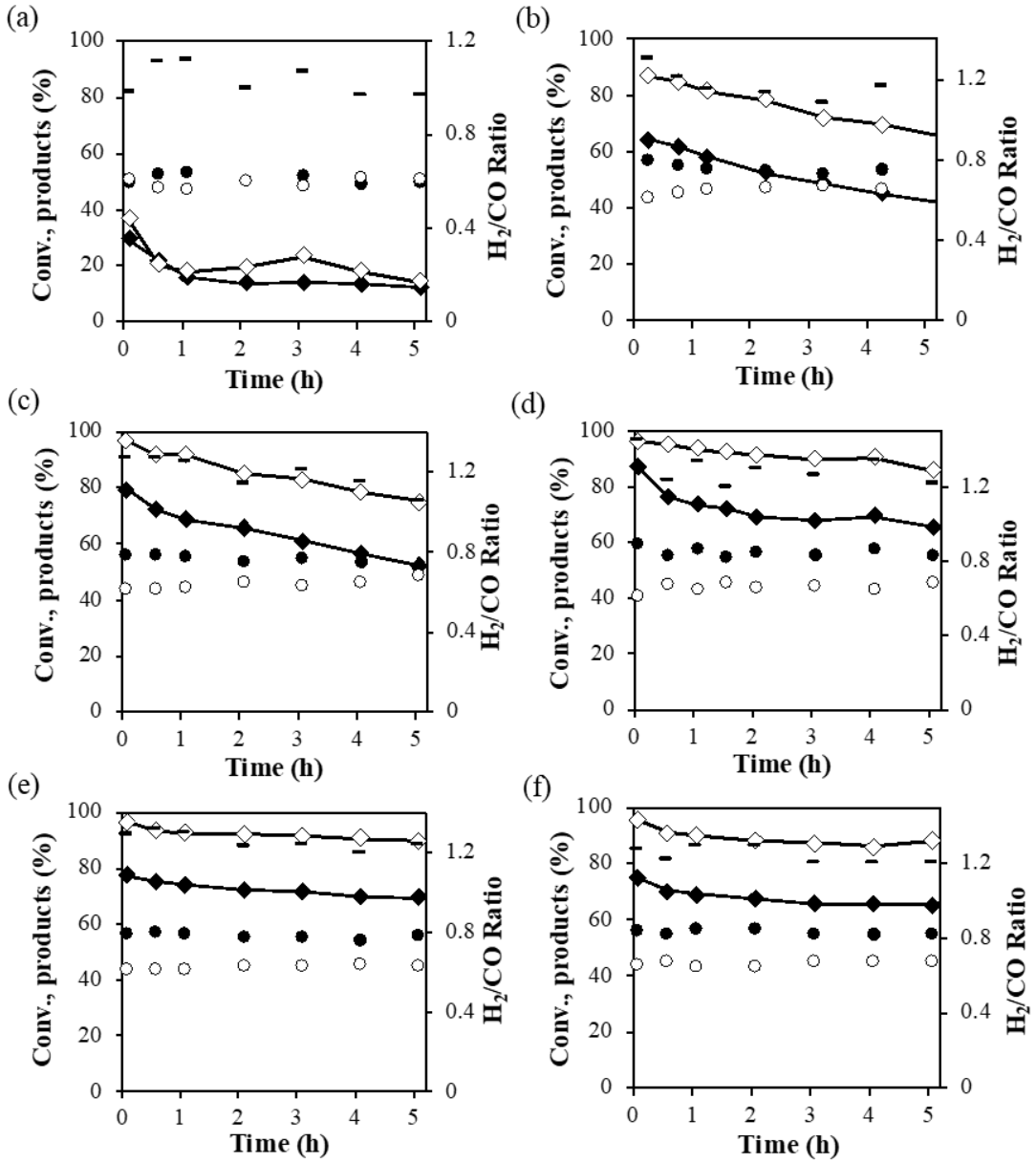

Fig. 2-62 DRM catalytic performance at 800 °C on calcined a) $CeNi_{0.1}O_Y$, b) $CeNi_{0.2}O_Y$, c) $CeNi_{0.3}O_Y$, d) $CeNi_{0.5}O_Y$, e) $CeNi_1O_Y$, and f) $CeNi_2O_Y$ catalysts (50 mg) without H_2 pretreatment. CH_4 (◆), CO_2 (◇) conversions, H_2 (●), CO (○), in mol % and H_2/CO ratio (-). $CH_4/CO_2/N_2$ = 7:5:88%.

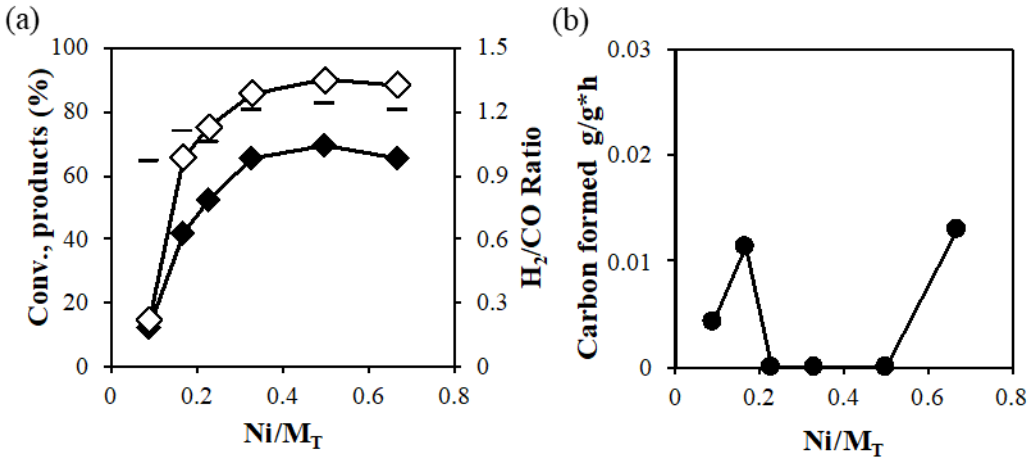

Fig. 2-63 DRM catalytic performance and carbon formation at 800 °C on calcined $CeNi_XO_Y$ catalysts (50 mg) without H_2 pretreatment. $CO_2/CH_4/N_2$ = 5:7:88%. CH_4 (◆), CO_2 (◇) and H_2/CO (-) ratio. $Ni/M_T = x/(x+1)$. Time of experiments = 5h.

2.B.4.1.c Influence of reaction temperature

On $CeNi_{0.5}O_Y$ catalyst (50 mg) without pretreatment in hydrogen Fig. 2-38 and 2-62 show particularly good catalytic performance at 800 °C compared to at 600 °C. CH_4 and CO_2 conversions rise from 65.3% and 68.2% at 600 °C to 86.8% and 96.1% at 800°C, separately. The experimental data perfectly align with the outcome of thermodynamic equilibrium computation in this condition, though stoichiometric equilibrium isn't totally reached in each scope of detected temperatures[200,201].

How temperature affects the catalytic performance of $CeNi_XO_Y$ catalyst is presented in Fig. 2-64. Generally, CH_4 and CO_2 conversions increase as the reaction temperature rises from 600 °C to 800 °C, anticipated as the reaction is a highly endothermic reaction and higher temperature helps shift chemical equilibrium towards syngas generation. CO_2 conversion exceeds paralleled CH_4 conversion for all specimens, mainly resulting from lower concentration of CO_2 in reactants[142].

2.B.4.2 On $CeZr_{0.5}Ni_XO_Y$ catalysts

2.B.4.2.a Influence of time

Fig. 2-64 illustrates catalytic performance of the $CeZr_{0.5}Ni_XO_Y$ catalysts without H_2 pretreatment in DRM reaction at 800 °C (10 mg of catalyst) with CO_2:CH_4 ratio 0.7. For $CeZr_{0.5}Ni_{0.5}O_Y$, the catalytic performance drops significantly with time. After 5 hours, the CH_4 and CO_2 conversions are of 29.8 % and 44.1 %, respectively. The H_2/CO ratio is around 0.9, the carbon formation rate is of 0.05 $g \cdot g_{cat}^{-1} \cdot h^{-1}$. For $CeZr_{0.5}Ni_1O_Y$ the reactants conversions decrease slightly in first 1 h then stay around 66.9 % and 86.7 %, respectively. The two high Ni content catalysts ($CeZr_{0.5}Ni_2O_Y$

and $CeZr_{0.5}Ni_5O_Y$) present very good catalytic performances, with CH_4 and CO_2 conversions around 99 % and 93 %, respectively, at the stable state (5h). Moreover, the $CeZr_{0.5}Ni_2O_Y$ compound presents even an activation under the feed, conversions increasing with time. And H_2/CO ratio is 1.2, carbon formation rate is 0.12 $g \cdot g_{cat}^{-1} \cdot h^{-1}$.

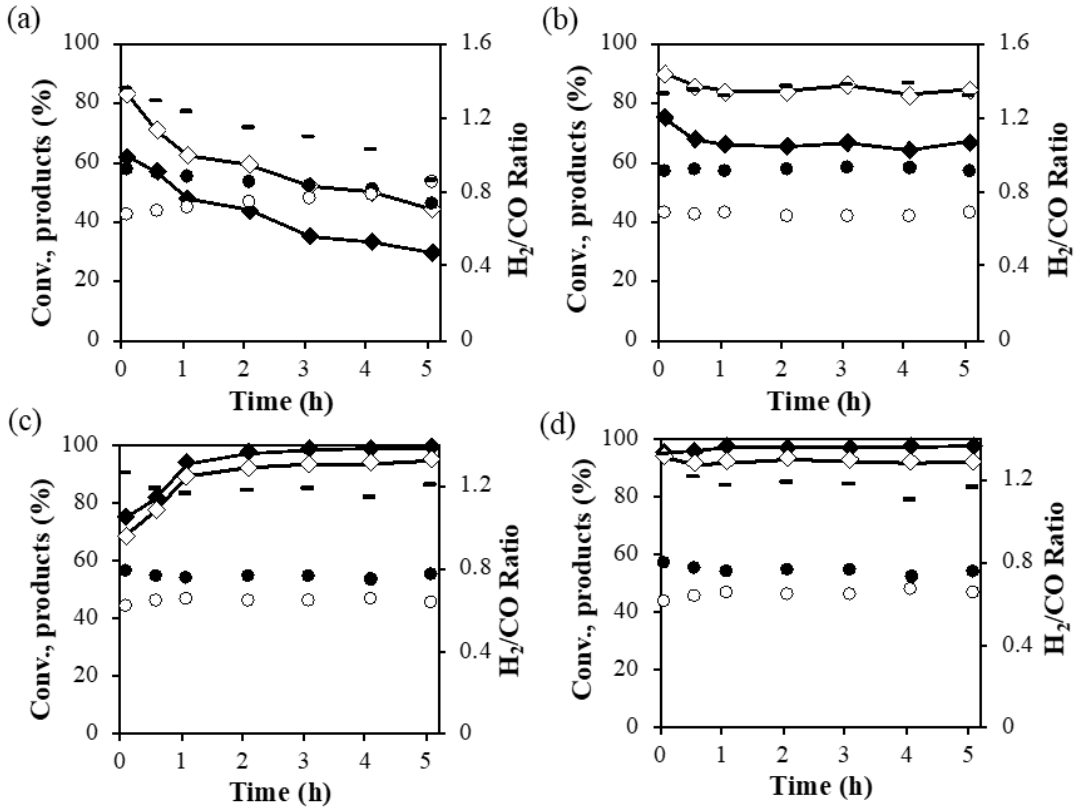

Fig. 2-64 DRM catalytic performance at 800 °C on calcined a) $CeZr_{0.5}Ni_{0.5}O_Y$, b) $CeZr_{0.5}Ni_1O_Y$, c) $CeZr_{0.5}Ni_2O_Y$, and d) $CeZr_{0.5}Ni_5O_Y$ catalysts (10 mg) without H_2 pretreatment. CH_4 (◆), CO_2 (◇) conversions, H_2 (●), CO (○), in mol % and H_2/CO ratio (-). $CH_4/CO_2/N_2$ = 7:5:88%.

2.B.4.2.b Influence of Ni content

On the $CeZr_{0.5}Ni_XO_Y$ catalysts without H_2 pretreatment in DRM reaction at 800 °C, when the Ni/M_T ratio increases, the ternary catalysts provide higher CH_4 and CO_2 conversions (Fig. 2-65). Moreover, the H_2/CO ratio slightly increases with the Ni/M_T increasing from 0.87 on $CeZr_{0.5}Ni_{0.5}O_Y$ to 1.32 on $CeZr_{0.5}Ni_1O_Y$. Carbon formation rate increases from 0.0542 $g \cdot g_{cat}^{-1} \cdot h^{-1}$ to 0.4987 $g \cdot g_{cat}^{-1} \cdot h^{-1}$ when the Ni/M_T ratio increases from 0.5 to 1. With the further increase of nickel content, the carbon formation rate decreases to 0 $g \cdot g_{cat}^{-1} \cdot h^{-1}$ on $CeZr_{0.5}Ni_5O_Y$. In this condition, $CeZr_{0.5}Ni_5O_Y$ catalyst presents a best catalytic performance, with 97.8 % and 89.6 % of CH_4 and CO_2 conversions and 1.16 of H_2/CO ratio.

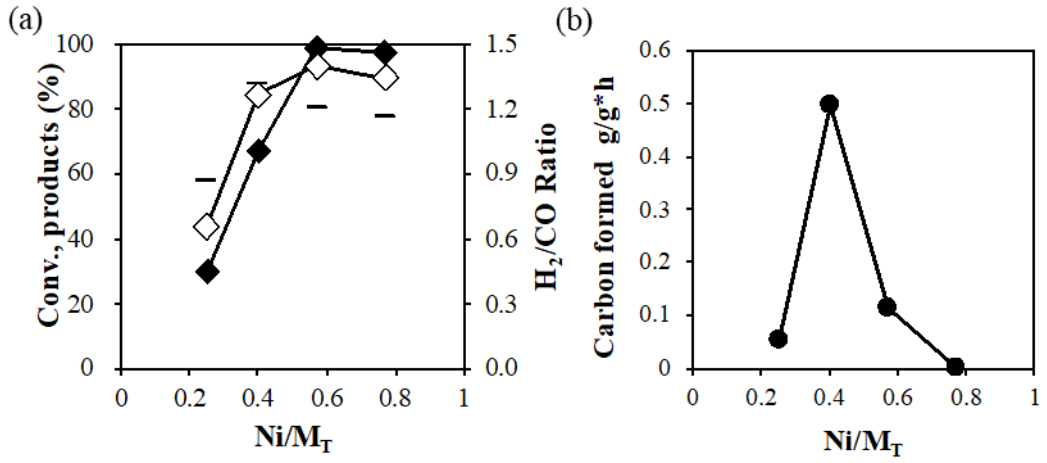

Fig. 2-65 DRM catalytic performance and carbon formation at 800 °C on calcined $CeZr_{0.5}Ni_XO_Y$ catalysts (10 mg) without H_2 pretreatment. $CO_2/CH_4/N_2$ = 5:7:88%. CH_4 (◆), CO_2 (◇) and H_2/CO (-) ratio. Ni/M_T = x/(x+1+0.5). Time of experiments = 5h.

2.B.4.3 On $CeAl_{0.5}Ni_XO_Y$ catalysts

2.B.4.3.a Influence of time

The catalytic performance of $CeAl_{0.5}Ni_XO_Y$ catalysts is also examined without H_2 pretreatment. The conversion as a function of time is presented in Fig. 2-66. During first hour under feed, a decrease in conversions is found for low Ni content catalysts ($CeAl_{0.5}Ni_1O_Y$ and $CeAl_{0.5}Ni_{0.5}O_Y$), and a variation of the CH_4 conversion is observed for the highest Ni content catalyst. The H_2/CO molar ratio is always higher than unity, and relatively stable at around 1.2.

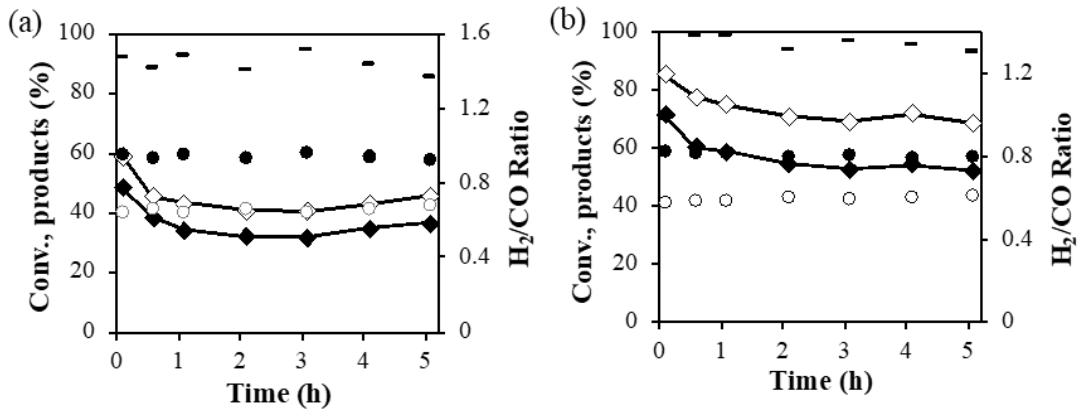

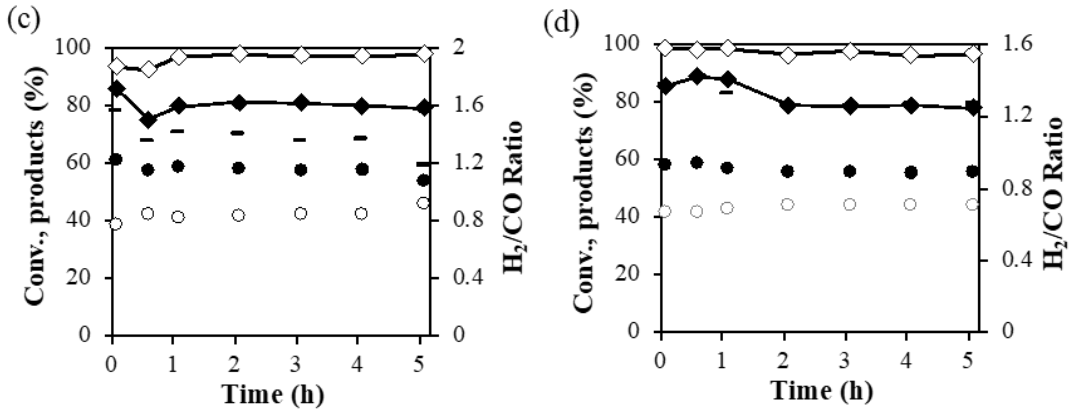

Fig. 2-66 DRM catalytic performance at 800 °C on calcined a) $CeAl_{0.5}Ni_{0.5}O_Y$, b) $CeAl_{0.5}Ni_1O_Y$, c) $CeAl_{0.5}Ni_2O_Y$, and d) $CeAl_{0.5}Ni_5O_Y$ catalysts (10 mg) without H_2 pretreatment. CH_4 (◆), CO_2 (◇) conversions, H_2 (●), CO (○), in mol % and H_2/CO ratio (-). $CH_4/CO_2/N_2$ = 7:5:88%.

2.B.4.3.b Influence of Ni content

On the $CeAl_{0.5}Ni_XO_Y$ catalysts, conversions globally increase with Ni content and the conversion of CO_2 is always higher than the conversion of CH_4 in such conditions (Fig. 2-67). At 800 °C, like an optimum is found when Ni/M_T is of 0.6, as for higher value of Ni/M_T similar conversions are obtained. The $CeAl_{0.5}Ni_2O_Y$ compound allows to get methane conversion of 79.3 % and CO_2 conversion almost total of 97.9 %, with a H_2/CO ratio at about 1.2, and a carbon formation around 0.16 $g \cdot g_{cat}^{-1} \cdot h^{-1}$. The highest Ni content $CeAl_{0.5}Ni_5O_Y$ compound leads to slightly lower conversions than $CeAl_{0.5}Ni_2O_Y$, but with much higher carbon formation rate (about 0.35 $g \cdot g_{cat}^{-1} \cdot h^{-1}$). The highest methane conversion is observed for the $CeAl_{0.5}Ni_2O_Y$ catalyst, followed by $CeAl_{0.5}Ni_5O_Y$, $CeAl_{0.5}Ni_1O_Y$, $CeAl_{0.5}Ni_{0.5}O_Y$.

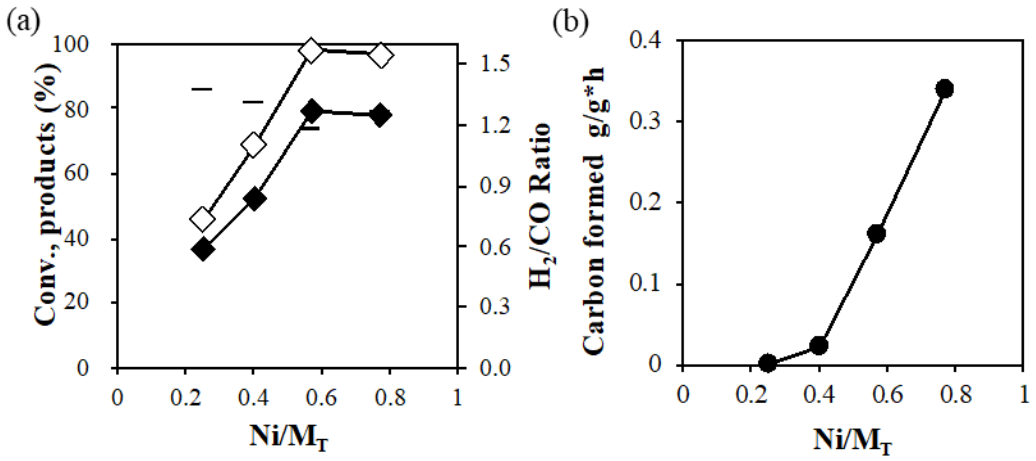

Fig. 2-67 DRM catalytic performance and carbon formation at 800 °C on calcined $CeAl_{0.5}Ni_XO_Y$ catalysts (10 mg) without H_2 pretreatment. $CO_2/CH_4/N_2$ = 5:7:88%. CH_4 (◆), CO_2 (◇) and H_2/CO (-) ratio. Ni/M_T = x/(x+1+0.5). Time of experiments = 5h.

2.B.4.4 On $AlMg_2Ni_XO_Y$ catalysts

2.B.4.4.a Influence of time

Fig. 2-68 shows the DRM results obtained on $AlMg_2Ni_XO_Y$ catalysts at 800 °C, 10 mg, without H_2 pretreatment, $CO_2/CH_4/N_2$ = 5:7:88%. The catalysts present very good stabilities after first hour, with even an increase in conversions in some cases. For $AlMg_2Ni_1O_Y$, the CH_4 and CO_2 conversions stay at 79.0 % and 98.0 %, respectively, from beginning to the end of the test during 5h, and the H_2/CO molar ratio keeps at 1.2. For $AlMg_2Ni_3O_Y$, the CH_4 and CO_2 conversions increase at the first half hour, then keep stable around 77.2 % and 96.4 %, respectively. For high Ni content catalyst $AlMg_2Ni_{12}O_Y$, the reactants conversions are lower at the initial state and then increase to 93.1 % and 86.3 %, respectively, for CH_4 and CO_2.

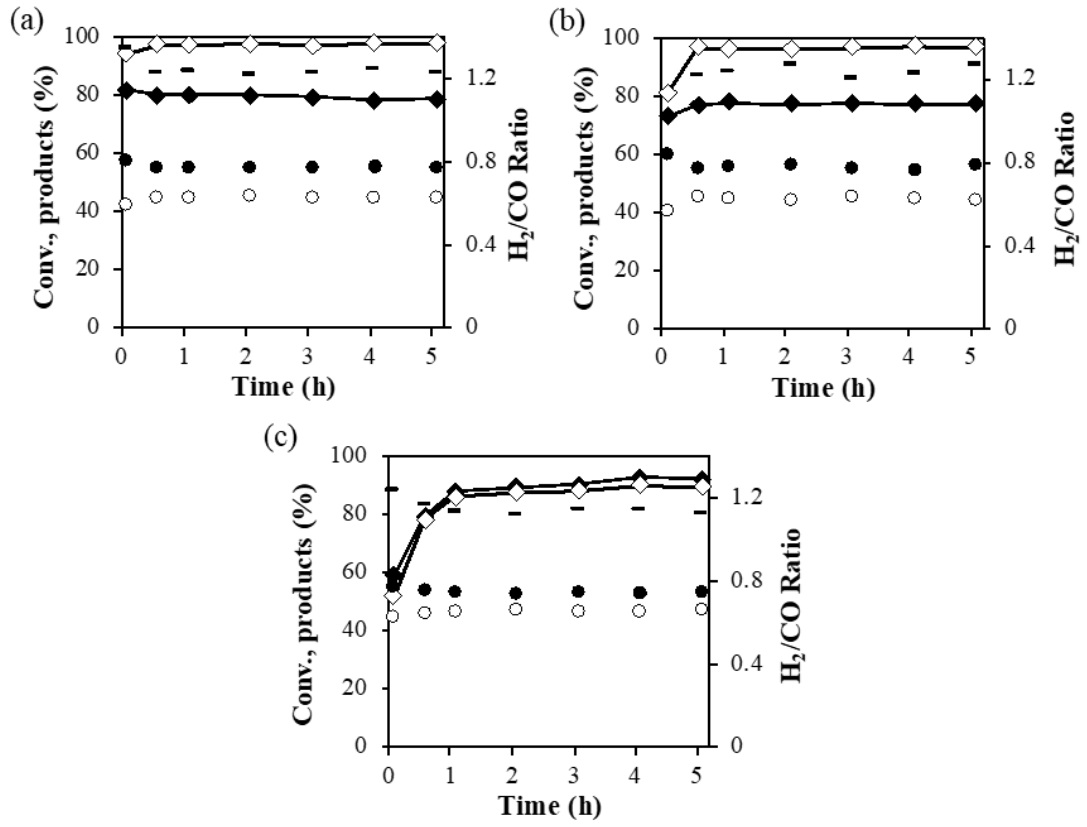

Fig. 2-68 DRM catalytic performance at 800 °C on calcined a) $AlMg_2Ni_1O_Y$, b) $AlMg_2Ni_3O_Y$, and c) $AlMg_2Ni_{12}O_Y$ catalysts (10 mg) without H_2 pretreatment. CH_4 (◆), CO_2 (◇) conversions, H_2 (●), CO (○), in mol % and H_2/CO ratio (-). $CH_4/CO_2/N_2$ = 7:5:88%.

2.B.4.4.b Influence of Ni content

Fig. 2-69 shows the evolution on this series of catalysts versus Ni content. For catalysts with lower Ni content, the CO_2 conversion is higher than the CH_4 conversion. The CH_4 conversion is higher than CO_2 conversion in the case of the high Ni content

catalyst. The H_2/CO ratio is always around 1.2 no matter the Ni content of the catalysts. The carbon formation rate increases with the Ni content increasing.

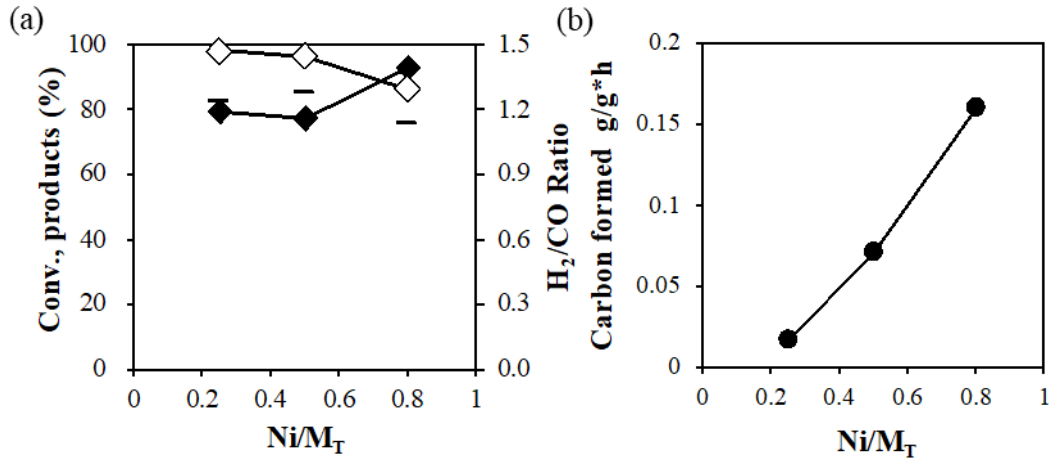

Fig. 2-69 DRM catalytic performance and carbon formation at 800 °C on calcined $AlMg_2Ni_XO_Y$ catalysts (10 mg) without H_2 pretreatment. $CO_2/CH_4/N_2$ = 5:7:88%. CH_4 (◆), CO_2 (◇) and H_2/CO (-) ratio. Ni/M_T = x/(x+1+2). Time of experiments = 5h.

Han et al. studied the CH_4 and CO_2 conversion rates and the syngas yield for different ratios of CO_2/CH_4 (0.5, 1, and 2). The simulation results showed that the optimum CO_2/CH_4 ratio was of 0.5. Under this condition, the CH_4 conversion rate was close to 92 %, and the CO_2 conversion rate was close to 85 %, the H_2/CO ratio of 1.6, at 800 °C on 3 wt. % Ni/Ce-MgO-ZrO_2/Al_2O_3 catalyst[117].

Conclusion of part B

The catalysts are studied in DRM with CO_2/CH_4 = 0.7 (CH_4/ CO_2/ N_2 = 7: 5: 88 %). At 600 °C, on 50 mg of catalyst, with in situ H_2 pretreatment, calcined $CeNi_{0.5}O_Y$ shows a similar conversion as using higher content of nickel and exhibits less carbon deposition. CH_4 and CO_2 conversions are about 52.9% and 67.1% after 5 h of test, with a H_2/CO ratio of around 1.28. Dried $CeNi_{0.5}O_Y$ compound also shows the similar result, but with lower carbon formation rate. 73.1 % and 65.9 % conversions of CH_4 and CO_2 are obtained with a H_2/CO ratio of 1.9 on $CeAl_{0.5}Ni_2O_Y$. The carbon formation rate is of 0.52 $g \cdot gcat^{-1} \cdot h^{-1}$.

Without H_2 pretreatment, among the binary catalysts, $CeNi_1O_Y$ displays best conversions of CH_4 and CO_2 at 59.8 % and 76.6 %, a H_2/CO ratio of 1.3, and carbon formation rate of 0.75 $g \cdot gcat^{-1} \cdot h^{-1}$. For $CeNi_XO_Y$ catalysts, at 600 °C, on 50 mg of catalyst, pretreatment provides no advantages on catalytic performance, it means that the catalyst is already activated even without the pretreatment under H_2. The reactor is blocked after 4.5 hours on $CeZr_{0.5}Ni_1O_Y$, with CH_4 and CO_2 conversions of 55.4 % and

68.5 %, a H_2/CO ratio of 1.37, and a carbon formation rate so high around 0.75 $g \cdot gcat^{-1} \cdot h^{-1}$. In Al compound series, the highest conversions of CH_4 and CO_2 are obtained at 82.2 % and 75.6 % on $CeAl_{0.5}Ni_5O_Y$ catalyst, with carbon formation rate of 0.76 $g \cdot gcat^{-1} \cdot h^{-1}$.

Then the catalytic performance is analyzed at 800 °C, on 10 mg of catalyst. $CeNi_{0.2}O_Y$ shows an excellent catalytic performance with 31.8 % and 38.2 % of CH_4 and CO_2 conversions after 5 hours on stream. Increasing the mass of catalyst to 50 mg, increase the conversions to 74.0 % and 93.9 %. On 10 mg of $CeNi_1O_Y$ final conversion of methane and CO_2 are of 23.8 % and 21.0 % after 80 h. The H_2/CO ratio is of 0.9 and carbon formation rate of 0.0012 $g \cdot gcat^{-1} \cdot h^{-1}$. The $CeZr_{0.5}Ni_2O_Y$ catalyst exhibits a deactivation in stability test. The conversions of methane and CO_2 drop from 78.8 % and 95.6 % to 59.1 % and 65.1 %. The carbon formation rate is of 0.045 $g \cdot gcat^{-1} \cdot h^{-1}$. $CeAl_{0.5}Ni_2O_Y$ presents CH_4 and CO_2 conversions of 80.4 % and 93.5 %, the H_2/CO ratio of 1.3, and carbon formation rate of 0.23 $g \cdot gcat^{-1} \cdot h^{-1}$. For the stability of $AlMg_2Ni_{12}O_Y$ catalyst, 76.8 % and 84.1 % of CH_4 and CO_2 conversions are obtained after 80 h, with a H_2/CO ratio 1.1 and a carbon formation rate of 0.008 $g \cdot gcat^{-1} \cdot h^{-1}$.

Without H_2 pretreatment, the $CeNi_2O_Y$ catalyst has the best performance at the end of 5 h, with CH_4 and CO_2 conversions of 62.7 % and 83.5 %, and carbon formation rate of 0.04 $g \cdot gcat^{-1} \cdot h^{-1}$. Increasing the mass of catalyst to 50 mg, the conversions stay the same on $CeNi_2O_Y$ but increase on low Ni content catalysts. For ternary catalysts, $CeZr_{0.5}Ni_2O_Y$ shows CH_4 and CO_2 conversions around 99 % and 93 %, and carbon formation rate of 0.12 $g \cdot gcat^{-1} \cdot h^{-1}$. $CeAl_{0.5}Ni_2O_Y$ compound allows methane and CO_2 conversions to 79.3 % and 97.9 %, with H_2/CO ratio about 1.2, and carbon formation rate of 0.16 $g \cdot g_{cat}^{-1} \cdot h^{-1}$. For $AlMg_2Ni_1O_Y$, the CH_4 and CO_2 conversions stay stable at 79.0 % and 98.0 % during 5 h. The H_2/CO molar ratio keeps at 1.23, and carbon formation rate of 0.016 $g \cdot g_{cat}^{-1} \cdot h^{-1}$.

2.3 Conclusion

Dry reforming of methane is studied on $CeNi_XO_Y$, $CeZr_{0.5}Ni_XO_Y$, $CeAl_{0.5}Ni_XO_Y$, and $AlMg_2Ni_XO_Y$ catalysts with reactants ratio CO_2/CH_4 = 1 (CH_4/ CO_2/ N_2 = 5: 5: 90 %) and CO_2/CH_4 = 0.7 (CH_4/ CO_2/ N_2 = 7: 5: 88 %). Different parameters are analyzed on four series of nickel-based catalysts, such as the reaction temperature at 600 °C and 800 °C, in situ H_2 pretreatment and without pretreatment, to study the catalytic performance.

With H_2 pretreatment overnight, after 80 h on stream at 600 °C, with CH_4/ CO_2 = 1, $AlMg_2Ni_1O_Y$ compound (50 mg) presents the best performance with 75.9 % and 83.2 % of CH_4 and CO_2 conversions, a H_2/CO ratio of 1.2, and a carbon deposition rate of 0.017 $g \cdot gcat^{-1} \cdot h^{-1}$ after 80 h. In same condition but without pretreatment, $AlMg_2Ni_{12}O_Y$ catalyst shows the highest CH_4 and CO_2 conversions at 83.6 % and 80.0 %, respectively, but has a carbon formation rate of 0.61 $g \cdot gcat^{-1} \cdot h^{-1}$. $CeZr_{0.5}Ni_{0.5}O_Y$ also shows good catalytic performance with CH_4 and CO_2 conversions of 66.2 % and 72.7 % and a carbon formation rate of 0.004 $g \cdot gcat^{-1} \cdot h^{-1}$ after 80 h of stability test.

In DRM reaction at 800 °C, with 10 mg of catalyst pretreated, and under CH_4/CO_2 = 1, the best result is obtained on $AlMg_2Ni_{12}O_Y$, the conversions of methane and CO_2 are of 99.7 % and 93.8 %, respectively, after 80 hours, with a H_2/CO ratio of 1.2 and carbon formation rate of 0.006 $g \cdot gcat^{-1} \cdot h^{-1}$. For $CeNi_{0.5}Zr_2O_Y$, CH_4 and CO_2 conversions are of 98.8% and 93.5%, with a H_2/CO ratio of 1.2 and a carbon formation rate of 0.004 $g \cdot gcat^{-1} \cdot h^{-1}$ after 80 hours. Without H_2 pretreatment, dried $CeZr_{0.5}Ni_2O_Y$ presents CH_4 and CO_2 conversions of 95.8 % and 91.7 % after 80 h. The H_2/CO molar ratio is about 1.2 during the reaction. Moreover, the carbon deposition is of 0.0151 $g \cdot gcat^{-1} \cdot h^{-1}$.

The catalysts are studied also in DRM with CO_2/CH_4 = 0.7 (CH_4/ CO_2/ N_2 = 7: 5: 88 %). At 600 °C, on 50 mg of catalyst, with in situ H_2 pretreatment, 73.1 % and 65.9 % conversions of CH_4 and CO_2 are obtained with a H_2/CO ratio of 1.9 on $CeAl_{0.5}Ni_2O_Y$. The carbon formation rate is of 0.52 $g \cdot gcat^{-1} \cdot h^{-1}$. Without H_2 pretreatment, the highest conversion of CH_4 and CO_2 are obtained at 82.2 % and 75.6 % on $CeAl_{0.5}Ni_5O_Y$ catalyst, with a carbon formation rate of 0.76 $g \cdot gcat^{-1} \cdot h^{-1}$.

At 800 °C, with CO_2/CH_4 = 0.7, $CeNi_{0.2}O_Y$ (50 mg) with in situ H_2 pretreatment, shows an excellent catalytic performance with 74.0 % and 93.9 % of CH_4 and CO_2 conversions after 5 hours on stream. $CeAl_{0.5}Ni_2O_Y$ presents CH_4 and CO_2 conversions of 80.4 % and 93.5 %, respectively, a H_2/CO ratio of 1.3, and carbon formation rate of 0.23 $g \cdot gcat^{-1} \cdot h^{-1}$. Without H_2 pretreatment, $CeZr_{0.5}Ni_2O_Y$ shows CH_4 and CO_2 conversions around 99 % and 93 %, respectively, with a carbon formation rate of 0.12 $g \cdot gcat^{-1} \cdot h^{-1}$.

In general, CH_4 and CO_2 conversions increase with the increase of the reaction temperature from 600 °C to 800 °C, which is expected since the reaction is a highly endothermic. Conversions globally increase with Ni content while H_2/CO ratio seems not be influenced by Ni content. Pretreatment helps to decrease carbon formation in

some cases. When the reactants CO_2/CH_4 ratio changes from 1 to 0.7, the CO_2 conversion and H_2/CO ratio increase.

Chapter 3
Catalysts characterizations

Chapter 3 Catalysts characterizations

As reported, the co-precipitation method has the advantages of simple and rapid preparation, easy control of particle size and composition, various possibilities to modify the particle surface state and overall homogeneity, energy-efficient, organic solvent not involved[202], and also is known to increase the interaction between cations[203]. In this work $CeNi_XO_Y$, $CeZr_{0.5}Ni_XO_Y$, $CeAl_{0.5}Ni_XO_Y$, $AlMg_2Ni_XO_Y$ catalysts are prepared by coprecipitation (details are given in Annex 1) and characterized. Some chosen catalysts are also characterized after DRM reaction to analyze their evolution.

3.1 $CeNi_XO_Y$ catalysts characterization results

3.1.1 Elemental analysis and textural properties

In Table 3-1, the textural analyzes of the dried and calcined $CeNi_XO_Y$ catalysts are presented as a function of the nickel content. The dried catalysts all have a larger specific surface area (S. A.) than those of the calcined catalysts. In fact, this one varies between 77 and 123 m^2/g for the calcined catalysts and between 110 and 215 m^2/g for the dried catalysts. By increasing the nickel content, the specific surface of the dried catalysts increases. For calcined catalysts, the maximum surface area is of 123 m^2/g, for $CeNi_{0.5}O_Y$, then decreases to 107 m^2/g for the highest Ni content compound.

Table 3-1 Ni content and specific surface area (BET) of $CeNi_XO_Y$ compounds.

Sample	Ni (wt.%)	Ni/M_T	Surface area dried (m^2/g)	Surface area calcined (m^2/g)	CeO_2 (nm)	NiO (nm)
$CeNi_{0.1}O_Y$	3.2	0.09	110	77	6.5	/
$CeNi_{0.2}O_Y$	6.2	0.17	175	117		/
$CeNi_{0.3}O_Y$	9.5	0.23	160	116		/
$CeNi_{0.5}O_Y$	14.0	0.33	198	123	6.3	13.9
$CeNi_1O_Y$	23.8	0.50	190	110	6.4	11.8
$CeNi_2O_Y$	36.5	0.67	215	107	5.3	11.3

3.1.2 XRD studies

Fig. 3-1 and 3-2 display the typical XRD patterns of $CeNi_XO_Y$ catalysts with different Ni contents. The X-Ray diffraction patterns of dried $CeNi_XO_Y$ compounds shown in Fig. 3-1 contain six prominent diffraction peaks at $2\theta = 28.5°$, 33.1°, 47.5°,

56.3°, 69.4°, 77.6°, which respectively correspond to (111), (200), (220), (311), (222), (400) planes of typical CeO_2 fluorite structure (JCPDS 34-0394)[204]. The CeO_2 average crystallites size decreases from 5.1 to 4.6 nm with increasing Ni loading from 3.2 to 36.5 wt %, suggesting the possibly further incorporation of Ni into the catalyst. There are characteristic peaks of $Ni(OH)_2$ observed for dried $CeNi_{0.5}O_Y$, $CeNi_1O_Y$, and $CeNi_2O_Y$. The absence of $Ni(OH)_2$ diffraction peaks in low Ni content catalysts and the broadness and shift of CeO_2 peaks apparent in the XRD pattern of dried $CeNi_XO_Y$ compounds suggest the formation of a cerium-nickel solid solution, which adopts a simple ceria structure.

Fig. 3-2 illustrates the XRD peaks of calcined $CeNi_XO_Y$ catalysts. Consistent with dried catalyst, the typical diffraction peaks of ceria are also seen in the calcined catalysts. With the increasing of Ni content, the diffraction peaks of ceria become gradually broad and the peak position shifts, which comes from the substitution of the smaller Ni^{2+} (0.7 Å) ions into Ce^{4+} sites (0.9 Å) inside the CeO_2 lattice and the formation of the cerium-nickel solid solution. In addition, the diffraction peaks of nickel oxide also appear for a specific value of $x \geq 0.5$ (corresponding to the Ni wt% ≥ 14 wt%). The diffraction patterns observed at $2\theta = 37.2°$, 43.4°, 62.8°, are attributed to the (101), (012) and (110) planes of NiO (JCPDS 4-0835) respectively[205]. The intensities of NiO diffraction peaks gradually strengthen along with the increase of the Ni content. Thus, there are two kinds of Ni species in $CeNi_XO_Y$ catalysts, in a solid solution with the substitution of Ni^{2+} ions in the CeO_2 lattice, and in crystallized NiO. According to the XRD results, the Scherrer Equation is used to measure the average crystallites size. For NiO it is found between 11.3 and 13.9 nm and for CeO_2 between 5.3 and 6.5 nm, when the Ni content increases, the crystallites size increases slightly.

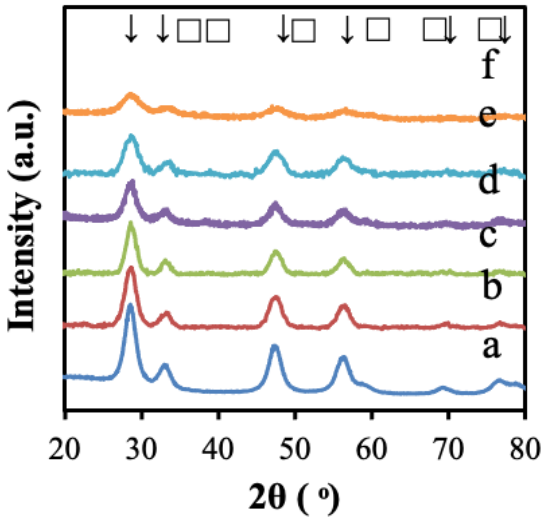

Fig. 3-1 XRD patterns of dried $CeNi_XO_Y$ catalysts: a) x = 0.1, b) x = 0.2, c) x = 0.3, d) x = 0.5, e) x = 1, f) x = 2. CeO_2 (↓), $Ni(OH)_2$ (□).

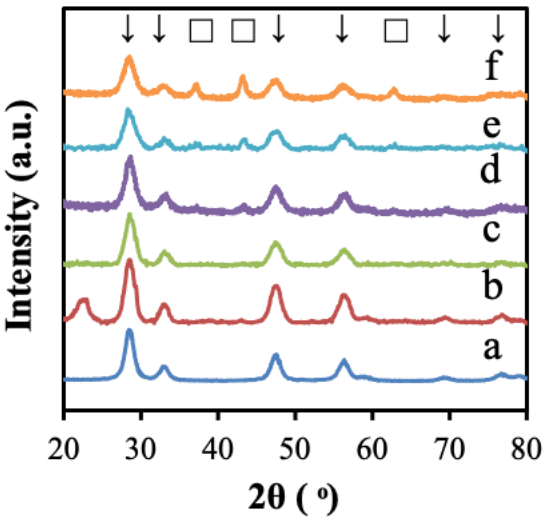

Fig. 3-2 XRD patterns of calcined $CeNi_XO_Y$ catalysts: a) x = 0.1, b) x = 0.2, c) x = 0.3, d) x = 0.5, e) x = 1, f) x= 2. CeO_2 (↓), NiO (□).

3.1.3 Raman studies

Fig. 3-3 and 3-4 show the Raman spectra of $CeNi_XO_Y$ catalysts. The results of dried compounds in Fig. 3-3 present an intense band around 460 cm^{-1} assigned to the first-order F_{2g} peak of CeO_2[206]. This band related to a symmetrical stretching mode of the Ce-O8 vibrational unit, corresponding to the frequency of ωR = 466 cm^{-1}, is very sensitive to any disorder in the oxygen sublattice and/or grain size induced non-stoichiometry. It has been known that the line shifts and broadens with decreasing grain size (increasing lattice defects)[207]. Compared with the pure ceria, the

peak of dried binary catalysts shifts to lower frequency and becomes broad. Among them, the peak of $CeNi_{0.3}O_Y$ shifts to 450 cm^{-1}, which is lower than reported on the cerium-nickel mixed oxides[205]. This can be explained as a result of the incorporation of nickel species into the ceria, which is consistent with the existence of solid solution. In the current case, it seems that lattice distortion and the generation of oxygen vacancies are higher.

Broad peaks between 500 cm^{-1} and 650 cm^{-1} are observed in all catalysts. This is due to the oxygen vacancies generated by the incorporation of the dopant in the ceria[208]. It can be divided into two parts: 547 cm^{-1} and 615 cm^{-1}. The 547 cm^{-1} is considered to be an external defect mode caused by oxygen vacancies. When Ce^{4+} cations in the solid solution are replaced by low valent cations, the defect rate increases[209]. According to the reports, 600 cm^{-1} is due to the presence of the Ce^{3+} -V_O complex in the ceria lattice[210]. Therefore, Raman analysis shows the existence of a solid solution of cerium and nickel and verified the XRD results. This indicates that there is a strong interaction between Ni and Ce species. Moreover, there is a small peak at 225 cm^{-1} in $CeNi_{0.3}O_Y$ catalyst corresponding to the ceria nanostructure observed.

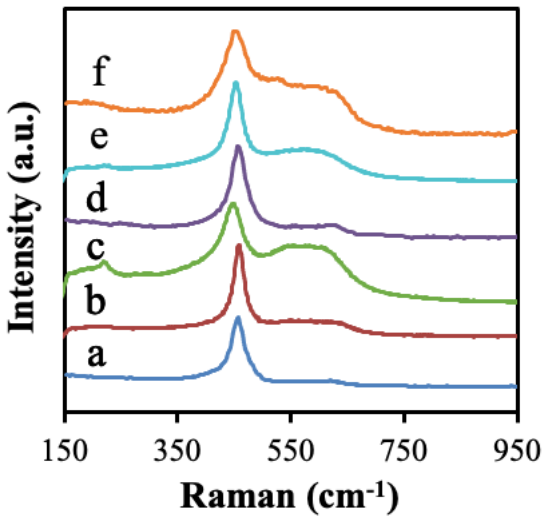

Fig. 3-3 Raman spectra of dried $CeNi_XO_Y$ catalysts: a) x = 0.1, b) x = 0.2, c) x = 0.3, d) x = 0.5, e) x = 1, f) x = 2.

The Raman spectra of calcined $CeNi_XO_Y$ catalysts are presented in Fig. 3-4. Four main bands are observed in calcined compounds. The intense one at 460 cm^{-1} is assigned to the F_{2g} active mode of ceria fluorite structure, due to a symmetric

breathing mode of the oxygen atoms around Ce^{4+} ions. The one located at 230 cm^{-1} is also corresponding to the CeO_2 nanostructure. Whereas the peak at 640 cm^{-1} is ascribed to the oxygen vacancies which appearance is an evidence for the presence of Ce^{3+} ions. The one at 560 cm^{-1} is related to the external defect mode caused by oxygen vacancies, suggesting lower valence cations replacing Ce^{4+} in solid solution[211].

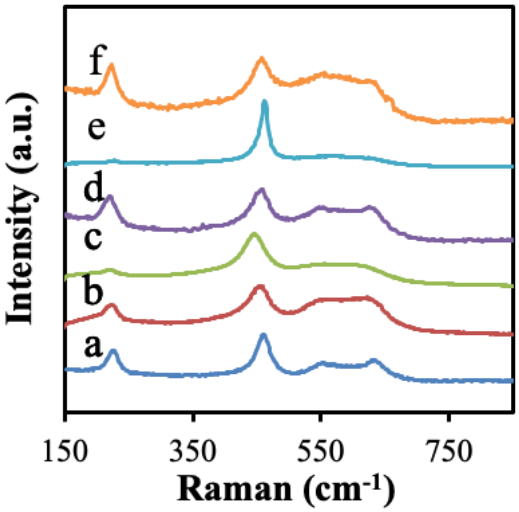

Fig. 3-4 Raman spectra of calcined $CeNi_XO_Y$ catalysts: a) x = 0.1, b) x = 0.2, c) x = 0.3, d) x = 0.5, e) x = 1, f) x = 2.

3.1.4 XPS studies

The XPS analysis is carried out to check the surface elements states of the $CeNi_XO_Y$ catalysts. Fig. 3-5 shows the XPS profiles of O 1s, Ni 2p, and Ce 3d obtained on the dried $CeNi_XO_Y$ catalysts. The relevant binding energies of the main peaks are summarized in Table 3-2. The O 1s spectra of dried binary compounds are shown in Fig. 3-5 a. When the Ni/M_T is lower than or equal to 0.5, the spectra exhibit the main feature at 529.4-529.9 eV, assigned to the presence of typical O^{2-} lattice oxygen species[206], this is in agreement with the presence of the ceria phase observed in XRD. When the Ni/M_T ratio is higher than 0.5, the main peak located at 531.2-531.5 eV corresponds to the presence of hydroxyl groups like in $Ni(OH)_2$[212].

The Ni $2p_{3/2}$ spectra of the dried compounds are presented in Fig. 3-5 b. There are two peaks seen on dried catalysts. The binding energy (B. E.) varying between 855.1 and 855.8 eV is related to Ni^{2+} species[209]. The peak at 860.8-861.4 eV is attributed to the Ni $2p_{3/2}$ core-level satellite peak, which located at 6 eV above the main peak,

indicating the presence of Ni^{2+} species. It must be noted that there is an uncertainty for low Ni content. Moreover, compared with the B.E. of $Ni(OH)_2$ reported in literature[213], close to 854.9 eV[214], the relatively high binding energy indicates the presence of strongly interacting Ni species with Ce species, which is consistent with the existence of a solid solution of cerium and nickel. Therefore, all results indicate the presence of Ni^{2+} cations that strongly interact with other cations.

The XPS spectra of Ce 3d locating from 875 to 925 eV are gathered in Fig. 3-5 c. There are eight components inside the Ce 3d spectra, the four "v" components related to Ce $3d_{5/2}$, the other four "u" components correspond to Ce $3d_{3/2}$ [215]. The peaks at 882.3 eV, 888.7 eV, 898.3 eV are assigned to v, v'', v''', the peaks at 900.6 eV, 911.3 eV, and 916.6 eV are related to u, u'', u''', all considered to be evidence of the existence of Ce^{4+}. However, the peaks at 884.3 and 907.2 eV are corresponding to v' and u', showing the presence of Ce^{3+}. These manifest that Ce^{4+} is the primary chemical states for Ce species with the presence of Ce^{3+}. The existence of Ce^{3+} is ascribed to the presence of oxygen vacancies, due to the creation of Ce-Ni solid solution[216].

Table 3-2 Binding energies of the dried $CeNi_XO_Y$ compounds.

Catalysts dried	O 1s (eV)	Ni $2p_{3/2}$ (eV)	Ce 3d (eV)
$CeNi_{0.1}O_Y$	529.7	861.2/855.6	916.7/ 900.9/ 898.4/ 882.5
$CeNi_{0.2}O_Y$	529.4	860.9/855.1	916.4/ 900.3/ 898.0/ 882.1
$CeNi_{0.3}O_Y$	529.5	861.4/855.8	916.8/ 900.7/ 898.6/ 882.9
$CeNi_{0.5}O_Y$	529.9	861.3/855.6	916.7/ 900.6/ 898.5/ 882.5
$CeNi_1O_Y$	531.5	861.4/855.8	917.1/ 901.1/ 898.8/ 882.6
$CeNi_2O_Y$	531.2	860.8/855.5	916.6/ 901.7/ 898.3/ 882.3

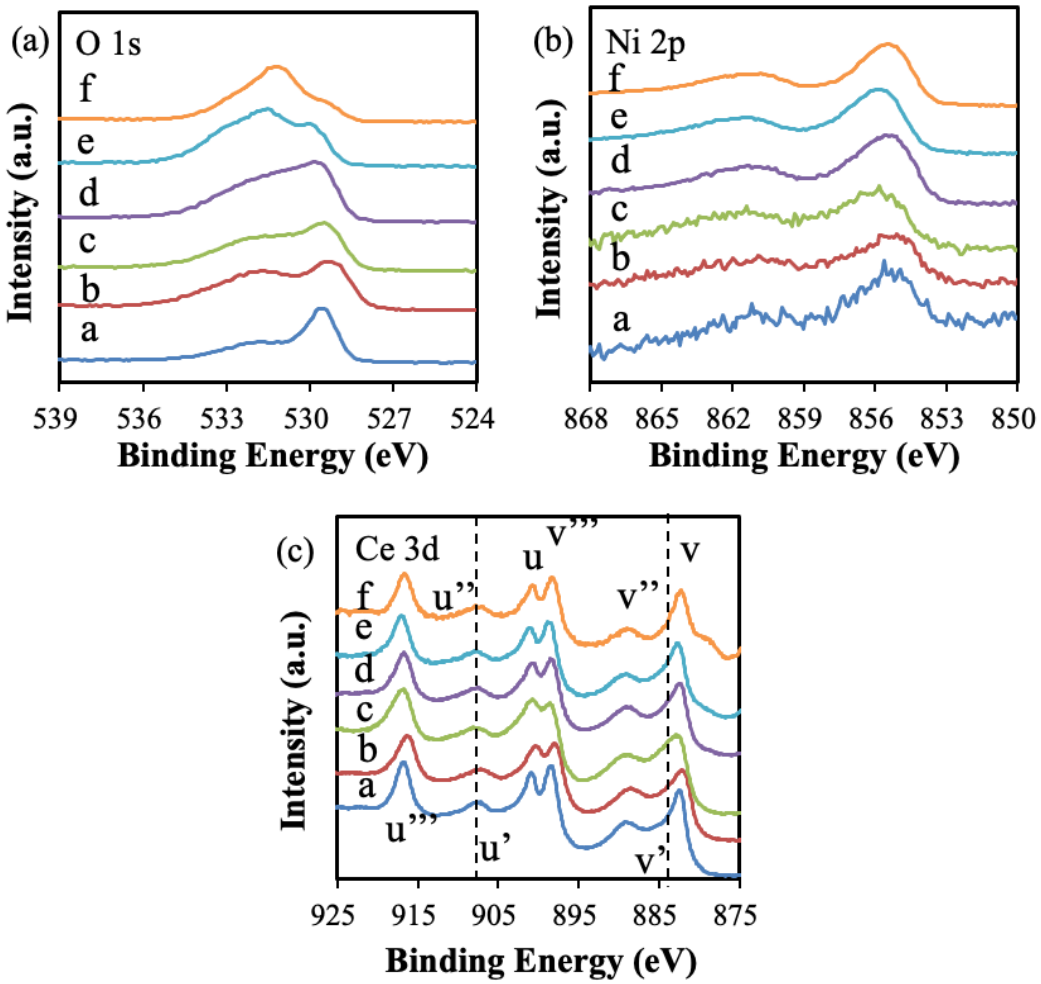

Fig. 3-5: XPS spectra of (a) O 1s, (b) Ni 2p, (c) Ce 3d of the dried $CeNi_XO_Y$ catalysts: a) x = 0.1, b) x = 0.2, c) x = 0.3, d) x = 0.5, e) x = 1, f) x = 2.

The XPS profiles of the calcined compounds are shown in Fig. 3-6. The relevant binding energies of the main peaks are summarized in Table 3-3. The O 1s spectra of calcined binary catalysts are shown in Fig. 3-6 a. All of the catalysts present the main feature at 529.1-529.8 eV, ascribed to the presence of typical O^{2-} lattice oxygen species[206]. Meanwhile, the catalysts exhibit a higher B.E. around 531 eV, that can be assigned to oxygen species related to the presence of hydroxyl groups (OH^-) at the surface of the compounds[212].

The Ni $2p_{3/2}$ spectra are shown in Fig. 3-6 b. Table 3-3 summarizes the values of the binding energies observed in Fig. 3-6 b. For the catalysts with Ni/M_T ratios lower than 0.33, there is a singlet peak around 855 eV, corresponding to the Ni^{2+} species in strong interaction with other species, in agreement with the formation of a solid solution[217]. For high Ni contents catalysts, Ni/M_T equal to or more than 0.33, two

peaks are observed for Ni $2p_{3/2}$, at 853.8 and 855.2 eV. Two peaks have been also observed on the simple NiO oxide, with the main peak located at 853.8 eV[214,218]. Globally, the obtained results can reveal the presence of two different environments for Ni^{2+}: Ni^{2+} in NiO and Ni^{2+} in solid solution. These results are perfectly consistent with the XRD results, the XRD diffraction patterns of nickel oxide can be seen when the Ni/M_T ratio is equal or higher than 0.33. Moreover, all the samples show the satellite peak around 861 eV, evidencing the presence of Ni^{2+} species.

The related Ce 3d peaks are presented in Fig. 3-6 c. As mentioned before, the Ce spectrum consists of two multiple peaks (v and u). These multiplets correspond to the spin-orbit split $3d_{5/2}$ and $3d_{3/2}$ core holes[219]. For example, the peaks v, v'', v''' and u, u'', u''' respectively located at 882.2, 888.9, 898.2 and 900.5, 911.5, 916.5 eV of $CeNi_{0.1}O_Y$ are the result of tetravalent Ce (Ce^{4+}). The peak v' and u' associated with the Ce 3d is characteristic of the presence of Ce^{3+} in Ce compounds. The presence of trivalent cerium indicates the formation of oxygen vacancies in the solid solution, which is consistent with the result of XRD.

Table 3-3 Binding energies of the calcined $CeNi_XO_Y$ compounds.

Catalysts calcined	O 1s (eV)	Ni $2p_{3/2}$ (eV)	Ce 3d (eV)
$CeNi_{0.1}O_Y$	529.2	860.9/854.7	916.5/ 900.5/ 898.2/ 882.2
$CeNi_{0.2}O_Y$	529.1	861.1/854.6	916.1/ 900.1/ 897.8/ 881.8
$CeNi_{0.3}O_Y$	529.8	860.4/855.3	916.8/ 900.7/ 898.4/ 882.5
$CeNi_{0.5}O_Y$	529.5	861.1/855.2/853.8	916.6/ 900.8/ 898.4/ 882.3
$CeNi_1O_Y$	529.4	860.5/855.1/853.8	916.6/ 900.8/ 898.3/ 882.3
$CeNi_2O_Y$	529.4	860.9/855.5/853.6	916.8/ 900.9/ 898.3/ 882.4

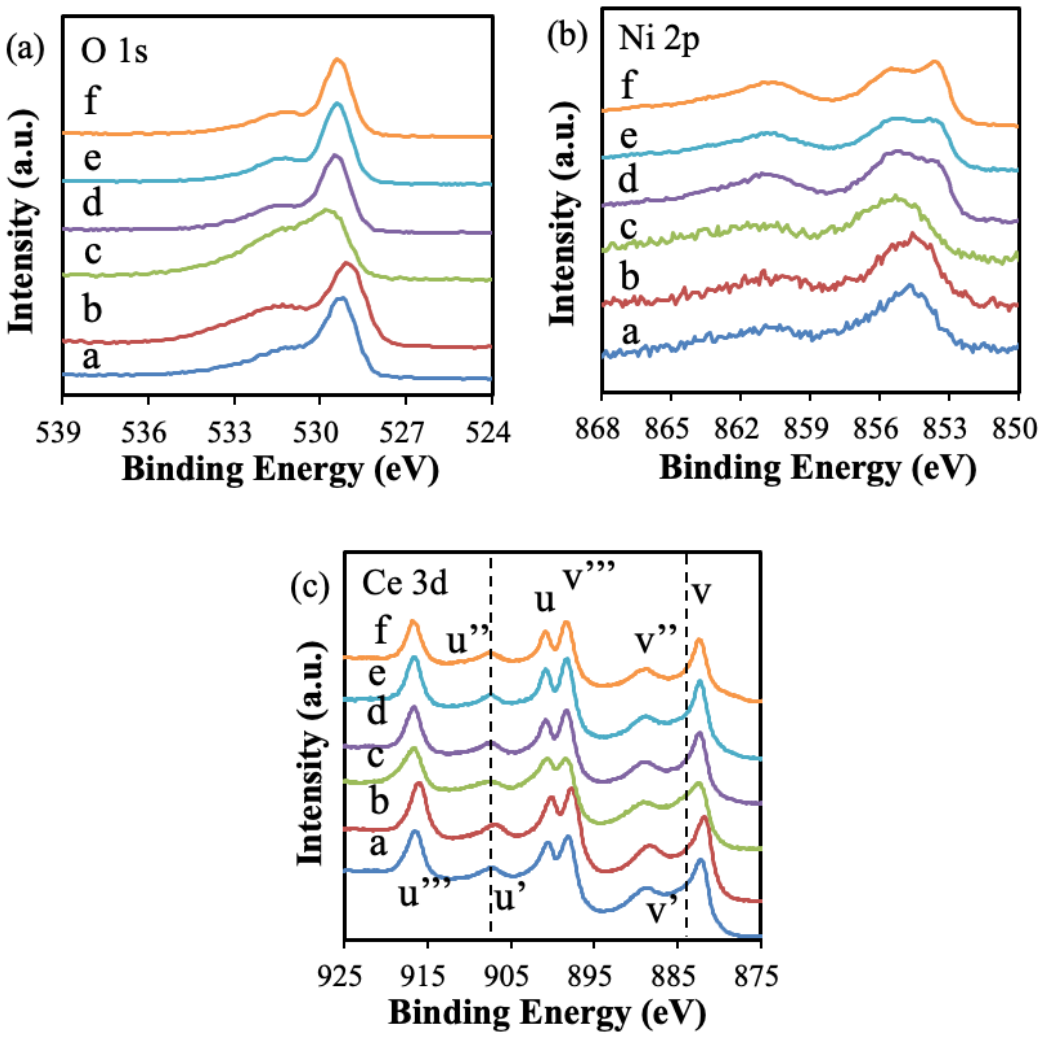

Fig. 3-6: XPS spectra of (a) O 1s, (b) Ni 2p, (c) Ce 3d of the calcined $CeNi_XO_Y$ catalysts: a) x = 0.1, b) x = 0.2, c) x = 0.3, d) x = 0.5, e) x = 1, f) x = 2.

3.1.5 TPR studies

Fig. 3-7 shows the different TPR results of the dried catalysts. The first peak obtained at low temperature (250-300 °C) has a peak area that decreases with the increase of Ni content. Then a second peak appears at 300-400 °C, and the peak area increases with the increase of Ni content. In addition, by increasing Ni content, a slight shift of the peak to high temperature can be seen. Therefore, the presence of two peaks indicates the presence of two types of nickel.

According to previous work, the first peak can be attributed to the nickel in solid solution in the ceria phase, or to the reduction of very small nanoparticles of the phase connected to Ni, which is invisible in XRD caused by the low content. For high Ni content catalysts, the second peak could correspond to the transformation of $Ni(OH)_2$ (phase faintly seen in XRD). It is also possible that $Ni(OH)_2$ (that could be present in

amorphous form) is transformed into NiO and then reduced to metallic Ni depending on the temperature resulting in two peaks. So, whatever the nickel content, the second peak could correspond to the reduction of nickel oxide. The same conclusions were made by Huang et al[220].

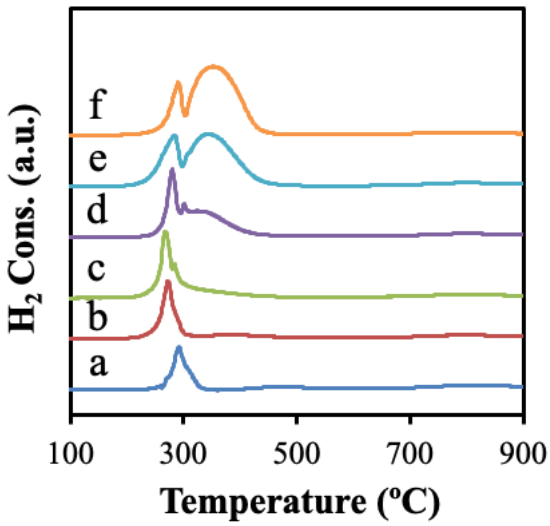

Fig. 3-7: TPR of the dried $CeNi_XO_Y$ catalysts: a) x = 0.1, b) x = 0.2, c) x = 0.3, d) x = 0.5, e) x = 1, f) x = 2.

The TPR curves of the calcined catalysts in H_2 are shown in Fig. 3-8. For all catalysts, a reduction peak is obtained at a low temperature of about 270 °C. This peak is probably related to the presence of Ni^{2+} in the solid solution of cerium and nickel and/or the presence of small particles where Ni^{2+} strongly interacts with other cations. When x is greater than or equal to 0.3, the second reduction peak appears at 330 °C. Moreover, the intensity of this peak increases and moves to a higher temperature of 370 °C with increasing the Ni content. The high-temperature peak corresponds to the NiO reduction commonly observed in the literature[221]. In addition, it is generally believed that the two peaks appearing at about 500 °C and 820 °C belong to ceria, which can be vaguely seen in this case (without zooming).

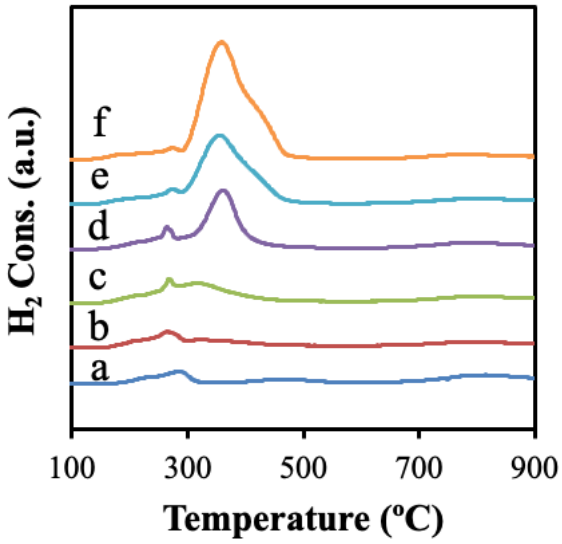

Fig. 3-8: TPR of the calcined $CeNi_XO_Y$ catalysts: a) x = 0.1, b) x = 0.2, c) x = 0.3, d) x = 0.5, e) x = 1, f) x = 2.

3.1.6 Characterizations of spent $CeNi_1O_Y$ catalyst

The catalytic performance of the $CeNi_1O_Y$ catalyst (10 mg, without H_2 pretreatment), tested in stream (CH_4/ CO_2/ N_2 = 5 %: 5 %: 90 %) for 80 h at 800 °C, has been shown previously in Fig. 2-28. A rapid decline of conversions and H_2/CO ratio are observed. The CH_4 and CO_2 conversions drop from 99.6 % and 90.9 % to 50.7 % and 55.8 % respectively after 80 hours. Moreover, the initial H_2/CO molar ratio of 1.19 decreases to 0.9 and carbon formation rate is of 0.018 $g \cdot gcat^{-1} \cdot h^{-1}$. After stability test this spent $CeNi_1O_Y$ catalyst is characterized by Raman and XPS, and the results are compared to the one obtained before test (on calcined compound).

The Raman spectrum is presented in Fig. 3-9. In Fig. 3-9 a, the peak assigned to the F_{2g} active mode of ceria fluorite structure shifts from 461.9 cm^{-1} to 459.3 cm^{-1} after test. It indicates that nickel species incorporates into ceria structure, showing the presence of Ce-Ni-O solid solution. Moreover, the peak at 532.5 cm^{-1} related to the oxygen vacancies is more intense than that observed in fresh catalyst. It means that more Ce^{4+} are replaced by low valent cations and more oxygen vacancies are generated after test.

The carbon formed can be analyzed by Raman as shown in Figure 3-9 b. The signal is weak in this zone and very noisy. The two main peaks in Figure 3-9 b are D band ascribed to vibration mode of sp^3 hybridized carbon atoms at 1350 cm^{-1} and the G band assigned to the stretching mode of sp^2 hybridized carbon atoms at 1600 cm^{-1}.

The D band represents disordered carbonaceous materials, and the G band represents ordered graphite. The intensity ratio of I_D/I_G means the order of graphitization of carbon material. The spent $CeNi_1O_Y$ catalyst exhibits the I_D/I_G ratio higher than unity showing the disorder of carbon deposited[222].

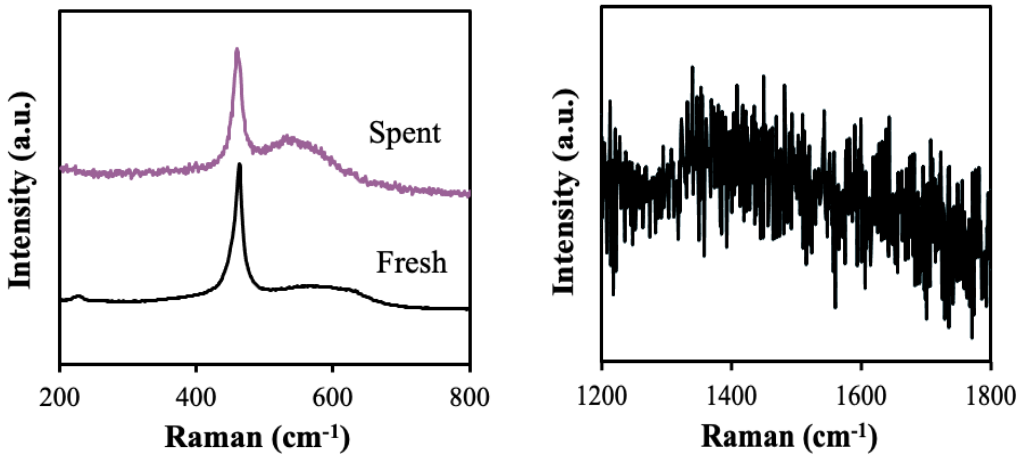

Fig. 3-9: Raman spectra of fresh (calcined) $CeNi_1O_Y$ compound and spent $CeNi_1O_Y$ catalyst after test at 800 °C, 10 mg, without H_2 pretreatment, CH_4/ CO_2/ N_2 = 5 %: 5 %: 90 %.

Table 3-4 Raman peaks of the fresh (calcined) $CeNi_1O_Y$ compound and spent $CeNi_1O_Y$ after test at 800 °C, 10 mg, without H_2 pretreatment, CH_4/ CO_2/ N_2 = 5 %: 5 %: 90 %.

Catalyst	Raman (cm^{-1})			
Fresh $CeNi_1O_Y$	461.9	578.3	-	-
Spent $CeNi_1O_Y$	459.3	532.5	1349.5	1599.3

The binding energies obtained on the fresh catalyst and the spent catalyst are compared in Table 3-5. The C 1s spectrum is shown in Fig. 3-10 a. To analyze the eventual carbon formation, for XPS after test, Ce at 917.0 eV is taken as a reference. The C 1s peak appears at 285.5 eV evidencing a slight shift to higher value (in comparison to 285 eV), ascribed to C-C bond which means the carbon formation takes place during the DRM reaction.

The O 1s spectrum of spent catalyst reveals two peaks at 532.2 eV and 530.3 eV. The peak at 530.3 eV ascribed to typical O^{2-} lattice species, compared with fresh catalyst, the peak appears at a higher binding energy. The peak at 532.2 eV is corresponding to the oxygen species in OH^- groups and the oxygen species in the

surface-absorbed organic functional groups[223]. After the DRM test, the hydroxyl group around 531.2 eV cannot be detected.

The catalyst shows a main emission peak in the Ni $2p_{3/2}$ region (Fig. 3-10 c). The BE shifts after DRM reaction compared to the calcined state. There are two peaks obtained for the Ni $2p_{3/2}$, one at slightly lower position than the calcined state (853.4 eV compared to 853.8 eV) and the other one at slightly higher BE (855.8 eV compared to 855.1 eV). The peak at 853.4 eV can be related to Ni^{2+} cations like in the NiO phase even if the obtained value is a little bit low. The peak at 855.8 eV is corresponding to Ni^{2+} with high interaction with other cations[223]. There is 12.5 % metallic Ni formed in spent catalyst after 80 hours on DRM reaction.

Ce 3d spectrum of spent $CeNi_1O_Y$ catalyst is given in Fig. 3-10 d and compared to calcined compound. This spectrum shows main peaks at 917.0, 901.2, 898.8, 882.9 eV. As discussed before, the peaks labeled v and u are from the spin-orbit coupling of $3d_{5/2}$ and $3d_{3/2}$, respectively. The peaks at 885.3 and 907.9 eV are ascribed the presence of Ce^{3+} and other peaks correspond to Ce^{4+}. This spectrum illustrates that in the spent catalyst Ce exits in both Ce 3+ and Ce 4+ oxidation states. Moreover, compared to 14 % of Ce^{3+} in fresh catalyst, there is 18.4 % of Ce^{3+} in spent compound.

Table 3-5 Binding energies of fresh (calcined) and spent $CeNi_1O_Y$ catalyst after test 80 h, at 800 °C, 10 mg, without H_2 pretreatment, CH_4/ CO_2/ N_2 = 5 %: 5 %: 90 %.

Catalysts	C 1s (eV)	O 1s (eV)	Ni $2p_{3/2}$ (eV)	Ce 3d (eV)
Fresh $CeNi_1O_Y$	285.0	531.2/ 529.4	860.5/ 855.1/ 853.8	916.6/ 900.8/ 898.3/ 882.3
Spent $CeNi_1O_Y$	285.5	532.2/ 530.3	861.2/ 855.8/ 853.4	917.0/ 901.2/ 898.8/ 882.9

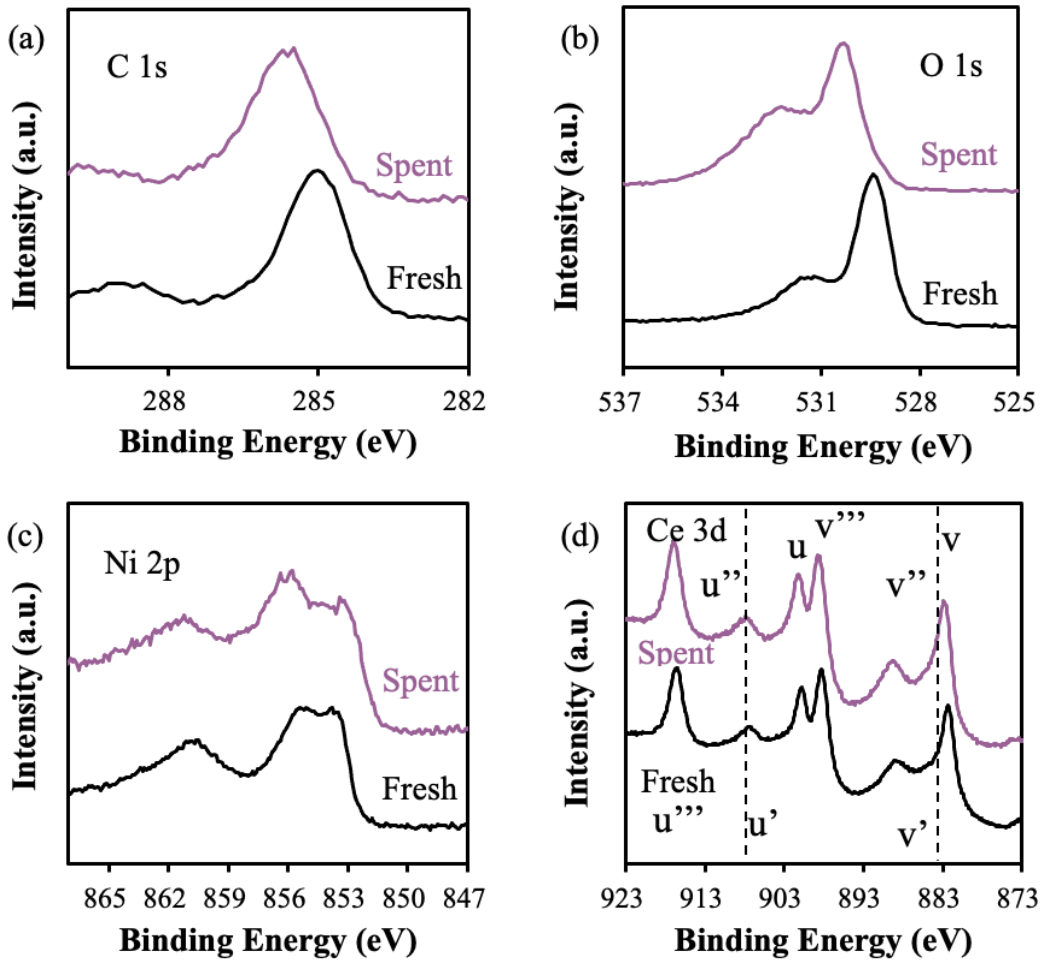

Fig. 3-10: XPS spectra of (a) C 1s, (b) O 1s, (c) Ni $2p_{3/2}$, (d) Ce 3d of fresh and spent $CeNi_1O_y$ catalyst, after test 80 h, at 800 °C, 10 mg, without H_2 pretreatment, CH_4/ CO_2/ N_2 = 5 %: 5 %: 90 %.

3.2 $CeZr_{0.5}Ni_XO_Y$ catalysts characterization results

3.2.1 Elemental analysis and textural properties

The precise Ni contents and the specific surface areas of dried and calcined $CeZr_{0.5}Ni_XO_Y$ catalysts are analyzed and summarized in Table 3-6. The elemental chemical analysis confirms that the Ni compositions of the catalysts are similar to the nominal values. All the ternary catalysts exhibit surface areas higher than 71 m^2/g. With the same nickel content, the specific surface area of the dried catalyst is larger than that of the calcined catalyst. For the dried catalysts, $CeZr_{0.5}Ni_{0.5}O_Y$ shows the largest specific surface area of 186 m^2/g. As the nickel content increases, the specific surface area of the catalyst decreases. For calcined compounds, the $CeZr_{0.5}Ni_1O_Y$ presents the largest specific area of 130 m^2/g.

Table 3-6 Ni content and specific surface area (BET) of $CeZr_{0.5}Ni_XO_Y$ compounds.

Sample	Ni (wt.%)	Ni/M_T	Surface area dried (m^2/g)	Surface area calcined (m^2/g)
$CeZr_{0.5}Ni_{0.5}O_Y$	10.8	0.25	186	86
$CeZr_{0.5}Ni_1O_Y$	19.0	0.40	135	130
$CeZr_{0.5}Ni_2O_Y$	30.6	0.57	133	120
$CeZr_{0.5}Ni_5O_Y$	48.3	0.77	112	71

3.2.2 XRD studies

X-Ray powder diffraction is conducted to determine the crystallinity of dried and calcined $CeZr_{0.5}Ni_XO_Y$ catalysts and the results are presented in Fig. 3-11 and 3-12. The dried $CeZr_{0.5}Ni_XO_Y$ catalysts show the typical patterns of CeO_2 at 2θ = 28.5°, 33.0°, 47.6°, 56.7°, 59.0°, 69.3°, 77.0°, 79.1°, and 88.4° representing the plane indices of (111), (200), (220), (311), (222), (400), (311), (420) and (422), respectively (JCPDS 34-0394)[204]. The reflections of $Ni(OH)_2$ (JCPDS 01-1047) are also observed, the peaks are detectable at 2θ = 19.1°, 33.0°, 38.4°, 52.0°, 59.0°, 62.6°, 69.3°, and 72.8°, corresponding to (001), (100), (101), (102), (110), (111), (200) and (112) planes, respectively[224, 225]. The diffraction patterns of the crystallized $Ni(OH)_2$ become more intense with increasing the Ni content. The XRD patterns of the catalysts do not present any zirconia phase, while the XRD patterns of the CeO_2 phase are broaden compared to pure ceria. This shift is due to the smaller size of Zr^{4+} (ionic radius r=0.84 Å) cations replacing Ce^{4+} cations (ionic radius r=0.97 Å). It indicates that a (Ni)-Ce-Zr-O solid solution is formed during synthesis[226].

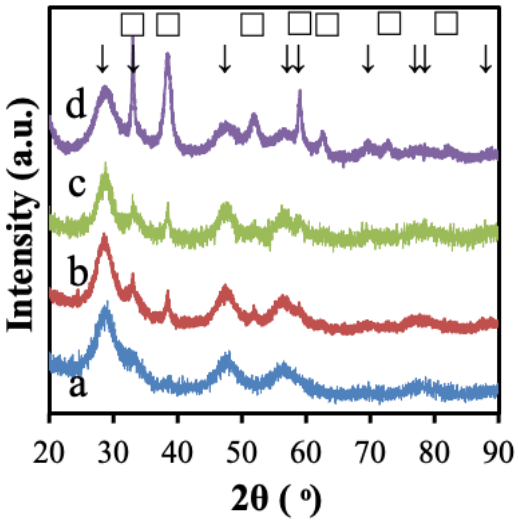

Fig. 3-11 XRD patterns of dried $CeZr_{0.5}Ni_XO_Y$ catalysts: a) x = 0.5, b) x = 1, c) x = 2, d) x = 5. CeO_2 (↓), $Ni(OH)_2$ (□).

For calcined $CeZr_{0.5}Ni_XO_Y$ catalysts, XRD patterns are shown in Fig. 3-12. A typical ceria structure (JCPDS 34-0394) is observed, with the main reflections at 28.5°, 33.0°, 47.6°, 56.7°, 59.0°, 69.3°, 77.0°, 79.1°, and 88.4°[204]. The XRD patterns broaden and which demonstrates that Ni^{2+} and/or Zr^{4+} cations are inside the CeO_2 lattice and that a cerium-nickel-(zirconium) solid solution is formed. Meanwhile, catalysts show the typical patterns of NiO at 2θ = 37.2°, 43.4°, 62.9°, 75.7°, and 79.5° related to the plane indices of (100), (012), (110), (113), and (202), respectively (JCPDS 4-0835)[205]. No phase related to zirconia is detected by XRD, indicating the successful formation of (Ni)-Ce-Zr-O solid solution which is expected in consideration of the low doping percentage.

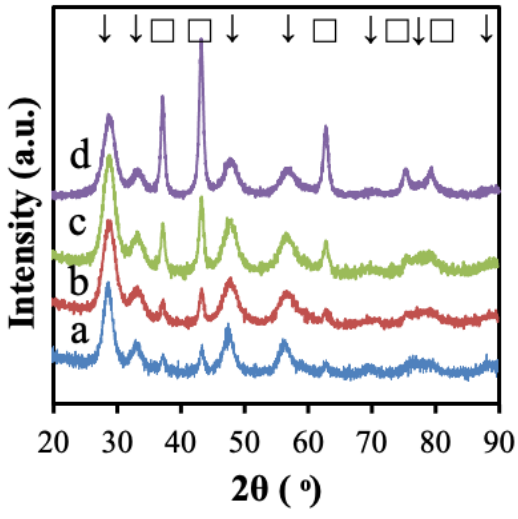

Fig. 3-12 XRD patterns of calcined $CeZr_{0.5}Ni_XO_Y$ catalysts: a) x = 0.5, b) x = 1, c) x = 2, d) x = 5. CeO_2 (↓), NiO (□).

3.2.3 Raman studies

The Raman spectra of dried $CeZr_{0.5}Ni_XO_Y$ compounds are shown in Fig. 3-13. The characteristic peak detected at 460 cm^{-1} is related to fluorite ceria and can be designated as symmetric F_{2g} stretching mode of oxygen surrounding the Ce^{4+} ions[206]. On the other hand, the protruding band in the region of 590-670 cm^{-1} corresponds to the oxygen vacancies and defects in the CeO_2 lattice, which comes from the Ce^{3+} ions and/or the substitution of Zr^{4+} into the ceria lattice[227]. The band near 1050 cm^{-1} is assigned to ceria phase, which agrees with the XRD result[228,229,230]. According to Wang's research, the peak at approximately 309 cm^{-1}; could show the Ni-OH lattice vibration and the Ni-OH tensile vibration mode, which follows the previously reported $Ni(OH)_2$[231].

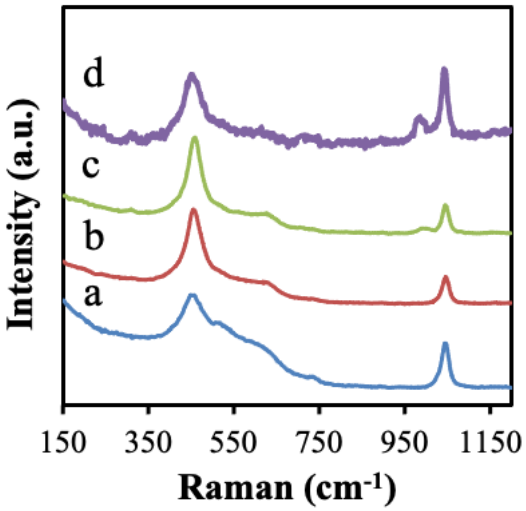

Fig. 3-13 Raman spectra of dried $CeZr_{0.5}Ni_XO_Y$ catalysts: a) x = 0.5, b) x = 1, c) x = 2, d) x = 5.

For calcined $CeZr_{0.5}Ni_XO_Y$ catalysts, compared to the peak from pure ceria, the ceria F_{2g} peak in Fig. 3-14 becomes broader and seems to be shifted to higher value (470 cm^{-1}), which could be attributed to the formation of ceria-zirconia solid solution[232]. The positive band shift may be the outcome of substitution of Ce^{4+} with Zr^{4+}, which resulted in the drop of the length of the CeO_2 bond and shifted to higher energy. It is worth mentioning that Chan's research indicates the two nickel-related bands overlapped at 400 and 500 cm^{-1} and Dharmaraj also identified one broad band located at 518 cm^{-1} corresponding to nickel species[233,234]. Therefore, the characteristic bands of nickel oxide and ceria may overlap in the range of study.

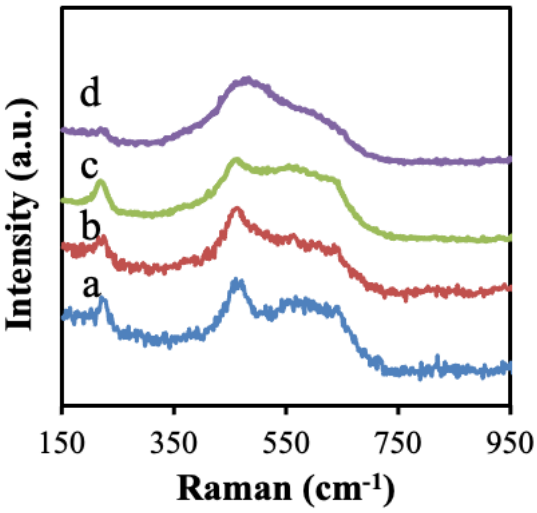

Fig. 3-14 Raman spectra of calcined $CeZr_{0.5}Ni_XO_Y$ catalysts: a) x = 0.5, b) x = 1, c) x = 2, d) x = 5.

3.2.4 XPS studies

The XPS analysis is carried out to check the composition and coordination states of the surface elements of the $CeZr_{0.5}Ni_XO_Y$ catalysts. The XPS profiles of O 1s, Ni 2p, Ce 3d, and Zr 3d of dried $CeZr_{0.5}Ni_XO_Y$ compounds with different Ni contents are displayed in Fig. 3-15 and the relevant binding energies of the main peaks are summarized in Table 3-7.

The O 1s spectra of dried Zr based compounds are shown in Fig. 3-15 a. The $CeZr_{0.5}Ni_{0.5}O_Y$ O 1s spectrum exhibits a feature at 530.0 eV, distinctive to lattice O^{2-} of ceria and/or ZrO_2 structures[235,236]. The main peak located at 531.2-531.5 eV can be clearly assigned to the presence of oxygen species as in hydroxide in relation to the presence of $Ni(OH)_2$[212]. The other peak at 533.0 eV is revealing another type of oxygen species as in adsorbed water[237]. The Ni $2p_{3/2}$ spectra of the catalysts are shown in Fig. 3-15 b. Two peaks at about 855.6 and 861.4 eV are assigned to Ni $2p_{3/2}$ and Ni $2p_{3/2}$ core-level satellite lines, respectively, clearly evidencing the presence of Ni^{2+} cations and their strong interaction with other cations, for example, with Ce species (or Zr species). According to the literature, a main peak at 855.8 eV can be also related to Ni^{2+} cations like in $Ni(OH)_2$ phase[238], which is in agreement with the XRD results. The related Ce 3d peaks of the dried samples are presented in Fig. 3-15 c. The Ce 3d spectra are composed of eight components, the four "v" components correspond to the Ce $3d_{5/2}$ and the other four "u" components to the Ce $3d_{3/2}$[239]. The features v, v'', v''' and u, u'',

u''' correlate cerium in a 4+ oxidation state, while the features v' and u' correlate cerium in a 3+ oxidation state[240]. The three main peaks of $3d_{5/2}$ at 882.4 eV (v), 888.9 eV (v''), 898.4 eV (v''') and three prominent features of $3d_{3/2}$ at 900.9 eV (u), 911.6 eV (u''), and 916.6 eV (u''') are observed, indicating the presence of cerium in a 4+ oxidation state. The presence of Ce^{3+} is established from the appearance of v' and u' features in the Ce 3d spectra at 886.3 and 907.4 eV, probably related to the presence of oxygen vacancies in Ce-Zr-Ni solid solution[241,242]. It is generally known that Ce^{3+} can produce unsaturated chemical bonds and charge imbalance, meanwhile, the presence of Ce^{3+} can lead to the formation of oxygen vacancies to maintain the electrostatic balance, these natures are beneficial to the redox property and promote the adsorption and oxidation of CH_4 [243].

The Zr 3d spectrum is presented in Fig. 3-15 d and shows doublet peaks. As can be noted from Table 3-7, the BE values are in the range of 182.2-182.4 eV and 184.6-184.7 eV, which agrees well with literature reports corresponding to Zr^{4+} ions[244]. The binding energy shifts to higher binding energy compared to the reference ZrO_2[245], which indicates the formation of a (Ni)-Ce-Zr solid solution, which is also discussed in the XRD results.

Table 3-7 Binding energies of the dried $CeZr_{0.5}Ni_XO_Y$ compounds.

Catalysts dried	O 1s (eV)	Ni $2p_{3/2}$ (eV)	Ce 3d (eV)	Zr 3d (eV)
$CeZr_{0.5}Ni_{0.5}O_Y$	531.4/ 530.0	861.6/855.8	917.0/ 901.1/ 898.6/ 882.7	184.6/182.3
$CeZr_{0.5}Ni_1O_Y$	531.2	861.6/855.8	917.1/ 901.3/ 898.7/ 882.6	184.7/182.4
$CeZr_{0.5}Ni_2O_Y$	533.0/ 531.5	861.4/855.6	917.1/ 901.1/ 898.8/ 882.6	184.6/182.3
$CeZr_{0.5}Ni_5O_Y$	531.3	861.3/855.6	916.9/ 901.1/ 898.6/ 882.5	184.6/182.2

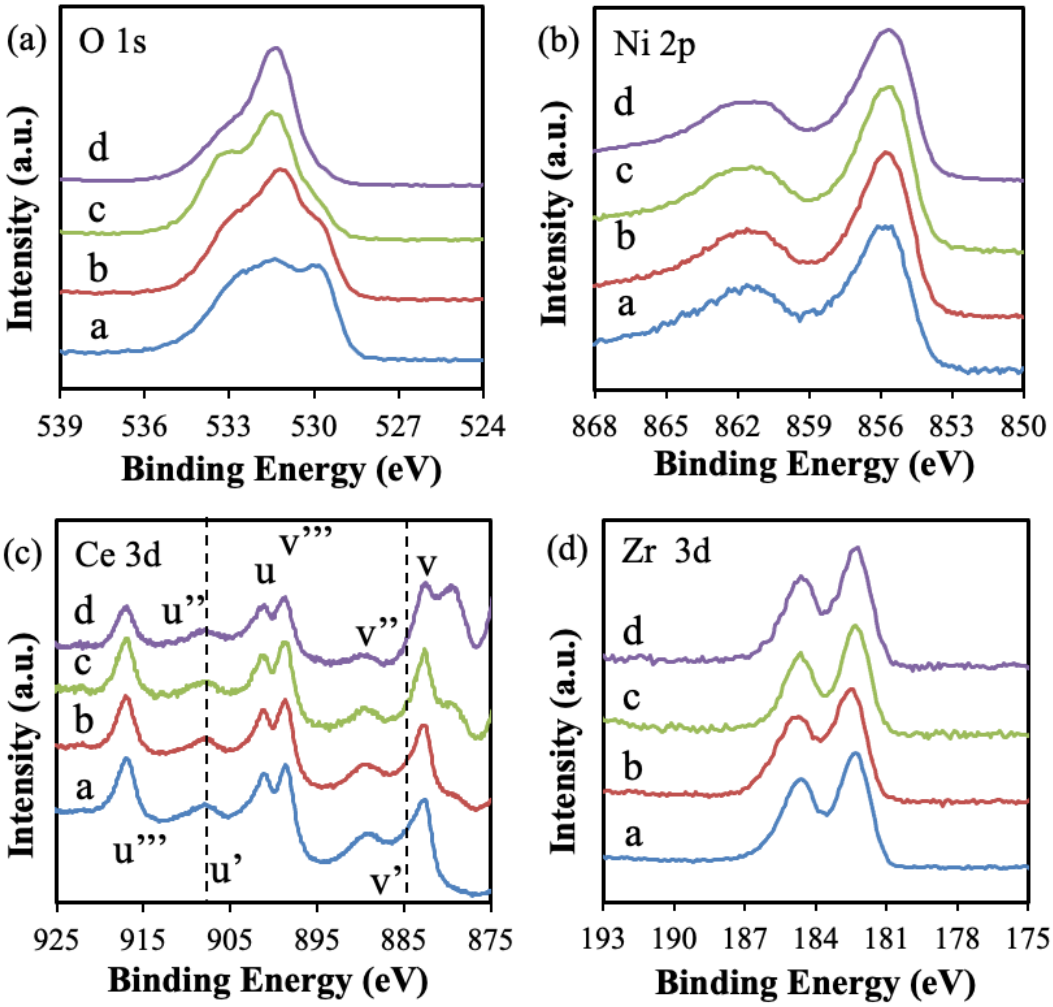

Fig. 3-15: XPS spectra of (a) O 1s, (b) Ni 2p, (c) Ce 3d, (d) Zr 3d of the dried $CeZr_{0.5}Ni_XO_Y$ catalysts: a) x = 0.5, b) x = 1, c) x = 2, d) x = 5.

The XPS profiles of calcined $CeZr_{0.5}Ni_XO_Y$ compounds with different Ni contents are displayed in Fig. 3-16. As shown in Fig. 3-16 a, the O 1s peaks of catalysts are located at 529.4 - 529.6 eV and 531.0 - 531.5 eV. The peak at 529.4 - 529.6 eV is related to the lattice oxygen ions, O^{2-} in the ceria phase[246]. Whereas the peaks located at 531.0 - 531.5 eV are attributed to oxygen species form hydroxyl groups.

For the Ni $2p_{3/2}$ spectra, it is found in Fig. 3-16 b that two main peaks of Ni $2p_{3/2}$ are observed for all samples. For low Ni content $CeZr_{0.5}Ni_{0.5}O_Y$ catalyst, the main peak centered at 855.3 eV, indicates the presence of Ni^{2+} species in strong interaction with other cations, in agreement with the formation of a solid solution. For high Ni content $CeZr_{0.5}Ni_XO_Y$ catalysts (x more than 0.5), the main peak located at 853.6 eV could be a contribution of the Ni species in NiO[247]. Moreover, the satellite peak of Ni $2p_{3/2}$ is seen

for all the compounds at around 861 eV, about 6 eV up to the main peak confirming the presence of Ni^{2+} species.

The spectra of Ce 3d (Fig. 3-16 c) show the two sets of spin-orbit multiple peaks according to the classification of Burroughs et al[248]. Specifically, the peaks located at 885.3 eV (v') and 903.4 eV (u') are corresponding to the Ce^{3+} cations. The peak at 882.4 eV (v), 889.2 eV (v''), 898.4 eV (v'''), 900.9 eV (u), 907.5 eV (u"), and 916.8 eV (u''') are related to the Ce^{4+} species. It is confirmed that Ce^{4+} and Ce^{3+} cations are coexisting over the surface of these catalysts, which could endow the catalysts with redox properties[249].

The ternary catalysts exhibit the expected Zr 3d peaks in Fig. 3-16 d. The peaks at around 184.4 eV and 182.0 eV correspond to the contribution of the Zr species in +4 oxidation state according to previous reports. The 2.4 eV energy difference that is found between Zr $3d_{3/2}$ and Zr $3d_{5/2}$ is in good agreement with the reported values for ZrO_2 samples, even if here no ZrO_2 phase has been observed by XRD[250].

Table 3-8 Binding energies of the calcined $CeZr_{0.5}Ni_XO_Y$ compounds.

Catalysts calcined	O 1s (eV)	Ni $2p_{3/2}$ (eV)	Ce 3d (eV)	Zr 3d (eV)
$CeZr_{0.5}Ni_{0.5}O_Y$	529.6/531.2	861.2/855.3	916.8/ 900.9/ 898.4/ 882.4	184.3/182.0
$CeZr_{0.5}Ni_1O_Y$	529.5/531.4	860.7/853.6	916.6/ 901.0/ 898.3/ 882.4	184.4/182.1
$CeZr_{0.5}Ni_2O_Y$	529.5/531.5	861.1/853.7	916.6/ 900.9/ 898.4/ 882.5	184.5/182.1
$CeZr_{0.5}Ni_5O_Y$	529.4/531.0	860.8/853.6	916.8/ 900.9/ 898.5/ 882.3	184.2/182.0

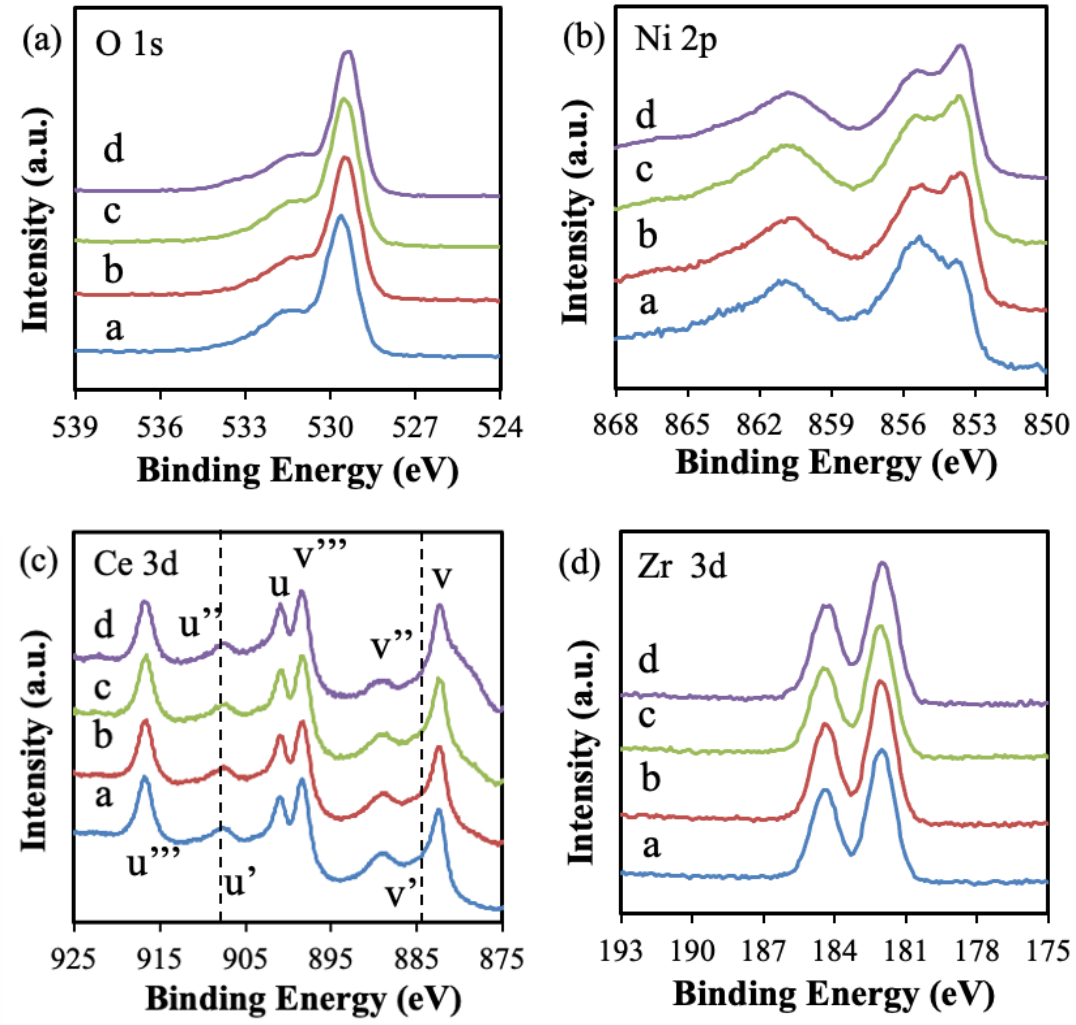

Fig. 3-16: XPS spectra of (a) O 1s, (b) Ni 2p, (c) Ce 3d, (d) Zr 3d of the calcined $CeZr_{0.5}Ni_XO_Y$ catalysts: a) x = 0.5, b) x = 1, c) x = 2, d) x = 5.

3.2.5 TPR studies

The H_2-TPR experiments for dried and calcined $CeZr_{0.5}Ni_XO_Y$ catalysts are performed to investigate the reducibility of all the catalysts, their results are presented in Fig. 3-17 and 3-18. For dried compounds, there are two reduction peaks before 900 °C. The TPR peaks of nickel species reduced at a low temperature around 240-310 °C is ascribable to the reduction of Ni^{2+} which has strong interaction with ceria [251]. The TPR peaks at higher temperatures around 360-380 °C are corresponding to the reduction of relatively free Ni species[252]. As increasing Ni content in the solid solution, the position of the main peak is shifted to a higher temperature.

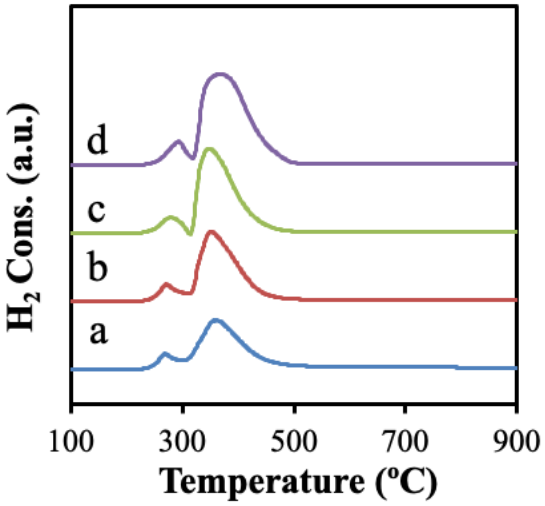

Fig. 3-17: TPR of the dried $CeZr_{0.5}Ni_XO_Y$ catalysts: a) x = 0.5, b) x = 1, c) x = 2, d) x = 5.

The reduction peaks of calcined $CeZr_{0.5}Ni_XO_Y$ catalysts are shown in Fig. 3-18. The first peak at 305 °C corresponds to the reduction of nickel species in solid solution or the small NiO particles. Compared with the reduction temperature of bulk nickel oxide of 370 °C, the second higher intensity peak at 360-400 °C is related to the reduction of NiO (visible by XRD) interacting with ceria. The peaks are shifted to the higher temperatures with an increase of the nickel content, which indicates a more difficult reduction of Ni species in high nickel content compounds. That could be explained by Ni incorporation into the (Zr)-Ce-Ni solid solution as XPS data have shown.

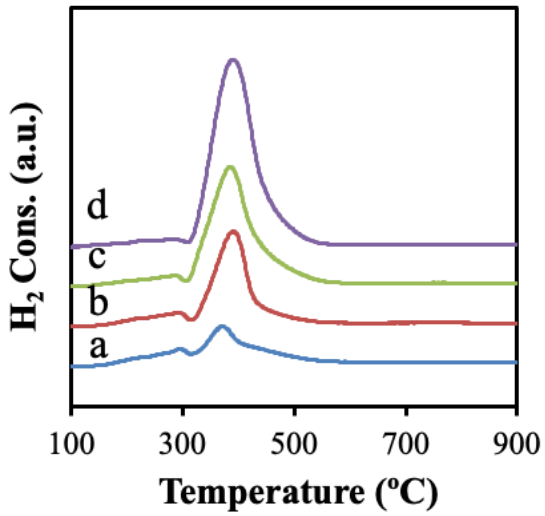

Fig. 3-18: TPR of the calcined $CeZr_{0.5}Ni_XO_Y$ catalysts: a) x = 0.5, b) x = 1, c) x = 2, d) x = 5.

3.2.6 Characterizations of spent $CeZr_{0.5}Ni_XO_Y$ catalysts

The stability in DRM catalytic test of 80 hours was previously reported on $CeZr_{0.5}Ni_2O_Y$ catalyst at 800 °C, 10 mg, with in situ H_2 pretreatment at 250 °C, CH_4/ CO_2/ N_2 = 5 %: 5 %: 90 % (Chapter 2, Fig. 2-25). The catalyst shows no decay in CH_4 and CO_2 conversions, the methane and CO_2 conversions are stable at 98.8% and 93.5% after 80 h of reaction. Moreover, the initial H_2/CO molar ratio is at 1.1 and the value increases to 1.2 in 80 h of time on stream. The carbon formation is of 0.004 $g \cdot gcat^{-1} \cdot h^{-1}$.

After stability test, the spent $CeZr_{0.5}Ni_2O_Y$ catalyst is characterized by Raman and XPS. The Raman spectrum of spent $CeZr_{0.5}Ni_2O_Y$ catalyst is shown in Fig 3-19. The band around 460 cm^{-1} ascribed to CeO_2 is similar with the band of fresh $CeZr_{0.5}Ni_2O_Y$ catalyst, and there is broadening effect compared to pure CeO_2 due to the formation of Ce-Ni-(Zr)-O solid solution. The peak around 538 cm^{-1} attributed to oxygen vacancies shifts to a lower position and becomes more intense compared to the one in fresh catalyst. It indicates that Ce^{4+} cations are replaced by low valent cations and shows the stable existence of oxygen vacancies. Raman analysis in the zone of carbon shows that there are two peaks appearing at 1306 cm^{-1} and 1594 cm^{-1} corresponding to the D band and G band, respectively, of graphitic carbon (Fig 3-19 b). The D-band revealing the presence of defects， evidences the disordered type of carbonaceous materials. The intensity of the G-band is used for comparison[253]. In this case, the D band is more intense than the G band, evidencing the highly disordered carbon species[222].

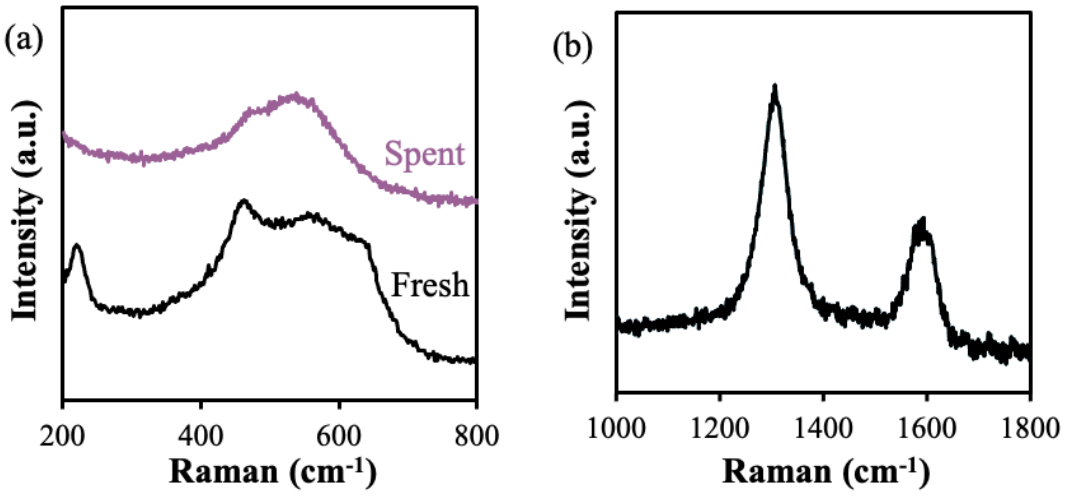

Fig. 3-19: Raman spectra of fresh and spent $CeZr_{0.5}Ni_2O_Y$ catalysts after test at 800 °C, 10 mg, with H_2 pretreatment at 250 °C, CH_4/ CO_2/ N_2 = 5 %: 5 %: 90 %.

Table 3-9 Raman peaks of the fresh and spent $CeZr_{0.5}Ni_2O_Y$ catalyst after test at 800 °C, 10 mg, with H_2 pretreatment at 250 °C, CH_4/ CO_2/ N_2 = 5 %: 5 %: 90 %.

Catalysts	Raman (cm^{-1})			
Fresh $CeZr_{0.5}Ni_2O_Y$	462.0	554.6		
Spent $CeZr_{0.5}Ni_2O_Y$	465.3	538.4	1306.2	1593.7

The binding energy values of spent $CeZr_{0.5}Ni_2O_Y$ catalyst are summarized in Table 3-10 and the spectra are shown in Fig. 3-20. As shown in Fig. 3-20 a, for the C 1s spectrum, the peak at 284.3 eV can be assigned to C–C or C=C bands[254]. It suggests the carbon species is formed in DRM reaction. As presented in Fig. 3-20 b, the O 1s spectra demonstrate two peaks at 531.3 and 529.7 eV for the spent $CeZr_{0.5}Ni_2O_Y$ catalyst. The lattice oxygen species are observed at 529.7 eV which is consistent with the catalyst before the reaction. Meanwhile the peak at 531.3 eV is assigned to the hydroxyl groups around metal cations, which is more intense than the one in fresh compound. Fig. 3-20 c shows the Ni $2p_{3/2}$ photoelectron spectra of the catalyst. The peak with binding energy at 855.7 eV is similar with the one in fresh catalyst, but the peak intensity is higher, corresponding to Ni^{2+} species interacting with other cations. The peak at 852.6 eV is characterizing the existence of metallic Ni^0 species. After catalytic stability test on the spent catalyst there is 10.5 % of metallic Ni and 89.5 % of Ni^{2+} cations (species with interactions with other cations and like in NiO). Changes in the oxidation state of the cerium cations are also detected and presented in Fig. 3-20 d. Specifically, the peaks located at 885.8 eV (v') and 907.4 eV (u') are corresponding to the Ce^{3+} cations. The other peaks are related to the Ce^{4+} species. It is confirmed that Ce^{4+} and Ce^{3+} cations are coexisting over the surface of these catalysts. 23.2 % of Ce^{3+} and 76.8 of Ce^{4+} are present in spent $CeZr_{0.5}Ni_2O_Y$ catalyst which could endow the catalyst with redox properties. The Zr 3d spectrum is presented in Fig. 3-20 e and shows doublet peaks. As can be noted from Table 3-10, the BE values are at 184.6 eV and 182.3 eV, which agrees well with the results of fresh catalyst. Compared to pure ZrO_2, the binding energy shifted slightly which indicates the formation of a (Ni)-Ce-Zr solid solution[245].

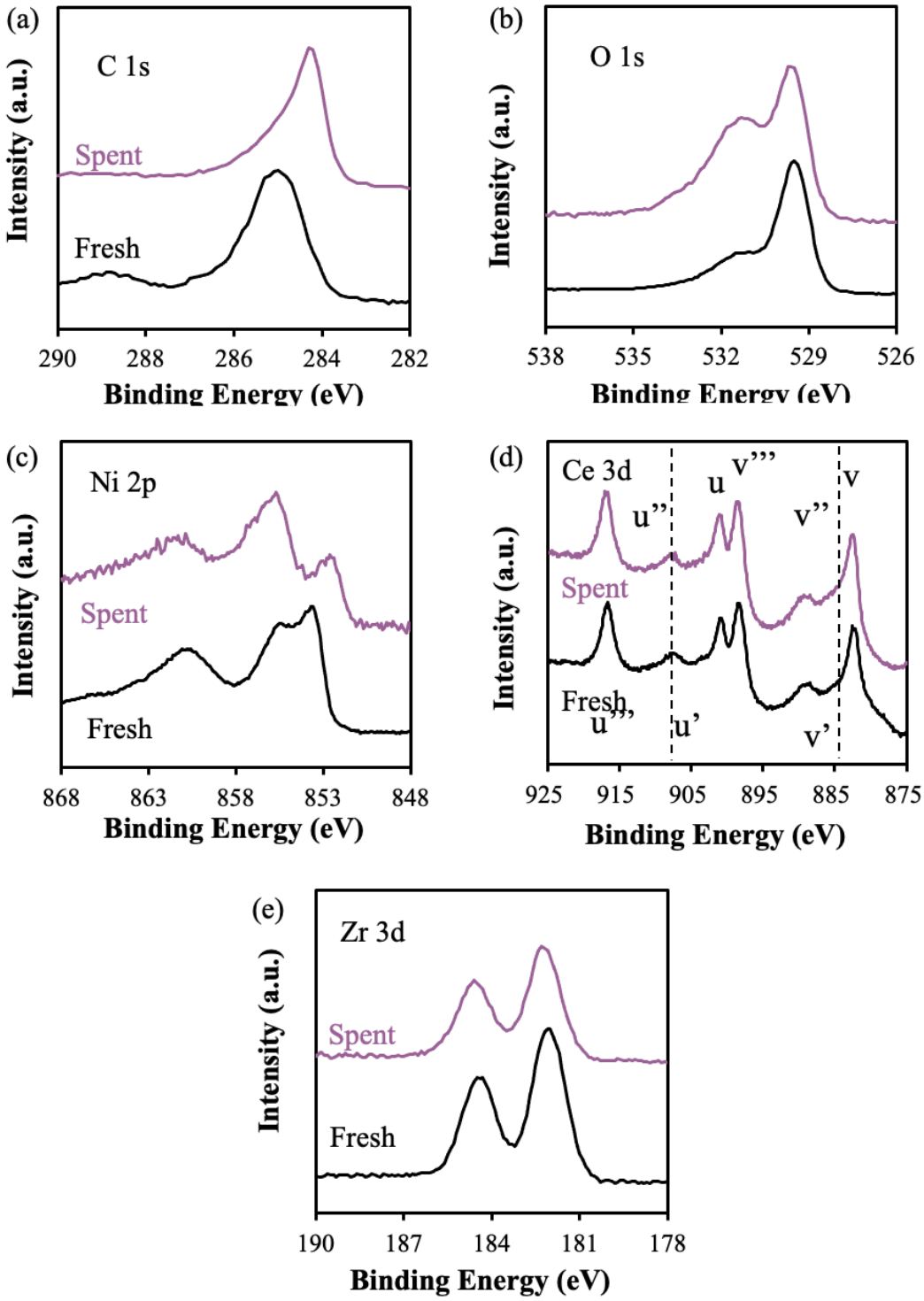

Fig. 3-20: XPS spectra of (a) C 1s, (b) O 1s, (c) Ni 2p, (d) Ce 3d, (e) Al 2p - Ni 3p of the fresh and spent $CeZr_{0.5}Ni_2O_Y$ catalyst, after test 80 h, at 800 °C, 10 mg, with H_2 pretreatment at 250 °C, CH_4/ CO_2/ N_2 = 5 %: 5 %: 90 %.

Table 3-10 Binding energies of the fresh (calcined) and spent $CeZr_{0.5}Ni_2O_Y$ catalyst after test 80 h, at 800 °C, 10 mg, with H_2 pretreatment at 250 °C, CH_4/ CO_2/ N_2 = 5 %: 5 %: 90 %.

$CeZr_{0.5}Ni_2O_Y$	C 1s (eV)	O 1s (eV)	Ni $2p_{3/2}$ (eV)	Ce 3d (eV)	Zr 3d (eV)
Fresh	285.0	531.5/ 529.5	861.1/855.5/ 853.7	916.6/900.9/ 898.4/ 882.5	184.5/182.1
Spent	284.3*	531.3/ 529.7	860.9/855.7/ 852.6	917.0/901.1/898.6/ 882.5	184.6/ 182.3

*The Ce 3d peak at 917.0 eV is taken as reference

3.3 $CeAl_{0.5}Ni_XO_Y$ catalysts characterization results

3.3.1 Elemental analysis and textural properties

The Ni content, specific surface area, and average crystallites size of the catalysts are studied and summarized in Table 3-11. The actual metal content is close to the nominal value. The $CeAl_{0.5}Ni_XO_Y$ compounds have large surface areas ranging from 106 to 154 m^2/g depending on Ni content. For low Ni content compounds, the specific surface area increases with increasing the Ni content from 12 to 30.8 wt.%. The $CeAl_{0.5}Ni_2O_Y$ catalyst exhibits the largest surface area of 154 m^2/g. When the nickel content is increased to 49.2 wt.%, the specific surface area of $CeAl_{0.5}Ni_5O_Y$ decreases to 106 m^2/g.

Table 3-11 Ni content, specific surface area (BET) and average crystallites size of $CeAl_{0.5}Ni_XO_Y$ compounds.

Sample	Ni (wt.%)	Ni/M_T	Surface area (m^2/g)	$dCeO_2$ (nm)	dNiO (nm)
$CeAl_{0.5}Ni_{0.5}O_Y$	12.0	0.25	126	3.9	-
$CeAl_{0.5}Ni_1O_Y$	19.5	0.40	136	4.1	7.2
$CeAl_{0.5}Ni_2O_Y$	30.8	0.57	154	3.8	5.9
$CeAl_{0.5}Ni_5O_Y$	49.2	0.77	106	4.4	5.5

3.3.2 XRD studies

The XRD patterns of the calcined $CeAl_{0.5}Ni_XO_Y$ catalysts are shown in Fig. 3-21. The CeO_2 phase (34-0394 JCPDS file) is always present, while no structure related to aluminum could be observed, which can be due to the presence of an amorphous

phase, the high dispersion, and/or the insertion of aluminum species into ceria phase[255]. NiO phase (4-0835 JCPDS file) appears when the value of x is above 0.5. It has been shown that aluminum doping ameliorates dispersion[218]. The $CeAl_{0.5}Ni_XO_Y$ compounds have an average crystallites size at about 4 nm for the CeO_2 phase and at about 6 nm for the NiO phase.

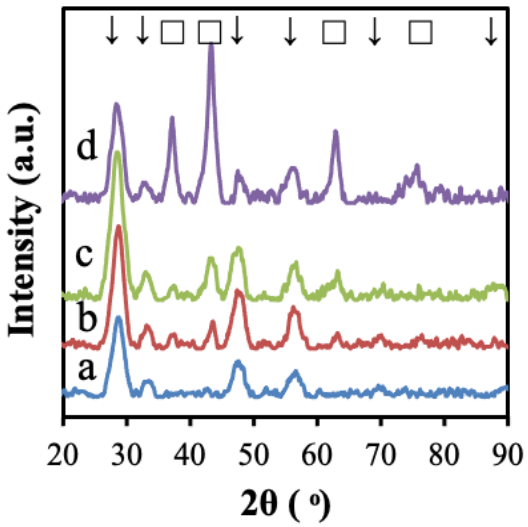

Fig. 3-21 XRD patterns of calcined $CeAl_{0.5}Ni_XO_Y$ catalysts: a) x = 0.5, b) x = 1, c) x = 2, d) x = 5. CeO_2 (↓), NiO (□).

3.3.3 Raman studies

The catalysts are also investigated using Raman spectroscopy. Raman spectra of $CeAl_{0.5}Ni_XO_Y$ compounds are presented in Fig. 3-22. The typical first-order F_{2g} peaks of CeO_2 is observed in all the compounds, located near 460 cm^{-1} related to fluorite nano-crystalline ceria. For the Al ternary catalysts, the first-order F_{2g} ceria peak shifts to lower frequencies around 435 cm^{-1} and presents a broadening effect. That illustrates the presence of small nanoparticles and the insertion of Ni^{2+} (and Al^{3+}) into ceria creating anionic vacancies. Among all the samples, the $CeAl_{0.5}Ni_2O_Y$ shows the maximum shift at 434 cm^{-1}. It can be concluded that the insertion of Ni in the ceria phase increases with Ni content and is maximum for the $CeAl_{0.5}Ni_2O_Y$ compound. In addition, there are the bands between 500 cm^{-1} and 650 cm^{-1} observed for all samples, corresponding to oxygen vacancies created by the incorporation of the dopant in ceria, in agreement with the presence of a solid solution[255].

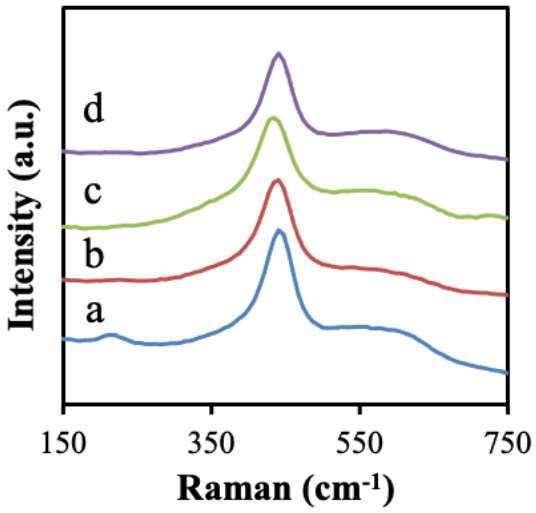

Figure 3-22 Raman spectra of calcined $CeAl_{0.5}Ni_XO_Y$ catalysts: a) x = 0.5, b) x = 1, c) x = 2, d) x = 5.

3.3.4 XPS studies

To further understand the interaction of the catalysts, fresh catalysts are also analyzed by XPS, the spectra are shown in Fig. 3-23. The O 1s core level presents two major oxygen species at 529.3 - 529.8 eV and 531.3 - 532.0 eV (Fig. 3-23 a). The first peak is assigned to typical O^{2-} lattice species, while the second peak is usually ascribed to oxygen species of hydroxyl groups (OH^-)[212].

The Ni 2p spectra show the presence of Ni^{2+} cations with the characteristic satellite line (Fig. 3-23 b). As summarized in Table 3-12, the BE of the main emission Ni $2p_{3/2}$ peak is varying between 855.5 and 855.7 eV on $CeNi_xAl_{0.5}O_Y$ compounds when x varying between 0.5 and 2, while for higher Ni content the main Ni $2p_{3/2}$ peak is at 854.6 eV with a shoulder at 856 eV. When $x \leq 2$, the values are slightly higher than the values reported previously for binary cerium nickel mixed oxides (854.5 - 854.8eV), but very close to that observed for $NiAl_2O_4$ (856.0 eV). Therefore, besides a contribution of Ni^{2+} cations in NiO, and even if a contribution peak at 855.7 eV can be also attributed to Ni^{2+}species related to the presence of a $Ni(OH)_2$ hydroxide[209], the Ni^{2+} cations in strong interaction with other cations are probably in the highest amount when x = 2, in agreement with Raman results. For the compound with the highest Ni content, the values become close to those obtained on binary cerium nickel mixed oxides. Therefore, XPS results show the presence of Ni^{2+} cations presenting

strong interactions with other cations (Ce^{4+}, Ce^{3+}, Al^{3+}), together with the presence of O^{2-} species and hydroxyl groups at the surface.

The Ce 3d spectra of calcined $CeAl_{0.5}Ni_XO_Y$ catalysts are shown in Fig. 3-23 c. The characteristic peak of Ce^{4+} is observed at approximately 917 eV, and a slightly lower value (916.1 eV) is obtained only when x = 1 (Table 3-12). In addition, considering that the double v'/u' is corresponding to the existence of Ce^{3+}. Based on this, the relative contribution of the Ce^{3+} species to the spectrum can be determined at 6 %.

The Al^{3+} species are present on the surface, as shown by the Al 2p peak (Fig. 3-23 d) obtained at about 74 eV (Table 3-12). However, the spectra of Al 2p and Ni 3p are very close, the uncertainty of the light peak position of Al 2p does not allow discussion on the environment of Al species[218]

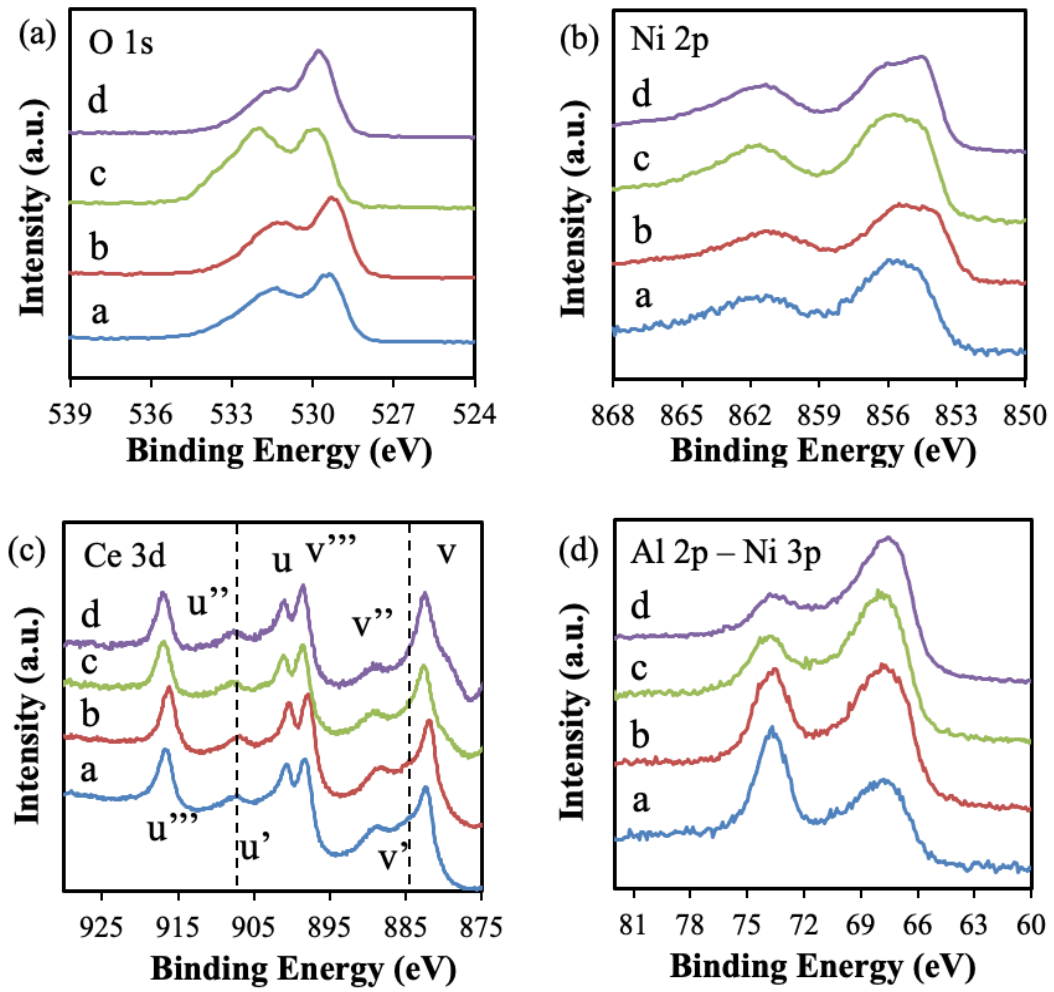

Fig. 3-23: XPS spectra of (a) O 1s, (b) Ni 2p, (c) Ce 3d, (d) Al 2p of the calcined $CeAl_{0.5}Ni_XO_Y$ catalysts: a) x = 0.5, b) x = 1, c) x = 2, d) x = 5.

Table 3-12 Binding energies of the calcined $CeAl_{0.5}Ni_XO_Y$ compounds.

Catalysts	O 1s (eV)	Ni $2p_{3/2}$ (eV)	Ce 3d (eV)	Al 2p (eV)
$CeAl_{0.5}Ni_{0.5}O_Y$	529.4/531.3	855.6	916.7/ 900.7/ 898.4/ 882.3	73.7
$CeAl_{0.5}Ni_1O_Y$	529.3/531.3	855.5	916.1/ 900.4/ 897.8/ 882.0	73.8
$CeAl_{0.5}Ni_2O_Y$	529.8/532.0	855.7	916.8/ 901.1/ 898.7/ 882.6	73.9
$CeAl_{0.5}Ni_5O_Y$	529.8/531.3	854.6	917.1/ 901.0/ 898.5/ 882.5	73.8

3.3.5 TPR studies

The H_2-TPR profiles of $CeAl_{0.5}Ni_xO_Y$ samples, shown in Fig. 3-24, has three main peaks centered at ~300 °C, 500 °C, and 900 °C. The reduction peaks at low temperature (210-354 °C) are assigned to the reduction of Ni species in small NiO nanoparticles and/or solid solution which are easily reducible. The reduction peaks at 400-700 °C are corresponding to the reduction of larger NiO nanoparticles which can be detected by XRD. As the nickel content increases the peaks become more intense and move to a higher temperature. Compared with the reduction temperature of bulk nickel oxide of 370 °C, the higher reduction temperature of nickel oxide in the $CeAl_{0.5}Ni_xO_Y$ catalyst proves the strong interaction between Ni cations with other cations. The peak at 900 °C can be associated with the reduction of bulk Ce^{4+} cations to Ce^{3+} [256].

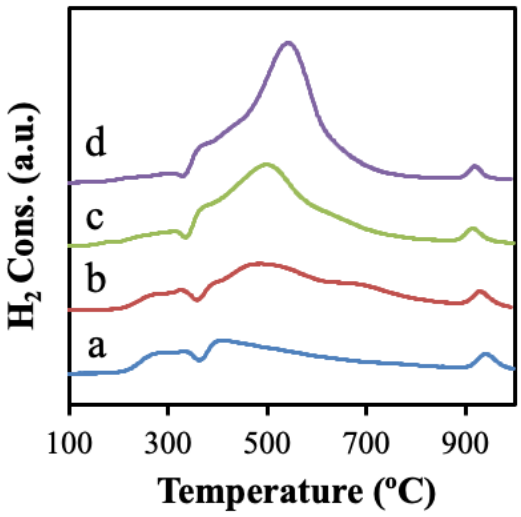

Figure 3-24 TPR of the calcined $CeAl_{0.5}Ni_XO_Y$ catalysts: a) x = 0.5, b) x = 1, c) x = 2, d) x = 5.

3.3.6 Characterizations of spent $CeAl_{0.5}Ni_XO_Y$ catalysts

The $CeAl_{0.5}Ni_2O_Y$ catalyst exhibits CH_4 and CO_2 conversions of 80% and 92%, respectively after 80 hours of stability in catalytic test at 800 °C, 10 mg, with H_2 pretreatment at 250 °C, CH_4/ CO_2/ N_2 = 5 %: 5 %: 90 % (according to the result in Fig. 2-26). The H_2/CO ratio is found at 1.1 and the carbon formation rate is of 0.0077 $g \cdot g_{cat}^{-1} \cdot h^{-1}$. To analyze the eventual evolution of the catalyst and the type of carbon formed, the spent $CeAl_{0.5}Ni_2O_Y$ catalyst is characterized by Raman and XPS.

In Fig. 3-25 a, the typical first-order F_{2g} peak of CeO_2 is observed in the spent compounds, located near 464 cm^{-1}, at higher frequencies than the fresh one. The peak around 525 cm^{-1} is evidencing the presence of oxygen vacancies created by the incorporation of the dopant in ceria, in agreement with the presence of a solid solution after DRM reaction. In the carbon zone, the Raman spectrum exhibits two bands at around 1306 cm^{-1} and 1604 cm^{-1}, which are associated with the D and G vibration modes of graphitic carbon. In addition, the intensity of D-band is much higher than the G-band, showing the high disorder of the material (low degree of graphitization). Therefore, the catalytic stability of the $CeAl_{0.5}Ni_2O_Y$ compound is apparently not perturbed by the formation of this type of carbon formed[206].

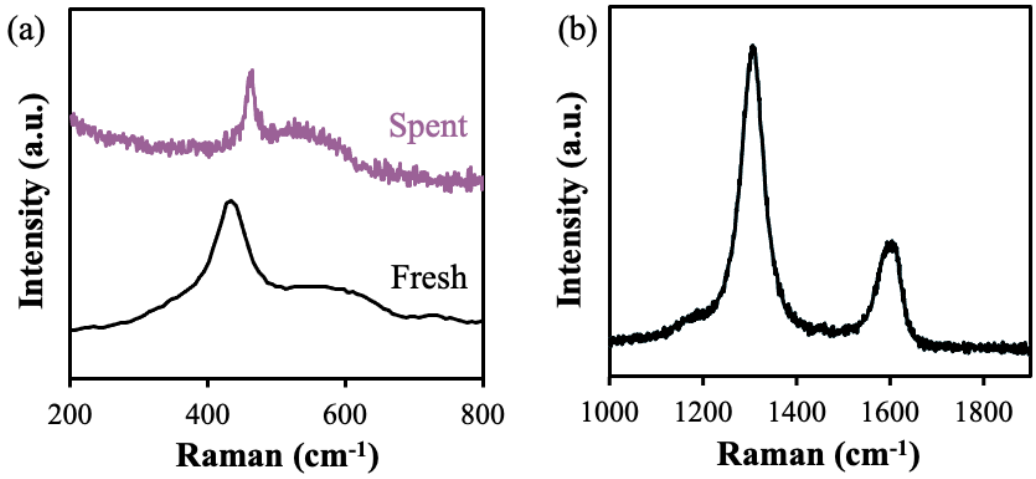

Fig. 3-25: Raman spectra of the $CeAl_{0.5}Ni_2O_Y$ catalyst after test at 800 °C, 10 mg, with H_2 pretreatment at 250 °C, CH_4/ CO_2/ N_2 = 5 %:5 %:90 %.

Table 3-13 Raman peaks of the fresh and spent $CeAl_{0.5}Ni_2O_Y$ catalyst after test at 800 °C, 10 mg, with H_2 pretreatment at 250 °C, CH_4/ CO_2/ N_2 = 5 %: 5 %: 90 %.

Catalysts	Raman (cm^{-1})			
Fresh $CeAl_{0.5}Ni_2O_Y$	434.1	545.7	-	-
Spent $CeAl_{0.5}Ni_2O_Y$	464.1	525.3	1306.2	1604.0

The XPS spectra of spent $CeAl_{0.5}Ni_2O_Y$ catalyst are shown in Fig. 3-26. To analyze the eventual carbon formed, the Al peak at 74.0 eV is taken as a reference in order to be able to report the C 1s BE. The C 1s peak at 285 eV (before test) presents a slight shift to 284.6 eV after test, that can correspond to some CH_X groups (formed by dissociation of CH_4) that can be normally recovered at the surface of the compound after stopping the catalytic test under CH_4 and CO_2 mixture[257]. As on the compound before test, in spent $CeAl_{0.5}Ni_2O_Y$ catalyst, the O 1s core level presents also two major oxygen species at 529.7 eV and 531.7 eV (Fig. 3-26 b) showing the presence of O^{2-} lattice species and oxygen species in hydroxyl groups (OH^-)[255]. However, the proportion of O^{2-} is higher after test compared to the fresh catalyst. The Ni $2p_{3/2}$ spectra of spent $CeAl_{0.5}Ni_2O_Y$ catalyst is shown in Fig. 3-26 c. The main peak shifts from 855.7 and 854.3 eV to 856.2 and 852.6 eV after DRM test. The one at 852.6 eV means that metallic Ni (Ni°) is formed after DRM reaction. The peak at 856.2 eV is demonstrating the presence of Ni^{2+} cations with strong interactions with other cations. The Ni 2p spectrum indicates that Ni species change from 100 % as Ni^{2+} cations (like in NiO and Ni^{2+} interacting with other cations) to 5.8 % of metallic Ni and 94.2 % of Ni^{2+} species after a long-time test. The Ce 3d spectra of spent catalyst presents two peaks assigned to Ce^{3+} at 907.9 eV and 888.9 eV, and the intensity of the two features are much higher than the ones of fresh catalyst. The peaks corresponding to Ce^{4+} are also well detected. It is confirmed that Ce^{4+} and Ce^{3+} cations are coexisting over the surface of spent catalysts. The used catalyst still has redox properties, as the amount of Ce^{3+} cations increases from 31.3 % to 45.9 %, in agreement with the Raman results.

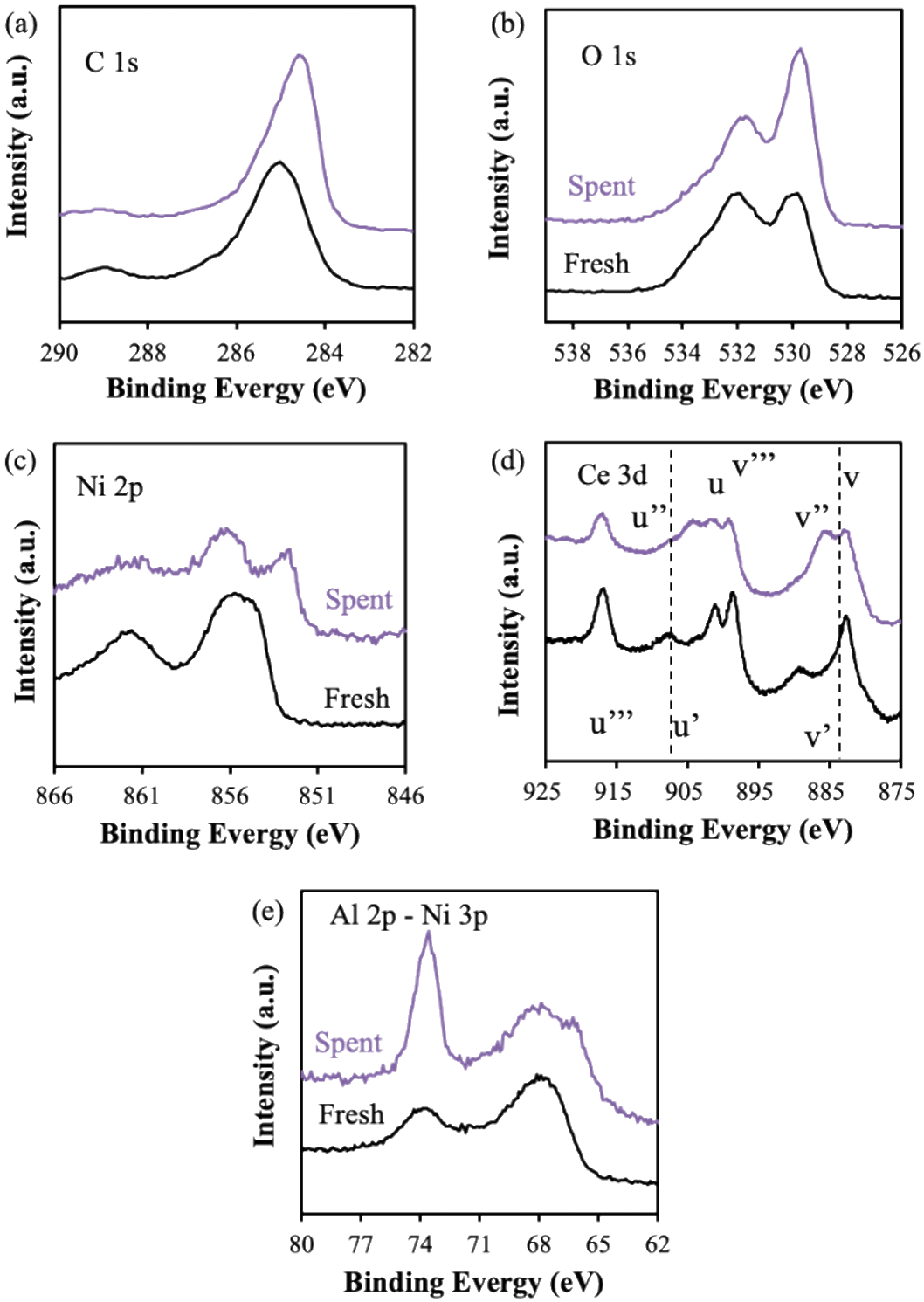

Fig. 3-26: XPS spectra of (a) C 1s, (b) O 1s, (c) Ni 2p, (d) Ce 3d, (e) Al 2p - Ni 3p of the calcined $CeAl_{0.5}Ni_2O_Y$ catalyst, after test 80 h, at 800 °C, 10 mg, with H_2 pretreatment at 250 °C, CH_4/ CO_2/ N_2 = 5 %:5 %:90 %.

Table 3-14 Binding energies of the calcined $CeAl_{0.5}Ni_2O_Y$ catalyst after test 80 h, at 800 °C, 10 mg, with H_2 pretreatment at 250 °C, CH_4/ CO_2/ N_2 = 5 %:5 %:90 %.

$CeAl_{0.5}Ni_2O_Y$	C 1s (eV)	O 1s (eV)	Ni $2p_{3/2}$ (eV)	Ce 3d (eV)
Fresh	285.0	532.0/ 529.8	861.6/ 855.7/ 854.3	916.8/ 901.1/ 898.7/ 882.6
Spent	284.6	531.7/ 529.7	862.4/ 856.2/ 852.6	917.0/ 901.3/ 899.2/ 883.0

*The Al 2p peak at 74.0 eV was taken as reference

The spent $CeAl_{0.5}Ni_XO_Y$ catalysts after 5 h of test at 600 °C in CH_4/ CO_2/ N_2 = 5 %:5 %:90 % reaction mixture (according to the catalytic result in Fig. 2-6 and 2-16) are characterized by XPS. The peak of Al 2p at 74.0 eV is taken as a reference to be able to analyze the C 1s BE evolution. The C 1s main peak at 284.2-284.9 eV varies only slightly due to C-C or C=C bands. Fig. 3-27 b and 3-28 b show the XPS profiles of O 1s for the spent catalysts. The low binding energy peak located at 529.9-530.2 eV is attributed to the typical O^{2-} lattice oxygen species. While the high binding energy peak located at 531.6-532.7 eV is assigned to oxygen species related to the hydroxyl groups. The spectra obtained in the Ni $2p_{3/2}$ energy region are included in Fig. 3-27 c and 3-28 c, showing the most intense peaks at 852.5 - 856.3 eV (with the satellite of Ni^{2+} cations at around 861 eV). For spent $CeAl_{0.5}Ni_{0.5}O_Y$ catalyst, the Ni $2p_{3/2}$ spectrum shows a main peak at 855.9 eV assigned to Ni^{2+} species interacting with other cations. For spent $CeAl_{0.5}Ni_XO_Y$ (X=1, 2, 5), there are two peaks at 852.0 - 853.2 eV and 854.7 - 856.3 eV which confirms the presence of metallic Ni (Ni°) and Ni^{2+} cations. The Ni° proportion seems to increase with Ni content. The Ce 3d spectra shown in Fig. 3-27 and 3-28 d, referring to as u, u″, v and v″ are assigned to Ce^{3+} and peaks u′, u‴, u⁗, v′, v‴, v⁗ represent the presence of Ce^{4+}. The results show the presence of Ce^{3+} and Ce^{4+} cations after test.

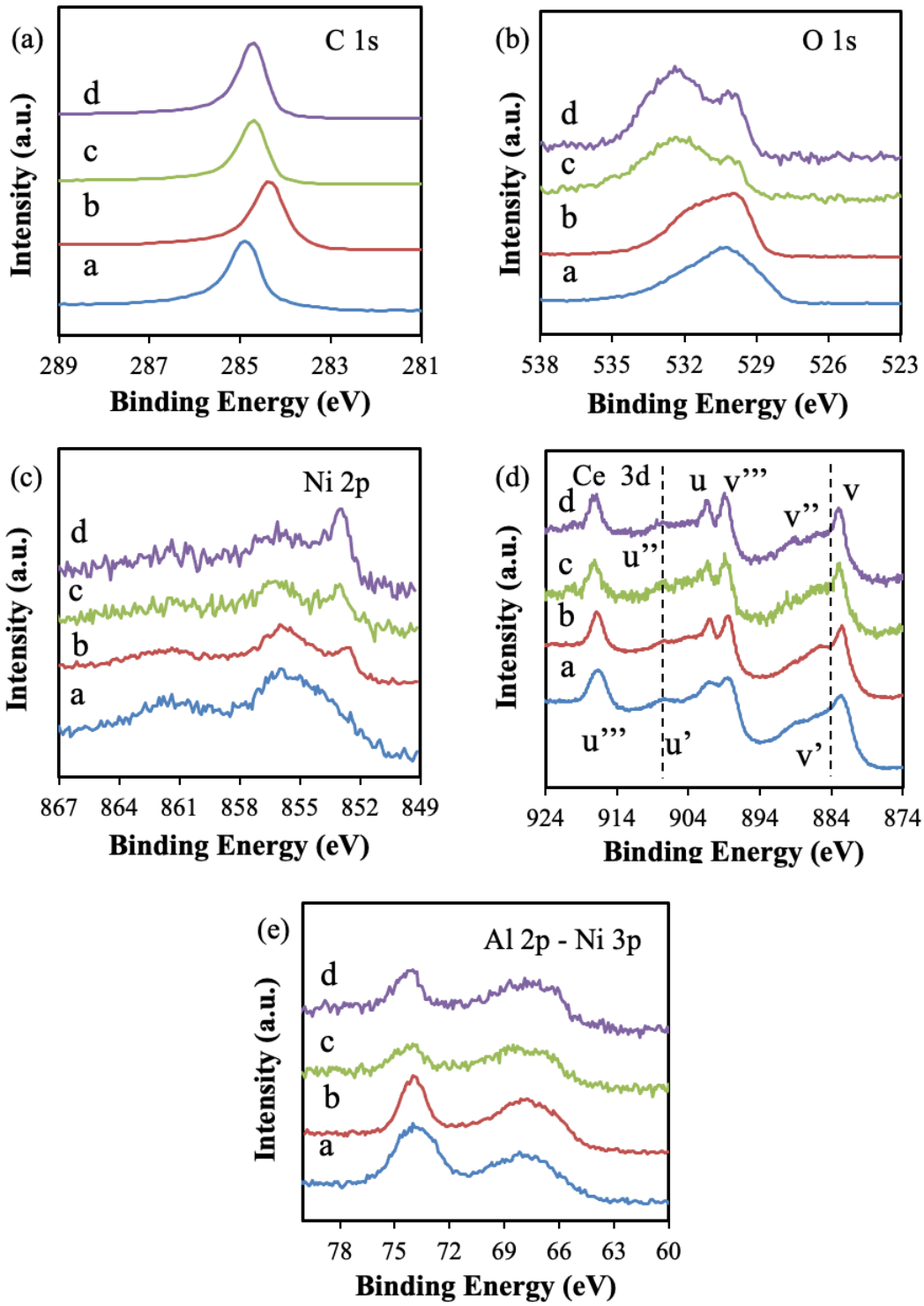

Fig. 3-27: XPS spectra of (a) C 1s, (b) O 1s, (c) Ni 2p, (d) Ce 3d, (e) Al 2p - Ni 3p of the calcined $CeAl_{0.5}Ni_XO_Y$ catalysts a) x = 0.5, b) x = 1, c) x = 2, d) x = 5, after test at 600 °C, 50 mg, with H_2 pretreatment at 250 °C, CH_4/ CO_2/ N_2 = 5 %:5 %:90 %.

Table 3-15 Binding energies of the calcined $CeAl_{0.5}Ni_XO_Y$ catalysts after test at 600 °C, 50 mg, with H_2 pretreatment at 250 °C, CH_4/ CO_2/ N_2 = 5 %:5 %:90 %.

Catalysts	C 1s (eV)	O 1s (eV)	Ni $2p_{3/2}$ (eV)	Ce 3d (eV)
$CeAl_{0.5}Ni_{0.5}O_Y$	284.9	530.2	861.4/ 855.9	916.0/ 900.5/ 898.5/ 882.6
$CeAl_{0.5}Ni_1O_Y$	284.4	529.9	861.4/ 856.0/ 852.5	916.2/ 900.5/ 898.4/ 882.5
$CeAl_{0.5}Ni_2O_Y$	284.7	531.8	862.3/854.7/ 853.0	917.1/ 900.7/ 898.9/ 882.9
$CeAl_{0.5}Ni_5O_Y$	284.7	532.4	861.4/ 856.1/ 852.9	916.9/ 900.8/ 898.6/ 883.0

*The Al 2p peak at 74.0 eV was taken as reference

Table 3-16 Binding energies of the calcined $CeAl_{0.5}Ni_XO_Y$ catalysts after test at 600 °C, 50 mg, without H_2 pretreatment, CH_4/ CO_2/ N_2 = 5 %:5 %:90 %.

Catalysts	C 1s (eV)	O 1s (eV)	Ni $2p_{3/2}$ (eV)	Ce 3d (eV)
$CeAl_{0.5}Ni_{0.5}O_Y$	284.2	531.6	855.3	917.0/ 901.2/ 898.6/ 882.8
$CeAl_{0.5}Ni_1O_Y$	284.8	532.7	856.3/ 853.2	917.3/ 901.5/ 899.0 /882.8
$CeAl_{0.5}Ni_2O_Y$	284.6	532.5	852.7	917.1/ 901.3/ 898.7/ 882.7
$CeAl_{0.5}Ni_5O_Y$	284.7	532.6	856.0/ 853.0	917.2/ 901.4/ 898.7/ 882.9

*The Al 2p peak at 74.0 eV is taken as reference

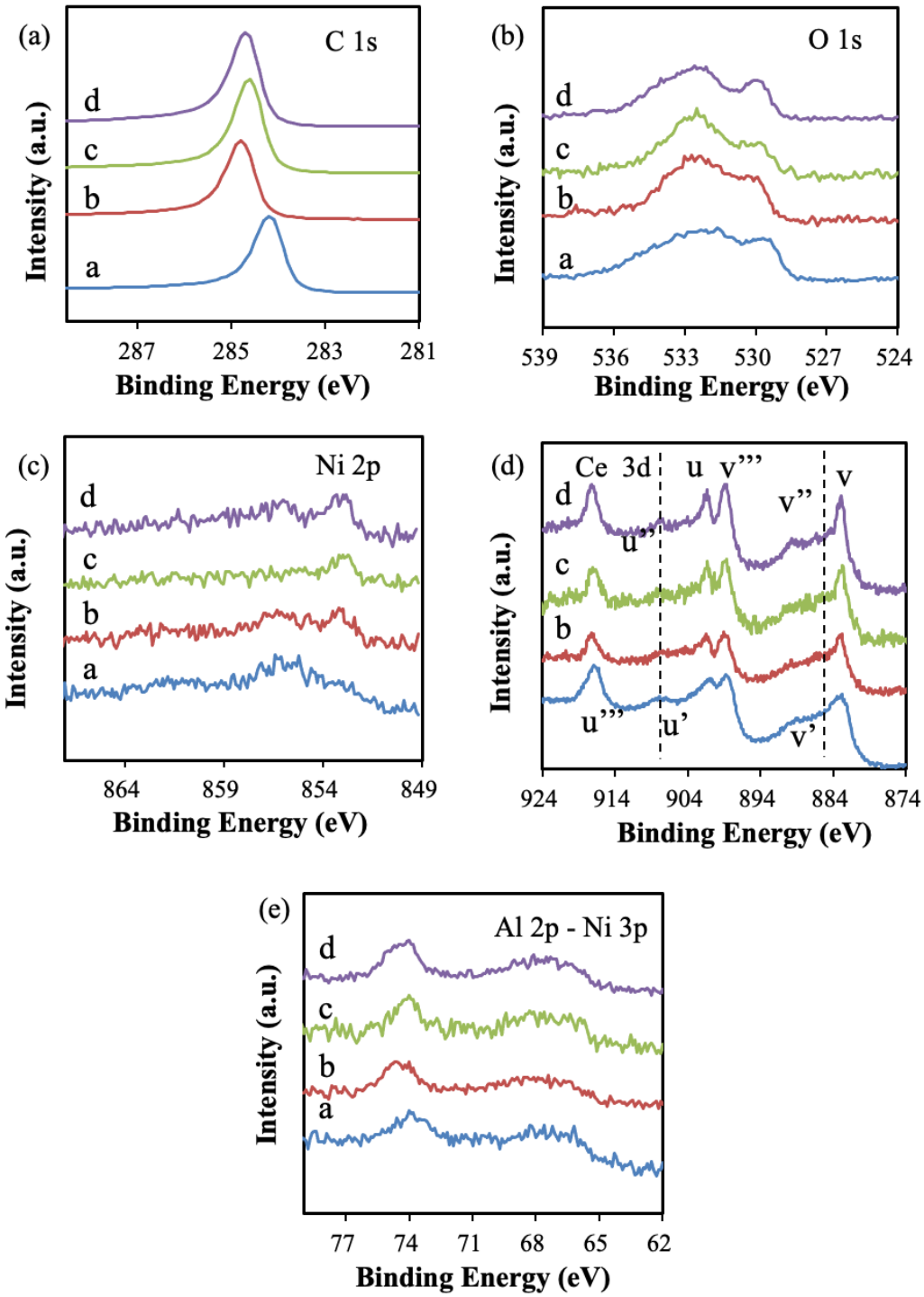

Fig. 3-28: XPS spectra of (a) C 1s, (b) O 1s, (c) Ni 2p, (d) Ce 3d, (e) Al 2p - Ni 3p of the calcined $CeAl_{0.5}Ni_XO_Y$ catalysts a) x = 0.5, b) x = 1, c) x = 2, d) x = 5, after test at 600 °C, 50 mg, without H_2 pretreatment, CH_4/ CO_2/ N_2 = 5 %:5 %:90 %.

3.4 $AlMg_2Ni_XO_Y$ catalysts characterization results

3.4.1 Elemental analysis and textural properties

The molar compositions, specific surface areas, and crystallites size of $AlMg_2Ni_XO_Y$ catalysts are investigated and shown in Table 3-17. The loading of the catalyst is 21.9, 43.7, and 61.4 wt.% on $AlMg_2Ni_1O_Y$, $AlMg_2Ni_3O_Y$, and $AlMg_2Ni_{12}O_Y$ catalysts. The actual loading is close to the nominal value. The BET surface areas of the catalysts are also presented in Table 3-18, the BET surface area increases with more addition of Ni content. The $AlMg_2Ni_{12}O_Y$ catalyst presents the maximum value of 196 m^2g^{-1} in the series.

Table 3-17 Compositions, specific surface areas, and average crystallites size of the $AlMg_2Ni_XO_Y$ catalysts.

Catalysts	Ni loading wt%	Ni/M_T	S_{BET}/m^2g^{-1}	d oxide crystal (nm)
$AlMg_2Ni_1O_Y$	21.9	0.25	127	3.6
$AlMg_2Ni_3O_Y$	43.7	0.50	168	3.9
$AlMg_2Ni_{12}O_Y$	61.4	0.80	196	5.9

3.4.2 XRD studies

The XRD patterns of the $AlMg_2Ni_XO_Y$ catalysts are exhibited in Fig. 3-29. The diffraction patterns observed could be attributed either to MgO (JCPDS 65-0476), Ni-Mg-O (JCPDS 24-0712), and NiO (JCPDS 47-1049)[258]. In fact, the diffraction peaks almost overlap with each other and can barely be distinguished from one another. When the Ni content increases, the diffraction patterns become thinner and more intense, which is consistent with the growth in the average crystallites size of the compounds. As the Ni loading increases, the average crystallites size grows from 3.6 to 5.9 nm. Moreover, it is found that adding nickel influences not only the intensity of the peak but also the broadness of the peak. It can be put down to the incorporation of Ni species into the MgO phase through the formation of Mg-Ni-(Al)-O solid solution[259]. In addition, no correlation peak corresponding to Al_2O_3 is found, which may be due to the high dispersion of Al species, the amorphous phase, and/or the insertion of Al into the Mg-Ni-O phase to form Mg-Ni-Al-O solid solution where some of the Mg^{2+} are replaced by Al^{3+} [260].

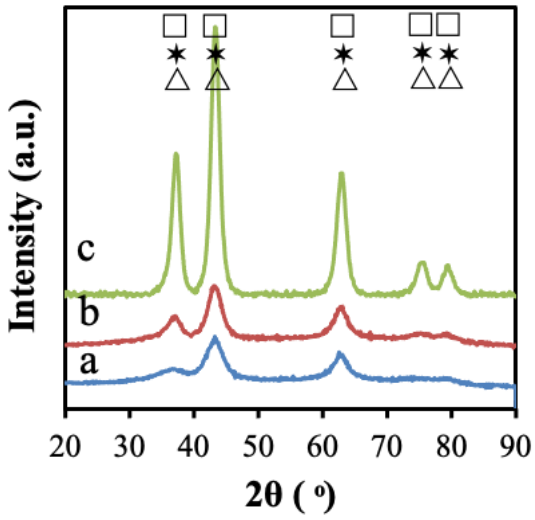

Fig. 3-29 XRD patterns of $AlMg_2Ni_XO_Y$ catalysts: a) x = 1, b) x = 3, c) x = 12. NiO (□), MgO (✶), Ni-Mg-O (△).

3.4.3 XPS studies

The surface of the catalysts is characterized by XPS to know the chemical state of the elements. As shown in Fig. 3-30 a, the O 1s peaks of the catalysts can be deconvoluted into two peaks at 531.7 and 530.6 eV. The $AlMg_2Ni_1O_Y$ catalyst presents the main peak at 531.7 eV, which corresponds to oxygen species like in hydroxyl groups. While the $AlMg_2Ni_3O_Y$ and $AlMg_2Ni_{12}O_Y$ catalysts present main peak at 530.6 eV, which is assigned to the typical O^{2-} lattice oxygen in oxides of NiO and/or MgO and/or Ni-Mg-(Al)-O solid solution[261].

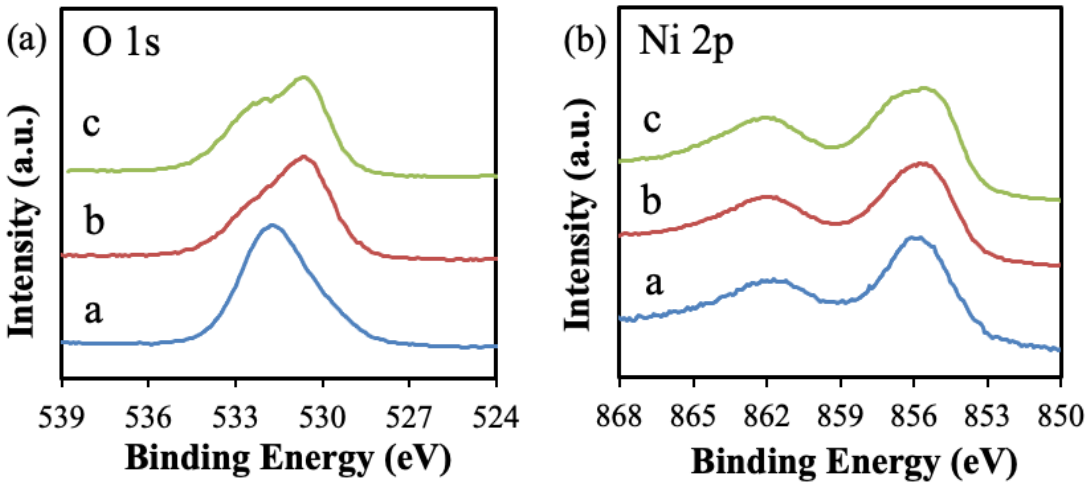

Fig. 3-30: XPS spectra of (a) O 1s, (b) Ni 2p of the calcined $AlMg_2Ni_XO_Y$ catalysts: a) x = 1, b) x = 3, c) x = 12.

The Ni 2p spectra are shown in Fig. 3-30 b and the binding energies obtained from the XPS spectra are listed in Table 3-18. The peaks at about 856 eV and 862 eV are assigned to the Ni $2p_{3/2}$ region, respectively. Compared to the BE of bulk nickel oxide reported in the literature (853.7-854.6 eV), the $AlMg_2Ni_{12}O_Y$ and $AlMg_2Ni_3O_Y$ catalysts present a BE at 855.6-855.7 eV, which is very similar to the Ni-Mg-Al mixed oxides (855.5 eV)[262]. While the $AlMg_2Ni_1O_Y$ catalyst shows a higher BE at 856.1 eV, it is close to $NiAl_2O_4$ (856 eV)[263]. It illustrates that the nickel species, aluminum species (magnesium species) have a strong interaction. The XPS results indicate that Ni-Mg-(Al)-O solid solution may be formed. Therefore, the transfer of electrons from Ni to Mg or Al in the structure will result in a transition to a higher BE of 855.7 eV. Meanwhile, the satellite line of Ni $2p_{2/3}$ present at 861.7-862.2 eV, proves the presence of Ni^{2+} species[264].

Table 3-18 Binding energies of the calcined $AlMg_2Ni_XO_Y$ compounds.

Catalysts	O 1s (eV)	Ni $2p_{3/2}$ (eV)
$AlMg_2Ni_1O_Y$	531.7	861.7/ 856.1
$AlMg_2Ni_3O_Y$	530.6	861.9/ 855.7
$AlMg_2Ni_{12}O$	530.6	862.2/ 855.6

3.4.4 TPR studies

The $AlMg_2Ni_XO_Y$ catalysts are examined by H_2-TPR and displayed in Fig. 3-31. For all catalysts, regardless of the Ni content, a major broad peak is observed for each sample, located in the temperature range of 580-780 °C. In addition, the reduction temperature is obviously related to the Ni content of the catalyst. The peak shifts to a higher temperature as the Ni content decreases. The reduction peak of $AlMg_2Ni_{12}O_Y$ catalyst appears at 580 °C, while the reduction peak of $AlMg_2Ni_3O_Y$ catalyst appears at higher temperature of 640 °C, and at 780 °C for $AlMg_2Ni_1O_Y$. It reveals that catalysts with lower nickel content are less likely to be reduced.

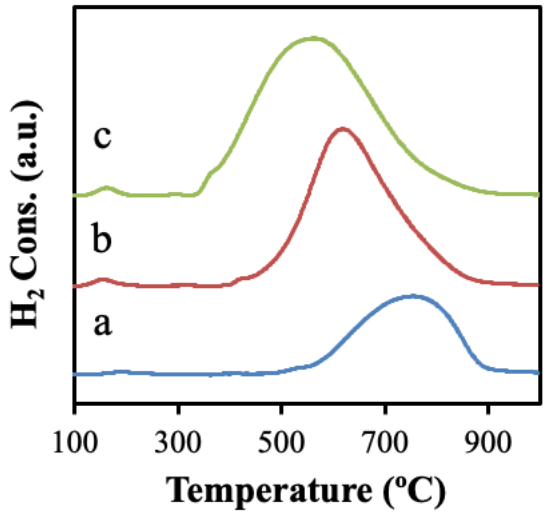

Figure 3-31 TPR profiles of $AlMg_2Ni_XO_Y$ catalysts: a) x = 1, b) x = 3, c) x = 12.

As mentioned in the literature, the reduction peak ranging from 580-780 °C is assigned to the reduction of Ni-Mg-(Al)-O or Ni-Al-(Mg)-O solid solution[265]. For low Ni content catalyst ($AlMg_2Ni_1O_Y$), the reduction peak around 750-850 °C was explained by the incorporation of Ni into the Mg-Al support, $NiMgO_2$, and/or $NiAl_2O_4$[258]. For higher Ni content catalysts ($AlMg_2Ni_3O_Y$ and $AlMg_2Ni_{12}O_Y$), the higher nickel content has an impact on the reducibility of nickel species, and significantly changes the interaction between Ni and Mg or/and Al. As a result, the reduction peak of the catalyst with higher Ni content appears in a lower temperature range.

A small shoulder at 350-435 °C could be assigned to the presence of NiO. The area of the reduction peak of NiO increases with the increase of Ni content. When the content of Ni increases, the peak moves to a lower temperature, which could be due to the different chemical environments around the NiO particles.

3.4.5 Characterizations of spent $AlMg_2Ni_XO_Y$ catalysts

The $AlMg_2Ni_{12}O_Y$ catalyst exhibits high CH_4 and CO_2 conversions and good carbon resistant performance (according to the catalytic result in Fig. 2-27). The CH_4 and CO_2 conversions are of 99.7 % and 93.8 %, respectively, after 80 hours at 800 °C, (10 mg, with in situ H_2 pretreatment at 450 °C) in CH_4/ CO_2/ N_2 = 5 %:5 %:90 % reaction mixture, and the H_2/CO ratio is around 1.2. The carbon formation rate in this case is of 0.006 $g \cdot gcat^{-1} \cdot h^{-1}$.

The spent $AlMg_2Ni_{12}O_y$ catalyst is analyzed by Raman spectroscopy in the region allowing carbon analysis. The signal is relatively noisy, but two peaks are

observed at 1307 cm^{-1} and 1585 cm^{-1} related to the D and G bands of graphitic type of carbon. The highest intensity of the D-band compared to G-band illustrates the high disorder of the carbonaceous species as byproducts of the reaction, as reported the I_D/I_G value of 1.15, higher than one.

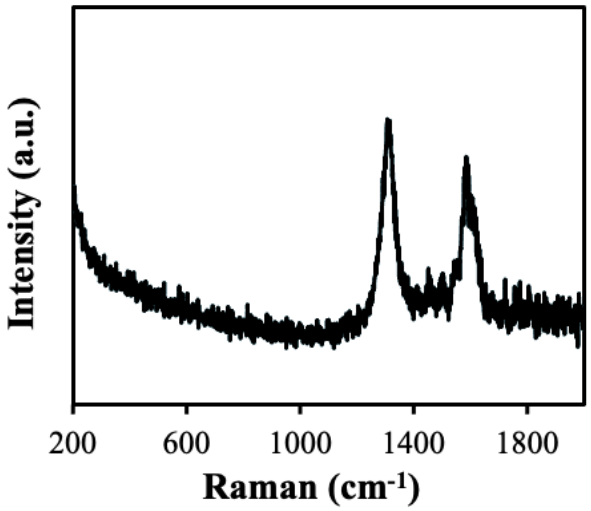

Fig. 3-32: Raman spectrum of the $AlMg_2Ni_{12}O_Y$ catalyst after test at 800 °C, 10 mg, with H_2 pretreatment at 450 °C, CH_4/ CO_2/ N_2 = 5 %:5 %:90 %.

Table 3-19 Raman peaks of the spent $AlMg_2Ni_{12}O_Y$ catalyst after test at 800 °C, 10 mg, with H_2 pretreatment at 450 °C, CH_4/ CO_2/ N_2 = 5 %: 5 %: 90 %.

Catalysts	Raman (cm^{-1})	
Spent $AlMg_2Ni_{12}O_Y$	1307.1	1585.3

The XPS spectrum of spent $AlMg_2Ni_{12}O_Y$ is shown in Fig. 3-33. The peak of Al 2p at 74.0 eV is taken as a reference to be able to analyze the C 1s BE evolution. The peak of C 1s in Fig. 3-33 a is observed at 281.7 eV which is ascribed to the carbidic species[266]. Fig. 3-33 b displays O 1s core level of spent $AlMg_2Ni_{12}O_Y$ catalyst. The main BE observed at 531.3 eV corresponds to oxygen species related to the presence of hydroxyl groups. However, a shoulder with BE close to 529 eV is emerging showing the presence of O^{2-} species. Ni $2p_{2/3}$ spectrum of spent $AlMg_2Ni_{12}O_Y$ is depicted in Fig. 3-33 c. In this spectrum 2 bands are clearly observed along with satellite peak. The BE at 856.3 eV is due to the presence Ni^{2+} species (with its satellite around 860 eV). The value of this BE is higher compared to the one observed on the calcined compound (855.6 eV) on which the presence of Ni^{2+} cations in strong

interaction with other cations has been shown, therefore these species are also present after test. The peak with binding energy at 852.8 eV can be assigned to metallic Ni. It demonstrates that 22.3 % of metallic Ni and 77.7 % of Ni^{2+} cations (in solid solution) are present after DRM test during 80 hours at 800 °C.

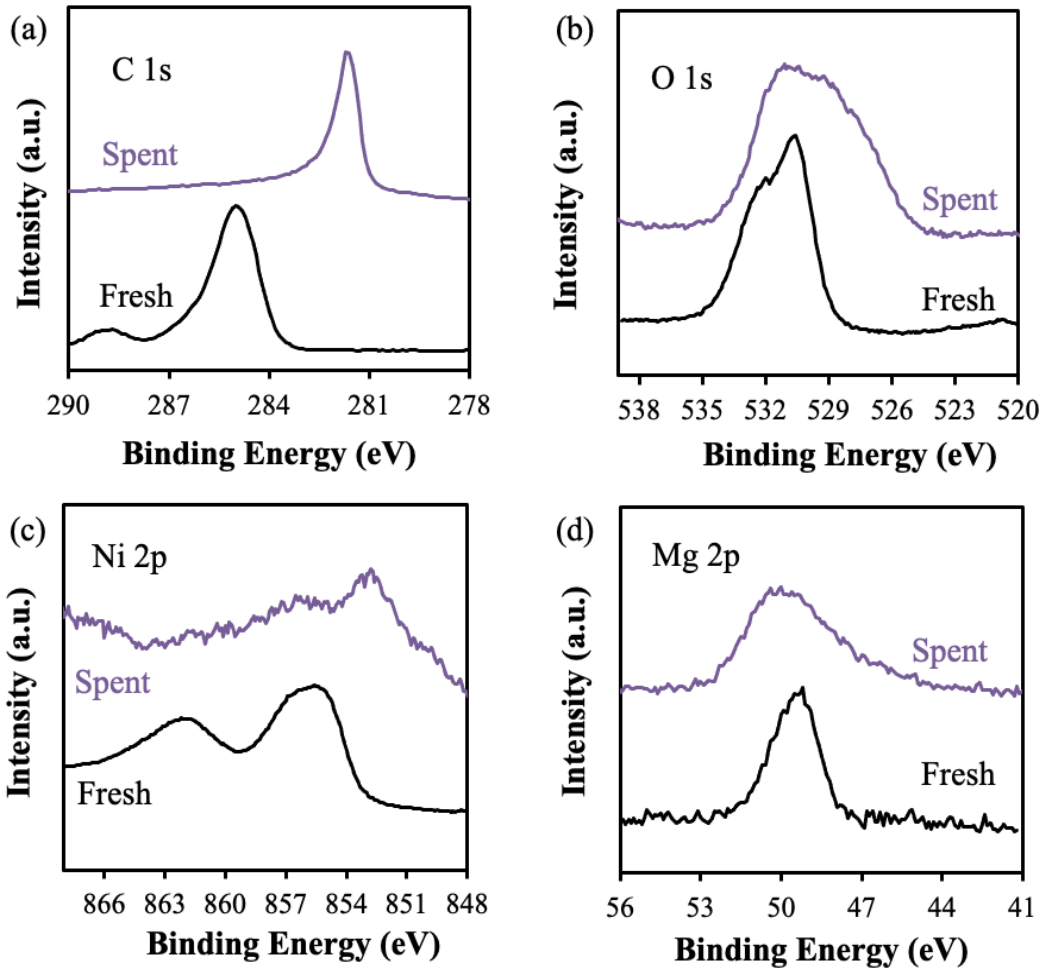

Fig. 3-33: XPS spectra of (a) C 1s, (b) O 1s, (c) Ni 2p, (d) Mg 2p, (e) Al 2p - Ni 3p of the fresh and spent $AlMg_2Ni_{12}O_Y$ catalyst, after test 80 h, at 800 °C, 10 mg, with H_2 pretreatment at 450 °C, CH_4/ CO_2/ N_2 = 5 %:5 %:90 %.

Table 3-20 Binding energies of the calcined $AlMg_2Ni_xO_y$ catalysts after test 80 h, at 800 °C, 10 mg, with H_2 pretreatment at 450 °C, CH_4/ CO_2/ N_2 = 5 %:5 %:90 %.

$AlMg_2Ni_{12}O_Y$	C 1s (eV)	O 1s (eV)	Ni $2p_{3/2}$ (eV)	Mg 2p (eV)	Al 2p (eV)
Fresh	285.0	530.6	855.6	49.2	73.6
Spent	281.7	531.3	856.3/ 852.8	50.0	74.0

*The Al 2p peak at 74.0 eV was taken as reference

The spent $AlMg_2Ni_XO_Y$ catalysts after test of 5 hours, at 600 °C, 50 mg, with H_2 pretreatment at 450 °C, CH_4/ CO_2/ N_2 = 5 %:5 %:90 % (according to the catalytic result in Fig. 2-8) are also characterized by XPS (Figure 3-34 and Table 3-21). The C1s spectrum is deconvoluted to reveal the types of carbonaceous species. The peaks of spent $AlMg_2Ni_1O_Y$ are assigned to carbidic carbon (280.2 eV and 282.4 eV). The peaks of spent $AlMg_2Ni_3O_Y$ and $AlMg_2Ni_{12}O_Y$ are assigned to graphitic carbon (BE 283.45 eV)[267]. The O 1s spectrum presents one major oxygen species, for $AlMg_2Ni_1O_Y$, at 529.5 eV assigned to typical O^{2-} lattice species in oxides of NiO and/or MgO and/or Ni-Mg-(Al)-O solid solution[258]. For $AlMg_2Ni_3O_Y$ and $AlMg_2Ni_{12}O_Y$ at 531.9 and 531.7 eV usually ascribed to oxygen species of hydroxyl groups (OH^-). The Ni $2p_{3/2}$ spectra of used $AlMg_2Ni_XO_Y$ are shown in Fig. 3-34 c and Table 3-21. The peak at binding energy of 855.0 - 856.0 eV is corresponding to the Ni^{2+} species with strong interaction with other cations. The peak around 851 eV, which intensity increases with Ni content, is ascribed to metallic Ni (Ni°), and well observed at 851.5 eV in spent $AlMg_2Ni_{12}O_Y$. The Mg 2p spectra of the used $AlMg_2Ni_XO_Y$ are shown in Fig. 3-34 d. The main peak corresponds to Mg^{2+} cations like in MgO with BE at 49.6 eV to 50.1 eV.

Table 3-21 Binding energies of the calcined $AlMg_2Ni_xO_Y$ catalysts after test at 600 °C, 50 mg, with H_2 pretreatment at 450 °C, CH_4/ CO_2/ N_2 = 5 %:5 %:90 %.

Catalysts	C 1s (eV)	O 1s (eV)	Ni $2p_{3/2}$ (eV)	Mg 2p (eV)
$AlMg_2Ni_1O_Y$	280.2	529.5	855.0	50.0
$AlMg_2Ni_3O_Y$	283.4	531.9	856.0	49.6
$AlMg_2Ni_{12}O_Y$	283.4	531.7	856.0/ 851.5	50.1

*The Al 2p peak at 74.0 eV was taken as reference

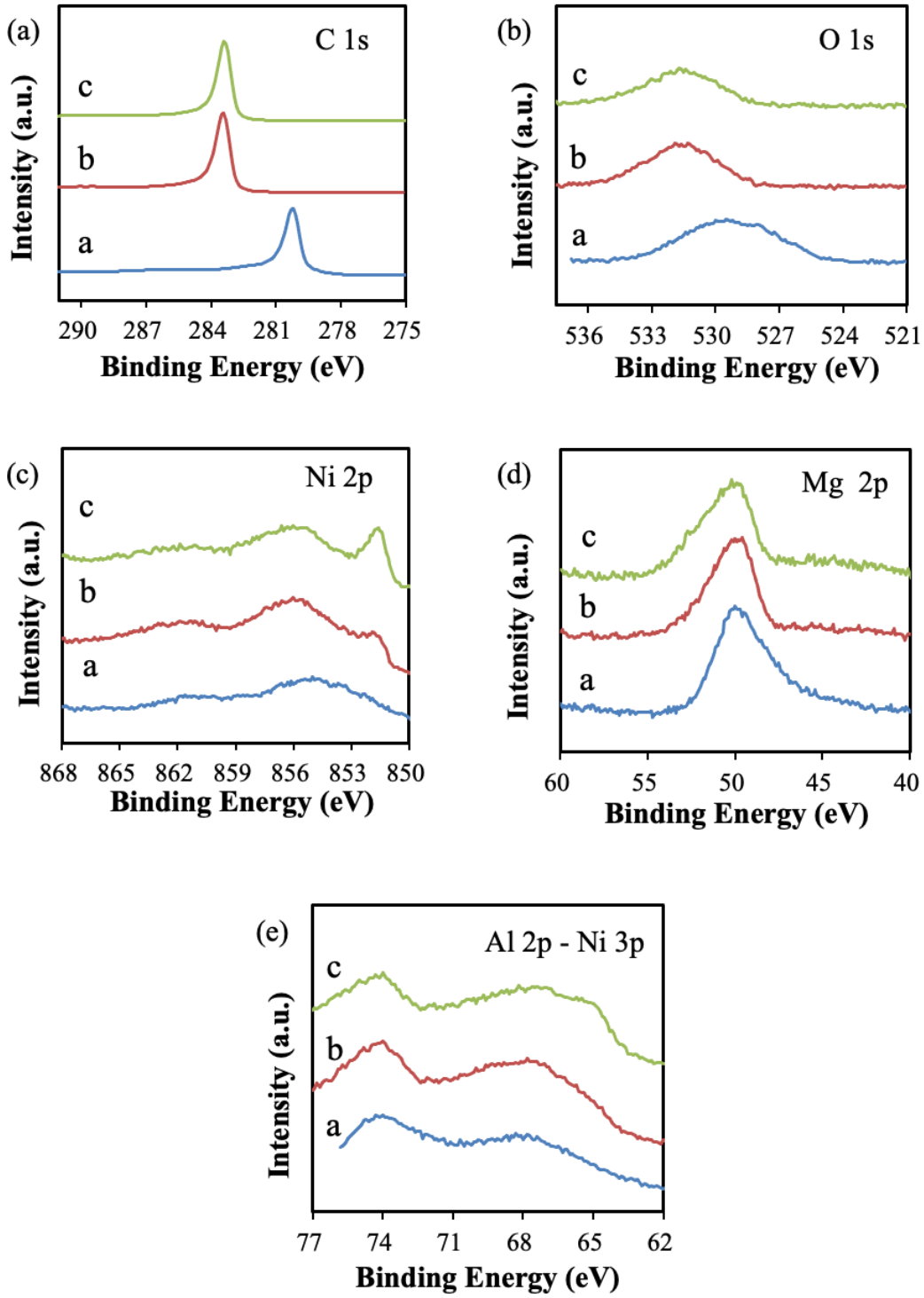

Fig. 3-34: XPS spectra of (a) C 1s, (b) O 1s, (c) Ni 2p, (d) Mg 2p, (e) Al 2p - Ni 3p of the calcined $AlMg_2Ni_xO_Y$ catalysts a) x = 1, b) x = 3, c) x = 12, after test at 600 °C, 50 mg, with H_2 pretreatment at 450 °C, CH_4/ CO_2/ N_2 = 5 %:5 %:90 %.

3.5 Conclusion

In this study, $CeNi_XO_Y$, $CeZr_{0.5}Ni_XO_Y$, $CeAl_{0.5}Ni_XO_Y$, and $AlMg_2Ni_XO_Y$ catalysts are prepared by the co-precipitation method (CP). The above Ni-based catalysts are studied by different physicochemical techniques, such as ICP-MS, N_2 physisorption, XRD, Raman, H_2-TPR, XPS, and some chosen compounds are also characterized after some tests by Raman and XPS.

The surface areas for $CeNi_XO_Y$ compounds are ranging between 77-215 $m^2\ g^{-1}$ (with x = 0.1, 0.2, 0.3, 0.5, 1 and 2 corresponding to Ni wt.% ranging from 5 % to 40 %). The dried compounds have a larger surface area than the calcined compounds with same Ni content. In dried $CeNi_XO_Y$ catalysts, the ceria like phase is clearly apparent in all samples, and there might be presence of $Ni(OH)_2$. The broadness and shift of CeO_2 XRD diffraction patterns suggest the formation of a cerium-nickel solid solution. The NiO crystalline phase is detected in high Ni content calcined catalysts ($x \geq 0.5$). The average crystallites size is distributed in the range of 4-5 nm for CeO_2 and 8-10 nm for NiO. Raman results evidence the existence of strong interactions between nickel and cerium species in dried and calcined catalysts. XPS analysis proves that Ni^{2+} cations which has strong interaction with other cations are present on the surface of the solids, which is in agreement with the formation of Ce-Ni-O solid solution. TPR analysis discloses that $CeNi_XO_Y$ solids possess a proportion of Ni species which present a characteristic reduction peak at about 270 °C. Such Ni species are able to be reduced and re-oxidized easily and reversibly, which is due to the existence of strong interactions between nickel and cerium species in $CeNi_XO_Y$ solids. After stability test of 80 h, the performed characterizations lead to conclude that the Ce-Ni-O solid solution is still present in spent $CeNi_1O_Y$ catalyst (with the presence of Ni^{2+} cations) and that there are more oxygen vacancies and Ce^{3+} generated.

In $CeZr_{0.5}Ni_XO_Y$ series, the dried $CeZr_{0.5}Ni_{0.5}O_Y$ shows the largest specific surface area of 186 m^2/g. The high nickel content and calcination decreases the specific surface area of the catalysts. The ceria and $Ni(OH)_2$ phase are detected by XRD in dried $CeZr_{0.5}Ni_XO_Y$ catalysts while ceria and NiO crystalline phase are detected in calcined catalysts. The XRD patterns of the catalysts do not show the presence of zirconia phase, while the peaks of CeO_2 are slightly broaden to pure ceria. The peaks broadening and shifts demonstrate that Ni^{2+} and/or Zr^{4+} cations enter inside the CeO_2 lattice and the cerium-nickel-(zirconium) solid solution is formed. Raman results

presents a broader ceria peak indicates the formation of ceria-zirconia solid solution. And XPS results evidence the existence of strong interactions between nickel and cerium (and zirconium) species in dried and calcined catalysts. The characterizations performed on spent $CeZr_{0.5}Ni_2O_Y$ catalyst after DRM reaction of 80 h shows the presence of oxygen vacancies and Ce-Ni-Zr-O solid solution. The Ni species mainly exists in the form of Ni^{2+} interacting with other cations and 10.5 % of metallic Ni (Ni°) appears.

For calcined $CeAl_{0.5}Ni_XO_Y$ compounds, the surface areas are between 125-154 $m^2 g^{-1}$. The reduction of Ni^{2+} species in various environments is seen in $CeAl_{0.5}Ni_XO_Y$ compounds. Concretely, the Ce-Ni-(Al)-O based blended oxides exhibit two peak low temperature at 250 °C and higher temperatures at 500 °C This phenomenon is considered to be reduction of Ni^{2+} species in solid solution and/or small NiO nano-crystals at low temperature, and bigger NiO nano-crystals at higher temperature. Looking from another aspect, adding Al obviously affects the catalyst reducibility. Furthermore, Ni^{2+} species exhibit the capacity of being reduced and re-oxidized easily and reversibly allowed through high interaction with other cations, especially Ce species. According to the Raman and XPS result of spent $CeAl_{0.5}Ni_2O_Y$ catalyst, there are more oxygen vacancies generated by incorporating the dopant in ceria, which means the presence of a solid solution after DRM reaction. The Ni^{2+} cations are present before and also after test, but the species change from NiO and Ni^{2+} interacting with other cations to 5.8 % of metallic Ni (Ni°) and 94.2 % of Ni^{2+} cations after DRM test.

The $AlMg_2Ni_XO_Y$ catalysts have surface areas ranging between 100 and 200 m^2/g. According to the XRD result, the catalyst could be assigned to a blend of NPs of NiO, MgO and/or to the Ni-Mg-(Al)-O solid solution. Very small and uniform nano-crystals between three-six nm are acquired dependent on the Ni concentration. The XPS and TPR outcomes exhibit close interaction presence between nickel cations and magnesium and/or aluminum cations resulting from the shaping of Ni-Mg-O and/or Ni-Mg-Al-O solid solution. For low Ni concentration the close interactions between Ni cations and other cations either in Ni-Mg-(Al)-O solid solution and/or at the interfaces between small NPs of NiO, MgO and/or Ni-Mg-(Al)-O render the solid hard to decrease. After that, the rise in nickel concentration renders the solid nearer that of bulk NiO, easier to be reduced. Nevertheless, close interactions still exist between Ni^{2+} cations and some other cations, since the needed temperature for reducing Ni species still much exceeds the one necessary to reduce bulk NiO. After DRM stability test, Ni^{2+}

cations in solid solution are shown in spent catalyst with appearance of 22.3 % of metallic Ni (Ni°).

Chapter 4
General discussion

Chapter 4 General discussion

4.1 Comparison and discussion

In the present study, several series of Ni-based catalysts are studied, $CeNi_XO_Y$, $CeZr_{0.5}Ni_XO_Y$, $CeAl_{0.5}Ni_XO_Y$, and $AlMg_2Ni_XO_Y$, prepared by co-precipitation method.

The surface areas for dried and calcined $CeNi_XO_Y$ (x= 0.1, 0.2, 0.3, 0.5, 1, 2) compounds are ranging between 110 - 215 m^2/g and 77 - 123 m^2/g. Whereas dried and calcined ternary $CeZr_{0.5}Ni_XO_Y$ (x= 0.5, 1, 2, 5) compounds have larger surface areas ranging 112 - 186 m^2/g and from 71 to 130 m^2/g. The calcined ternary $CeAl_{0.5}Ni_XO_Y$ (x= 0.5, 1, 2, 5) compounds surface areas are ranging in 106 - 154 m^2/g. The surface areas of $AlMg_2Ni_XO_Y$ compounds are ranging between 127 and 196 m^2/g.

In dried $CeNi_XO_Y$ catalysts, the X-Ray diffraction patterns of CeO_2 are always visible and there might be presence of $Ni(OH)_2$. The CeO_2 average crystallites size decreases from 5.1 to 4.6 nm with increasing Ni loading. It suggests the formation of a cerium-nickel solid solution. In calcined $CeNi_XO_Y$ catalysts, the ceria like phase is clearly apparent in each sample, while the NiO crystalline phase can be detected in high Ni content compounds. The average crystallites size is found at about 6.5 - 5.3 nm for CeO_2 and 13.9 - 11.3 nm for NiO. There are also Ni^{2+} cations in calcined $CeNi_XO_Y$ catalysts, in solid solution with ceria where Ni^{2+} cations substitute Ce^{4+} cations in the CeO_2 lattice.

The dried $CeZr_{0.5}Ni_XO_Y$ catalysts show the typical patterns of CeO_2 and reflections of $Ni(OH)_2$. While the CeO_2 and NiO structures are found by XRD in calcined $CeZr_{0.5}Ni_XO_Y$ catalysts. For both dried and calcined $CeZr_{0.5}Ni_XO_Y$ catalysts, no crystallographic structure involving zirconium has even been detected in these catalysts. However, the smaller size of Zr^{4+} cations replacing Ce^{4+} cations in ceria allows the formation of a (Ni)-Ce-Zr-O solid solution during synthesis.

For the calcined $CeAl_{0.5}Ni_XO_Y$ catalysts, the CeO_2 and NiO phase are observed, while no structure related to aluminum could be observed. The average crystallites size of CeO_2 is of 3.8 - 4.4 nm and the average crystallites size of NiO is of 7.2 - 5.5 nm. The aluminum doping ameliorates dispersion and the formation of (Ni)-Ce-Al-O solid solution.

The XRD analysis do not allow to conclude on the presence of NiO, MgO and/or Ni-Mg-(Al)-O solid solution, as the XRD diffractions patterns of these phases overlap each over. Very small and uniform nano-crystals between 3.6 - 5.9 nm are acquired dependent on the nickel concentration.

Reducing nickel species in different compounds can be observed by TPR. Dried $CeNi_XO_Y$ features Ni species exhibiting a reduction peak at about 250 °C, having the capacity of being reduced and reoxidized easily and reversibly allowed through strong interaction with Ce species, complementing nickel species associated with the nickel hydroxide exhibiting a reduction peak at a higher temperature 300 - 400 °C. Calcined $CeNi_XO_Y$ catalysts show a reduction peak at about 270 °, considered to be Ni species reduction in cerium-nickel solid solution or small NiO nanoparticles where Ni^{2+} strongly interacts with other cations. The second reduction peak appearing at 370 °C corresponds to the NiO reduction which can be detected by XRD.

The $CeZr_{0.5}Ni_XO_Y$ and $CeAl_{0.5}Ni_XO_Y$ compounds show two major reduction peaks. The first peak at low temperature (around 250 °C -300 °C) is assigned to nickel species reduction in small NiO NPs and/or solid solution easily reducible and easily re-oxidized. The second peak at higher temperature corresponds to NiO ($Ni(OH)_2$ reduction for dried $CeZr_{0.5}Ni_XO_Y$) nanoparticles which can be detected by XRD. Adding Al or Zr affects catalyst reducibility.

$AlMg_2Ni_XO_Y$ blended oxides exhibit a single wide TPR peak between 580 °C and 780 °C assigned to Ni species reduction. For low Ni concentration the close interactions between Ni species and other cations either in Ni-Mg-(Al)-O solid solution and/or at the interfaces between small NPs of NiO, MgO and/or Ni-Mg-(Al)-O render the solid hard to reduce. Then, the rise in nickel concentration renders solid reducibility nearer that of bulk NiO, easier to be reduced. Nevertheless, close interactions still exist between nickel cations and some other cations.

For dried and calcined $CeNi_XO_Y$, $CeZr_{0.5}Ni_XO_Y$ catalysts, Raman outcomes evidence close interactions presence between Ni and cerium species cations in catalysts. XPS analysis proves that Ni^{2+} species presenting close interaction with other cations are present on solids surface, which aligns with the main shaping of Ce-Ni-(Zr)-O solid solution.

For calcined $CeAl_{0.5}Ni_XO_Y$ catalysts, Raman and XPS outcomes evidence close interactions presence between Ni and Ce (and Al) species aligning with a solid solution

existence. Hence, the compounds are depicted as a blend of NiO and CeO_2 NPs, coexisting with a Ce-Ni-(Al) solid solution. The XPS and Raman analysis of $AlMg_2Ni_XO_Y$ compounds present close interactions presence between nickel species and magnesium and/or aluminum species aligning with the shaping of nickel-magnesium-oxygen and/or nickel-magnesium-aluminum-oxygen solid solution.

According to the characterizations results, there are two kinds of Ni species existing in catalysts, Ni^{2+} ions in solid solution or small NiO not visible through XRD, and in crystallized NiO. The average crystallites size of catalysts is close to 10 nm. Small particles size is a major consideration for methane reform reaction, for the activity, and for selectivity.

All the catalysts are studied in dry reforming of methane (DRM). The influence of reaction temperature, mass of catalyst, calcination, Ni content, in situ H_2 pretreatment, and reactants concentration are examined.

The catalytic performance is analyzed at 600 °C and 800 °C to see the effect of reaction temperature with 50 mg of calcined $CeNi_XO_Y$ catalysts, under a reaction mixture with CO_2/ CH_4= 0.7, pretreated in H_2 and without in situ H_2 pretreatment (Fig. 4-1 and 4-2). In general, the methane and CO_2 conversions at 800 °C are higher than that at 600 °C. Moreover, the H_2/CO ratio and carbon formation rate at 800 °C are less than that at 600 °C, in agreement with the known highest carbon formation at lower temperature. The maximum carbon formation rate of $CeNi_XO_Y$ catalysts is of 0.016 $g \cdot gcat^{-1} \cdot h^{-1}$ at 800 °C, while the catalysts show a higher carbon deposition rate at 600 °C with maximum value of 1.1 $g \cdot gcat^{-1} \cdot h^{-1}$. This is duo to the dry reforming of methane reaction is an endothermic reaction, high temperature at 800 °C facilitates the progress of the reaction and increases the reactants conversions. The Boudouard reaction (Eq. (1-8)) which causes carbon deposition is an exothermic reaction, inhibited at high temperatures.

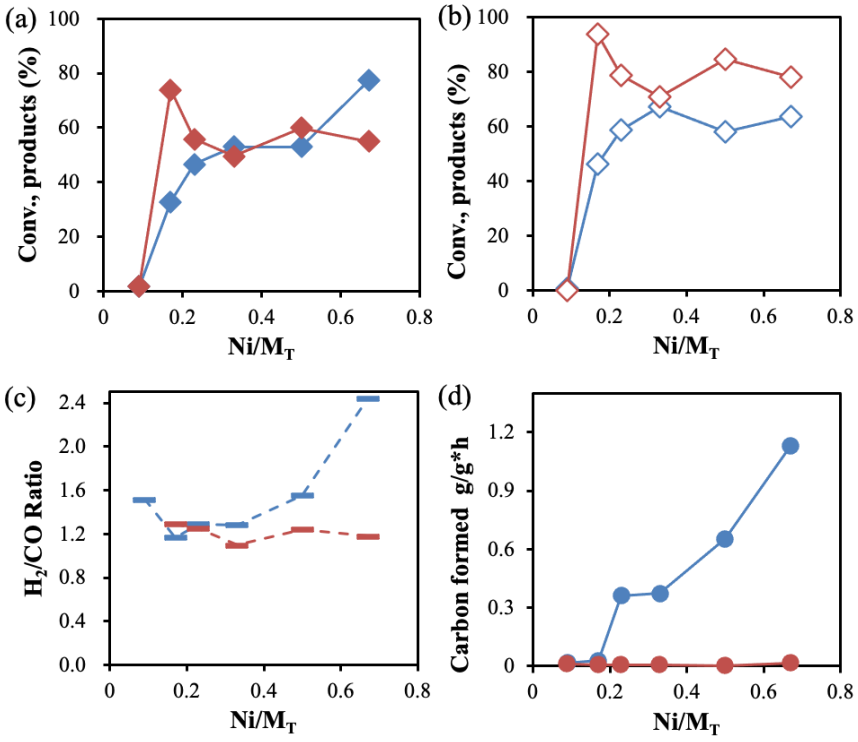

Fig. 4-1 (a) CH_4 conversion, (b) CO_2 conversion, (c) H_2/CO ratio, (d) carbon formation rate in DRM reaction on calcined $CeNi_XO_Y$ (50 mg), with in situ H_2 pretreatment, CO_2/ CH_4 ratio = 0.7, at 600 °C (◆), at 800 °C (◆).

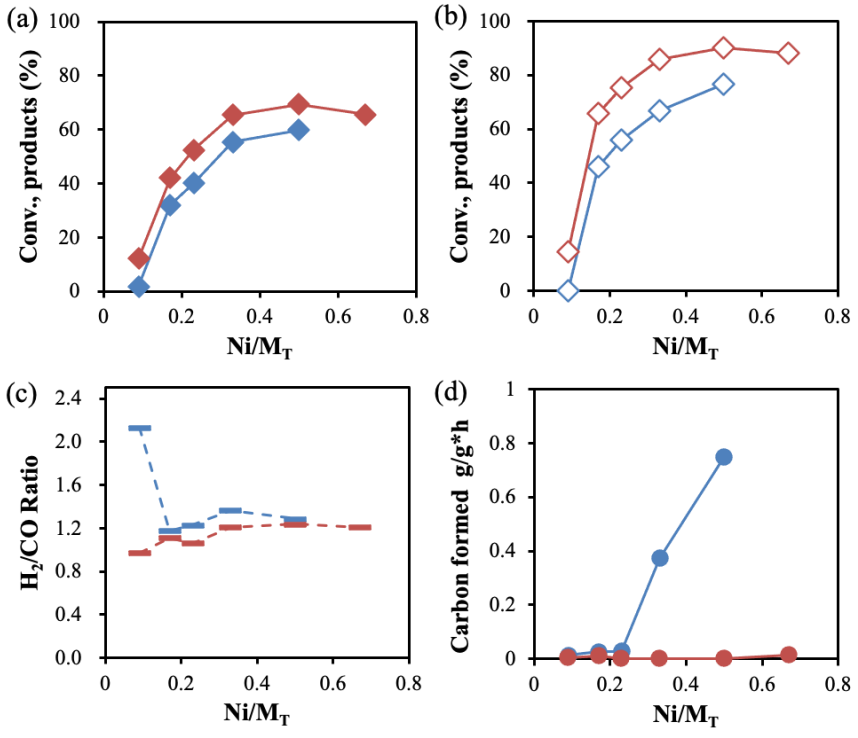

Fig. 4-2 (a) CH_4 conversion, (b) CO_2 conversion, (c) H_2/CO ratio, (d) carbon formation rate in DRM reaction on calcined $CeNi_XO_Y$ (50 mg), without H_2 pretreatment, CO_2/ CH_4 ratio = 0.7, at 600 °C (◆), at 800 °C (◆).

The influence of calcination is studied at 600 °C, on 50 mg of $CeNi_XO_Y$ catalysts, under a reaction mixture with CH_4/ CO_2 = 0.7, pretreated in H_2 and without in situ H_2 pretreatment (Fig. 4-3 and 4-4). Calcination of the catalysts increases the CO_4 and CO_2 conversions for the $CeNi_{0.3}O_Y$ with in situ H_2 pretreatment. However, for other catalysts tested, there is almost no difference for the conversions and H_2/CO ratio between the dried and calcined compounds. At the same time, there is less carbon deposition on dried catalysts compared to calcined catalysts. It is interesting as a step of calcination of the catalyst can be avoided, saving energy.

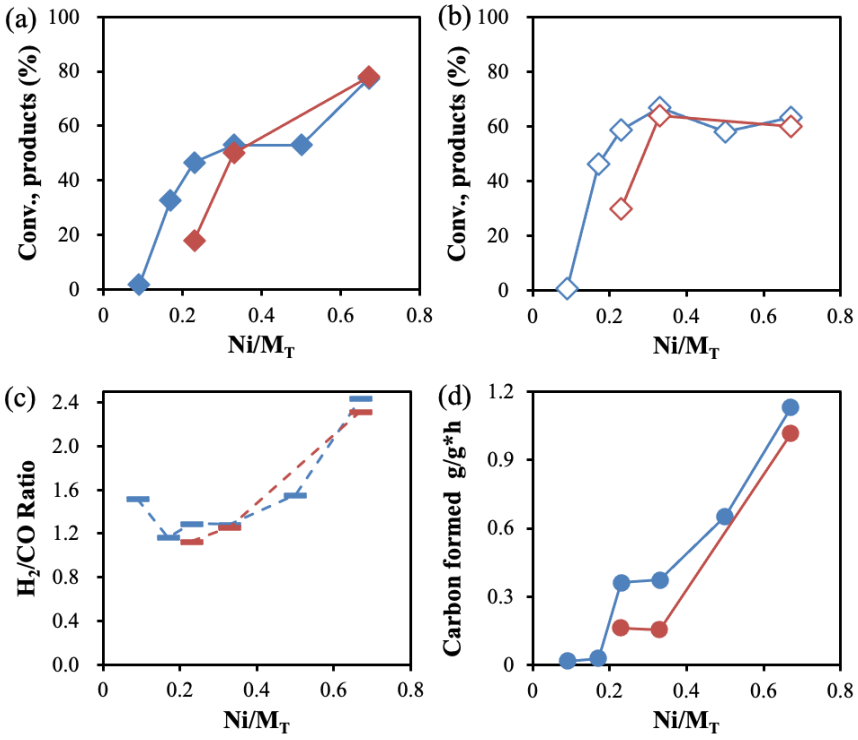

Fig. 4-3 (a) CH_4 conversion, (b) CO_2 conversion, (c) H_2/CO ratio, (d) carbon formation rate in DRM reaction at 600 °C on $CeNi_XO_Y$ (50 mg), with in situ H_2 pretreatment, CO_2/ CH_4 ratio = 0.7, calcined (◆), dried (◆).

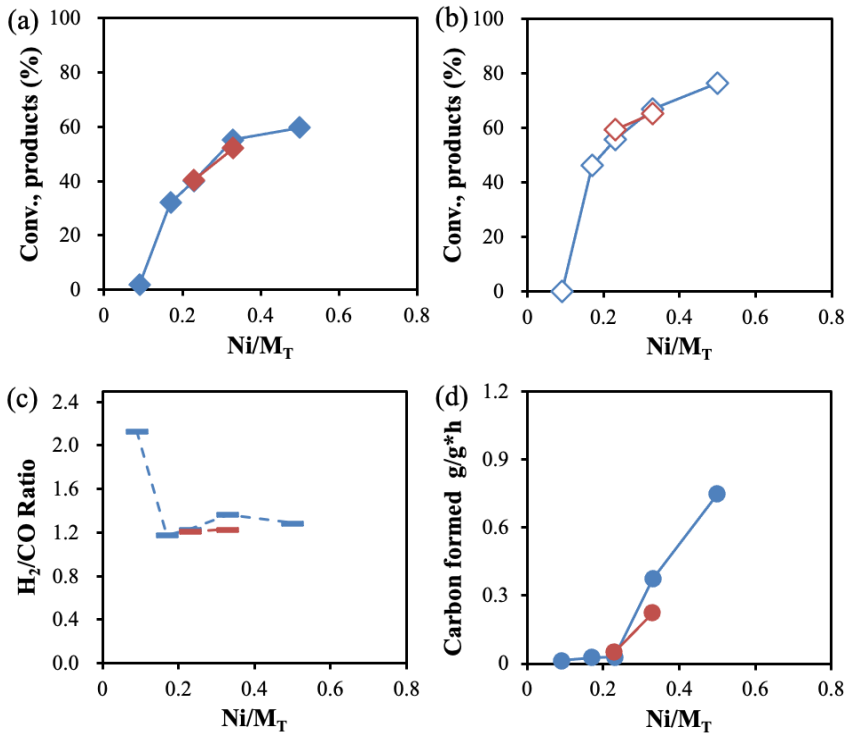

Fig. 4-4 (a) CH_4 conversion, (b) CO_2 conversion, (c) H_2/CO ratio, (d) carbon formation rate in DRM reaction at 600 °C on $CeNi_XO_Y$ (50 mg), without H_2 pretreatment, CO_2/ CH_4 ratio = 0.7, calcined (◆), dried (◆).

The catalytic performance is conducted under a reaction mixture with CO_2/ CH_4 = 0.7 on 10 mg and 50 mg of catalysts to investigate the effect of mass of catalysts at 800 °C, on calcined $CeNi_XO_Y$ catalysts, pretreated in H_2 and without in situ H_2 pretreatment (Fig. 4-5 and 4-6). As the mass of the catalyst increases from 10 mg to 50 mg, the reactants conversions increase significantly. Moreover, 50 mg of catalysts leads to lower H_2/CO ratio and less carbon deposition. Obviously, the increase in the quantity of the catalyst means that more active sites are added in the reaction and the conversions are improved.

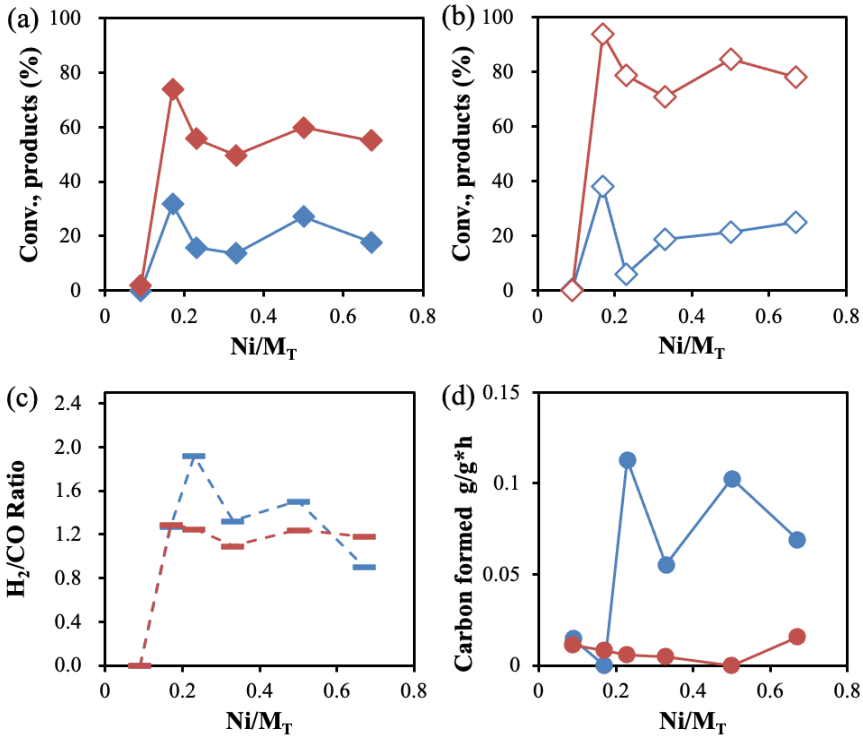

Fig. 4-5 (a) CH_4 conversion, (b) CO_2 conversion, (c) H_2/CO ratio, (d) carbon formation rate in DRM reaction at 800 °C on calcined $CeNi_XO_Y$, with H_2 pretreatment, CO_2/ CH_4 ratio = 0.7, 10 mg (◆), 50 mg (◆).

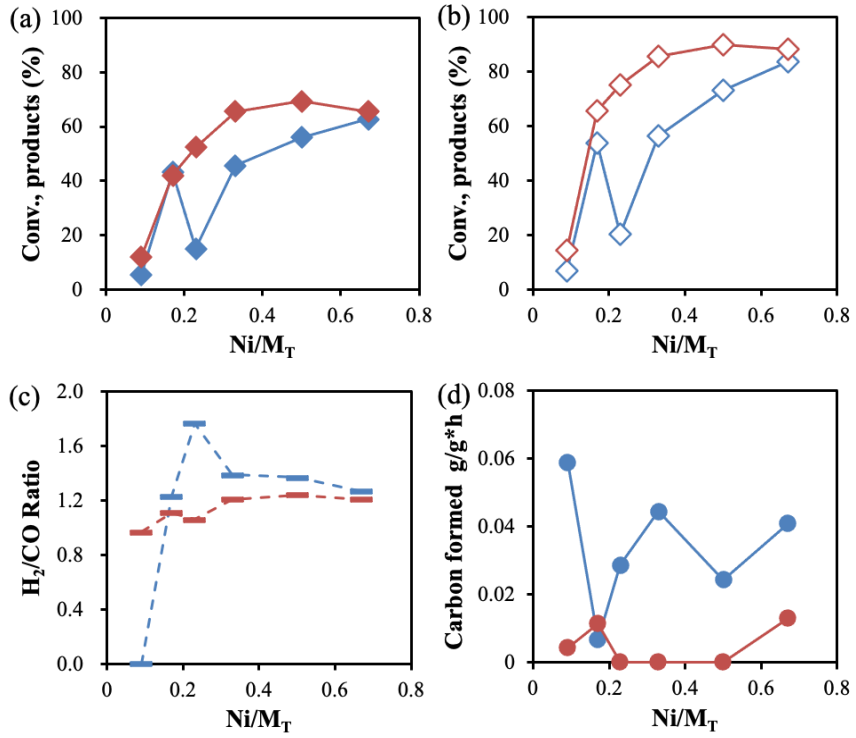

Fig. 4-6 (a) CH_4 conversion, (b) CO_2 conversion, (c) H_2/CO ratio, (d) carbon formation rate in DRM reaction at 800 °C on calcined $CeNi_XO_Y$, without H_2 pretreatment, CO_2/ CH_4 ratio = 0.7, 10 mg (◆), 50 mg (◆).

The influence of in situ H_2 pretreatment is studied on four series of catalysts (Fig. 4-7, 4-8, 4-9, 4-10). Interestingly, the in situ H_2 pretreatment has not always the same effect on the catalytic performance of different catalysts under different conditions. For $CeNi_XO_Y$ catalysts, in situ H_2 pretreatment has no influence on DRM catalytic performance at 600 °C, with 50 mg of catalyst, under $CO_2/CH_4 = 0.7$. At 800 °C, on 10 or 50 mg of catalyst, under $CO_2/CH_4 = 0.7$, in situ H_2 pretreatment decreases the CH_4 and CO_2 conversions and increases carbon formation rate of high Ni content $CeNi_XO_Y$ ($x > 0.3$) catalysts. On dried $CeZr_{0.5}Ni_XO_Y$ catalysts, in situ H_2 pretreatment makes no different CH_4 and CO_2 conversions but leads to a lower carbon formation rate at 800 °C, on 10 mg of catalyst, under $CO_2/CH_4 = 1$. Calcined $CeZr_{0.5}Ni_{0.5}O_Y$ and $CeZr_{0.5}Ni_1O_Y$ catalysts present higher CH_4 and CO_2 conversions and lower carbon formation rate with in situ H_2 pretreatment than without pretreatment at 800 °C, on 10 mg of catalyst, and under $CO_2/CH_4 = 0.7$. For $CeAl_{0.5}Ni_XO_Y$ catalysts, at 600 °C, with 50 mg of catalyst, under $CO_2/CH_4 = 0.7$, there is no difference with in situ H_2 pretreatment and without H_2 pretreatment. At 800 °C, with 10 mg of catalyst, under $CO_2/CH_4 = 0.7$, in situ H_2 pretreatment increases the CH_4 and CO_2 conversions on $CeAl_{0.5}Ni_{0.5}O_Y$, and $CeAl_{0.5}Ni_1O_Y$, catalysts, and increases the carbon deposition on all $CeAl_{0.5}Ni_XO_Y$, catalysts. For $AlMg_2Ni_XO_Y$ catalysts, in situ H_2 pretreatment has almost no influence on CH_4 and CO_2 conversions, H_2/CO ratio, and carbon formation rate, whether at 800 °C, on 10 mg of catalyst, under $CO_2/CH_4 = 0.7$, or at 600 °C, on 50 mg of catalyst, under $CO_2/CH_4 = 1$.

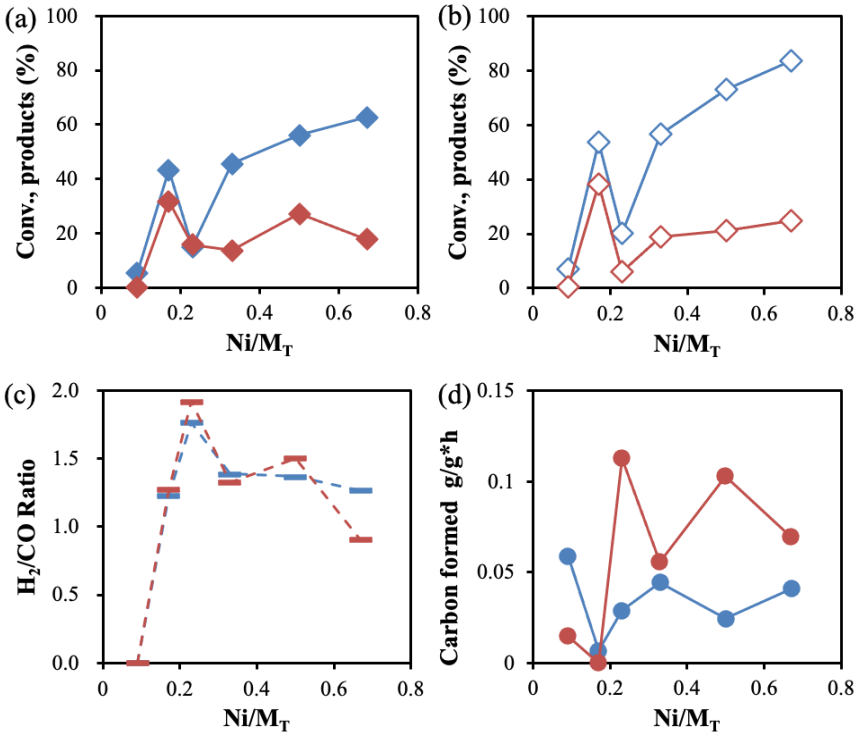

Fig. 4-7 (a) CH_4 conversion, (b) CO_2 conversion, (c) H_2/CO ratio, (d) carbon formation rate in DRM reaction at 800 °C on calcined $CeNi_XO_Y$ (10 mg), CO_2/ CH_4 ratio = 0.7, without H_2 pretreatment (◆), with in situ H_2 pretreatment (◆).

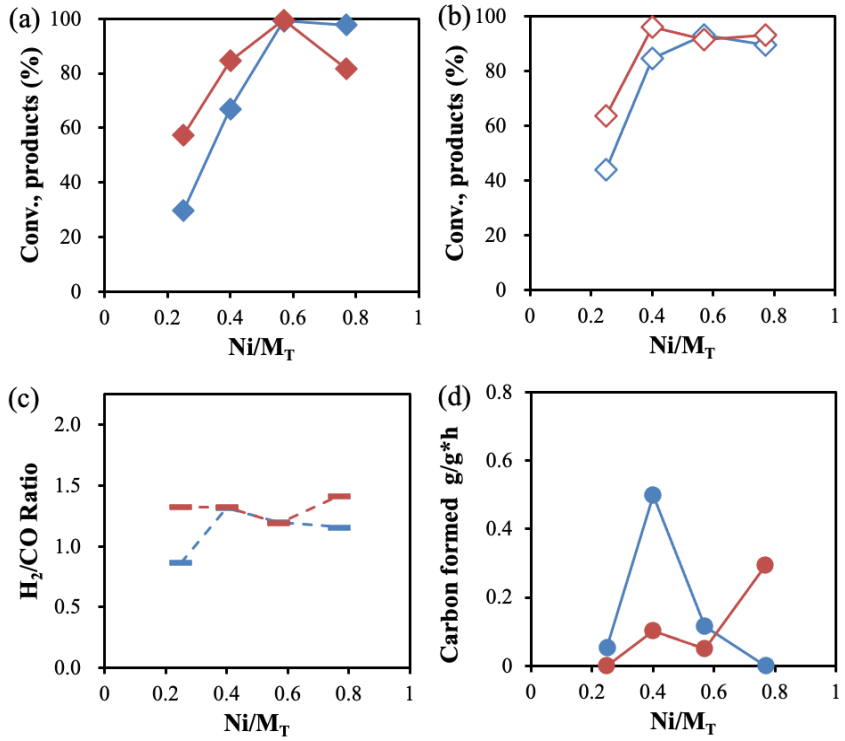

Fig. 4-8 (a) CH_4 conversion, (b) CO_2 conversion, (c) H_2/CO ratio, (d) carbon formation rate in DRM reaction at 800 °C on calcined $CeZr_{0.5}Ni_XO_Y$ (10 mg), CO_2/ CH_4 ratio = 0.7, without H_2 pretreatment (◆), with in situ H_2 pretreatment (◆).

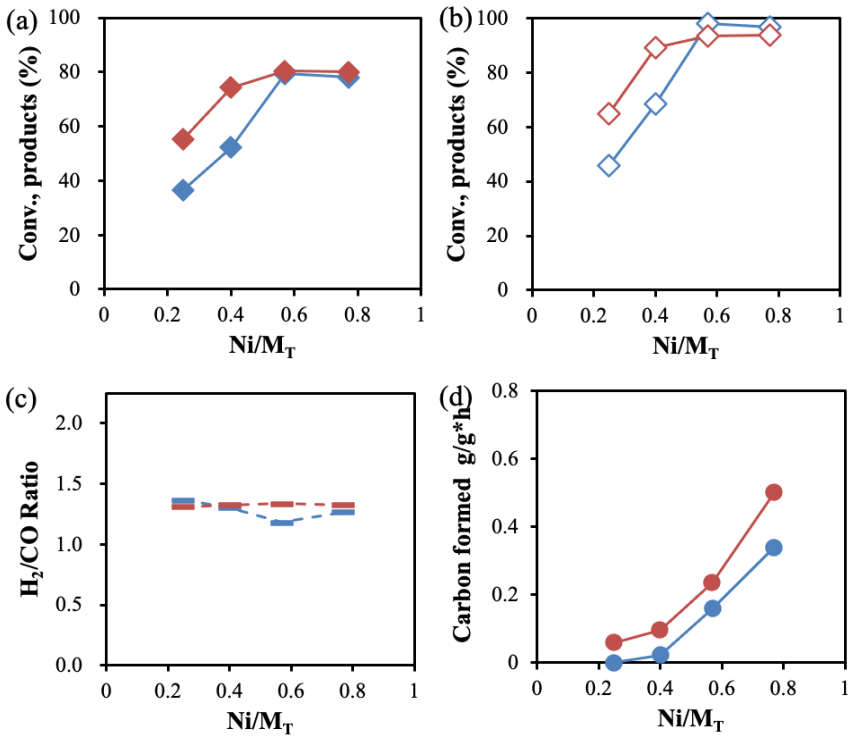

Fig. 4-9 (a) CH_4 conversion, (b) CO_2 conversion, (c) H_2/CO ratio, (d) carbon formation rate in DRM reaction at 800 °C on calcined $CeAl_{0.5}Ni_XO_Y$ (10 mg), CO_2/ CH_4 ratio = 0.7, without H_2 pretreatment (◆), with in situ H_2 pretreatment (◆).

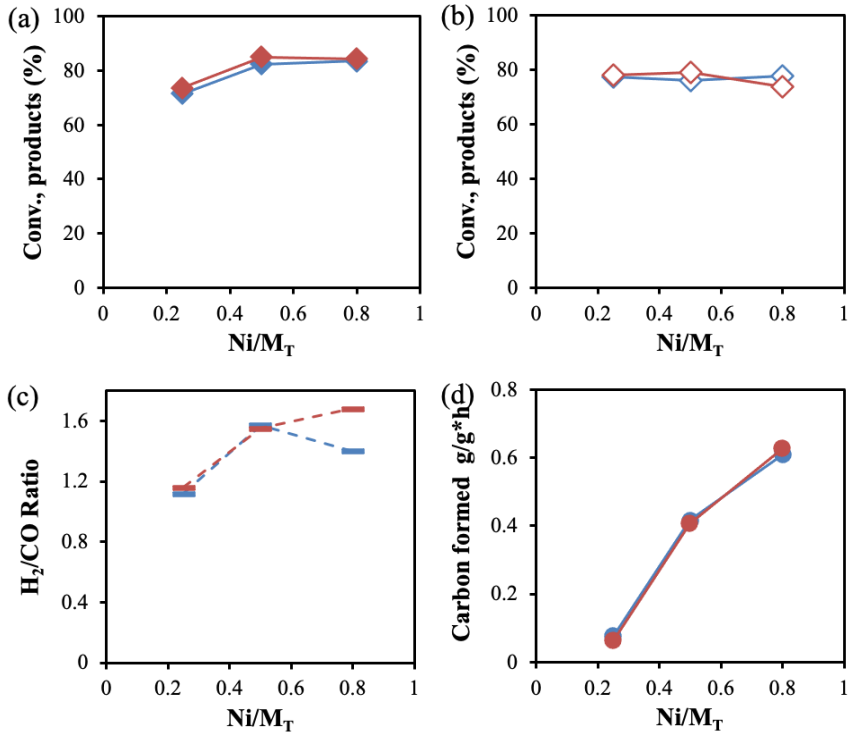

Fig. 4-10 (a) CH_4 conversion, (b) CO_2 conversion, (c) H_2/CO ratio, (d) carbon formation rate of DRM reaction at 600 °C on calcined $AlMg_2Ni_XO_Y$ (50 mg), CO_2/ CH_4 ratio = 1, without H_2 pretreatment (◆), with in situ H_2 pretreatment (◆).

The influence of reactants concentration is also studied on $CeNi_XO_Y$, $CeZr_{0.5}Ni_XO_Y$, $CeAl_{0.5}Ni_XO_Y$ catalysts with the CO_2/CH_4 ratio = 1 and 0.7. The CH_4 conversion obtained with CO_2/CH_4 ratio = 0.7 is lower than that with CO_2/CH_4 ratio = 1. The H_2/CO ratio and carbon formation rate are higher when CO_2/ CH_4 ratio = 0.7.

According to the catalytic results, some catalysts presenting very high performance under specific conditions have been found. Among the $CeNi_XO_Y$ catalysts, the calcined $CeNi_{0.5}O_Y$ presents CH_4 and CO_2 conversions of 53.4% and 59.1%, a carbon formation rate of 0.0037 $g\cdot gcat^{-1}\cdot h^{-1}$ after stability test of 80 h at 600 °C on 50 mg of catalyst with in situ H_2 pretreatment at 250 °C and under a reaction mixture with CH_4/CO_2 = 1). And calcined $CeNi_1O_Y$ leads to the highest conversions (CH_4 and CO_2 conversions of 69.4 % and 90.0 %, respectively) and without carbon formation, H_2/CO ratio of 1.2, at 800 °C (on 50 mg of catalyst without in situ H_2 pretreatment and under a reaction mixture with CH_4/CO_2 = 0.7).

For $CeZr_{0.5}Ni_XO_Y$ compounds, at 800 °C, on 10 mg of catalyst pretreated, and under CH_4/CO_2 = 1, the best result is obtained on $CeZr_{0.5}Ni_2O_Y$, with CH_4 and CO_2 conversions of 98.8% and 94.1 %, respectively, H_2/CO ratio of 1.2, and carbon formation rate of 0.004 $g\cdot gcat^{-1}\cdot h^{-1}$ after 80 hours. Dried $CeZr_{0.5}Ni_2O_Y$ catalyst also presents methane and CO_2 conversions of 95.8 % and 91.7 % after 80 h. The H_2/CO molar ratio is about 1.2, and the carbon deposition is of 0.0151 $g\cdot gcat^{-1}\cdot h^{-1}$. At 600 °C, $CeZr_{0.5}Ni_{0.5}O_Y$ shows CH_4 and CO_2 conversions of 66.2 % and 72.7 % and carbon formation rate of 0.004 $g\cdot gcat^{-1}\cdot h^{-1}$ after 80 h of stability test.

In $CeAl_{0.5}Ni_XO_Y$ compounds, $CeAl_{0.5}Ni_2O_Y$ is the most competitive one with CH_4 and CO_2 conversions of 79.3 % and 97.9 %, H_2/CO ratio of 1.18, and carbon deposition rate of 0.16 $g\cdot gcat^{-1}\cdot h^{-1}$ at 800 °C (on 10 mg of catalyst without H_2 pretreatment, and under CO_2/CH_4 = 0.7). The stability test is conducted over $CeAl_{0.5}Ni_1O_Y$, at 600 °C, with 50 mg of catalyst pretreated, and under CH_4/CO_2 = 1, conversions of CH_4 and CO_2 reach 66.5 % and 72.6 %, respectively. The H_2/CO molar ratio obtained is at about 1.07, and the carbon formation rate is of 0.009 $g\cdot gcat^{-1}\cdot h^{-1}$. At 800 °C, with 10 mg catalyst pretreated, and under CH_4/CO_2 = 1, $CeAl_{0.5}Ni_2O_Y$ also presents a good result, with CH_4 and CO_2 conversions around 82 %, and a H_2/CO ratio of 1.1, and carbon formation rate of 0.008 $g\cdot gcat^{-1}\cdot h^{-1}$ after 80 hours.

In $AlMg_2Ni_XO_Y$ series, at 600 °C, with in situ H_2 pretreatment, CH_4/CO_2 = 1, $AlMg_2Ni_1O_Y$ is tested on stream for 80 hours. 75.9 % and 83.2 % of CH_4 and CO_2

conversions are obtained, H_2/CO ratio of 1.2, and carbon deposition rate of 0.017 $g \cdot gcat^{-1} \cdot h^{-1}$. At 800 °C, with 10 mg of catalyst pretreated, under CH_4/CO_2 = 1, $AlMg_2Ni_{12}O_Y$ shows the conversions of methane and CO_2 of 99.7 % and 93.8 % after 80 hours, with a H_2/CO ratio of 1.2, and a carbon formation rate of 0.006 $g \cdot gcat^{-1} \cdot h^{-1}$. At 800 °C, on 10 mg of pretreated catalysts, CO_2/CH_4 = 0.7, 76.8 % and 84.1 % of CH_4 and CO_2 conversions are obtained after 80 h, on $AlMg_2Ni_{12}O_Y$ catalyst, with H_2/CO ratio of 1.1 and carbon formation rate of 0.008 $g \cdot gcat^{-1} \cdot h^{-1}$.

4.2 Proposal of active site and possible mechanism

In order to determine the active phase/active species converting CH_4 and CO_2, a comparison is illustrated in Fig. 4-11, which reports conversion, selectivity and carbon formation rate in DRM measured at 600 °C as a function of the Ni proportion in the different studied compounds.

Fig. 4-11 a and b reports the conversions of CH_4 and CO_2 versus Ni/M_T molar ratio, at 600 °C with the conditions CO_2/ CH_4 = 1, on different catalysts without H_2 pretreatment. Methane conversions increase with Ni content ascension on the four series of catalysts, CO_2 conversions increase on Zr and Al doped compounds. Moreover, Fig. 4-11 c and d display the H_2/CO ratio and carbon formation rate versus Ni molar ratio. The different catalysts studied exhibit same tendency on H_2/CO ratio and carbon formation rate. When Ni/M_T ratio is higher than 0.4, the H_2/CO ratio and carbon formation rate increase sharply with the increase of nickel content. This shows the important role that nickel plays in the dry reforming reaction.

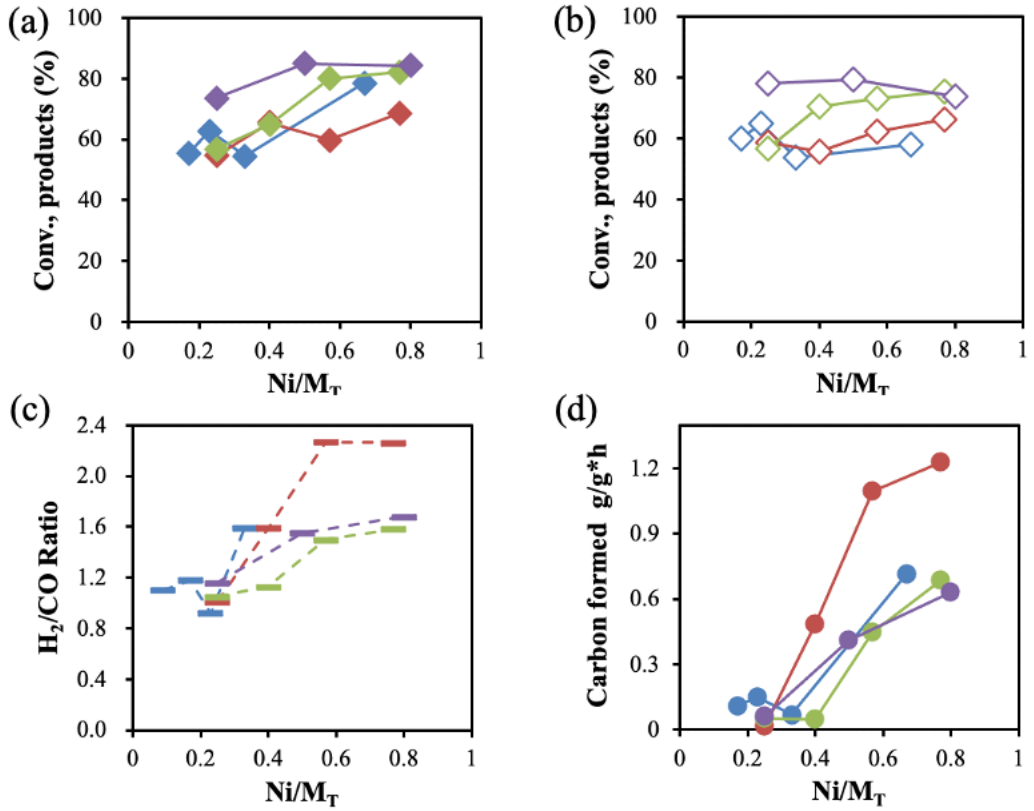

Fig. 4-11 (a) CH_4 conversion, (b) CO_2 conversion, (c) H_2/CO ratio, (d) carbon formation rate of DRM reaction at 600 °C with CO_2/CH_4 ratio = 1, on $CeNi_XO_Y$ (◆), $CeZr_{0.5}Ni_XO_Y$ (◆), $CeAl_{0.5}Ni_XO_Y$ (◆), and $AlMg_2Ni_XO_Y$ (◆) catalysts without pretreatment.

The DRM catalytic performances at 800 °C with CO_2/CH_4 ratio = 0.7, on different catalysts with H_2 pretreatment, are compared and shown in Fig. 4-12. Increasing with Ni molar ratio, the conversions on ternary catalysts are much higher than that on binary catalysts. But it has to be noticed, more nickel is needed in the ternary compounds in order to obtain the same Ni/M_T molar ratio to the binary compounds. The ternary catalysts exhibit very similar H_2/CO ratio around 1.2, due to the CO_2/CH_4 feed ratio of reactants is 0.7. As shown in Fig. 4-12 d, globally, the Ni content has no effect on carbon deposition on $CeNi_XO_Y$ and $AlMg_2Ni_XO_Y$ catalysts. But carbon formation rate increases with Ni content on Zr and Al doped catalysts.

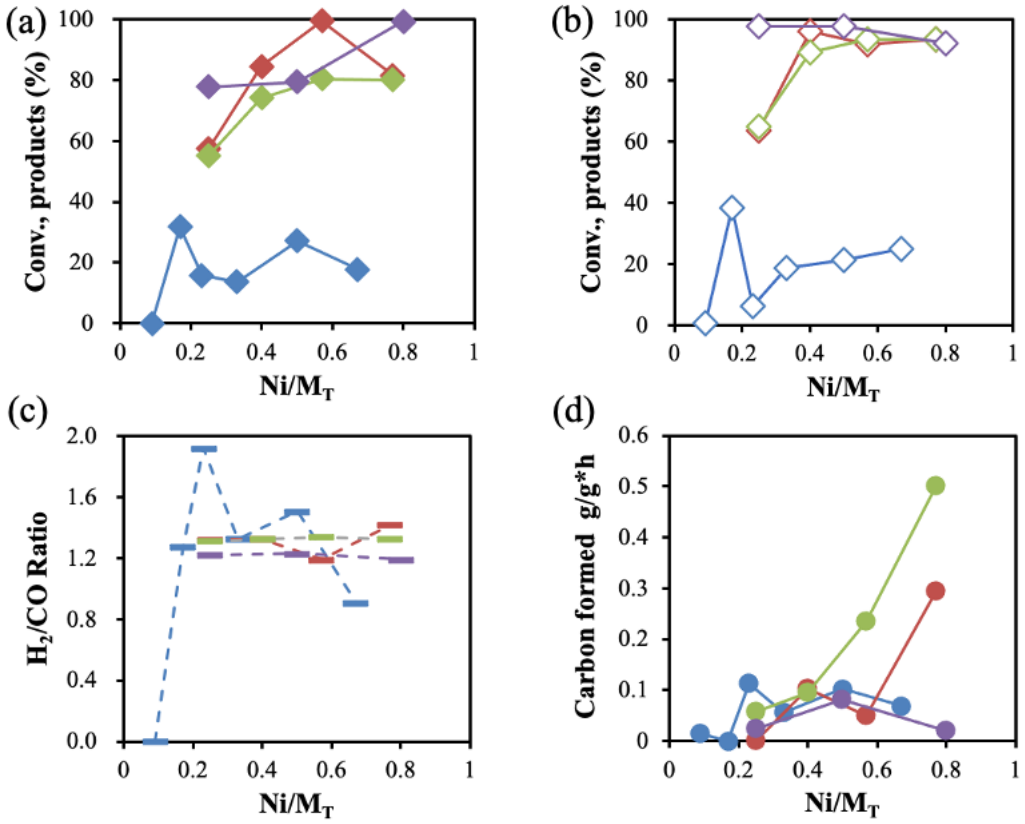

Fig. 4-12 (a) CH_4 conversion, (b) CO_2 conversion, (c) H_2/CO ratio, (d) carbon formation rate of DRM reaction at 800 °C with CO_2/CH_4 ratio = 0.7, with pretreatment, on $CeNi_XO_Y$ (◆), $CeZr_{0.5}Ni_XO_Y$ (◆), $CeAl_{0.5}Ni_XO_Y$ (◆), and $AlMg_2Ni_XO_Y$ (◆) catalysts.

In order to understand the correlations between the activity and the Ni species in the different catalysts, Fig. 4-13 reports DRM activity in mol of methane and CO_2 converted per gram of Ni per hour, measured at 600 °C as a function of the Ni/M_T ratio. Reporting activity in this way, it is possible to extract the activity of a mole of Ni species, so the activity of a Ni species in the different environments (in four series of compounds) can be seen.

All catalysts show an index fell in activity with increasing Ni content, which indicates that the number of active sites does not increase with Ni loading. The highest activity is reported on $CeNi_{0.2}O_Y$ (6 wt.% Ni), while the lowest value is obtained on $AlMg_2Ni_{12}O_Y$ (61 wt.% Ni). It suggests that not all the Ni species in the catalysts can behave as active sites; the number of active sites is diluted by the growing Ni content and for some compounds the growing of surface area (117 m^2/g for $CeNi_{0.2}O_Y$, and 196 m^2/g for $AlMg_2Ni_{12}O_Y$). It appears clearly that the Ni species which are active are obtained in higher proportion at low Ni content. Then when the Ni content increases, even if active Ni species are added inactive Ni species are also added in higher

proportion. In other words, if Ni content increases, the proportion of inactive Ni species added is higher compared to the proportion of active Ni species added. Therefore, as metallic Ni increases with the Ni content, there is a low probability that the active Ni species correspond to metallic Ni., For example, the $CeNi_XO_Y$ compounds with $x < 0.5$ correspond to a solid solution with the substitution of Ni^{2+} cations in CeO_2 lattice, and to a mixture of crystallized NiO coexisting with the solid solution when $0.5 \leq x < 5$. Moreover, very small nanoparticles of NiO can be always present whatever the Ni content.

Hence more active sites (with the same activity) can be generated in the compound with higher Ni loading. When the Ni content increases, the added Ni species present all the same activity, or in the added Ni species there is always the same proportion of active and inactive Ni species.

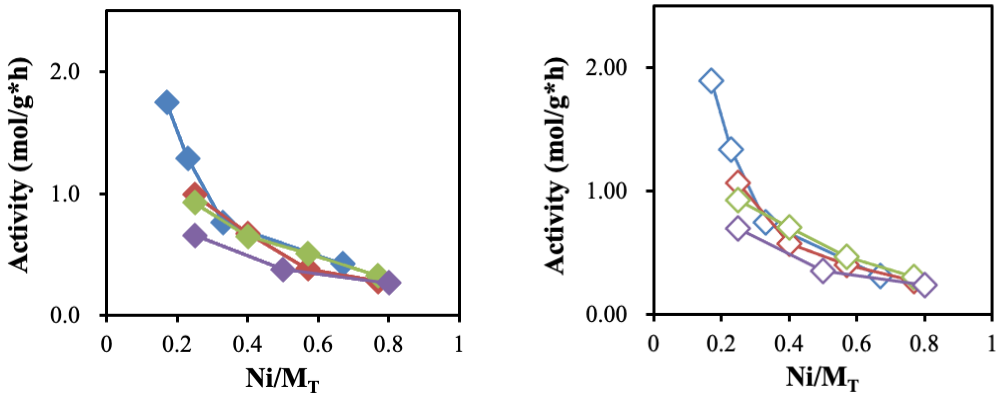

Fig. 4-13 Activity of $CeNi_XO_Y$ (CH_4 (◆), CO_2 (◇)), $CeZr_{0.5}Ni_XO_Y$ (CH_4 (◆), CO_2 (◇)), $CeAl_{0.5}Ni_XO_Y$ (CH_4 (◆), CO_2 (◇)), and $AlMg_2Ni_XO_Y$ (CH_4 (◆), CO_2 (◇)) catalysts without pretreatment in DRM at 600 °C with CO_2/CH_4 ratio = 1.

The activity (in mol of CH_4 and CO_2 converted per gram of Ni per hour) of catalysts at 800 °C with CO_2/ CH_4 ratio = 0.7 is also compared in Fig. 4-14. In this case, the activity curves with the same trend are obtained for the four series of catalysts, respectively.

It is found that the activity of all Ni-based catalysts for DRM at 800 °C with CO_2/ CH_4 ratio = 0.7 shows a decreasing tendency versus Ni content. The activity declines almost linearly when the Ni loading increases. It can be explained by the fact that activity is divided by the growing Ni molar ratio when the reactants conversions are constant. However, it is important to recall that the activity is already very high with the low Ni content, so the active sites are created with the low Ni concentration. Moreover, whatever the Ni content is, $CeZr_{0.5}Ni_XO_Y$ and $CeAl_{0.5}Ni_XO_Y$ catalysts always

demonstrate higher activity than the value obtained on $AlMg_2Ni_XO_Y$ and $CeNi_XO_Y$ catalysts. Some slight differences in the activity curves can be seen which indicate that the number of active sites and/or the activity of the sites (Ni species) in different catalysts is different. It might be due to that the Zr and Al doping allows forming solid solutions, and/or decreasing average crystallites size, which yield ample oxygen vacancies and strong interaction between cations. The highest activity is reported when Ni/M_T is close to 0.2, like on the $CeZr_{0.5}Ni_{0.5}O_Y$ catalyst (10.8 wt.% Ni). Based on the correlation between activity and Ni/M_T molar ratio, an active site certainly involving Ni species in close interaction with other cations can be predicted which presence has been shown after test by characterizations on some compounds.

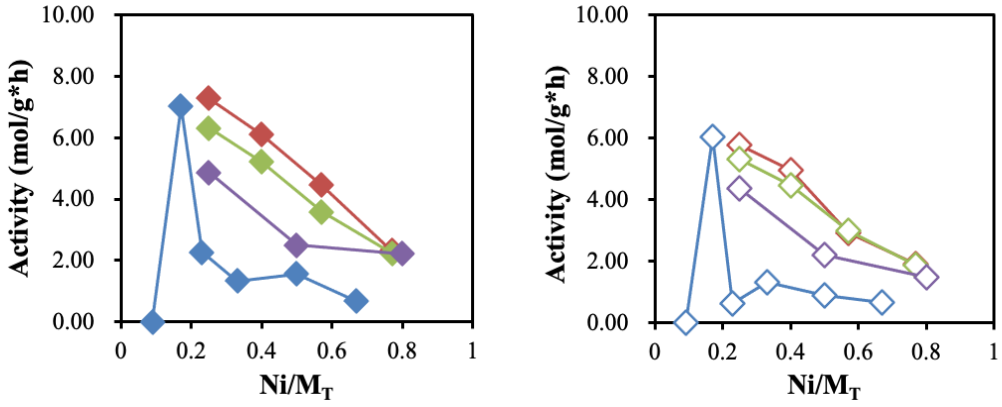

Fig. 4-14 Activity of $CeNi_XO_Y$ (CH_4 (◆), CO_2 (◇)), $CeZr_{0.5}Ni_XO_Y$ (CH_4 (◆), CO_2 (◇)), $CeAl_{0.5}Ni_XO_Y$ (CH_4 (◆), CO_2 (◇)), and $AlMg_2Ni_XO_Y$ (CH_4 (◆), CO_2 (◇)) catalysts with H_2 pretreatment for DRM at 800 °C with CO_2/CH_4 ratio = 0.7, as a function of Ni molar ratio.

After the above comparison, it is found that all the catalysts have Ni species as the active species. In low nickel content catalysts, nickel has a large proportion in small nanoparticles and/or solid solutions as cations presenting strong interaction with other cations. For example, there is a strong interaction between the nickel and cerium species in cerium and nickel-based catalysts. Ni species are surrounded by different neighboring atoms, and Ni species strongly interact with Ce, Al or Mg cations, which is confirmed by the previous XRD, Raman, XPS, and TPR characterization results. In catalysts with high nickel content, nickel exists in small nanoparticles and/or solid solutions and in crystalline nickel oxide. The catalytic performance is promoted to a certain extent, but carbon deposition is also promoted.

In the literature, Ni has been used as active metal in DRM reaction[66]. It is reported that Ni species could dissociate C-H bond in methane[112]. The support such as ZrO_2, CeO_2, CaO, is also considered as having an active role duo to its basicity, oxygen

storage capacity, and reducibility[268,269]. Moreover, promoter is thought to provide additional new active sites relating to the reactivity of the catalysts such as basicity or redox property[270].

Some researchers proposed metallic Ni^0 as an active site in the dry reforming of methane[187]. It was mentioned that metallic Ni^0 decomposed methane and helped remove carbon deposition[271]. However, it was also proposed that the nickel species with different oxidation state or with strong interaction with other cations might act as active sites in DRM reaction[272].

10Ni1Ce/PZr catalyst was tested on methane dry reforming reaction[271]. Ceria induced surface reducibility, reduced NiO and $Ni_2P_2O_7$ and provided active sites for CH_4 decomposition. The loading amount of ceria at 1 wt.% and 2 wt.% in catalysts showed catalytic activity. However, the 3 wt.% of ceria leaded a worse catalytic performance due to the masking of catalytic active sites or the re-oxidation of metallic nickel by excessive cerium oxide. The cycle experiment of H_2 TPR - CO_2 TPD - H_2 TPR clearly showed the role of CO_2 in oxygen supplementation at empty lattice sites, while the TPH experiment showed that in the presence of ceria, more types of CHx species are hydrogenated under H_2 flow.

Li et al. studied the reaction activity of Ni/Al_2O_3-ZrO_2 catalyst for methane dry reforming[273]. The introduction of ZrO_2 improved the reducibility of the catalyst. At the same time, ZrO_2 helped to reduce NiO species to metallic Ni while avoiding the formation of inactive $NiAl_2O_4$.

Rogers et al. investigated the active site on $NiAl_4O_7$, $NiAl_2O_5$, and $NiAl_2O_4$ catalysts[274]. After analyzing the catalysis and characterization results, it was found that there is no metallic nickel in $NiAl_4O_7$ and a small amount of metallic nickel in $NiAl_2O_4$. Both two catalysts presented the activity in dry reforming of methane reaction, which strongly proved that the active site was the oxide species. Moreover, these two catalysts formed a few carbon deposition. On the contrary, the metallic nickel particles mainly presented in $NiAl_2O_5$ caused a large amount of carbon formation during the dry reforming of methane.

Ni-CeZrAl catalyst was prepared and applied in dry reforming of methane reaction in Wen's group[275]. They found that the interacting Ni species and the oxygen vacancies brought the catalyst good activity. On the contrary, the Ni-CeZr catalyst with poor dispersion and weak interaction with the support exhibited poor catalytic performance. The basic sites in the catalyst reduced the carbon formation and

effectively protected the active sites of Ni. And the high concentration of disordered carbon in Ni-CeZrAl from TGA and Raman proved that the interaction between active sites and supports could help catalysts keeping activity in DRM reaction.

According to all the catalytic and characterization results in this study, the activity in DRM reaction is more likely to be related to the partially reduced solid containing Ni cations. The redox process between Ni and Ce cations also promote the formation of anionic vacancies (Eq. 4-1 and 4-2). As reported in literature, CeO_2 has redox properties, and provides active oxygen species[158,276]. These oxygen species which are labile on the surface of the catalyst help to resist coking and sintering[159]. Anionic vacancies can also be produced by H_2 pretreatment, which is the reason why pretreatment can reduce carbon deposition (Eq. 4-1).

$$Ni^{2+} + O^{2-} + H_2 \rightarrow Ni^0 + H_2O + \square \text{ (with } \square\text{: anionic vacancy)} \text{ (Eq. 4-1)}$$

$$2Ce^{4+} + Ni^0 \leftrightarrow 2Ce^{3+} + Ni^{2+} \text{ (Eq. 4-2)}$$

Consistent with the commonly believed bifunctional mechanism[91], in this study the active site can be modeled by the collection of two cations, which involves cations in strong interactions. This ^{X}M-^{Y}M site is composed of two closely interacting cations and surrounding O^{2-} species and anionic vacancies, X and Y are the number of coordination unsaturations, that is, the anionic vacancies on each cation, leading to coordination unsaturation sites. The dehydrogenation of CH_4 first needs to extract hydrogen species from CH_4 and break the C-H bond at the same time. Therefore, an active site containing anionic vacancies and O^{2-} species at the surface of the solid can dissociate CH_4, leading to the formation of C species. The C species can then react with oxygen atoms from the solid to form gaseous CO.

Chapter 5

General conclusion

Chapter 5 General conclusion

In this study, Ni-based $CeNi_XO_Y$, $CeZr_{0.5}Ni_XO_Y$, $CeAl_{0.5}Ni_XO_Y$, and $AlMg_2Ni_XO_Y$ catalysts are prepared by co-precipitation method and tested in DRM reaction.

The surface areas for $CeNi_XO_Y$ compounds are ranging between 77-215 $m^2\ g^{-1}$ (with x = 0.1, 0.2, 0.3, 0.5, 1 and 2 corresponding to Ni wt.% ranging from 5 % to 40 %). The dried compounds have a larger surface area than the calcined compounds with same Ni content. In dried $CeNi_XO_Y$ catalysts, the ceria like phase is clearly apparent in all samples, and there might be presence of $Ni(OH)_2$. The broadness and shift of CeO_2 XRD diffraction patterns suggest the formation of a cerium-nickel solid solution. The NiO crystalline phase is detected in high Ni content calcined catalysts ($x \geq 0.5$). The average crystallites size is distributed in the range of 4-5 nm for CeO_2 and 8-10 nm for NiO. Raman results evidence the existence of strong interactions between nickel and cerium cations in dried and calcined catalysts. XPS analysis proves that Ni^{2+} cations which has strong interaction with other cations are present on the surface of the solids, which is in agreement with the formation of Ce-Ni-O solid solution. TPR analysis discloses that $CeNi_XO_Y$ solids possess a proportion of Ni species which present a characteristic reduction peak at about 270 °C. Such Ni species are able to be reduced and re-oxidized easily and reversibly, which is due to the existence of strong interactions between nickel and cerium species in $CeNi_XO_Y$ solids. The Ni species related to the presence of NiO are reduced at higher temperature of about 370 °C.

Among the $CeNi_XO_Y$ catalysts, the calcined $CeNi_{0.5}O_Y$ presents CH_4 and CO_2 conversions of 53.4% and 59.1, carbon formation rate of 0.0037 $g{\cdot}gcat^{-1}{\cdot}h^{-1}$ after stability test of 80 h, at 600 °C, on 50 mg of catalyst with in situ H_2 pretreatment at 250 °C, and under DRM reaction mixture with $CH_4/CO_2 = 1$. After stability test of 80 h, the performed characterizations lead to conclude that the Ce-Ni-O solid solution is still present in spent $CeNi_1O_Y$ catalyst and that there are more oxygen vacancies, Ni^{2+} interacting with other cations, and Ce^{3+} generated. Calcined $CeNi_1O_Y$ leads to the highest conversions (CH_4 and CO_2 conversions of 69.4 % and 90.0 %, respectively) and without carbon formation, H_2/CO ratio of 1.2, at 800 °C, with 50 mg of catalyst without in situ H_2 pretreatment, and under a reaction mixture with $CH_4/CO_2 = 0.7$.

In $CeZr_{0.5}Ni_XO_Y$ series, the dried $CeZr_{0.5}Ni_{0.5}O_Y$ compound shows the largest specific surface area of 186 m^2/g. The high nickel content and calcination decreases the specific surface area of the catalysts. The ceria and $Ni(OH)_2$ phase are detected by

XRD in dried $CeZr_{0.5}Ni_XO_Y$ catalysts while ceria and NiO crystalline phase are detected in calcined catalysts. The XRD patterns of the catalysts do not show the presence of zirconia phase, while the peaks of CeO_2 are slightly broaden to pure ceria. The peaks broadening and shifts demonstrate that Ni^{2+} and/or Zr^{4+} cations enter inside the CeO_2 lattice and the cerium-nickel-(zirconium) solid solution is formed. Raman results indicates the formation of ceria-zirconia solid solution. The XPS results evidence the existence of strong interactions between nickel and cerium (and zirconium) cations in dried and calcined catalysts.

For $CeZr_{0.5}Ni_XO_Y$ compounds, at 800 °C, with 10 mg catalyst pretreated, and CH_4/CO_2 = 1, the best result is obtained on $CeZr_{0.5}Ni_2O_Y$, with CH_4 and CO_2 conversions of 98.8% and 94.1 %, a H_2/CO ratio at 1.2, and carbon formation rate of 0.004 $g \cdot gcat^{-1} \cdot h^{-1}$ after 80 hours. The characterizations performed on spent $CeZr_{0.5}Ni_2O_Y$ catalyst after DRM reaction of 80 h show the presence of oxygen vacancies and Ce-Ni-Zr-O solid solution. The Ni species mainly exists in the form of Ni^{2+} interacting with other cations and metallic Ni (Ni°) appears. Dried $CeZr_{0.5}Ni_2O_Y$ also presents methane and CO_2 conversions of 95.8 % and 91.7 % after 80 h. The H_2/CO molar ratio is about 1.2, and the carbon deposition is of 0.0151 $g \cdot gcat^{-1} \cdot h^{-1}$. At 600 °C, $CeZr_{0.5}Ni_{0.5}O_Y$ shows CH_4 and CO_2 conversions of 66.2 % and 72.7 % and carbon formation rate of 0.004 $g \cdot gcat^{-1} \cdot h^{-1}$ after 80 h of stability test.

For calcined $CeAl_{0.5}Ni_XO_Y$ compounds, the surface areas are between 125-154 $m^2 \cdot g^{-1}$. The XRD patterns of $CeAl_{0.5}Ni_XO_Y$ show CeO_2 phase and NiO phase, while no structure related to aluminum could be observed. This might be due to the presence of an amorphous phase, and/or the insertion of aluminum species into ceria phase. The Raman spectra also illustrates the insertion of Ni^{2+} (and Al^{3+}) into ceria creating anionic vacancies. Two kind of reduction peaks of Ni^{2+} species are observed in $CeAl_{0.5}Ni_XO_Y$ compounds. This phenomenon is assigned to reduction of Ni^{2+} species in solid solution and/or small NiO nano-crystallites at low temperature, and larger NiO nano-crystallites at higher temperature. The addition of Al significantly influences the reducibility of the catalysts. Moreover, XPS results show the presence of Ni^{2+} cations presenting strong interactions with other cations (Ce^{4+}, Ce^{3+}, Al^{3+}), together with the presence of O^{2-} species and hydroxyl groups at the surface.

Among $CeAl_{0.5}Ni_XO_Y$ compounds, $CeAl_{0.5}Ni_2O_Y$ is the most competitive one with CH_4 and CO_2 conversions of 79.3 % and 97.9 %, H_2/CO ratio of 1.18, however with a

carbon deposition rate of 0.16 $g \cdot gcat^{-1} \cdot h^{-1}$ at 800 °C, on 10 mg of catalyst, without H_2 pretreatment, and under $CO_2/CH_4 = 0.7$. The stability test on $CeAl_{0.5}Ni_1O_Y$, at 600 °C, with 50 mg of catalyst pretreated, and under $CH_4/CO_2 = 1$, shows that conversions of CH_4 and CO_2 reach 66.5 % and 72.6 %, respectively. The H_2/CO molar ratio obtained is about 1.07. The carbon formation rate is of 0.009 $g \cdot gcat^{-1} \cdot h^{-1}$. At 800 °C, with 10 mg of catalyst pretreated, and under $CH_4/CO_2 = 1$, $CeAl_{0.5}Ni_2O_Y$ also presents a good result, with CH_4 and CO_2 conversions around 82%, a H_2/CO ratio of 1.1, and a carbon formation rate of 0.008 $g \cdot gcat^{-1} \cdot h^{-1}$ after 80 hours. According to the Raman and XPS result of spent $CeAl_{0.5}Ni_2O_Y$ catalyst, there are more oxygen vacancies created by the incorporation of the dopant in ceria, which means the presence of a solid solution after DRM reaction. The Ni^{2+} cations are present before and also after test, but the species changed from NiO to Ni^{2+} interacting with other cations and some metallic Ni (Ni°) after DRM test.

The $AlMg_2Ni_XO_Y$ catalysts have surface areas between 100 and 200 m^2/g. The XRD analysis do not allow to conclude on the presence of NiO, MgO and/or nickel-magnesium-(aluminum)-oxygen solid solution, as the XRD diffractions patterns of these phases overlap each over. Very small and uniform nano-crystals between three-six nm are acquired dependent on the nickel concentration. The XPS and TPR outcomes exhibit close interactions presence between nickel cations and magnesium and/or aluminum cations aligning with the shaping of nickel-magnesium-oxygen and/or nickel-magnesium-aluminum-oxygen solid solution. For low nickel concentration close interactions between Ni cations and other cations either in nickel-magnesium-(aluminum)-oxygen solid solution and/or at the interfaces between small NPs of NiO, MgO and/or Ni-Mg-(Al)-O render the solid hard to reduce. After that, the rise in nickel concentration renders the solid nearer that of bulk NiO, easier to be reduced. Nevertheless, close interactions still exist between nickel cations and some other cations, since the needed temperature for reducing Ni species still much exceeds the one necessary to reduce bulk NiO.

In the $AlMg_2Ni_XO_Y$ series, at 600 °C, with in situ H_2 pretreatment, under $CH_4/CO_2 = 1$, $AlMg_2Ni_1O_Y$ is tested in stream for 80 hours. 75.9 % and 83.2 % of CH_4 and CO_2 conversions are obtained, H_2/CO ratio of 1.2, and carbon deposition rate of 0.017 $g \cdot gcat^{-1} \cdot h^{-1}$. At 800 °C, with 10 mg of catalyst pretreated, under $CH_4/CO_2 = 1$, $AlMg_2Ni_{12}O_Y$ shows the conversions of methane and CO_2 of 99.7 % and 93.8 % after 80 hours, a H_2/CO ratio of 1.2, and carbon formation rate of 0.006 $g \cdot gcat^{-1} \cdot h^{-1}$. After

stability test, Ni^{2+} cations in solid solution are shown in spent catalyst with appearance of some metallic Ni (Ni°). At 800 °C, on 10 mg of pretreated catalysts, under CO_2/CH_4 = 0.7, 76.8 % and 84.1 % of CH_4 and CO_2 conversions are obtained after 80 h, on $AlMg_2Ni_{12}O_Y$ catalyst, with a H_2/CO ratio of 1.1 and carbon formation rate of 0.008 $g \cdot gcat^{-1} \cdot h^{-1}$.

The catalytic performance is also analyzed at 600 °C and 800 °C to see the effect of reaction temperature on calcined $CeNi_XO_Y$ catalysts, under a reaction mixture with CO_2/CH_4= 0.7. In general, the methane and CO_2 conversions at 800 °C are higher than that at 600 °C. However, the H_2/CO ratio and carbon formation rate at 800 °C are less than that at 600 °C.

The influence of calcination is studied at 600 °C, on 50 mg $CeNi_XO_Y$ catalysts, under a reaction mixture with CH_4/CO_2 = 0.7. Calcination of the catalysts increases the CO_4 and CO_2 conversions for the $CeNi_{0.3}O_Y$ with in situ H_2 pretreatment. However, for other catalysts tested, there is almost no difference for the conversions and H_2/CO ratio between the dried and calcined compounds. At the same time, there is less carbon deposition on dried catalysts compared to calcined catalysts.

The catalytic performance is conducted with 10 mg and 50 mg catalysts to investigate the effect of mass of catalysts at 800 °C, on calcined $CeNi_XO_Y$ catalysts, under a reaction mixture with CO_2/CH_4= 0.7. As the mass of the catalyst increases from 10 mg to 50 mg, the reactants conversions increase significantly. Moreover, 50 mg of catalysts exhibit lower H_2/CO ratio and less carbon deposition.

The influence of in situ H_2 pretreatment is studied on four series of catalysts. Interestingly, the in situ H_2 pretreatment has not same effects on the catalytic performance of the different catalysts under different conditions. For $CeNi_XO_Y$ catalysts, in situ H_2 pretreatment has no influence on DRM catalytic performance at 600 °C, with 50 mg of catalyst, and under CO_2/CH_4 = 0.7. At 800 °C, on 10 or 50 mg of catalyst, under CO_2/CH_4 = 0.7, in situ H_2 pretreatment decreases the CH_4 and CO_2 conversions and increases carbon formation rate of high Ni content $CeNi_XO_Y$ (x > 0.3) compounds. On dried $CeZr_{0.5}Ni_XO_Y$ catalysts, in situ H_2 pretreatment makes no different CH_4 and CO_2 conversions but leads to a lower carbon formation rate at 800 °C, on 10 mg of catalyst, and under CO_2/CH_4 = 1. Calcined $CeZr_{0.5}Ni_{0.5}O_Y$ and $CeZr_{0.5}Ni_1O_Y$ catalysts present higher CH_4 and CO_2 conversions and a lower carbon formation rate with in situ H_2 pretreatment than without pretreatment at 800 °C, on 10

mg of catalyst, and under CO_2/CH_4 = 0.7. For $CeAl_{0.5}Ni_XO_Y$ catalysts, at 600 °C, with 50 mg of catalyst, under CO_2/CH_4 = 0.7, there is no difference with in situ H_2 pretreatment and without H_2 pretreatment. At 800 °C, with 10 mg of catalyst, under CO_2/CH_4 = 0.7, in situ H_2 pretreatment increases the CH_4 and CO_2 conversions on $CeAl_{0.5}Ni_{0.5}O_Y$, and $CeAl_{0.5}Ni_1O_Y$, catalysts, and increases the carbon deposition on all $CeAl_{0.5}Ni_XO_Y$ catalysts. For $AlMg_2Ni_XO_Y$ catalysts, in situ H_2 pretreatment has almost no influence on CH_4 and CO_2 conversions, H_2/CO ratio, and carbon formation rate, whether at 800 °C, on 10 mg of catalyst, under CO_2/CH_4 = 0.7, or at 600 °C, on 50 mg of catalyst, and under CO_2/CH_4 = 1.

The influence of reactants concentration is also analyzed on $CeNi_XO_Y$, $CeZr_{0.5}Ni_XO_Y$, $CeAl_{0.5}Ni_XO_Y$ catalysts with the CO_2/CH_4 ratio = 1 and 0.7. The CH_4 conversion obtained under CO_2/CH_4 ratio = 0.7 is lower than that under CO_2/CH_4 ratio = 1. The H_2/CO ratio and carbon formation rate are higher under CO_2/CH_4 ratio = 0.7 compared to when this ratio is of 1.

Concerning the influence of Ni content, in general, the methane and CO_2 conversions increase with Ni content increasing, however, the carbon formation rate increases also.

Finally, in this study, possible mechanisms and active sites are discussed, and an active site is modeled by the collection of two cations, which involves cations in strong interactions and anionic vacancies.

Annex

Annex 1 Catalysts preparation

Preparation of $CeNi_XO_Y$ catalysts

The $CeNi_XO_Y$ catalysts are synthesized via the co-precipitation method by using triethylamine $(C_2H_5)_3N$ (TEA, Sigma-Aldrich, ≥ 99.5 % assay) as precipitant in the presence of methanol (Sigma-Aldrich, ≥ 99.8 % assay), the corresponding hydroxides from mixtures of nickel and cerium nitrates. In the typical preparation, $Ni(NO_3)_2{\cdot}6H_2O$ and $Ce(NO_3)_3{\cdot}6H_2O$ were dissolved in distilled water respectively to obtain the precursor solution 0.5 M. An appropriate volume of each nitrate solution was mixed to get an appropriate molar ratio, then the mixture was added dropwise to triethylamine diluted in a methanol solution while stirring. The solids were recovered by filtration and washing, then dried at 100 °C overnight, calcined in air at 500 °C for 4 hours. The obtained catalysts were named $CeNi_{0.1}O_Y$, $CeNi_{0.2}O_Y$, $CeNi_{0.3}O_Y$, $CeNi_{0.5}O_Y$, $CeNi_1O_Y$, $CeNi_2O_Y$.

Preparation of $CeZr_{0.5}Ni_XO_Y$ catalysts

The $CeZr_{0.5}Ni_XO_Y$ catalysts (ternary) are prepared by the co-precipitation method. First, the reaction reagents $Ni(NO_3)_2{\cdot}6H_2O$, $Ce(NO_3)_3{\cdot}6H_2O$, and $Zr(NO_3)_3{\cdot}6H_2O$ are respectively dissolved in a certain volume of distilled water and the three solutions are mixed together. Then, the methanol and triethylamine (TEA) are mixed, and the above two mixtures are mixed together under stirring. After keeping the mixed solution under stirring for one hour, the mixed solution was filtered and washed. After filtration, the solid was dried at 100 °C to obtain dried $CeZr_{0.5}Ni_XO_Y$ catalyst and then calcined in air at 500 °C for 4 hours to obtain calcined $CeZr_{0.5}Ni_XO_Y$ catalyst. The molar ratio of Ni/M_T depends on the molar ratio of nickel in all metals. The catalysts were named $CeZr_{0.5}Ni_{0.5}O_Y$, $CeZr_{0.5}Ni_1O_Y$, $CeZr_{0.5}Ni_2O_Y$, $CeZr_{0.5}Ni_5O_Y$.

Preparation of $CeAl_{0.5}Ni_XO_Y$ catalysts

The $CeAl_{0.5}Ni_XO_Y$ catalysts (ternary), where x is the Ni/Ce atomic ratio, are prepared by the same synthetic route mentioned before. The corresponding hydroxides came from mixtures of nickel, aluminum, and cerium nitrates solutions. At first, the nitrate precursors $Ni(NO_3)_2{\cdot}6H_2O$, $Ce(NO_3)_3{\cdot}6H_2O$, and $Al(NO_3)_3{\cdot}6H_2O$ were dissolved in distilled water, respectively, to get 0.5 M solutions. After mixing the appropriate volume of each nitrate solution in order to get the adequate molar ratio of

each element, the mixture was added dropwise into triethylamine (1.5 M) diluted in methanol solution while stirring. After filtration, the hydroxide mixture was washed, dried at 100 °C for 24 h, and calcined in air at 500 °C for 4h. The catalysts were named $CeAl_{0.5}Ni_{0.5}O_Y$, $CeAl_{0.5}Ni_1O_Y$, $CeAl_{0.5}Ni_2O_Y$, $CeAl_{0.5}Ni_5O_Y$.

Preparation of $AlMg_2Ni_XO_Y$ catalysts

The $AlMg_2Ni_XO_Y$ nanocomposite catalysts are formulated by coprecipitation of nickel, magnesium, and aluminum hydroxides from a mixture of their nitrate solutions by using NaOH/Na_2CO_3 as a precipitant agent. An aqueous mixed solution (1 M) of nitrate metals with a desired molar ratio of Al: Mg: Ni =1: 2: x was added dropwise into NaOH (1 M) and Na_2CO_3 (0.5 M) mixed solution at room temperature until pH = 8. Then the mixture was kept stirring at 80 °C for 18 h. After filtration and washing, obtained compounds were dried at 100 °C then calcined in air at 500 °C for 4 hours. The catalysts were named $AlMg_2Ni_1O_Y$, $AlMg_2Ni_3O_Y$, $AlMg_2Ni_{12}O_Y$.

Annex 2 Characterization method

Elemental analysis:

For all the catalysts prepared by the co-precipitation method, the metal loading of Ni, Ce, Mg, and Al were analyzed by the ICP technique (Agilent 720-ES ICP-OES). The Ni/M_T molar ratio reported corresponds to the nickel molar proportion in all the metals. For Ce-Ni based catalysts, $M_T = x + 1$, $Ni/M_T = x/(x + 1)$; For Ce-Ni-Al and Ce-Ni-Zr catalysts, $M_T = x + 1.5$, $Ni/M_T = x/(x + 1.5)$; For Ni-Mg-Al catalysts, $M_T = x + 3$, $Ni/M_T = x/(x + 3)$.

Surface area measurements:

The specific surface area (BET) was estimated from the N_2 adsorption by using (TriStar II 3020) analyzer. The samples were degassed for 40 min at 150°C prior to each measurement.

X-Ray diffraction (XRD) analysis:

X-Ray powder diffraction measurements were performed with a Bruker D8 Advance x-ray diffractometer equipped using a fast detector type LynxEye with a copper anticathode. The XRD patterns were registered in the 2θ domain (10-90°) with a measured step of 0.02 ° and the time integration of 0.3 s. The particle size was calculated based on the width of the main diffraction peak as assessed with the software using the Scherrer equation. From the most intense reflections observed for the NiO and CeO_2 crystallographic structures: (1 1 1), (2 0 0), and (2 2 0). Crystallites sizes were calculated using the Scherrer equation: $Dhkl = K \cdot \lambda / B \cdot \cos\theta$, where K is a structure constant (0.9 for spherical crystals); λ is the incident ray wavelength; B is the peak width at half height after correction for instrumental broadening, and θ is the Bragg angle. The lattice parameter 'a' was calculated using the most prominent peak (200) according to the following formulas: (1) $d = \lambda / 2\sin\theta$ (2) Where d represents the inter-planar spacing and θ represents the diffraction angle of the (111) plane.

Raman:

Raman spectra were acquired on a Labram Infinity HORIBA JOBIN YVON Raman spectrometer using a visible laser with an output laser power of λ = 532 nm at room temperature.

XPS:

The X-Ray photoelectron spectroscopy (XPS) of the sample was obtained on a KRATOS Axis Ultra spectrometer under ultrahigh vacuum condition, using a twin Al x-ray source (1486.6 eV) at pass energy of 40 eV. The solids in the form of pellets were fixed on a copper holder with copper tape. For calibration of the binding energy (BE) scale of photoemission features, the charge effect was adjusted by taking the C 1s peak at 285.0 eV as a reference for all the samples before the reaction. While for the catalysts after the reaction, a reference to the Al 2p peak at 74.0 eV and Ce 3d at 917.0 eV were taken into account.

H_2-TPR:

Temperature programmed reduction (TPR) analyses of the catalysts were conducted on a Micromeritics Autochem II Chemisorption analyzer, and the hydrogen consumption was measured by a thermal conductivity detector (TCD). Treatment was performed by heating 50 mg of catalyst sample from room temperature to 1000 °C in the 5% H_2-95 % Ar (v/v) gas mixture with a slope of 10 °C/min.

O_2-TPO:

The TPO measurements were performed on a Micromeritics Autochem 2920 analyzer. The sample was treated in the 5 vol % O_2-95 vol % He mixture with a flow rate of 50 ml/min. The temperature was increased to 900 °C at a heating rate of 5 °C/min.

Annex 3 Experimental

In dry reforming test, the catalytic test was conducted under atmospheric pressure in a fixed-bed quartz reactor (i.d. = 4 mm for 10 mg catalyst and 8 mm for 50 mg catalyst). The reactor was mounted into a tubular electric furnace and the temperature was controlled by a temperature controller. Prior to experiment with pretreatment, the sample was reduced in pure H_2 for 12 h and the reduction temperature depending on the catalysts, then the catalyst bed was washed for 30 minutes with a flow of pure He, followed by the sample was brought to the reaction temperature by 10 °C/min. Finally, the reactant mixture with N_2 as carry gas wse fed in, with total flow rate 80 mL/min. The stoichiometric molar ratio CO_2/CH_4 in reactants was maintained at 1 (CH_4/ CO_2/ N_2 = 5 %: 5 %: 90 %) or 0.7 (CH_4/ CO_2/ N_2 = 7 %: 5 %: 88 %). When doing a test without pretreatment, the reactants directly introduced into the reactor then the oven was headed to a target temperature in He. Gas flow was controlled by calibrated MFCs (Bronkhorst High-Tech BV, various models). The result reported in the thesis is the value after 5 h of TOS if no special instructions. The time of stability test is 80 h. **Fig.** 1 illustrated the scheme of experimental apparatus.

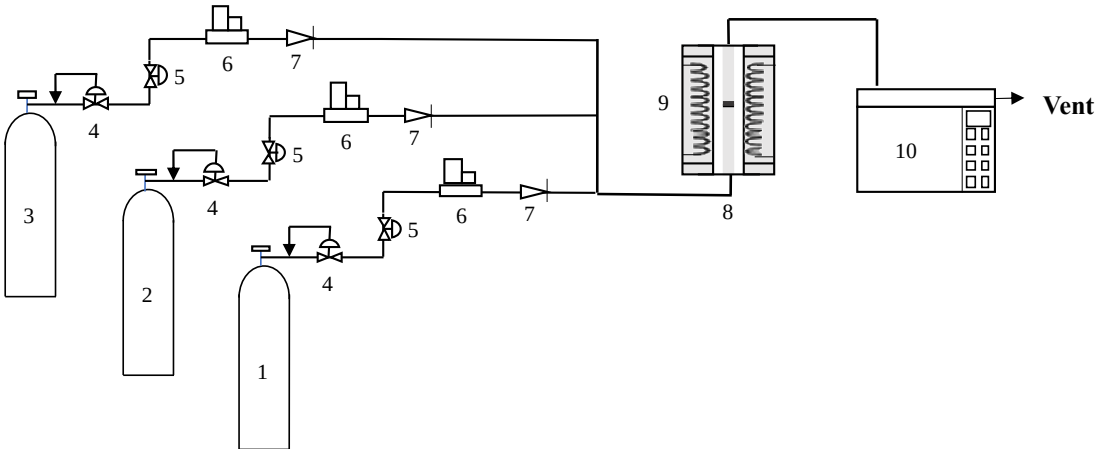

Fig. 1 Schematic diagram of experimental apparatus.1-CH_4; 2-CO_2; 3-N_2; 4-pressure regulator; 5-ball valve; 6-mass flow controller; 7-check valve; 8-reactor; 9-heater and thermal insulator; 10-gas chromatography.

All the products were analyzed on-line by gas chromatography (TRACE GC ULTRA) equipped with a thermal-conductivity detector (TCD) and a flame ionization detector (FID). The chromatography uses helium as carrier gas, is made up of two

ovens: a central furnace at 100°C with a column filled with HaysepQ 80-100 mesh and a PS255 30m-0.32mm-5micron film capillary column. And an auxiliary furnace at 130°C where there are two injection loops and the molecular sieve.

After reaction, the product gas mixture reaches the on-line GC, in the injection loops. When the first valve switches, the mixture in the first loop goes towards the TCD and the mixture in the second loop goes towards the FID.

The TCD analysis begins with a first separation of the products with the HaysepQ column which will separate the gaseous mixture into several peaks.

When this first separation is done, we switch valve 3 before the arrival of CO_2 so as not to poison the sieve and we re-switch valve 3 when the water has passed, these 4 peaks go directly to the TCD. Then the different gases CH_4, CO, N_2 and H_2 which have passed through the sieve, are separated and analyzed on the TCD.

Calibration of all products was performed online at a fixed flow rate (50ml/min). The concentration of the product is calculated from the response factor.

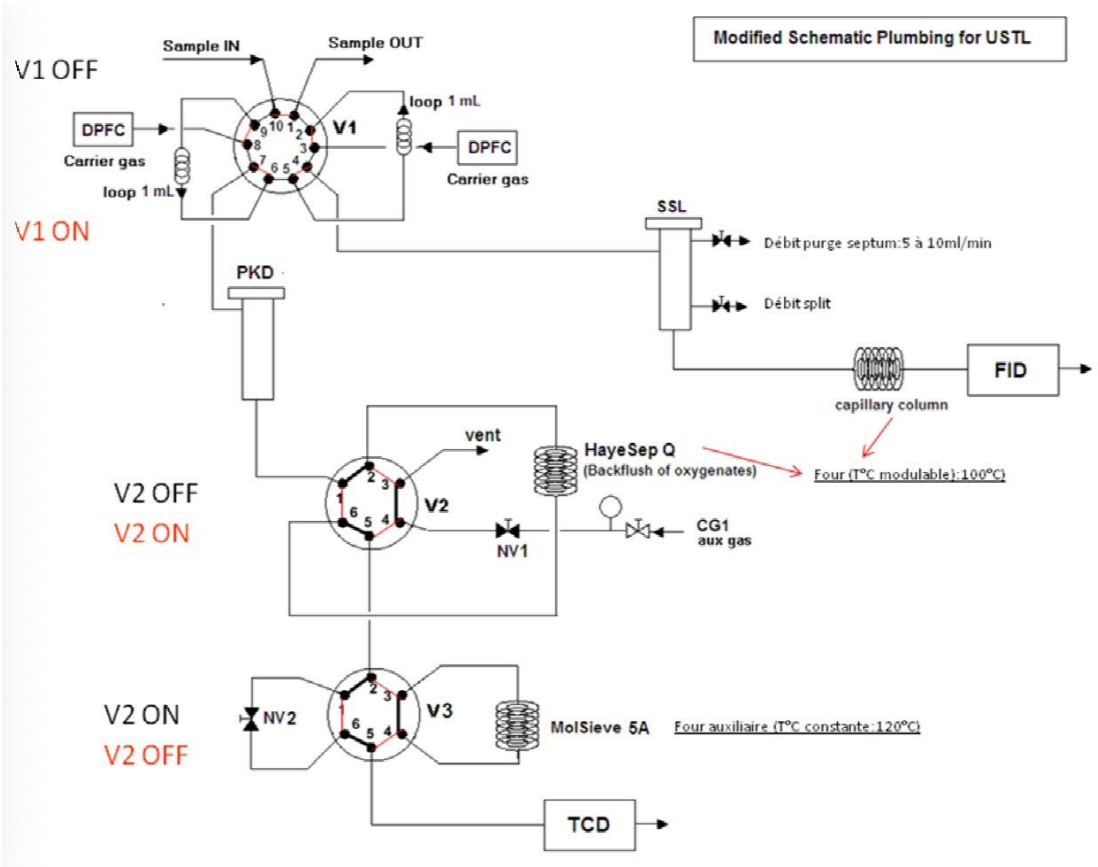

Fig. 2 Schematic of Ultra GC Trace chromatography

The catalytic performance was assessed using reactant conversion (CH_4, CO_2), and distribution of the products (H_2 and CO), dry basis, given also as H_2/CO molar ratio

during dry reforming reaction as given in Eqs. (1, 2 and 3). H_2O was also formed but the quantity was not reported due to the high uncertainty on the analysis of water.

(1) $X_{CH_4} = \frac{CH_{4\,in} - CH_{4\,out}}{CH_{4\,in}} * 100\%$

(2) $X_{CO_2} = \frac{CO_{2\,in} - CO_{2\,out}}{CO_{2\,in}} * 100\%$

(3) H_2/CO ratio = $H_{2\ out}/CO_{\ out}$

Where $CH_{4\ in}$, $CH_{4\ out}$, $CO_{2\ in}$, $CO_{2\ out}$, $H_{2\ out}$ and $CO_{\ out}$ are in moles of each component in the feed or effluent.

Résumé

CHAPITRE 1 - Introduction générale

Avec le développement de l'industrialisation, la demande d'énergie et de ses ressources augmentent. La consommation massive de combustibles fossiles entraîne des pénuries d'énergie et l'effet de serre. Par conséquent, il est nécessaire de développer des sources d'énergie renouvelables et propres pour remplacer les combustibles fossiles. L'hydrogène est une source d'énergie propre et renouvelable, mais la principale méthode de production d'hydrogène n'est ni durable ni respectueuse de l'environnement. L'hydrogène devrait également être produit à partir de sources renouvelables, par exemple, la production d'hydrogène à partir de biogaz (principalement composé de CH_4 et de CO_2).

Ce chapitre présente la technologie et la littérature sur la production d'hydrogène par reformage du méthane, en rendant compte des différents procédés de production (vaporeformage, oxydation partielle, reformage à sec et reformage oxydant) et des catalyseurs utilisés pour les réactions de reformage à sec. Les catalyseurs à base de Ni ont été largement étudiés dans la littérature en raison de leur faible coût et activité très élevée, mais ils sont souvent désactivés en raison du dépôt de carbone et/ou du fait du frittage. Dans ce contexte, l'objectif de cette thèse est de développer des catalyseurs actifs et sélectifs à base de nickel en limitant la formation de carbone et en évitant le frittage.

CHAPITRE 2 - Reformage à sec du méthane sur des catalyseurs à base de Ni

Dans cette thèse, des catalyseurs à base de Ni, $CeNi_XO_Y$, $CeZr_{0.5}Ni_XO_Y$, $CeAl_{0.5}Ni_XO_Y$, et $AlMg_2Ni_XO_Y$ sont étudiés pour la réaction de reformage à sec du méthane (DRM) qui conduit à la formation de H_2 et CO dont le rapport molaire (H_2/CO) est analysé. L'effet de la température de réaction, de la teneur en Ni, du prétraitement in situ sous H_2, de la masse de catalyseur, de la calcination et du rapport molaire des réactifs CO_2/CH_4 sont analysés. Sur certains composés choisis, des tests de stabilité de longue durée sont aussi reportés. L'optimisation des performances catalytiques avec une formation réduite de carbone, sont obtenues sur des catalyseurs partiellement réduits.

Avec un prétraitement sous H_2 pendant une nuit du catalyseur, et 80 h de fonctionnement à 600 °C sous un mélange réactionnel $CH_4/ CO_2/ N_2$ = 5 : 5 : 90 % avec CH_4/CO_2 = 1, le composé $AlMg_2Ni_1O_Y$ (50 mg) présente les meilleures performances

avec 75,9 % et 83,2 % de conversions du CH_4 et de CO_2, respectivement, et conduisant à la formation des produits H_2 et CO (rapport H_2/CO de 1,2) et un taux de dépôt de carbone de 0,017 $g \cdot gcat^{-1} \cdot h^{-1}$ après 80 h. Dans les mêmes conditions mais sans prétraitement, le catalyseur $AlMg_2Ni_{12}O_Y$ permet les conversions de CH_4 et CO_2 les plus élevées à 83,6 % et 80,0 %, respectivement, mais conduit à une formation de carbone de 0,61 $g \cdot gcat^{-1} \cdot h^{-1}$. $CeZr_{0.5}Ni_{0.5}O_Y$ montre également de bonnes performances catalytiques avec des conversions de CH_4 et CO_2 de 66,2 % et 72,7 %, respectivement, et un taux de formation de carbone de 0,004 $g \cdot gcat^{-1} \cdot h^{-1}$ après 80 h de test en stabilité.

En DRM à 800 °C (CH_4/CO_2 = 1) sur 10 mg de catalyseur prétraité sous H_2 , le meilleur résultat est obtenu sur $AlMg_2Ni_{12}O_Y$, les conversions du méthane et du CO_2 sont de 99,7 % et 93,8 %, respectivement, après 80 heures, avec un rapport H_2/CO de 1,2 et un taux de formation de carbone de 0,006 $g \cdot gcat^{-1} \cdot h^{-1}$. Sur le catalyseur $CeNi_{0.5}Zr_2O_Y$, les conversions du CH_4 et de CO_2 sont de 98,8% et 93,5%, respectivement, avec un rapport H_2/CO de 1,2 et un taux de formation de carbone de 0,004 $g \cdot gcat^{-1} \cdot h^{-1}$ après 80 heures. Sans prétraitement du catalyseur sous H_2, $CeZr_{0.5}Ni_2O_Y$ séché présente des conversions du CH_4 et de CO_2 de 95,8 % et 91,7 %, respectivement, après 80 h. Le rapport molaire H_2/CO est d'environ 1,2 pendant la réaction. De plus, le dépôt de carbone est de 0,0151 $g \cdot gcat^{-1} \cdot h^{-1}$.

Les catalyseurs sont étudiés également en DRM sous un mélange réactionnel avec CO_2/CH_4 = 0,7 (CH_4/ CO_2/ N_2 = 7 : 5 : 88 %). A 600 °C, sur 50 mg de catalyseur ayant subi un prétraitement in situ sous H_2 à 250 °C, des conversions de 73,1 % et 65,9 % de CH_4 et CO_2 sont obtenues avec un rapport H_2/CO de 1,9 sur $CeAl_{0.5}Ni_2O_Y$. Le taux de formation de carbone est de 0,52 $g \cdot gcat^{-1} \cdot h^{-1}$. Sans prétraitement sous H_2, les conversions les plus élevées de CH_4 et CO_2 sont obtenues à 82,2 % et 75,6 % sur le catalyseur $CeAl_{0.5}Ni_5O_Y$, avec un taux de formation de carbone de 0,76 $g \cdot gcat^{-1} \cdot h^{-1}$.

A 800 °C, avec CO_2/CH_4 = 0,7, $CeNi_{0.2}O_Y$ (50 mg) avec un prétraitement in situ sous H_2 à 250 °C, montre une excellente performance catalytique avec 74,0 % et 93,9 % de conversions de CH_4 et CO_2 après 5 heures de fonctionnement. $CeAl_{0.5}Ni_2O_Y$ présente des conversions de CH_4 et CO_2 de 80,4 % et 93,5 %, respectivement, un rapport H_2/CO de 1,3 et un taux de formation de carbone de 0,23 $g \cdot gcat^{-1} \cdot h^{-1}$. Sans prétraitement sous H_2, $CeZr_{0.5}Ni_2O_Y$ montre des conversions de CH_4 et CO_2 autour de 99 % et 93 %, respectivement, avec un taux de formation de carbone de 0,12 $g \cdot gcat^{-1} \cdot h^{-1}$.

En général, les conversions de CH_4 et de CO_2 augmentent avec l'augmentation de la température de réaction de 600 °C à 800 °C, ce qui est attendu puisque la réaction est hautement endothermique. Les conversions augmentent globalement avec la teneur en Ni tandis que le rapport H_2/CO ne semble pas être influencé par la teneur en Ni. Le prétraitement in situ sous H_2 aide à diminuer la formation de carbone dans certains cas. Lorsque le rapport CO_2/CH_4 des réactifs passe de 1 à 0,7, la conversion du CO_2 et le rapport H_2/CO augmentent.

CHAPITRE 3 - Caractérisations des catalyseurs

Dans cette étude, les catalyseurs $CeNi_XO_Y$, $CeZr_{0.5}Ni_XO_Y$, $CeAl_{0.5}Ni_XO_Y$ et $AlMg_2Ni_XO_Y$ sont préparés par la méthode de co-précipitation (CP). Les catalyseurs à base de Ni ci-dessus sont étudiés par différentes techniques physico-chimiques, telles que XRD, Raman, XPS et TPR, et certains composés choisis sont également caractérisés après quelques tests par Raman et XPS.

Les surfaces pour les composés $CeNi_XO_Y$ sont comprises entre 77 et 215 $m^2\ g^{-1}$ (avec x = 0,1, 0,2, 0,3, 0,5, 1 et 2 correspondant à un % massique en Ni allant de 5 % à 40 %). Les composés séchés ont une surface spécifique plus grande que les composés calcinés à même teneur en Ni. Dans les catalyseurs $CeNi_XO_Y$ séchés, la phase de type oxyde de cérium est clairement apparente dans tous les échantillons, et il peut y avoir présence de $Ni(OH)_2$. La largeur et le décalage des raies de diffraction (XRD) de CeO_2 suggèrent la formation d'une solution solide de cérium-nickel. La phase cristalline NiO est détectée dans les catalyseurs calcinés à haute teneur en Ni ($x \geq 0,5$). La taille moyenne des cristallites est répartie entre 4-5 nm pour CeO_2 et 8-10 nm pour NiO. Les résultats Raman mettent en évidence l'existence de fortes interactions entre les espèces nickel et cérium dans les catalyseurs séchés et calcinés. L'analyse XPS prouve que des cations Ni^{2+} qui ont une forte interaction avec d'autres cations sont présents à la surface des solides, ce qui est en accord avec la formation de solution solide Ce-Ni-O. L'analyse TPR révèle que les solides $CeNi_XO_Y$ possèdent une proportion d'espèces Ni qui présentent un pic de réduction caractéristique à environ 270 °C. De telles espèces de Ni peuvent être réduites et réoxydées facilement et de manière réversible, ce qui est dû à l'existence de fortes interactions entre les espèces nickel et cérium dans les solides $CeNi_XO_Y$. Après un test de stabilité de 80 h, les caractérisations effectuées conduisent à conclure que la solution solide de Ce-Ni-O est toujours présente dans le catalyseur $CeNi_1O_Y$ usé (avec la présence de cations Ni^{2+}) et qu'il y a davantage de lacunes d'oxygène et de cations Ce^{3+} générés.

Dans la série $CeZr_{0.5}Ni_XO_Y$, le $CeZr_{0.5}Ni_{0.5}O_Y$ séché présente la plus grande surface spécifique de 186 m^2/g. La forte teneur en nickel et la calcination diminuent la surface spécifique des catalyseurs. Les phases d'oxyde de cérium et de $Ni(OH)_2$ sont détectées par XRD dans les catalyseurs $CeZr_{0.5}Ni_XO_Y$ séchés, tandis que les phases cristallines d'oxyde de cérium et de NiO sont détectées dans les catalyseurs calcinés. L'analyse XRD des catalyseurs ne montrent pas la présence de phase zircone, tandis que les raies de diffraction de CeO_2 sont légèrement élargies comparativement à l'oxyde de cérium simple. L'élargissement et les déplacements des raies de diffraction démontrent que les cations Ni^{2+} et/ou Zr^{4+} pénètrent à l'intérieur du réseau CeO_2 et la solution solide de cérium-nickel-(zirconium) se forme. Les résultats Raman présentent un pic d'oxyde de cérium plus large comparativement à la cérine seule indiquant la formation d'une solution solide d'oxyde de cérium et de zirconium. Et les résultats XPS mettent en évidence l'existence de fortes interactions entre les espèces nickel et cérium (et zirconium) dans les catalyseurs séchés et calcinés. Les caractérisations effectuées sur le catalyseur $CeZr_{0.5}Ni_2O_Y$ usé après une réaction DRM de 80 h montrent la présence de lacunes d'oxygène et de solution solide Ce-Ni-Zr-O. L'espèce Ni existe principalement sous forme de Ni^{2+} en interaction avec d'autres cations et 10,5 % de Ni métallique (Ni°) apparaît.

Pour les composés $CeAl_{0.5}Ni_XO_Y$ calcinés, les surfaces sont comprises entre 125 et 154 $m^2\ g^{-1}$. La réduction des espèces Ni^{2+} dans divers environnements est observée dans les composés $CeAl_{0.5}Ni_XO_Y$. Concrètement, les oxydes mixtes à base de Ce-Ni-(Al)-O présentent deux pics à basse température vers 250 °C et à des températures plus élevées à environ 500 °C. Ce phénomène est considéré comme une réduction des espèces Ni^{2+} en solution solide et/ou présentes dans NiO sous forme de petits nanocristaux (à basse température), et plus gros nanocristaux (à haute température). L'ajout d'Al affecte évidemment la réductibilité du catalyseur. De plus, les espèces Ni^{2+} présentent la capacité d'être réduites et réoxydées facilement et de manière réversible grâce à une interaction élevée avec d'autres cations, en particulier les espèces Ce. Selon les résultats Raman et XPS du catalyseur $CeAl_{0.5}Ni_2O_Y$ usé, il y a davantage de lacunes d'oxygène générées par l'incorporation du dopant dans l'oxyde de cérium, ce qui signifie la présence de solution solide après la réaction DRM. Les cations Ni^{2+} sont présents avant et aussi après le test, mais la nature des espèces et leur proportion changent de NiO et Ni^{2+} interagissant avec d'autres cations à 5,8 % de Ni métallique (Ni°) et 94,2 % de cations Ni^{2+} après le test DRM.

Les catalyseurs $AlMg_2Ni_XO_Y$ ont des surfaces comprises entre 100 et 200 m^2/g. Selon les résultats XRD, les catalyseurs pourraient correspondre à un mélange de NiO, MgO et/ou à la solution solide de Ni-Mg-(Al)-O. Des nanocristaux avec une taille moyenne de cristallites entre 3 et 6 nm sont présents en fonction de la concentration en Ni. Les résultats XPS et TPR montrent la présence d'interactions fortes entre les cations nickel et les cations magnésium et/ou aluminium résultant de la présence de la solution solide Ni-Mg-O et/ou Ni-Mg-Al-O. Pour une faible concentration en Ni, les interactions fortes entre les cations Ni et les autres cations soit dans la solution solide Ni-Mg-(Al)-O et/ou aux interfaces entre les nanoparticules de NiO, MgO et/ou Ni-Mg-(Al)- O rendent le solide plus difficile à réduire. L'augmentation de la concentration en nickel rend le comportement du solide plus proche de celui du NiO massif, plus facile à réduire. Néanmoins, des interactions fortes existent toujours entre les cations Ni^{2+} et certains autres cations, puisque la température nécessaire pour réduire les espèces Ni reste encore supérieure à celle nécessaire pour réduire le NiO massif. Après le test de stabilité en DRM, les cations Ni^{2+} en solution solide sont mis en évidence dans le catalyseur usé avec l'apparition de 22,3 % de Ni métallique (Ni°).

CHAPITRE 4 - Discussion générale

Dans ce chapitre, les résultats catalytiques et les résultats des caractérisations des catalyseurs sont synthétisés, et la relation possible entre les propriétés des catalyseurs et leurs performances catalytiques est étudiée en profondeur. Des espèces actives et sélectives pour l'activation et la conversion des molécules CH_4 et CO_2 ont été identifiées, et un site actif impliquant des espèces Ni en interactions fortes avec d'autres cations est proposé. Ce site est obtenu sur un catalyseur partiellement réduit impliquant des lacunes anioniques, des espèces O^{2-} et des cations.

References

References

[1] H. Nazir, C. Louis, S. Jose, J. Prakash, N. Muthuswamy, M. E. Buan, T. Kallio, Is the H_2 economy realizable in the foreseeable future? Part I: H_2 production methods, *Int. J. Hydrogen Energy*, 41, 20693-20708 (2020).

[2] WMO Greenhouse Gas Bulletin-No. 15: The State of Greenhouse Gases in the Atmosphere Based on Global Observations through 2018 (2019).

[3] Y. Zhao, H. Li, H. Li, NiCo@ SiO_2 core-shell catalyst with high activity and long lifetime for CO_2 conversion through DRM reaction, *Nano Energy*, 45, 101-108 (2018).

[4] J. O. Abe, A. P. I. Popoola, E. Ajenifuja, O. M. Popoola, Hydrogen energy, economy and storage: review and recommendation, *Int. J. Hydrogen Energy*, 44, 15072-15086 (2019).

[5] J. L. Young, M. A. Steiner, H. Doscher, R. M. France, J. A. Turner, T. G. Deutsch, Direct solar-to-hydrogen conversion via inverted metamorphic multi-junction semiconductor architectures, *Nat. Energy*, 2, 17028 (2017).

[6] Z. Abdin, A. Zafaranloo, A. Rafiee, W. Merida, W. Lipinski, K. R. Khalilpour, Hydrogen as an energy vector, *Renew. Sust. Energ. Rev*., 120, 109620 (2020).

[7] H. Liu, Ammonia Synthesis Catalysts, Innovation and Practice, Singapore: World Scientific, 2013.

[8] International Energy Agency, The Future of Hydrogen, 2019.

[9] N. Sazali, Emerging technologies by hydrogen: A review, *Int. J. Hydrogen Energy*, 45, 18753-18771 (2020).

[10] F. Safari, I. Dincer, A review and comparative evaluation of thermochemical water splitting cycles for hydrogen production, *Energy Convers. Manag.*, 205, 112182 (2020).

[11] Hydrogen Strategy Enabling A Low-Carbon Economy, United States Department of Energy 2020.

[12] B. Heid, M. Linder, A. Orthofer, M. Wilthaner M. Hydrogen: The next wave for electric vehicles? 2017.

[13] I. Staffell, D. Scamman, A. A. Velazquez, P. Balcombe, P. E. Dodds, P. Ekins, N. Shah, K. R. Ward, The role of hydrogen and fuel cells in the global energy system, *Energy Environ. Sci*., 12, 463-91 (2019).

[14] F. Manenti, R. Pelosato, P. Vallevi, A. R. Leon-Garzon, G. Dotelli, A. Vita, M. Lo Faro, G. Maggio, L. Pino, A. S. Aricò, Biogas-fed solid oxide fuel cell (SOFC) coupled to tri-reforming process: Modelling and simulation, *Int. J. Hydrogen Energy*, 1-11 (2015).

[15] International Energy Agency, Hydrogen Production and Storage, R&D Priorities and Gaps, *Hydrog. Implement. Agreem*., 13, 392 (2006).

[16] Y. Yan, Y. Cui, L. Zhang, L. Li, J. Zhang, Y. Chen, T. Q. Qiang, C. Lin, Experimental investigation of methane auto-thermal reforming in hydrogen-permeable membrane reactor for pure

hydrogen production, *Int. J. Hydrogen Energy*, 41, 13069-76 (2016).

[17] S. Thangalazhy-Gopakumar, S. Adhikari, R. B. Gupta, M. Tu, S. Taylor, Production of hydrocarbon fuels from biomass using catalytic pyrolysis under helium and hydrogen environments, *Bioresour. Technol*., 102, 6742-9 (2011).

[18] H. Nazir, C. Louis, S. Jose, J. Prakash, N. Muthuswamy, M. E. M. Buan, C. Flox, S. Chavan, X. Shi, P. Kauranen, T. Kallio, G. Maia, K. Tammeveski, N. Lymperopoulos, E. Carcadea, E. Veziroglu, A. Iranzo, A. M. Kannan, Is the H_2 economy realizable in the foreseeable future? Part I: H_2 production methods, *Int. J. Hydrogen Energy*, 45, 13777-13788 (2020).

[19] G. Liu, Y. Sheng, J. W. Ager, M. Kraft, R. Xu, Research advances towards large-scale solar hydrogen production from water, *EnergyChem*, 1, 100014 (2019).

[20] M. R. Shaner, H. A. Atwater, N. S. Lewis, E. W. McFarland, A comparative technoeconomic analysis of renewable hydrogen production using solar energy, *Energy Environ. Sci*., 9, 2354-2371 (2016).

[21] P. Zhang, Y. J. Guo, J. Chen, Y. R. Zhao, J. Chang, H. Junge, M. Beller, Y. Li, Streamlined hydrogen production from biomass, *Nat. Catal.*, 1, 332-8 (2018).

[22] P. McKendry, Energy production from biomass (part 1): overview of biomass, *Bioresour. Technol*., 83, 37-46 (2002).

[23] A. Lalsarea, A. Sivrib, R. Egana, R. J. Vukmanovicha, C. E. Dumitrescub, J. Hu, Biomass-Flare gas synergistic co-processing in the presence of carbon dioxide for the controlled production of syngas (H_2:CO ~ 2-2.5), *Chem. Eng. J*., 385, 123783 (2020).

[24] M. Jaganmohan, Biomass energy production forecast in the U.S. 2020-2050, Feb 22, 2021.

[25] T. N. L. T. Ngo, K. Chiang, C. Liu, Y. Chang, H. Wan, Hydrogen production enhancement using hot gas cleaning system combined with prepared Ni-based catalyst in biomass gasification, *Int. J. Hydrogen Energy*, 46, 11269-11283 (2021).

[26] K. Goransson, U. Soderlind, J. He, W. Zhang, Review of syngas production via biomass DFBGs, *Renew. Sust. Energ. Rev.*, 15, 482-492 (2011).

[27] A. Arregi, M. Amutio, G. Lopez, J. Bilbao, M. Olazar, Evaluation of thermochemical routes for hydrogen production from biomass: a review, *Energy Convers. Manag.*, 165, 696-719 (2018).

[28] P. Mishra, S. Krishnan, S. Rana, L. Singh, M. Sakinah, Z. Ab Wahid, Outlook of fermentative hydrogen production techniques: an overview of dark, photo and integrated dark-photo fermentative approach to biomass, *Energy Strateg. Rev.*, 24, 27-37 (2019).

[29] K. Bolatkhan, B. D. Kossalbayev, B. K. Zayadan, T. Tomo, T. N. Veziroglu, S. I. Allakhverdiev, Hydrogen production from phototrophic microorganisms: reality and perspectives, *Int. J. Hydrogen Energy*, 44, 5799-811 (2019).

[30] A. Sharma, S. K. Arya, Hydrogen from algal biomass: a review of production process, *Biotechnol. Rep.*, 15, 63-69 (2017).

[31] M. Shahabuddin, B. B. Krishna, T. Bhaskar, G. Perkins, Advances in the thermo-chemical

production of hydrogen from biomass and residual wastes: Summary of recent techno-economic analyses, *Bioresour. Technol*., 299, 122557 (2020).

[32] M. J. Turner, G. Sverdrup, M. K. Mann, P. Maness, B. Kroposki, Renewable hydrogen production, *Int. J. energy Res*., 32, 379-407 (2008).

[33] S. Jung, J. Lee, D. H. Moon, K. Kim, E. E. Kwon, Upgrading biogas into syngas through dry reforming, *Renew. Sust. Energy Rev.*, 143, 110949 (2021).

[34] P. Kolbitsch, C. Pfeifer, H. Hofbauer, Catalytic steam reforming of model biogas, *Fuel*, 87, 701-706 (2008).

[35] W. H. Chen, S. C. Lin, Biogas partial oxidation in a heat recirculation reactor for syngas production and CO_2 utilization, *Appl. Energy*, 217, 113-125 (2018).

[36] A. Petersson, A. Wellinger, Biogas upgrading technologies-developments and innovations, *IEA bioenergy*, 20, 1-19 (2009).

[37] Y. J. O. Asencios, C. B. Rodella, E. M. Assaf, Oxidative reforming of model biogas over NiO-Y_2O_3-ZrO_2, catalysts, *Appl. Catal. B Environ.*, 132, 1-12 (2013).

[38] V. Chiodo, S. Maisano, G. Zafarana, F. Urbani, Effect of pollutants on biogas steam reforming, *Int. J. Hydrog. Energy*, 42, 1622-1628 (2017).

[39] P. L. Cruz, Z. Navas-Anguita, D. Iribarren, J. Dufour, Exergy analysis of hydrogen production via biogas dry reforming, *Int. J. Hydrogen Energy*, 43, 11688-11695 (2018).

[40] B. Su, W. Han, H. He, H. Jin, Z. Chen, J. Zheng, S. Yang, X. Zhang, Using moderate carbon dioxide separation to improve the performance of solar-driven biogas reforming process, *Appl. Energy*, 219, 115693 (2020).

[41] T. Yamamoto, S. Uchiyama, M. Kishida, R. Tanaka, Influence of Nozzle Shape on Partial Oxidation Reforming of Biogas Using Microwave Plasma, *Energy Fuels*, 35, 4203-4211 (2021).

[42] W. Yin, N. Guilhaume, Y. Schuurman, Model biogas reforming over Ni-Rh/$MgAl_2O_4$ catalyst. Effect of gas impurities, *Chem. Eng. J.*, 389, 125534 (2020).

[43] E. V. Kondratenko, T. Peppel, D. Seeburg, V. A. Kondratenko, N. Kalevaru, A. Martina, S. Wohlrab, Methane conversion into different hydrocarbons or oxygenates: current status and future perspectives in catalyst development and reactor operation, *Catal. Sci. Technol.*,7, 366-381 (2017).

[44] K. Hou, R. Hughes, The kinetics of methane steam reforming over a Ni/α-Al_2O_3 catalyst, *Chem. Eng. J.*, 82, 311-28 (2001).

[45] Q. Lu, Y. Hou, S. R. Laraib, O. Khalifa, K. Li, W. L. Xie, Y. P. Yang, Electro-catalytic steam reforming of methane over Ni-CeO_2/γ-Al_2O_3-MgO catalyst, *Fuel Process. Technol.*, 192, 57-64 (2019).

[46] F. Che, J. T. Gray, S. Ha, J. S. McEwen, Reducing reaction temperature, steam requirements, and coke formation during methane steam reforming using electric fields: a microkinetic modeling and experimental study, *ACS Catal.*, 7, 6957-6968 (2017).

[47] J. Xu, G. F. Froment, Methane steam reforming, methanation and water-gas shift: I. Intrinsic kinetics, *AIChE J*, 35, 88-96 (1989).

[48] S. D. Angeli, G. Monteleone, A. Giaconia, A. A. Lemonidou, State-of-the-art catalysts for CH_4 steam reforming at low temperature, *Int. J. Hydrogen Energy*, 39, 1979-1997 (2014).

[49] C. H. Chen, C. T. Yu, W. H. Chen, Improvement of steam methane reforming via in-situ CO_2 sorption over a nickel-calcium composite catalyst, *Int. J. Hydrogen Energy*, 46, 16655-16666 (2021).

[50] H. Kim, A. Al-Shahat Eissa, S. B. Kim, H. Lee, W. Kim, D. J. Seo, K. Lee, W. L. Yoon, One-pot synthesis of a highly mesoporous Ni/$MgAl_2O_4$ spinel catalyst for efficient steam methane reforming: influence of inert annealing, *Catal. Sci. Technol.*, 2021.

[51] Y. Meng, C. Ding, X. Gao, K. Zhang, J. Wang, Z. Li, Adsorption of Pd on the Cu (1 1 1) surface and its catalysis of methane partial oxidation: A density functional theory study. *Appl. Surf. Sci.*, 513, 145724 (2020).

[52] M. Ao, G. H. Pham, V. Sage, V. Pareek, Selectivity enhancement for higher alcohol product in Fischer-Tropsch synthesis over nickel-substituted $La_{0.9}Sr_{0.1}CoO_3$ perovskite catalysts, *Fuel*, 206, 390-400 (2017).

[53] J. Guo, C. Ding, Z. Ma, L. Ma, J. Wang, J. Shangguan, Q. Yuan, M. Zhao, Y. Li, M. Wang, K. Zhang, Highly dispersed and stable Pt clusters encapsulated within ZSM-5 with aid of sodium ion for partial oxidation of methane, *Fuel*, 289, 119839 (2021).

[54] Y. Ma, Y. Ma, Y. Chen, S. Ma, Q. Li, X. Hu, D. Dong, Highly stable nanofibrous La_2NiZrO_6 catalysts for fast methane partial oxidation. *Fuel*, 265, 116861 (2020).

[55] T. J. Siang, A. A. Jalil, M. Y. S. Hamid, A. A. Abdulrasheed, T. A. T. Abdullah, D. V. N. Vo, Role of oxygen vacancies in dendritic fibrous M/KCC-1 (M = Ru, Pd, Rh) catalysts for methane partial oxidation to H_2-rich syngas production, *Fuel*, 278, 118360 (2020).

[56] L. Ma, C. Ding, J. Wang, Y. Li, Y. Xue, J. Guo, K. Zhang, P. Liu, X. Gao, Highly dispersed Pt nanoparticles confined within hierarchical pores of silicalite-1 zeolite via crystal transformation of supported Pt/S-1 catalyst for partial oxidation of methane to syngas, *Int. J. Hydrogen Energy*, 44, 21847-21857 (2019).

[57] A. Scarabello, D. D. Nogare, P. Canu, R. Lanza, Partial oxidation of methane on Rh/ZrO_2 and Rh/Ce-ZrO_2 on monoliths: Catalyst restructuring at reaction conditions, *Appl. Catal. B Environ.*, 174-175, 308-322 (2015).

[58] S. Das, R. Gupta, A. Kumar, M. Shah, M. Sengupta, S. Bhandari, A. Bordoloi, Facile synthesis of ruthenium decorated $Zr_{0.5}Ce_{0.5}O_2$ nanorods for catalytic partial oxidation of methane, *ACS Appl. Nano Mater.*, 1, 2953-2961 (2018).

[59] A. Moral, I. Reyero, J. Llorca, F. Bimbela, L. M. Gandía, Partial oxidation of methane to syngas using Co/Mg and Co/Mg-Al oxide supported catalysts, *Catal. Today*, 333, 259-267 (2019).

[60] L. Li, N. H. MD Dostagir, A. Shrotri, A. Fukuoka, H. Kobayashi, Partial Oxidation of Methane to

Syngas via Formate Intermediate Found for a Ruthenium-Rhenium Bimetallic Catalyst, *ACS Catal.*, 11, 3782-3789 (2021).

[61] A. H. K. Owgi, A. A. Jalil, I. Hussain, N. S. Hassan, H. U. Hambali, T. J. Siang, D. V. N. Vo, Catalytic systems for enhanced carbon dioxide reforming of methane: a review, *Environ. Chem. Lett.*,19, 2157-2183 (2021).

[62] D. Selvatico, A. Lanzini, M. Santarelli, Low Temperature Fischer-Tropsch fuels from syngas: Kinetic modeling and process simulation of diferente plant configurations, *Fuel*, 186, 544-560 (2016).

[63] H. Ghezel-Ayagh, S. Jolly, D. Patel, D. Stauffer, Solid oxide fuel cell system utilizing syngas from coal gasifiers, *Ind. Eng. Chem. Res.*, 52, 3112-3120 (2013).

[64] R. Fan, M. Kyodo, L. Tan, X. Peng, G. Yang, Y. Yoneyama, R. Yang, Q. Zhang, N. Tsubaki, Preparation and application of Cu/ZnO catalyst by urea hydrolysis method for low-temperature metanol synthesis from syngas, *Fuel Process. Technol.*, 167, 69-77 (2017).

[65] Y. Wang, Y. Chen, F. Yu, D. Pan, B. Fan, J. Ma, R. Li, One-step synthesis of dimethyl ether from syngas on ordered mesoporous copper incorporated alumina, *J. Energy Chem.*, 25, 775-781 (2016).

[66] N. A. K. Aramouni, J. G. Touma, B. A. Tarboush, J. Zeaiter, M. N. Ahmad, Catalyst design for dry reforming of methane: Analysis review, *Renew. Sust. Energy Rev.*, 82, 2570-2585 (2018).

[67] W. Liu, L. Li, X. Zhang, Z. Wang, X. Wang, H. Peng, Design of Ni-ZrO_2@SiO_2 catalyst with ultra-high sintering and coking resistance for dry reforming of methane to prepare syngas, *J. CO_2 Util.*, 27, 297-307 (2018).

[68] S. Damyanova, I. Shtereva, B. Pawelec, L. Mihaylov, J. L. G. Fierro, Characterization of none and yttrium-modified Ni-based catalysts for dry reforming of methane, *Appl. Catal. B Environ.*, 278, 119335-119348 (2020).

[69] S. Chen, J. Zaffran, B. Yang, Dry reforming of methane over the cobalt catalyst: Theoretical insights into the reaction kinetics and mechanism for catalyst deactivation, *Appl. Catal. B Environ.*, 270, 118859-118867 (2020).

[70] S. Arora, R. Prasad, An overview on dry reforming of methane: strategies to reduce carbonaceous deactivation of catalysts, *RSC Adv.*, 6, 108668-108688 (2016).

[71] N. Kumar, M. Shojaee, J. Spivey, Catalytic bi-reforming of methane: from greenhouse gases to syngas, *Curr. Opin. Chem. Eng.*, 9, 8-15 (2015).

[72] S. Kawi, Y. Kathiraser, J. Ni, U. Oemar, Z. Li, E.T. Saw, Progress in synthesis of highly active and stable nickel-based catalysts for carbon dioxide reforming of methane, *ChemSusChem*, 8, 3556-75 (2015).

[73] A. T. Ashcroft, A. K. Cheetham, MLH. Green, PDF. Vernon, Partial oxidation of methane to synthesis gas using carbon dioxide, *Nat.*, 3525,225-226 (1991).

[74] PDF. Vernon, MLH. Green, AK. Cheetham, AT. Ashcroft, Partial oxidation of methane to synthesis gas and carbon dioxide as an oxidising agent for methane conversion, *Catal. Today*, 13,

417-426 (1992).

[75] A. Moral, I. Reyero, C. Alfaro, F. Bimbela, L.M. Gandia, Syngas production by means of biogas catalytic partial oxidation and dry reforming using Rh-based catalysts, *Catal. Today*, 299, 280-288 (2017).

[76] T. V. Choudhary, V. R. Choudhary, Energy-efficient syngas production through catalytic oxy-methane reforming reactions, *Angew. Chem. Int. Ed.*, 47,1828-1847 (2008).

[77] M. Li, A. C. van Veen, Coupled reforming of methane to syngas ($2H_2$-CO) over Mg-Al oxide supported Ni catalyst, *Appl. Catal. A Gen.*, 550,176-183 (2018).

[78] J. Guo, Z. Hou, J. Gao J, X. Zheng, Syngas production via combined oxy-CO_2 reforming of methane over Gd_2O_3-modified Ni/SiO_2 catalysts in a fluidized-bed reactor, *Fuel*, 87, 1348-1354 (2008).

[79] J. Shen, A. A. C. Reule, N. Semagina, Ni/$MgAl_2O_4$ catalyst for low-temperature oxidative dry methane reforming with CO_2, *Int. J. Hydrogen Energy*, 44, 4616-4629 (2019).

[80] P. Wang, L. Jin, H. Hu, CO_2 Reforming of Methane over Fe-Modified Ni-Based Catalyst for Syngas Production, *Energy Technol.*, 8, 1900231 (2020).

[81] S. Sepehri, M. Rezaei, Y. Wang, A. Younesi, H. Arandiyan, The evaluation of autothermal methane reforming for hydrogen production over Ni/CeO_2 catalysts, *Int. J. Hydrogen Energy*, 43, 22340-22346 (2018).

[82] S. Ayabe, H. Omoto, T. Utaka, R. Kikuchi, K. Sasaki, Y. Teraoka, K. Eguchi, Catalytic autothermal reforming of methane and propane over supported metal catalysts, *Appl. Catal. A Gen.*, 241, 261-269 (2003).

[83] D. J. Moon, K. Steekumar, S. D. Lee, B. G. Lee, H. S. Kim, *Appl. Catal. A Gen.*, 215, 1 (2001).

[84] E. V. Matus, I. Z. Ismagilov, S. A. Yashnik, V. A. Ushakov, I. P. Prosvirin, M. A. Kerzhentsev, Z. R. Ismagilov, Hydrogen production through autothermal reforming of CH_4: Efficiency and action mode of noble (M= Pt, Pd) and non-noble (M= Re, Mo, Sn) metal additives in the composition of Ni-M/$Ce_{0.5}Zr_{0.5}O_2$/Al_2O_3 catalysts, *Int. J. Hydrogen Energy*, 45, 33352-33369 (2020).

[85] A. Majewski, J. Wood, Tri-reforming of methane over Ni@SiO_2 catalyst, *Int. J. Hydrogen Energy*, 39, 12578-12585 (2014).

[86] A. V. P. Lino, E. M. Assaf, J. M. Assaf, Adjusting Process Variables in Methane Tri-reforming to Achieve Suitable Syngas Quality and Low Coke Deposition, *Energy Fuels*, 34, 16522-16531 (2020).

[87] M. Usman, W. M. A. W. Daud, H. F. Abbas, Dry reforming of methane: influence of process parameters: a review, *Renew. Sust. Energ. Rev.*, 45, 710-744 (2015).

[88] M. A. Goula, N. D. Charisiou, G. Siakavelas, L. Tzounis, I. Tsiaoussis, P. Panagiotopoulou, G. Goula, I. V. Yentekakis, Syngas production via the biogas dry reforming reaction over Ni supported on zirconia modified with CeO_2 or La_2O_3 catalysts, *Int. J. Hydrogen Energy*, 42, 13724-13740 (2017).

[89] Z. Zhang, X. E. Verykios, Carbon dioxide reforming of methane to synthesis gas over supported Ni catalysts, *Catal. Today*, 21, 589-595 (1994).

[90] M. K. Nikoo, N. A. S. Amin, Thermodynamic analysis of carbon dioxide reforming of methane in view of solid carbon formation, *Fuel Process. Technol.*, 92, 678-91 (2011).

[91] Z. Lian, S. O. Olanrele, C. Si, M. Yang, B. Li, Critical Role of Interfacial Sites between Nickel and CeO_2 Support in Dry Reforming of Methane: Revisit of Reaction Mechanism and Origin of Stability, *J. Phys. Chem. C*, 124, 5118-5124 (2020).

[92] X. Yan, T. Hu, P. Liu, S. Li, B. Zhao, Q. Zhang, L. Fan, Highly efficient and stable Ni/CeO_2-SiO_2 catalyst for dry reforming of methane: Effect of interfacial structure of Ni/CeO_2 on SiO_2, *Appl. Catal. B Environ.*, 246, 221-231 (2019).

[93] W. Tu, M. Ghoussoub, C. V. Singh, Y.H. C. Chin, Consequences of Surface Oxophilicity of Ni, Ni-Co, and Co Clusters on Methane Activation, *J. Am. Chem. Soc.*, 139, 6928-6945 (2017).

[94] L. B. Sun, X. Q. Liu, H. C. Zhou, Design and fabrication of mesoporous heterogeneous basic catalysts, *Chem. Soc. Rev.*, 44, 5092-5147 (2015).

[95] B. O. Nielsen, A. C. Luntz, P. M. Holmblad, I. Chorkendorff, Activated dissociative chemisorption of methane on Ni(100): a direct mechanism under thermal conditions, *Catal. Lett.*, 32, 15-30 (1995).

[96] H. Huang, Y. Yu, M. Zhang, Mechanistic insight into methane dry reforming over cobalt: a density functional theory study, *Phys. Chem. Chem. Phys.*, 22, 27320 (2020).

[97] C. Fan, Y. A. Zhu, M. L. Yang, Z. J. Sui, X. G. Zhou, D. Chen, Density Functional Theory-Assisted Microkinetic Analysis of Methane Dry Reforming on Ni Catalyst, *J. Phys. Chem. B*, 110, 9976-9983 (2006).

[98] P. Ferreira-Aparicio, I. Rodriguez-Ramos, J. A. Anderson, A. Guerrero-Ruiz, *Appl. Catal. A Gen.*, 202, 183-196 (2000).

[99] P. Ferreira-Aparicio, I. Rodriguez-Ramos, J. A. Anderson, A. Guerrero-Ruiz, Mechanistic aspects of the dry reforming of methane over ruthenium catalysts, *Appl. Catal. A Gen.*, 202, 183-196 (2000).

[100] P. Djinovic, J. Batista, A. Pintar, Efficient catalytic abatement of greenhouse gases: Methane reforming with CO_2 using a novel and thermally stable Rh-CeO_2 catalyst, *Int. J. Hydrogen Energy*, 37, 2699-2707 (2012).

[101] B. Bachiller-Baeza, C. Mateos-Pedrero, M. A. Soria, A. Guerrero-Ruiz, U. Rodemerck, I. Rodríguez-Ramos, Transient studies of low-temperature dry reforming of methane over Ni-CaO/ZrO_2-La_2O_3, *Appl. Catal. B Environ.*, 129, 450-459 (2013).

[102] D. Papurello, C. Soukoulis, L. Cappellin, S. Silvestri, M. Santarelli, F. Biasioli, Monitoring of volatile compound emission during dry anaerobic digestion of organic fraction of municipal solid waste by PTR-ToF-MS, *Bioresour Technol.*, 126, 254-65 (2012).

[103] P. K. Yadav, T. Das, P. Mondal, Effect of the magnesia and alumina in the modified-supported perovskite-type catalysts for the dry reforming of methane, *Fuel*, 302, 121233 (2021).

[104] E. le Saché, A. A. Moreno, T. R. Reina, Biogas Conversion to Syngas Using Advanced Ni-Promoted Pyrochlore Catalysts: Effect of the CH_4/CO_2 Ratio, *Front. Chem.*, 9, 672319 (2021).

[105] S. Rattanaphan, T. Rungrotmongkol, P. Kongsune, Biogas improving by adsorption of CO_2 on modified waste tea activated carbon, *Renew. Energ*., 145, 622-631 (2020).

[106] L. Jin, B. Ma, S. Zhao, X. He, Y. Li, H. Hu, Z. Lei, Ni/MgO-Al_2O_3 catalyst derived from modified [Ni, Mg, Al]-LDH with NaOH for CO_2 reforming of methane, *Int. J. Hydrogen Energy*, 43, 2689-2698 (2018).

[107] C. Wang, N. Sun, N. Zhao, W. Wei, Y. Sun, C. Sun, H. Liu, C. E. Snape, Coking and deactivation of a mesoporous Ni-CaO-ZrO_2 catalyst in dry reforming of methane: A study under different feeding compositions, *Fuel*, 143, 527-535 (2015).

[108] S. Yasyerli, S. Filizgok, H. Arbag, N. Yasyerly, G. Dogu, Ru incorporated Ni-MCM-41 mesoporous catalysts for dry reforming of methane: effects of Mg addition, feed composition and temperature, *Int. J. Hydrogen Energy*, 36, 4863-74 (2011).

[109] A. Serrano-Lotina, L. Daza, Influence of the operating parameters over dry reforming of methane to syngas, *Int. J. Hydrogen Energy*, 39, 4089-4094 (2014).

[110] H. O. Seo, Recent Scientific Progress on Developing Supported Ni Catalysts for Dry (CO_2) Reforming of Methane, *Catalysts*, 8, 110-127 (2018).

[111] S. Li, J. Gong, Strategies for improving the performance and stability of Ni-based catalysts for reforming reactions, *Chem. Soc. Rev.*, 43, 7245-7256 (2014).

[112] A. Abdulrasheed, A. A. Jalil, Y. Gambo, M. Ibrahim, H. U. Hambali, M. Y. S. Hamid, A review on catalyst development for dry reforming of methane to syngas: Recent advances, *Renew. Sust. Energ. Rev.*, 108, 175-193 (2019).

[113] Y. Gao, J. Jiang, Y. Meng, F. Yan, A. Aihemaiti, A review of recent developments in hydrogen production via biogas dry reforming, *Energ. Convers. Manage.*, 171, 133-155 (2018).

[114] K, Bu, J, Deng, X. Zhang, S. Kuboon, T. Yan, H. Li, L. Shi, D. Zhang, Promotional effects of B-terminated defective edges of Ni/boron nitride catalysts for coking- and sintering-resistant dry reforming of methane, *Appl. Catal. B Environ.*, 267, 118692 (2020).

[115] M. Li, A. C. van Veen, Tuning the catalytic performance of Ni-catalysed dry reforming of methane and carbon deposition via Ni-CeO_{2-x} interaction, *Appl. Catal. B Environ.*, 237, 641-648 (2018).

[116] E. Akbari, S. M. Alavi, M. Rezaei, Synthesis gas production over highly active and stable nanostructured Ni-MgO-Al_2O_3 catalysts in dry reforming of methane: Effects of Ni contents, *Fuel*, 194, 171-179 (2017).

[117] D. Han, Y. Kim, W. Cho, Y. Baek, Effect of Oxidants on Syngas Synthesis from Biogas over 3 wt % Ni-Ce-MgO-ZrO_2/Al_2O_3 Catalyst, *Energies*, 13, 297 (2020).

[118] R. Debek, M. Motak, M. E. Galvez, T. Grzybek, P. D. Costa, Promotion effect of zirconia on Mg(Ni,Al)O mixed oxides derived from hydrotalcites in CO_2 methane reforming, *Appl. Catal. B Environ.*, 243, 36-46 (2018).

[119] E. le Sache, L. Pastor-Perez, D. Watson, A. Sepulveda-Escribano, T. R. Reina, Ni stabilised on inorganic complex structures: superior catalysts for chemical CO_2 recycling via dry reforming of methane, *Appl. Catal. B Environ.*, 236, 458-465 (2018).

[120] T. Zhang, Z. Liu, Y. Zhu, Z. Liu, Z. Sui, K. Zhu, X. Zhou, Dry Reforming of Methane on Ni-Fe-MgO Catalysts: influence of Fe on carbon-resistant property and kinetics, *Appl. Catal. B Environ.*, 264, 118497 (2020).

[121] M. Zhanga, J. Zhang, Z. Zhoua, Shu. Chen, T. Zhang, F. Song, Q. Zhang, N. Tsubaki, Y. Tan, Y. Han, Effects of the surface adsorbed oxygen species tuned by rare-earth metal doping on dry reforming of methane over Ni/ZrO_2 catalyst, *Appl. Catal. B Environ.*, 264, 118522 (2020).

[122] K. Bu, S. Kuboon, J. Deng, H. Li, T. Yan, G. Chen, L. Shi, D. Zhang, Methane dry reforming over boron nitride interface-confined and LDHs-derived Ni catalysts, *Appl. Catal. B Environ.*, 252, 86-97 (2019).

[123] S. Dama, S. R. Ghodke, R. Bobade, H. R. Gurav, S. Chilukuri, Active and durable alkaline earth metal substituted perovskite catalysts for dry reforming of methane, *Appl. Catal. B Environ.*, 224, 146-158 (2018).

[124] V. Danghyan, S. C. Novoa, A. Mukasyan, E. E. Wolf, Pressure dilution, a new method to prepare a stable Ni/fumed silica catalyst for the dry reforming of methane, *Appl. Catal. B Environ.*, 234, 178-186 (2018).

[125] V. Danghyan, A. Kumar, A. Mukasyan, E. E. Wol, An active and stable NiOMgO solid solution based catalysts prepared by paper assisted combustion synthesis for the dry reforming of methane, *Appl. Catal. B Environ.*, 273, 119056 (2020).

[126] J. Dou, R. Zhang, X. Hao, Z. Bao, T. Wu, B. Wang, F. Yu, Sandwiched SiO_2@Ni@ZrO_2 as a coke resistant nanocatalyst for dry reforming of methane, *Appl. Catal. B Environ.*, 254, 612-623 (2019).

[127] J. Hu, V. V. Galvita, H. Poelman, C. Detavernier, G. B. Marin, Pressure-induced deactivation of core-shell nanomaterials for catalystassisted chemical looping, *Appl. Catal. B Environ.*, 247, 86-99 (2019).

[128] J. Huang, Y. Yan, S. Saqline, W. Liu, B. Liu, High performance Ni catalysts prepared by freeze drying for efficient dry reforming of methane, *Appl. Catal. B Environ.*, 275, 119109 (2020).

[129] M. Zhang, J. Zhang, Y. Wu, J. Pan, Q. Zhang, Y. Tan, Y. Han, Insight into the effects of the oxygen species over Ni/ZrO_2 catalyst surface on methane reforming with carbon dioxide, *Appl. Catal. B Environ.*, 244, 427-437 (2019).

[130] X. Zhang, L. Zhang, H. Peng, X. You, C. Peng, X. Xu, W. Liu, X. Fang, Z. Wang, N. Zhang, X. Wang, Nickel nanoparticles embedded in mesopores of AlSBA-15 with a perfect peasecod-like structure: A catalyst with superior sintering resistance and hydrothermal stability for methane dry

reforming, *Appl. Catal. B Environ.*, 224, 488-488 (2019).

[131] H. Wang, X. Dong, T. Zhao, H. Yu, M. Li, Dry reforming of methane over bimetallic Ni-Co catalyst prepared from $La(Co_xNi_{1-x})_{0.5}Fe_{0.5}O_3$ perovskite precursor: Catalytic activity and coking Resistance, *Appl. Catal. B Environ.*, 245, 302-313 (2019).

[132] A. P. Tathod, N. Hayek, D. Shpasser, D. S. A. Simakov, O. M. Gazit, Mediating interaction strength between nickel and zirconia using a mixed oxide nanosheets interlayer for methane dry reforming, *Appl. Catal. B Environ.*, 249, 106-115 (2019).

[133] Z. Y. Lim, X. Ma, B. Chen, Enhanced porosity of Ni@HSZ for dry reforming of methane, *New J. Chem.*, 44, 1707-1710 (2020).

[134] A. S. Al-Fatesh, Y. Arafat, S. O. Kasim, A. A. Ibrahim, A. E. Abasaeed, A. H. Fakeeha, In situ auto-gasification of coke deposits over a novel Ni-Ce/W-Zr catalyst by T sequential generation of oxygen vacancies for remarkably stable syngas production via CO_2-reforming of methane, *Appl. Catal. B Environ.*, 280, 119445 (2021).

[135] G. Deng, G. Zhang, X. Zhu, Q. Guo, X. Liao, X. Chen, K. Lia, Optimized Ni-based catalysts for methane reforming with O_2-containing CO_2, *Appl. Catal. B Environ.*, 289, 120033 (2021).

[136] M. Shah, S. Das, A. K. Nayak, P. Mondal, A. Bordoloi, Smart designing of metal-support interface for imperishable dry reforming catalyst, *Appl. Catal. A Gen.*, 556, 137-154 (2018).

[137] S. Das, A. Jangam, S. Jayaprakash, S. Xi, K. Hidajat, K. Tomishige, S. Kawi, Role of lattice oxygen in methane activation on Ni-phyllosilicate@$Ce_{1-x}Zr_xO_2$ core-shell catalyst for methane dry reforming: Zr doping effect, mechanism, and kinetic study, *Appl. Catal. B Environ.*, 290, 119998 (2021).

[138] L. Azancot, L. F. Bobadilla, M. A. Centeno, J. A. Odriozola, IR spectroscopic insights into the coking-resistance effect of potassium on nickel-based catalyst during dry reforming of methane, *Appl. Catal. B Environ.*, 285, 119822 (2021).

[139] J. Dou, Z. Bao, F. Yu, Mesoporous $Ni(OH)_2$/$CeNi_xO_y$ Composites Derived Ni/$CeNi_xO_y$ Catalysts for Dry Reforming of Methane, *ChemCatChem*, 10, 250-258 (2018).

[140] K. Swirk, M. Rønning, M. Motak, T. Grzybek, P. Da Costa, Synthesis strategies of Zr- and Y-promoted mixed oxides derived from double-layered hydroxides for syngas production via dry reforming of methane, *Int. J Hydrogen Energy*, 46, 12128-12144 (2021).

[141] S. M. Mousavi, F. Meshkani, M. Rezaei, Preparation of mesoporous nanocrystalline 10% Ni/$Ce_{1-x}Mn_xO_2$ catalysts for dry reforming reaction, *Int. J Hydrogen Energy*, 42, 24776-24784 (2017).

[142] W. Kong, Y. Fu, L. Shi, S. Li, E. Vovk, X. Zhou, R. Si, B. Pan, C. Yuan, S. Li, F. Cai, H. Zhu, J. Zhang, Y. Yang, Y. Sun, Nickel nanoparticles with interfacial confinement mimic noble metal catalyst in methane dry reforming, *Appl. Catal. B Environ.*, 285, 119873 (2021).

[143] R. D. Barbosa, M. A. S. Baldanza, N. Solange de Resende, F. B. Passos, V. L. S. Teixeira da Silva, Nickel-Promoted Molybdenum or Tungsten Carbides as Catalysts in Dry Reforming of Methane: Effects of Variation in CH_4/CO_2 Molar Ratio, Catalysis Letters, 151, 1578-1591 (2021).

[144] D. L. Serrano-Lotina A, Influence of the operating parameters over dry reforming of methane to syngas, *Int. J Hydrogen Energy*, 39, 4089-94 (2013).

[145] I. V. Yentekakis, G. Goula, M. Hatzisymeon, I. B. Argyropoulou, G. Botzolaki, K. Kousi, D. I. Kondarides, M. J. Taylor, C. M. A. Parlett, A. Osatiashtiani, G. Kyriakou, J. P. Holgado, R. M. Lambert, Effect of support oxygen storage capacity on the catalytic performance of Rh nanoparticles for CO_2 reforming of methane, *Appl. Catal. B Environ.*, 243, 490-501 (2019).

[146] H. Zhou, T. Zhang, Z. Sui, Y. Zhu, C. Han, K. Zhu, X. Zhou, A single source method to generate Ru-Ni-MgO catalysts for methane dry reforming and the kinetic effect of Ru on carbon deposition and gasification, *Appl. Catal. B Environ.*, 233, 143-159 (2018).

[147] J. A. Mendoza-Nieto, S. Tehuacanero-Cuapa, J. Arenas-Alatorre, H. Pfeiffer, Nickel-doped sodium zirconate catalysts for carbon dioxide storage and hydrogen production through dry methane reforming process, *Appl. Catal. B Environ.*, 22, 480-87 (2018).

[148] S. Dama, S. R. Ghodke, R. Bobade, H. R. Gurav, S. Chilukuri, Active and durable alkaline earth metal substituted perovskite catalysts for dry reforming of methane, *Appl. Catal. B Environ.*, 224, 146-158 (2018).

[149] M. Zhang, J. Zhang, Y. Wu, J. Pan, Q. Zhang, Y. Tan, Y. Han, Insight into the effects of the oxygen species over Ni/ZrO_2 catalyst surface on methane reforming with carbon dioxide, *Appl. Catal. B Environ.*, 244, 427-437 (2019).

[150] L. Pino, C. Italiano, A. Vita, M. Laganà, V. Recupero, $Ce_{0.70}La_{0.20}Ni_{0.10}O_{2-\delta}$ catalyst for methane dry reforming: Influence of reduction temperature on the catalytic activity and stability, *Appl. Catal. B Environ.*, 218, 779-792 (2017).

[151] Z. Shang, S. Li, L. Li, G. Liu, X. Liang, Highly active and stable alumina supported nickel nanoparticle catalysts for dry reforming of methane, *Appl. Catal. B Environ.*, 201, 302-309 (2017).

[152] H. Dai, P. Yu, H. Liu, S. Xiong, X. Xiao, J. Deng, L. Huang, Ni-Based catalysts supported on natural clay of attapulgite applied in the dry reforming of methane reaction, *New J. Chem.*, 44, 16101 (2020).

[153] H. A. Lara-Garcfia, D. G. Araiza, M. Mendez-Galvan, S. Tehuacanero-Cuapa, A. Gomez-Cortes, G. Diaz, Dry reforming of methane over nickel supported on Nd-ceria: enhancement of the catalytic properties and coke resistance, *RSC Adv.*,10, 33059 (2020).

[154] O. E. Samrout, L. Karam, K. Jabbour, P. Massiani, F. Launay, N. E. Hassan, Investigation of new routes for the preparation of mesoporous calcium oxide supported nickel materials used as catalysts for the methane dry reforming reaction, *Catal. Sci. Technol.*, 10, 6910-6922 (2020).

[155] I. V. Yentekakis, G. Goula, M. Hatzisymeon, I. Betsi-Argyropoulou, G. Botzolaki, K. Kousi, G. Kyriakou, Effect of support oxygen storage capacity on the catalytic performance of Rh

nanoparticles for CO_2 reforming of methane, *Appl. Catal. B Environ.*, 243, 490-501 (2019).

[156] L. Foppa, T. Margossian, S. M. Kim, C. Müller, C. Copéret, K. Larmier, A. ComasVives, Contrasting the role of Ni/Al_2O_3 interfaces in water-gas shift and dry reforming of methane, *J. Am. Chem. Soc.*, 139, 17128-17139 (2017).

[157] M. A. A. Aziz, A. A. Jalil, S. Wongsakulphasatch, Dai-Viet N. Vo, Understanding the role of surface basic sites of catalysts in CO_2 activation in dry reforming of methane: a short review, *Catal. Sci. Technol.*, 10, 35-45 (2020).

[158] T. Odedairo, J. L. Chen, Z. H. Zhu, Metal-support interface of a novel $Ni\text{-}CeO_2$ catalyst for dry reforming of methane, *Catal. Commun.*, 31, 25-31 (2013).

[159] X. Yan, T. Hu, P. Liu, S. Li, B. Zhao, Q. Zhang, L. Fan, Highly efficient and stable $Ni/CeO_2\text{-}SiO_2$ catalyst for dry reforming of methane: Effect of interfacial structure of Ni/CeO_2 on SiO_2, *Appl. Catal. B Environ.*, 246, 221-231 (2019).

[160] A. S. Ivanova, Physicochemical and catalytic properties of systems based on CeO_2, *Kinet. Catal.*, 50, 797-815 (2009).

[161] E. C. Faria, R. C. R. Neto, R. C. Colman, F. B. Noronha, Hydrogen production through CO_2 reforming of methane over $Ni/CeZrO_2/Al_2O_3$ catalysts, *Catal. Today*, 228, 138-144 (2014).

[162] P. H. Tu, D. N. Le, T. D. Dao, Q. T. Tran, T. C. D. Doan, Y. Shiratori, C. M. Dang, Paper-structured catalyst containing CeO_2-Ni flowers for dry reforming of methane, *Int. J. Hydrogen Energy*, 45, 18363-18375 (2020).

[163] A. L. A. Marinho, R. C. Rabelo-Neto, F. Epron, N. Bion, F. S. Toniolo, F. B. Noronha, Embedded Ni nanoparticles in $CeZrO_2$ as stable catalyst for dry reforming of methane, *Appl. Catal. B Environ.*, 268, 118387 (2020).

[164] N. Wang, Z. Xu, J. Deng, K. Shen, X. Yu, W. Qian, W. Chu, F. Wei, One-pot synthesis of ordered mesoporous niceal oxide catalysts and a study of their performance in methane dry reforming, *ChemCatChem*, 6, 1470-1480 (2014).

[165] R. Dębek, M. Motak, D. Duraczyska, F. Launay, M. E. Galvez, T. Grzybek, and P. Da Costa, Methane dry reforming over hydrotalcite-derived Ni-Mg-Al mixed oxides: the influence of Ni content on catalytic activity, selectivity and stability, *Catal. Sci. Technol.*, 1, 192-208 (2016).

[166] H. Wang, N. V. Srinath, H. Poelman, C. Detavernier, P. Li, G. B. Marin, V. V. Galvita, Hierarchical Fe-modified $MgAl_2O_4$ as a Ni-catalyst support for methane dry reforming, *Catal. Sci. Technol.*, 10, 6987-7001 (2020).

[167] K. Tanabe, Surface and catalytic properties of ZrO_2, *Mater. Chem. Phys.*, 13, 347-364 (1985).

[168] Y. Lou, M. Steib, Q. Zhang, K. Tiefenbacher, A. Horváth, A. Jentys, Y. Liu, J. A. Lercher, Design of stable Ni/ZrO_2 catalysts for dry reforming of methane, *J. Catal.*, 356, 147-156 (2017).

[169] D. Liu, X. Y. Quek, W. N. E. Cheo, R. Lau, A. Borgna, Y. Yang, MCM-41 supported nickel-based bimetallic catalysts with superior stability during carbon dioxide reforming of methane: Effect of strong metal-support interaction, *J. Catal.*, 266, 380-390 (2009).

[170] H. Wu, G. Pantaleo, V. La Parola, A. M. Venezia, X. Collard, C. Aprile, and L. F. Liotta, Bi- and trimetallic Ni catalysts over Al_2O_3 and Al_2O_3-MO_x (M=Ce or Mg) oxides for methane dry reforming: Au and Pt additive effects, *Appl. Catal. B Environ.*, 156, 350-361 (2014).

[171] M. B. Bahari, H. D. Setiabudi, T. D. Nguyen, P. T. T. Phuong, Q. D. Truong, A. A. Jalil, N. Ainirazali, D.-V. N. Vo, Insight into the influence of rare-earth promoter (CeO_2, La_2O_3, Y_2O_3, and Sm_2O_3) addition toward methane dry reforming over Co/mesoporous alumina catalysts, *Chem. Eng. Sci.*, 228, 115967 (2020).

[172] R. O. da Fonseca, R. C. Rabelo-Neto, R. C. C. Simoes, L.V. Mattos, F. B. Noronha, Pt supported on doped CeO_2/Al_2O_3 as catalyst for dry reforming of methane, *Int. J. Hydrogen Energy*, 45, 5182-5191 (2020).

[173] Y. Turap, I. Wang, T. Fu, Y. Wu, Y. Wang, W. Wang, Co-Ni alloy supported on CeO_2 as a bimetallic catalyst for dry reforming of methane, *Int. J. Hydrogen Energy*, 45, 6538-6548 (2020).

[174] T. Y. Liang, H. H. Chen, D. H. Tsai, Nickel hybrid nanoparticle decorating on alumina nanoparticle cluster for synergistic catalysis of methane dry reforming, *Fuel Process. Technol.*, 201, 106335 (2020).

[175] A. Jawad, F. Rezaei, A. A. Rownaghi, Highly efficient Pt/Mo-Fe/Ni-based Al_2O_3-CeO_2 catalysts for dry reforming of methane, *Catal. Today*, 350, 80-90 (2020).

[176] D. Guo, Y. Lu, Y. Ruan, Y. Zhao, Y. Zhao, S. Wang, X. Ma, Effects of extrinsic defects originating from the interfacial reaction of CeO_{2-x}-nickel silicate on catalytic performance in methane dry reforming, *Appl. Catal. B Environ.*, 277, 119278-119292 (2020).

[177] S. P. Padi, L. Shelly, E. P. Komarala, D. Schweke, S. Hayun, B. A. Rosen, Coke-free methane dry reforming over nano-sized NiO-CeO_2 solid solution after exsolution, *Catal. Commun.*, 138, 105951 (2020).

[178] H. Wang, B. Zhao, L. Qin, Y. Wang, F. Yu, J. Han, Non-thermal plasma-enhanced dry reforming of methane and CO_2 over Ce-promoted Ni/C catalysts, *Mol. Catal.*, 485, 110821 (2020).

[179] B. M. A. Swai, N. B. Osman, A. Ramli, B. Abdullah, A. S. Farooqi, B. V. Ayodele, D. O. Patrick, Low-temperature catalytic conversion of greenhouse gases (CO_2 and CH_4) to syngas over ceria-magnesia mixed oxide supported nickel catalysts, *Int. J. Hydrogen Energy*, 46, 24768-24780 (2021).

[180] S. Damyanova, B. Pawelec, R. Palcheva, Y. Karakirova, M. C. C. Sanchez, G. Tyuliev, E. Gaigneaux, J. L. G. Fierro, Structure and surface properties of ceria-modified Ni-based catalysts for hydrogen production, *Appl. Catal. B Environ.*, 225, 340-353 (2018).

[181] M. Lu, X. Zhang, J. Deng, S. Kuboon, K. Faungnawakij, S. Xiao, D. Zhang, Coking-resistant dry reforming of methane over BN-nanoceria interface-confined Ni catalysts, *Catal. Sci. Technol.*, 10, 4237-4244 (2020).

[182] D. Shen, M. Huo, L. Li, S. Lyu, J. Wang, X. Wang, Y. Zhang, J. L, Effects of alumina morphology on dry reforming of methane over Ni/Al_2O_3 catalysts, *Catal. Sci. Technol.*, 10, 510-516

(2020).

[183] Q. L. M. Ha, H. Lund, C. Kreyenschulte, S. Bartling, H. Atia, T. H. Vuong, S. Wohlrab, U. Armbruster, Development of Highly Stable Low Ni Content Catalyst for Dry Reforming of CH_4-Rich Feedstocks, *ChemCatChem*, 12, 1562-1568 (2020).

[184] B. R. de Vasconcelos, D. P. Minh, E. Martins, A. Germeau, P. Sharrock, A. Nzihou, A Comparative Study of Hydroxyapatiteand Alumina-Based Catalysts in Dry Reforming of Methane, *Chem. Eng. Technol.*, 43, 698-704 (2020).

[185] B. Jin, Z. Shang, S. Li, Y. Jiang, X. Gud, X. Liang, Reforming of methane with carbon dioxide over cerium oxide promoted nickel nanoparticles deposited on 4-channel hollow fibers by atomic layer deposition, *Catal. Sci. Technol.*, 10, 3212-3222 (2020).

[186] J. Wang, Y. Fu, W. Kong, F. Jin, J. Bai, J. Zhang, Y. Sun, Design of a carbon-resistant Ni@S-2 reforming catalyst: Controllable Ni nanoparticles sandwiched in a peasecod-like structure, *Appl. Catal. B Environ.*, 282, 119546 (2021).

[187] A. L. A. Marinho, F. S. Toniolo, F. B. Noronha, F. Epron, D. Duprez, N. Bion, Highly active and stable Ni dispersed on mesoporous CeO_2-Al_2O_3 catalysts for production of syngas by dry reforming of methane, *Appl. Catal. B Environ.*, 281, 119459 (2021).

[188] C. Bartholomew, M. Argyle, Advances in catalyst deactivation and regeneration, Catalysts, 5, 949-954 (2015).

[189] N.E. Tsakoumis, M. Rønning, Ø. Borg, E. Rytter, A. Holmen, Deactivation of cobalt based Fischer-Tropsch catalysts: a review, *Catal. Today*, 154, 162-182 (2010).

[190] M. A. Álvarez, L. F. Bobadilla, V. Garcilaso, M. A. Centeno, J. A. Odriozola, CO_2 reforming of methane over Ni-Ru supported catalysts: on the nature of active sites by operando DRIFTS study, *J CO_2 Util.*, 24, 509-15 (2018).

[191] N. Wang, Z. Xu, J. Deng, K. Shen, X. Yu, W. Qian, One-pot synthesis of ordered mesoporous NiCeAl oxide catalysts and a study of their performance in methane dry reforming, *ChemCatChem*, 6, 1470-80 (2014).

[192] U. Guharoy, E. Le Saché, Q. Cai, T. R. Reina, S. Gu, Understanding the role of Ni-Sn interaction to design highly effective CO_2 conversion catalysts for dry reforming of methane, *J CO_2 Util.*, 27, 1-10 (2018).

[193] M. Muraleedharan Nair, S. KaliaguinE, Structured catalysts for dry reforming of methane, *New J Chem*., 40, 4049-60 (2016).

[194] O. Muraza, A. Galadima, A review on coke management during dry reforming of methane, *Int. J. Energy Res*., 39, 1196-216 (2015).

[195] M. Tang, L. Xu, M. Fan, Progress in oxygen carrier development of methane-based chemical-looping reforming: a review, *Appl. Energy*, 151, 143-56 (2015).

[196] Y. Wang, L. Yao, S. Wang, D. Mao, C. Hu, Low-temperature catalytic CO_2 dry reforming of methane on Ni-based catalysts: a review, *Fuel Process. Technol*., 169, 199-206 (2018).

[197] S. Singh, R. Kumar, H. D. Setiabudi, S. Nanda, D. V. N. Vo, Advanced synthesis strategies of mesoporous SBA-15 supported catalysts for catalytic reforming applications: a state-of-the-art review, *Appl. Catal. A Gen*., 559, 57-74 (2018).

[198] S. Pavlova, M. Smirnova, A. Bobin, S. Cherepanova, V. Kaichev, A. Ishchenko, A. Selivanova, V. Rogov, A. Roger, V. Sadykov, Structural, Textural, and Catalytic Properties of Ni-$Ce_xZr_{1-x}O_2$ Catalysts for Methane Dry Reforming Prepared by Continuous Synthesis in Supercritical Isopropanol, *Energies*,13,3728(2020).

[199] H. Zhan, X. Shi, B. Ma, W. Liu, X. Jiao, X. Huang, Facile one-step preparation of ordered mesoporous Ni–M–Al (M = K, Mg, Y, and Ce) oxide catalysts for methane dry reforming, *New J. Chem.*, 43, 12292 (2019).

[200] P. G. Lustemberg, P. J. Ramirez, Z. Y. Liu, R. A. Gutierrez, D. G. Grinter, J. Carrasco, Room-temperature activation of methane and dry-reforming with CO_2 on Ni-CeO_2(111) surfaces: effect of Ce^{3+} sites and metal-support interactions on C-H bond cleavage. *ACS Catal*., 6, 8184-8191 (2016).

[201] Z. Liu, D. C. Grinter, P. G. Lustemberg, T. Nguyen-Phan, Y. Zhou, S. Luo, I. Waluyo, E. J. Crumlin, D. J. Stacchiola, J. Zhou, J. Carrasco, H. F. Busnengo, M. V. Ganduglia-Pirovano, S. D. Senanayake, J. A. Rodriguez, Dry Reforming of Methane on a highly active Ni-CeO_2 Catalyst: Effects of Metal-Support Interactions on C-H Bond Breaking, *Angew. Chem. Int. Ed.*, 55, 7455 -7459 (2016)

[202] S. M. Bhagyaraj, O. S. Oluwafemi, N. Kalarikkal, S. Thomas, Synthesis of inorganic nanomaterials: Advances and key technologies, Woodhead Publishing (2018).

[203] S. Mirzaee, Y. Azizian-Kalandaragh, P. Rahimzadeh, Modified co-precipitation process effects on the structural and magnetic properties of Mn- doped nickel ferrite nanoparticles, *Solid State Sci.*, 99, 106052, (2020).

[204] I. Iglesias, A. Quindimil, F. Mariño, U. De-La-Torre, J. R. González-Velasco, Zr promotion effect in CO_2 methanation over ceria supported nickel catalysts, *Int. J. Hydrogen Energy*, 44, 1710-1719 (2019).

[205] L. Jalowiecki-Duhamel, S. Debeusscher, H. Zarrou, A. D'Huysser, H. Jobic, E. Payen, Hydrogen storage in $CeNi_XO_Y$ and $CeM_{0.5}Ni_XO_Y$ (M= Zr or Al) mixed oxides, *Catal. Today*, 138, 266-271 (2008).

[206] W. Fang, C. Pirez, S. Paul, M. Capron, H. Jobic, F. Dumeignil, L. Jalowiecki-Duhamel, Room Temperature Hydrogen Production from Ethanol over $CeNi_XH_ZO_Y$ Nano-Oxyhydride Catalysts, *ChemCatChem*, 5, 2207-2216 (2013).

[207] I. Kosacki, T. Suzuki, H. U. Anderson, P. Colomban, Raman scattering and lattice defects in nanocrystalline CeO_2 thin films, *Solid State Ion.*, 149, 99-105 (2002).

[208] M. Palard, J. Balencie, A. Maguer, J. F. Hochepied, Effect of hydrothermal ripening on the photoluminescence properties of pure and doped cerium oxide nanoparticles, *Mater. Chem. Phys*., 120, 79-88 (2010).

[209] A. Löfberg, J. Guerrero-Caballero, T. Kane, A. Rubbens, L. Jalowiecki-Duhamel, Ni/CeO_2 based catalysts as oxygen vectors for the chemical looping dry reforming of methane for syngas production, *Appl. Catal. B Environ.*, 212, 159-174 (2017).

[210] N. Paunović, Z. Dohčević-Mitrović, R. Scurtu, S. Aškrabić, M. Prekajski, B. Matović, Z. V. Popović, Suppression of inherent ferromagnetism in Pr-doped CeO_2 nanocrystals, *Nanoscale*, 4, 5469 (2012).

[211] N. D. Charisiou, G. Siakavelas, K. N. Papageridis, A. Baklavaridis, L. Tzounis, D. G. Avraam, M. A. Goula, Syngas production via the biogas dry reforming reaction over nickel supported on modified with CeO_2 and/or La_2O_3 alumina catalysts, *J. Nat. Gas Sci. Eng.*, 31, 164-183 (2016).

[212] B. Payne, M. Biesinger, N. McIntyre, The Study of Polycrystalline Nickel Metal Oxidation by Water Vapour, *J. Electron. Spectrosc. Relat. Phenom*., 175, 55-65 (2009).

[213] B. Jin, Z. Shang, S. Li, Y. B. Jiang, X. Gud, X. Liang, Reforming of methane with carbon dioxide over cerium oxide promoted nickel nanoparticles deposited on 4-channel hollow fibers by atomic layer deposition, *Catal. Sci. Technol.*, 10, 3212-3222 (2020).

[214] M. C. Biesinger, B. P. Payne, L. W. M. Lau, A. Gerson, R. St. C. Smart, X-ray photoelectron spectroscopic chemical state quantification of mixed nickel metal, oxide and hydroxide systems, *Surf. Interface Anal.*, 41, 324-332 (2009).

[215] C. Xian, S. Wang, C. Sun, H. Li, S. Chan, L, Chen, Effect of Ni doping on the catalytic properties of nanostructured peony-like CeO_2, *Chinese J. Catal.*, 34, 305-312 (2013).

[216] Y. Guo, G. Wang, X. Yao, B. Liu, A comparison of NiO-CuO-CeO_2 composite catalysts prepared via different methods for CO oxidation, *J. Solid State Chem.*, 292, 121697 (2020).

[217] L. Jalowiecki-Duhamel, C. Pirez, M. Capron, F. Dumeignil, E. Payen, Hydrogen production from ethanol in presence of water over cerium and nickel mixed oxides, *Catal. Today*, 157, 456-461 (2010).

[218] A. Ponchel, A. D'huysser, C. Lamonier, L. Jalowiecki-duhamel, CeNixOy and CeAlzNixOy solids studied by electron microscopy, XRD, XPS and depth sputtering techniques, *Phys. Chem. Chem. Phys.*, 2, 303-312 (2000).

[219] E. Beche, P. Charvin, D. Perarnau, S. Abanades, G. Flaman, Ce 3d XPS investigation of cerium oxides and mixed cerium oxide (CexTiyOz), *Surf. Interface Anal.*, 40, 264-267(2008).

[220] H. H. Huang, S. W. Yu, C. L. Chuang, C. B. Wang, Application of boron-modified nickel catalysts on the steam reforming of ethanol, *Int. J. Hydrogen Energy*, 39, 20712-20721 (2014).

[221] F. Ju, M. Wang, T. Wu, H. Ling, The Role of NiO in Reactive Adsorption Desulfurization Over NiO/ZnO-Al_2O_3-SiO_2 Adsorbent, *Catalysts*, 9, 79 (2019).

[222] C. E. Figueira, P. F. M. Junior, R. Giudici, R. M. B. Alves, M. Schmal, Nanoparticles of Ce, Sr, Co in and out the multi-walled carbon nanotubes applied for dry reforming of methane, *Appl. Catal. A, Gen.*, 550 297-307 (2018).

[223] B. P. Payne, M. C. Biesinger, N. S. McIntyre, Use of oxygen/nickel ratios in the XPS characterisation of oxide phases on nickel metal and nickel alloy surfaces, *J. Electron Spectros. Relat. Phenomena*, 185, 159-166 (2012).

[224] M. Mansournia, E. Moradinia, β-$Ni(OH)_2$ and NiO nanostructures: novel template-free synthesis and their photocatalytic activity, *J. Mater. Sci. Mater. Electron.*, 27, 82-89 (2016).

[225] J. Yin, G. Zhou, X. Gao, J. Chen, L. Zhang, J. Xu, P. Zhao, F. Gao, α- and β-Phase Ni-Mg Hydroxide for High Performance Hybrid Supercapacitors, *Nanomaterials*, 9, 1686-1699 (2019).

[226] F. Zhang, Z. Liu, X. Chen, N. Rui, L. E. Betancourt, L. Lin, W. Xu, C. Sun, A. M. M. Abeykoon, J. A. Rodriguez, J. Teržan, K. Lorber, P. Djinović, S. D. Senanayake, Effects of Zr Doping into Ceria for the Dry Reforming of Methane over $Ni/CeZrO_2$ Catalysts: In Situ Studies with XRD, XAFS, and AP-XPS, *ACS Catal.*, 10, 3274-3284 (2020).

[227] B. Liu, C. Li, G. Zhang, X. Yao, S. S. C. Chuang, Z. Li, Oxygen vacancy promoting dimethyl carbonate synthesis from CO_2 and methanol over Zr-doped CeO_2 nanorods, *ACS Catal.*, 8, 10446-10456 (2018).

[228] A. Westermann, C. Geantet, P. Vernoux, S. Loridant, Defects band enhanced by resonance Raman effect in praseodymium doped CeO_2, *J.Raman Spectrosc.*, 47, 1276-1279 (2016).

[229] S. Loridant, Raman spectroscopy as a powerful tool to characterize ceria-based catalysts, *Catal. Toda*y, 373, 98-111 (2021).

[230] A. C. Garcia, T. Touzalin, C. Nieuwland, N. Perini, M. T. Koper, Enhancement of oxygen evolution activity of nickel oxyhydroxide by electrolyte alkali cations, *Angew. Chem. Int. Ed.*, 58, 12999-13003 (2019).

[231] F. Wang, Y. Li, T. A. Shifa, K. Liu, F. Wang, Z. Wang, P. Xu, Q. Wang, J. He, Selenium-Enriched Nickel Selenide Nanosheets as a Robust Electrocatalyst for Hydrogen Generation, *Angew. Chem. Int. Ed.*, 55, 6919-6924 (2016).

[232] H. Xu, M. Sun, S. Liu, Y. Li, J. Wang, Y. Chen, Effect of the calcination temperature of cerium-zirconium mixed oxides on the structure and catalytic performance of $WO_3/CeZrO_2$ monolithic catalyst for selective catalytic reduction of NO_x with NH_3, *RSC Adv.*, 7, 24177-24187 (2017).

[233] S. S. Chan, I. E. Wachs, In situ laser Raman spectroscopy of nickel oxide supported on γ-Al_2O_3, *J. Catal.*, 103, 224-227 (1987).

[234] N. Dharmaraj, P. Prabu, S. Nagarajan, C. H. Kim, J. H. Park, H. Y. Kim, Synthesis of nickel oxide nanoparticles using nickel acetate and poly(vinyl acetate) precursor, *Mater. Sci. Eng. B*, 128, 111-114 (2006).

[235] B. M. Reddy, A. Khan, Nanosized CeO_2-SiO_2, CeO_2-TiO_2, and CeO_2-ZrO_2 mixed oxides: influence of supporting oxide on thermal stability and oxygen storage properties of ceria, *Catal. Surv. from Asia*, 9, 155-171 (2005).

[236] B. M. Reddy, A. Khan, Y. Yamada, T. Kobayashi, S. Loridant, J. C. Volta, Raman and X-ray photoelectron spectroscopy study of CeO_2-ZrO_2 and V_2O_5/CeO_2-ZrO_2 catalysts, *Langmuir*, 19, 3025-3030 (2003).

[237] X. Li, X. Li, J. Li, J. Hao, High calcium resistance of CeO_2-WO_3 SCR catalysts: Structure investigation and deactivation analysis, *Chem. Eng. J.*, 317, 70-79 (2017).

[238] N. Weidler, J. Schuch, F. Knaus, P. Stenner, S. Hoch, A. Maljusch, R. Schafer, B. Kaiser, W. Jaegermann, X-ray Photoelectron Spectroscopic Investigation of Plasma Enhanced Chemical Vapor Deposited NiOx, NiOx(OH)y, and CoNiOx(OH)y: Influence of the Chemical Composition on the Catalytic Activity for the Oxygen Evolution Reaction, *J. Phys. Chem. C*, 121, 6455-6463 (2017).

[239] W. Cai, N. Homs, P. R. Piscina, Renewable hydrogen production from oxidative steam reforming of bio-butanol over CoIr/$CeZrO_2$ catalysts: Relationship between catalytic behaviour and catalyst structure, *Appl. Catal. B Environ.*, 150-151, 47-56 (2014).

[240] T. Sukonket, A. Khan, B. Saha, H. Ibrahim, S. Tantayanon, P. Kumar, R. Idem, Influence of the Catalyst Preparation Method, Surfactant Amount, and Steam on CO_2 Reforming of CH_4 over 5Ni/$Ce_{0.6}Zr_{0.4}O_2$ Catalysts, *Energy Fuels*, 25, 864-877 (2011).

[241] S. Liu, J. Liu, Q. Lin, S. Xu, J. Wang, H. Xu, Y. Chen, Solvent Effects on the Low-Temperature NH_3-SCR Activity and Hydrothermal Stability of WO_3/SiO_2@CeZrOx Catalyst, *ACS Sustain. Chem. Eng.*, 8, 13418-13429 (2020).

[242] A. Lamacz, K. Matus, B. Liszka, J. Silvestre-Albero, M. Lafjah, T. Dintzer, I. Janowska, The impact of synthesis method of CNT supported $CeZrO_2$ and Ni-$CeZrO_2$ on catalytic activity in WGS reaction, *Catal. Today*, 301, 172-182 (2018).

[243] C. Li, J. Cheng, Q. Ye, F. Meng, X. Wang, H. Dai, Poisoning Effects of Alkali and Alkaline Earth Metal Doping on Selective Catalytic Reduction of NO with NH_3 over the Nb-Ce/Zr-PILC Catalysts, *Catalysts*, 11, 329 (2021).

[244] A. V. P. Lino, Y. N. Colmenares-Calderon, V. R. Mastelaro, E. M. Assaf, J. M. Assaf, Syngas for Fischer-Tropsch synthesis by methane tri-reforming using nickel supported on $MgAl_2O_4$ promoted with Zr, Ce and Ce-Zr, *Appl. Surf. Sci.*, 481, 747-760 (2019).

[245] B. M. Reddy, G. K. Reddy, I. Ganesh, J. M. F. Ferreira, Microwave-assisted Synthesis and Structural Characterization of Nanosized $Ce_{0.5}Zr_{0.5}O_2$ for CO Oxidation, *Catal. Lett.*, 130, 227-234 (2009).

[246] X. Zhang, X. Fang, X. Feng, X. Li, W. Liu, X. Xu, N. Zhang, Z. Gao, X. Wang, W. Zhou, Ni/$Ln_2Zr_2O_7$ (Ln = La, Pr, Sm and Y) catalysts for methane steam reforming: the effects of A site replacement, *Catal. Sci. Technol.*, 7, 2729-2743 (2017).

[247] M. A.Peck, M. A. Langell, Comparison of nanoscaled and bulk NiO structural and environmental characteristics by XRD, XAFS, and XPS, *Chem. Mater*., 24, 4483-4490 (2012).

[248] P. Burroughs, A. Hamnett, A. F. Orchard, G. Thornton, Satellite structure in the X-ray photoelectron spectra of some binary and mixed oxides of lanthanum and cerium, *J. Chem. Soc*., Dalton Trans, 1686-98 (1976).

[249] A. S. Al-Fatesh, Y. Arafat, S. O. Kasim, A. A. Ibrahim, A. E. Abasaeed, A. H. Fakeeha, In situ auto-gasification of coke deposits over a novel Ni-Ce/W-Zr catalyst by sequential generation of oxygen vacancies for remarkably stable syngas production via CO_2-reforming of methane, *Appl. Catal. B Environ.*, 280, 119445-119456 (2021).

[250] A. V. P. Lino, C. B. Rodella, E. M. Assaf, J. M. Assaf, Methane tri-reforming for synthesis gas production using $Ni/CeZrO_2/MgAl_2O_4$ catalysts: Effect of Zr/Ce molar ratio, *Int. J. Hydrogen Energy*, 45, 8418-8432 (2020).

[251] N. Mahata, A. F. Cunha, J. J. M. Orfao, J. L. Figueiredo, Hydrogenation of nitrobenzene over nickel nanoparticles stabilized by filamentous carbon, *Appl. Catal. A Gen*., 351, 204-209 (2008).

[252] X. Lu, J. He, R. Jing, P. Tao, R. Nie, D. Zhou, Q. Xia, Microwave-activated Ni/carbon catalysts for highly selective hydrogenation of nitrobenzene to cyclohexylamine, *Sci. Rep.*, 7, 2676 (2017).

[253] Q. Ma, L. Guo, Y. Fang, H. Li, J. Zhang, T. Zhao, G. Yang, Y. Yoneyama, N. Tsubaki, Combined methane dry reforming and methane partial oxidization for syngas production over high dispersion Ni based mesoporous catalyst, Fuel Processing Technology, 188 (2019) 98-104.

[254] S. S. Kim, S. M. Lee, J. M. Won, H. J. Yang, S. C. Hong, Effect of Ce/Ti ratio on the catalytic activity and stability of Ni/CeO2-TiO2 catalyst for dry reforming of methane, Chemical Engineering Journal, 280 (2015) 433-440.

[255] Y. Wei, X. Liu, N. Haidar, H. Jobic, S. Paul, L. Jalowiecki-Duhamela, $CeNi_XAl_{0.5}H_ZO_Y$ nano-oxyhydrides for H_2 production by oxidative dry reforming of CH_4 without carbon formation, *Appl. Catal. A Gen*., 594, 117439-117448 (2020).

[256] C. Lamonier, A. Ponchel, A. D'Huysser, L. Jalowiecki- Duhamel, Studies of the cerium-metal-oxygen-hydrogen system (metal= Cu, Ni), *Catal. Today*, 50, 247-259 (1999).

[257] Z. Liu, P. Lustemberg, R. A. Gutiérrez, J. J. Carey, R. M. Palomino, M. Vorokhta, D. C. Grinter, P. J. Ramírez, V. Matolín, M. Nolan, M. V. Ganduglia-Pirovano, S. D. Senanayake, J. A. Rodriguez, In Situ Investigation of Methane Dry Reforming on Metal/Ceria(111) Surfaces: Metal-Support Interactions and C-H Bond Activation at Low Temperature, *Angew. Chem. Int. Ed.*, 56, 13041-13046 (2017).

[258] W. Fang, S. Paul, M. Capron, A. V. Biradar, S. B. Umbarkar, M. K. Dongare, F. Dumeignil, L. Jalowiecki-Duhamel, Highly loaded well dispersed stable Ni species in $Ni_XMg_2AlO_Y$ nanocomposites: Application to hydrogen production from bioethanol, *Appl. Catal. B Environ.*, 166-167, 485-496 (2015).

[259] C. Resini, T. Montanari, L. Barattini, G. Ramis, G. Busca, S. Presto, P. Riani, R. Marazza, M. Sisani, F. Marmottini, U. Costantino, Hydrogen production by ethanol steam reforming over Ni catalysts derived from hydrotalcite-like precursors: Catalyst characterization, catalytic activity and reaction path, *Appl. Catal. A Gen*., 355, 83-93 (2009).

[260] A. Corma, V. Fornés, F. Rey, Hydrotalcites as Base Catalysts: Influence of the Chemical Composition and Synthesis Conditions on the Dehydrogenation of Isopropanol, *J. Catal.*, 148, 205-212 (1994).

[261] W. Fang, S. Paul, M. Capron, F. Dumeignil, L. Jalowiecki-Duhamel, Hydrogen production from bioethanol catalyzed by $Ni_XMg_2AlO_Y$ ex-hydrotalcite catalysts, *Appl. Catal. B Environ.*, 152-153, 370-382 (2014).

[262] A. F. Lucrédio, J. D. A. Bellido, E. M. Assaf, Effects of adding La and Ce to hydrotalcite-type Ni/Mg/Al catalyst precursors on ethanol steam reforming reactions, *Appl. Catal. A Gen*., 388, 77-85 (2010).

[263] M. C. Biesinger, B. P. Payne, L. W. M. Lau, A. Gerson, R. S. C. Smart, X-ray photoelectron spectroscopic chemical state quantification of mixed nickel metal, oxide and hydroxide systems, *Surf. Interface Anal.*, 41 324-332 (2009).

[264] A. P. Grosvenor, M. C. Biesinger, R. S. C. Smart, N. S. McIntyre, New interpretations of XPS spectra of nickel metal and oxides, *Surf. Sci.*, 600, 1771-1779 (2006).

[265] G. Zeng, Q. Liu, R. Gu R, L. Zhang, Y. Li, Synergy effect of MgO and ZnO in a Ni/Mg-Zn-Al catalyst during ethanol steam reforming for H_2-rich gas production, *Catal. Today*, 178, 206-213 (2011).

[266] J. L. Ewbank, L. Kovarik, C. C. Kenvin, C. Sievers, Effect of preparation methods on the performance of Co/Al_2O_3 catalysts for dry reforming of methane, *Green Chem*., 16, 885-896 (2014).

[267] J. L. Ewbank, L. Kovarik, F. Z. Diallo, C. Sievers, Effect of metal-support interactions in Ni/Al_2O_3 catalysts with low metal loading for methane dry reforming, *Appl. Catal. A Gen*., 494 (2015) 57-67.

[268] P. Ferreira-Aparicio, I. Rodríguez-Ramos, J. A. Anderson, A. Guerrero-Ruiz, Mechanistic aspects of the dry reforming of methane over ruthenium catalysts, *Appl. Catal. A Gen.*, 202, 183-196 (2000).

[269] L. P. Teh, H. D. Setiabudi, S. N. Timmiati, M. A. A. Aziz, N. H. R. Annuar, N. N. Ruslan, Recent progress in ceria-based catalysts for the dry reforming of methane: A review, *Chem. Eng. Sci.*, 239, 116606 (2021).

[270] W. Jang, J. Shim, H. Kim, S. Yoo, H. Roh, A review on dry reforming of methane in aspect of catalytic properties, *Catal. Today*, 324, 15-26 (2019).

[271] J. Khatri, A. H. Fakeeha, S. O. Kasim, M. S. Lanre, A. E. Abasaeed, A. A. Ibrahim, R. Kumar, A. S. Al-Fatesh, Ceria promoted phosphate-zirconia supported Ni catalyst for hydrogen rich syngas production through dry reforming of methane, *Int. J Energy Res*., 45, 19289-19302 (2021).

[272] H. Tian, C. Pei, Y. Wu, S. Chen, Z. Zhao, J. Gong, Tunable metal-oxide interaction with balanced Ni^0/Ni^{2+} sites of $Ni_xMg_{1-x}O$ for ethanol steam reforming, *Appl. Catal. B Environ.*, 293, 120178 (2021).

[273] H. Li, J. Wang, Study on CO_2 reforming of methane to syngas over Al_2O_3-ZrO_2 supported Ni catalysts prepared via a direct sol-gel process, *Chem. Eng. Sci.*, 59, 4861-4867 (2004).

[274] J. L. Rogers, M. C. Mangarella, A. D. D'Amico, J. R. Gallagher, M. R. Dutzer, E. Stavitski, J. T. Miller, C. Sievers, Differences in the Nature of Active Sites for Methane Dry Reforming and Methane Steam Reforming over Nickel Aluminate Catalysts, *ACS Catal*., 6, 5873-5886 (2016).

[275] J. Wen, Y. Xie, Y. Ma, H. Sun, H. Wang, M. Liu, Q. Zhang, J. Chen, Engineering of surface properties of Ni-CeZrAl catalysts for dry reforming of methane, *Fuel*, 308, 122008 (2022).

[276] J. Fonseca, N. Bion, Y. E. Licea, C. M. Morais, M. D. C. Rangel, D. Duprez, F. Epron, Unexpected redox behaviour of large surface alumina containing highly dispersed ceria nanoclusters, *Nanoscale*, 11, 1273-1285 (2019).

Production d'hydrogène par reformage à sec de méthane sur catalyseurs au Ni à base de CeO_2, CeO_2 modifiée avec Zr ou Al, et nano-matériaux Mg-Al-O

La demande en hydrogène, en tant que produit chimique et énergie, augmente, mais les principales méthodes de production d'hydrogène ne sont ni durables ni respectueuses de l'environnement. La production d'hydrogène à partir de ressources renouvelables (comme le biogaz composé principalement de CH_4 et de CO_2) est requise. Le reformage à sec du méthane (DRM) est une méthode prometteuse pour produire H_2 et CO à partir des gaz. Dans cette thèse, des catalyseurs à base de Ni, $CeNi_XO_Y$, $CeZr_{0.5}Ni_XO_Y$, $CeAl_{0.5}Ni_XO_Y$, et $AlMg_2Ni_XO_Y$ sont étudiés pour la réaction de reformage à sec du méthane. L'effet de la température de réaction, de la teneur en Ni, du prétraitement in situ sous H_2, de la masse de catalyseur, de la calcination et du rapport CO_2/CH_4 sont analysés. Sur certains composés choisis, des tests de stabilité à long terme sont aussi reportés. L'optimisation des performances catalytiques avec une formation réduite de carbone, sont obtenues sur des catalyseurs partiellement réduits. Diverses méthodes de caractérisation sont utilisées pour analyser les propriétés physico-chimiques des catalyseurs, telles que XRD, Raman, XPS et TPR. Certains catalyseurs sont également caractérisés après la réaction catalytique (DRM) pour analyser leur évolution. Enfin, un site actif impliquant des espèces Ni en interactions fortes avec d'autres cations est proposé. Ce site est obtenu sur un catalyseur partiellement réduit impliquant des lacunes anioniques, des espèces O^{2-} et des cations.

Mots clés: Reformage à sec du méthane, Production d'hydrogène, Catalyseurs à base de Ni, Cérine, Zirconium, Aluminium, Mg-Al-O, Nano-matériaux.

Hydrogen production by dry reforming of methane on Ni catalysts based on CeO_2, modified CeO_2 with Zr or Al, and Mg-Al-O nano-materials

The demand for hydrogen, as a chemical product and as energy is increasing, but the main hydrogen production methods are unsustainable and not environmentally friendly. Hydrogen production from renewable resources (such as biogas mainly composed of CH_4 and CO_2) is required. Dry reforming of methane (DRM) is a promising method to produce H_2 and CO from greenhouse gases. In this thesis, Ni-based $CeNi_XO_Y$, $CeZr_{0.5}Ni_XO_Y$, $CeAl_{0.5}Ni_XO_Y$, and $AlMg_2Ni_XO_Y$ catalysts are studied in dry reforming of methane reaction. The effect of reaction temperature, Ni content, in situ H_2 pretreatment, mass of catalyst, calcination, and CO_2/CH_4 ratio are studied. Moreover, long duration stability tests are reported on some chosen samples. The optimized catalytic performance associated with resistance to carbon formation is obtained on partially reduced catalysts. Various physicochemical characterizations are used to analyze the properties of the catalysts, such as XRD, Raman, XPS, and H_2-TPR. Some chosen catalysts are also characterized after DRM reaction to analyze their evolution. Finally, an active site involving Ni species in close interactions with other cations is proposed. It is related to a partially reduced catalyst involving anionic vacancies, O^{2-} species, and cations.

Keywords: Dry reforming of methane, Hydrogen production, Ni-based catalysts, Ceria, Zirconium, Aluminum, Mg-Al-O nano-materials.